Final Report

SPS Free Flyer for Low Earth Orbits

by

Name	Student ID
A. Cabrera	**4439295**
J.J.M. Frijns	**4553713**
J.Y.H. Pho	**4541197**
K. Krüger	**4562259**
R.W.M. De Cock	**4547977**
S. Vlaskin	**4535308**
S.V. Lonis	**4313712**
T.J.B. Hendrix	**4446143**
W.F. van Lynden	**4534344**

July 2, 2019

in partial fulfilment of the requirements for the degree of

Bachelor of Science
in Aerospace Engineering

at the Delft University of Technology

	Change Record		
Issue	Date	Description	Author
1.0	25-06-2019	Final Report Draft	Entire team
1.1	July 2, 2019	Final Report Final	Entire team

Supervisor: Ir. M. C. Naeije, TU Delft
Tutors: Ir. L. Pasqualetto Cassinis, TU Delft
Ir. S. di Mascio, TU Delft

TU Delft
Delft University of Technology

PREFACE

This report is the last deliverable of Group 15 for the Spring 2019 Design Synthesis Exercise (DSE), as part of of the Bachelor of Science Programme offered at the Faculty of Aerospace Engineering at Delft University of Technology.

We would like to thank our supervisor Marc Naeije for the guidance offered during these 10 weeks intense work, as well as Lorenzo P. Cassinis and Stefano di Mascio, our project coaches, whose continued advice and support are strongly appreciated. Furthermore, we would like to thank Henk Cruijssen and his team at Airbus Defence & Space Netherlands, our client and main point of contact, who facilitated the definition of system requirements throughout the entire DSE.

DSE Group 15, Faculty of Aerospace Engineering, Delft University of Technology, The Netherlands
July 2^{nd}, 2019

Contents

Nomenclature

List of Abbreviations

ADCS	Attitude Determination & Control System
ADS	Airbus Defence & Space
AMOI	Area Moment of Inertia
AVUM	Attitude Vernier Upper Module
CCM	Continuous Conduction Mode
CG	Center of Gravity
CMG	Control Moment Gyro
CMG	Revolutions Per Minute
COTS	Commerical Off-The-Shelf
DET	Direct Energy Transfer
DP&SC	Data Processing & Storage Centre
DT	DeTumbling mode
EA	Earth Acquisition mode
EA	Sun-Pointing mode
EDRS	European Data Relay System
EIRP	Effective Isotropic Radiated Power
ESA	European Space Agency
FBD	Functional Breakdown Structure
FDP	Gross Domestic Product
FF	Free Flyer
FFD	Functional Flow Diagram
FOV	Field Of View
FS	Factor of Safety
GEI	Geocentric Equatorial Inertial
GEO	GEOgraphic
GMAT	General Mission Analysis Tool
GNSS	Guidance Navigation & Control System
GOM	Ground Operations Model
IOD	In Orbit Demonstation
IR	Infra Red
LEO	Low Earth Orbit
MCC	Mission Control Centre
MDC	Mission Design Centre
MIT	Manufacturing Integration and Testing
MJD	Modified Julian Date
MLI	Multi Layer Insulation
MPP	Maximum Power Point
MS	Margin of Safety
NASA	National Aeronautics and Space Administration
NL	The Netherlands
OBC	On Board Computer
OBDH	On Board Data Handling
OBP	On Board Processor
OBP	On- Board & Processing
ODCS	Orbital Determination & Control System
PGD&S	Power Generation Distribution & Storage
PPL	Primary PayLoad
PPT	Peak Power Tracking
PV	Photo-Voltaic
QSL	Quasi-Static Loads
SA	Sun Acquisition mode
SM	Science Mode
SMAD	Space Mission Analysis and Design
SNR	Signal to Noise Ratio
SPS	Secondary Payload Structure
SVM	Service Module
TBD	To Be Determined
TID	Total Ionizing Dose
TRL	Technology Readiness Level
UD	UniDirectional
UT	Universal Time

List of Symbols

α	Angle between the normalised Sun vector and the E-frame in the (z, y)-plane	rad
α	Central angle	deg
α^{th}	Absorptivity	–
$\alpha_{1/2}$	Antenna half-power beam width	deg
β	Angle between the normalised Sun vector and the E-frame in the (z, x)-plane	rad
β^{th}	Orbital Position Angle	deg
$\boldsymbol{\tau}$	Torque	Nm
$\boldsymbol{B}$	Magnetic field vector	T
$\boldsymbol{M}_s$	Moments acting on the spacecraft	Nm
$\boldsymbol{S}_E$	Normalised Sun vector	–
$\hat{\boldsymbol{r}}^{P*}$	Gravitation disturbance moment	Nm
$\hat{\boldsymbol{r}}^{P*}$	normalised distance vector in the P-frame	–
$\boldsymbol{A_c}$	vector coil area	m^2
$\boldsymbol{J}$	Mass Moment of Inertia matrix	kgm^2
$\boldsymbol{m}$	magnetic dipole moment	Am^2
$\boldsymbol{M}_{plate}$	Plate moment vector	Nm
$\boldsymbol{M}_{wall}$	Wall-induced moment vector	Nm
$\boldsymbol{r}^{P*}$	Distance vector in the P-frame	m
$\boldsymbol{r}_{com}$	Vector position of the center of mass with respect to body frame	m
$\boldsymbol{r}_{plate}$	Vector position of the plate center of pressure	m
$\boldsymbol{r}_{wall}$	Vector position of the wall center of pressure	m
$\boldsymbol{T_{C,elli}}$	Ellipsoidal to C-frame transformation matrix	–
$\boldsymbol{T_{CI}}$	I- to C-frame transformation matrix	–
$\boldsymbol{T_{E'E}}$	E- to E'-frame transformation matrix	–
$\boldsymbol{T_{EC}}$	C- to E-frame transformation matrix	–
$\boldsymbol{T_{P*P}}$	P- to P*-frame transformation matrix	–
$\boldsymbol{T_{PE'}}$	E'- to P-frame transformation matrix	–
$\boldsymbol{T_{PE}}$	E- to P-frame transformation matrix	–
$\boldsymbol{V}^P$	Velocity Direction Vector	m/s
$\boldsymbol{z}_{ref_C}$	Reference vector in the C-frame	dm
$\boldsymbol{z}_{ref_P}$	Reference vector in the P-frame	m
ΔV	Velocity difference	$m \cdot s^{-1}$
$\Delta\Omega$	Angular precession per orbit	rad
$\dot{\omega}$	angular rate	rad/s^2
$\dot{\omega}_x$	angular acceleration about the x-axis	rad/s^2
$\dot{\omega}_y$	angular acceleration about the y-axis	rad/s^2
$\dot{\omega}_z$	angular acceleration about the z-axis	rad/s^2
ϵ	Emissivity	–
η^{th}	Efficiency Solar Panels	–

η_{ant}	Antenna efficiency	$-$
γ	Angle between the reference vector and the P-frame in the (x, y)-plane	rad
λ	Longitude	rad
λ	Wavelength	m
μ	Earth's standard gravitational parameter	m^3/s^2
ν_{sol}	Total PV panel efficiency	$-$
ω_x	angular velocity about the x-axis	rad/s
ω_y	angular velocity about the y-axis	rad/s
ω_z	angular velocity about the z-axis	rad/s
$\overline{J}$	Inertia matrix	m^2
ϕ	Latitude	rad
ϕ	Signal incidence angle	deg
ρ	Precession rate	$deg \cdot yr^{-1}$
ρ	Total Atmospheric Mass Density	kg/m^3
σ	Boltzmann Constant	$m^2kgs^{-2}K^{-1}$
θ	Greenwich mean sidereal time	rad
A	Area	m^2
a	Semi-major axis	m
A_{sa}	Required Solar Array Area	m^2
A_{sa}	Solar Panel Area	m^2
B	Channel bandwidth	Hz
b	Semi-minor axis	m
C	Channel capacity	bit/s
C_D	Drag Coefficient	$-$
D	Degradaion Constant	$/year$
D_r	Receiver diameter	m
e	First eccentricity	$-$
e_t	Pointing offset angle	deg
E_{ADCS}	Error ADCS	deg
f	Flattening of the Earth	$-$
G_r	Receiver gain	dB
G_t	Transmitter gain	dBi
h	Altitude	m
h_ring	Height ring	m
H_z	Momentum build up around the z-axis, over the entire orbit	Nms
h_{sps}	SPS cylinder-equivalent height	m
H_{xy}	Momentum build up around the xy-axis, over the entire orbit	Nms
i	Inclination	rad
I_c	Current through a coil	A
Id	Inherent Photo-voltaic Degradation	$-$
J_2	J_2 effect of orbit perturbation	$-$
J_{xx}	MMOI around the x-axis	kgm^2
J_{yy}	MMOI around the y-axis	kgm^2
J_{zz}	MMOI around the z-axis	kgm^2
k	Boltzmann's constant	JK^{-1}
L	Mission lifetime	$years$
L_a	Transmission path loss	dB

L_l	Transmitter loss	dB
L_r	Receiver loss	dB
L_s	Space loss	dB
L_{pr}	Antenna pointing loss	dB
M_z	average torque that must be produced around the z-axis	Nm
M_{xy}	average torque that must be produced around the combined xy-axis	Nm
N	Radius of curvature in the prime vertical	m
n_c	Number of wire coils	$-$
P	Power	W
p	Semi-lattice rectum	m
P_d	Day System Power	W
P_{eol}	End-of-Life Specific Solar Array Power	W/m^2
P_e	Eclipse System Power	W
P_{front}	Actuated Front Solar Panel Area	m^2
P_{sa}	Required Solar Array Power	W
q	Heat flux	W/m^2
R	Data rate	bit/s
r	Distance of the satellite to the centre of the Earth	m
R_E	Radius Earth	m
R_{cont}	Range of contact	m
r_{SPS}	Radius of SPS-equivalent cylinder	m
SNR	Signal to noise ratio	dB
S	Distance	m
$SolFlux$	Solar Flux	W/m^2
T	Orbital Period	s
t	Time	s
T_0	Time in Julian centuries	a
T_s	System noise temperature	K
T_d	Day Time	s
T_e	Eclipse Time	s
V	Scalar Velocity	m/s
x_C	Distance in x-direction in the C-frame	m
x_E	Distance in x-direction in the E-frame	m
x_I	Distance in x-direction in the I-frame	m
x_P	Distance in x-direction in the P-frame	m
X_d	Day Cumulative Path Efficiency	$-$
X_e	Eclipse Cumulative Path Efficiency	$-$
y_C	Distance in y-direction in the C-frame	m
y_E	Distance in y-direction in the E-frame	m
y_I	Distance in y-direction in the I-frame	m
y_P	Distance in y-direction in the P-frame	m
z_C	Distance in z-direction in the C-frame	m
z_E	Distance in z-direction in the E-frame	m
z_I	Distance in z-direction in the I-frame	m
z_P	Distance in z-direction in the P-frame	m
F_{plate}	Plate (Cylinder Top) Force	N
F_{wall}	Wall (Cylinder Side) Force	N

Executive Overview

This executive overview is a summarised version of the main outputs and findings of the detailed design of the chosen concept after the trade-off presented in the Midterm Review. The most crucial aspects of the design are discussed and the most important design features are briefly covered. The detailed design offers the client insight on the overall feasibility of an improved version of the SPS-1, and serves as a baseline for the potential upcoming stages of the development of the upgraded product.

Three-Step Approach

The three-Step approach consists of dividing the design, development and production activities into three distinct versions of the design. Step 1 is a simple Sun-pointing design that must cater for 50 W of payload power. Step 2 changes the pointing requirement to Earth-pointing with a higher pointing accuracy, and an increased payload power of 70 W. Step 3 retains the Earth-pointing regime but drastically increases the pointing accuracy required and payload power to 100 W. The “Delta” (difference between the design and investment required to achieve it) must be kept as low as possible, in order to maximise the strength of the business strategy and SPS program going forward.

Risk & Sustainability

A holistic sustainability approach has been used, and mission risk analysis has been conducted. The detailed product configuration and subsystem design comply with the requirements imposed by the client. Each subsystem incorporates risk (including the mitigation of these risks) and sustainability within the design.

Mission Operations

The available ground segment facilities are studied to evaluate the potential level accessibility of the spacecraft. The ground stations studied are the ones included in the ESRTRACK network, the stations used by the European Space Agency [1]. Based on software based orbit propagation and the mission geometry, the communication times with the available ground stations is determined over a period of 224 orbits. This data is used for the sizing and verification of the data handling and communication subsystems. It is concluded that the considered ground station network offers sufficient contact opportunities with the spacecraft, being the polar ground stations located in Troll (Antarctica) and Svalbard (Norway) the stations with the highest contact times and pass frequency. In orbit maintenance activities are also considered and implemented in the mission operations. Three different maintenance procedures are defined and its effect on the scheduling of ground stations passes is found appropriate.

On-Board Data Handling System

The on-board data handling system is able to comply with the data generation requirements of the hosted payload. These values are illustrated in Table 1 and are the basis of the link budget calculations. The subsystem is composed by commercial off-the-shelf products manufactured by Gomspace, and provide optimal performance for the given mission requirements. The on-board motherboard used is the NanoDock SDR SDK [2], which offers all the required payload and subsystem integration interfaces specified by the client. The central processing unit is the NanoMind Z7000, which provides unrivalled storage and computing capabilities [3]. The exceptional performance of these components is measured relative to their size and weight, which is crucial for the limited volume available for service module components.

Table 1: IOD requirement table, indicating the IODs for each step and their telemetry needs.[4]

	OBCs/ OBPs	RF Comms	GNSS Receiver	ADCS sensor	Optical P/L	RF Payload	Space Weather	Radiation Hardness	CubeSats
Telemetry needs	n.a.	n.a.	<1 kbps	<1 kbps	few GB per day	<100 kbps	<100 kbps	<1 kbps	n.a.

Based on the processed ground station contact time data and the characteristics of the chosen commercial products, the final data generation and communication requirements are presented in Table 2 and Table 3. It has been confirmed that the system is able of processing the generated data every orbit and of storing the payload data and telemetry, taking into account safety margins for risks and scheduled spacecraft maintenance.

Table 2: Overview of communication characteristics for Step 1.

Average Passes Per Orbit	3.69
Data Generation Rate (kbps)	8.5
Orbit Storage (Mb/orbit)	49.24
Downlink Rate (kbps) ***(Average Passes / orbit)***	47.53
Downlink Rate (kbps) ***(1 Pass / orbit)***	175.47

Table 3: Overview of communication characteristics for Step 2.

Average Passes Per Orbit	3.69
Data Generation Rate (kbps)	751
Orbit Storage (Gb/orbit)	4.35
Downlink Rate (mbps) ***(Average Passes / orbit)***	4.2
Downlink Rate (mbps) ***(1 Pass / orbit)***	15.5

Communication System

This subsystem has been designed based on the data gathered from the data handling properties of the system and the requirements imposed by the client. It can be concluded that a communication system capable of meeting the requirements imposed by the ground segment constraints has been found feasible. Likewise the data handling, the communications uses commercial off-the-shelf products from Gomspace. The transceiver used is the NanoCom TR600 [5], which offers in-orbit reconfiguration and variable channel bandwidth. The product is used for S-band communications to ensure downlink capabilities with the ESTRACK network. The system uses three ANT-2000 [6]: powerful and loss efficient S-band patch antennas distributed over the SPS-2 FF as shown in Figure 1. This improves ground coverage and reduces the system failure risks. It has been confirmed through software based signal propagation software, that the signal strength is sufficient to establish successful communication with the ground stations. It has been found that the uplink requirements do not offer any design constraints, given the transmission performance of the considered ground facilities [1].

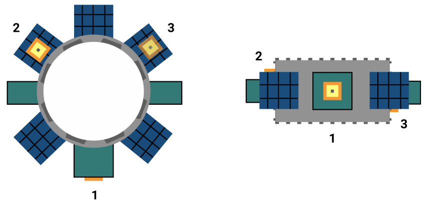

Figure 1: Schematic distribution of the three patch antennas on-board the SPS-2.

Guidance, Navigation & Control

For the Guidance, Navigation & Control models from SPENVIS[1] were used to analyse the aerodynamic, magnetic and gravitational forces acting on the spacecraft. Using this analysis the disturbance torques acting on the spacecraft were calculated. These disturbance torques were used to determine the needed torques to be provided by the reaction wheels. This resulted in a required torque of 0.0625 Nm around the x-axis, which lead to the use of 4 reaction wheels in a pyramid configuration. On basis of the angular momentum capacity and the maximum torque which can be delivered by the reaction wheel. The reaction wheels chosen are the RW-1 reaction wheels[2], as they complied with the requirements for provided torque and had angular momentum capacity which would not over- or underdesign the system.

The disturbance torques were also used during the analysis of detumbling of the spacecraft. A requirement was set to detumble within 1.5 orbit after separation from the AVUM+ stage. An analysis was performed to determine the linear dipole required from the magnetorquers to detumble within this required time. The result was a minimum linear dipole of 10 Am^2. Due to other constraints on the magnetorquers, like the size, the magnetorquer chosen were three orthogonal placed TQ15 (redundant winding)[3]. The magnetorquers will be used in combination with a magnetometer along each of the three axes, which were chosen to be NMRM-001-485[4].

To gain knowledge of the attitude of the spacecraft a gyroscope was implemented, together with sun sensors this gyroscope will determine the required torque from the reaction wheel to obtain Sun-pointing attitude. The used Sun-sensors and gyroscope are the NanoSSOC-A60[5] and the QRS116[6], respectively. The number of used Sun-sensors is two to employ redundancy, three gyroscopes are used, one for each axis on a Systron tri-axis mounting bracket.

Power Generation, Distribution & Storage

For Step 1, the required solar panel area is calculated to be 0.567 m^2. This is achieved by placing solar panels on top of the QuadPacks and the service module: it requires approximately 90% coverage of the top surfaces. After a trade-off, the Step 2 power generation system requires unfolding and fully actuated service-module attached arrays,

[1]URL: https://www.spenvis.oma.be/intro.php [cited on 24th of June]
[2]URL: "https://storage.googleapis.com/blue-canyon-tech-news/1/2019/05/BCT_DataSheet_Components_ReactionWheels.pdf" [cited on 24th of June]
[3]No source for this could be found other than the specification sheets from Airbus unfortunately, for more information Airbus shall be consulted
[4]URL:"https://www.cubesatshop.com/product/nss-magnetometer/" [cited on 24th of June]
[5]URL:"https://www.cubesatshop.com/product/nano-ssoc-a60-analog-sun-sensor/" [cited on 24th of June]
[6]URL:"https://www.systron.com/gyroscopes/qrs116-single-axis-tactical-grade-analog-gyroscope-non-itar"[cited on 24th of June]

with a total area of 0.785 m^2. The rest of the Power Generation, Distribution & Storage subsystem remains the same. Modes were estimated in terms of power requirement for all steps, which allowed for a more accurate sizing of the sub-components. The suppliers were selected, and are AzurSpace for the photo-voltaic panels and Saft S.A. for the batteries. The distribution and regulation subsystems could not be designed in detail. Step 3 was deemed feasible in terms of this subsystem alone when considering the cost, mass and volume budgets.

Thermal Control

In order to design and analyse the thermal control subsystem a transient thermal analysis based on a nodal model of the SPS2-FF was conducted. The results show that for both steps 1 and 2 passive thermal control can be used. Additionally the thermal control system architecture allows for iterations in the future without significant redesign, as well as a small development delta between step 1 and step 2.

Structural Analysis & Design

A conceptual analysis is performed on the SPS-1 structure by performing a conceptual analysis of the loads presented in the Vega-C launcher manual. Several materials are investigated from a selection which include aluminium 7075-T6 , Titanium Ti-6Al-4V and a CF/epoxy Prepreg material. The aluminium alloy is chosen as the best choice for a material for the ring structure after an assessment on the density, sustainability, risk and cost.

A design is made for the service module, based on requirements from [7] and [8]. The interface with the ring is analysed, where the QuadPack integration port is deemed as the best option for integrating the service module. All subsystem components are gathered, and are placed in the Service Module, ranging from integration to the inner structure to mounting on the external structure. This is done for all the subsystem components for step 1 and also for step 2.

An overview is made of all the separation systems of the SPS-2 FF, where the RUAG Space 937S is presented as the separation system on top of the SPS-2 FF, and also on the bottom.

A structural mass estimation is made, where the masses of the Marman clamp, the cylindrical ring structure and the complete service module structure is given.

Manufacturing, Integration & Testing

The Manufacturing, Integration & Testing process of the SPS-2 has been analysed by means of a production plan. This production plan is focused on the Manufacturing, Integration & Testing of the service module as this has not yet been tested and manufactured to the extent the other components of the other parts of the SPS-2 have been tested and manufactured.

Budget Control

The Mass and Cost budgets were controlled through the creation of initial estimates, which were then used to keep track of the progress and development during the design process. A Power budget was created for sizing the power subsystem. The Mass budget allows for 5 fully stacked QuadPacks and 1 service module without a propulsive system. For the cost budget, the recurring cost of the SPS-2-FF step 1 are €2.76 million, the initial investment €17.2 million and the launch operation costs will be €0.75 million per launch.

Project Development Planning

After the approval of the project, the set of activities to be performed after the completion of the Design Synthesis Exercise are presented. Based on the Space Flight Program and Project Management Handbook [9], the highest level phases of a general project life cycle for space development projects is presented in Figure 2.

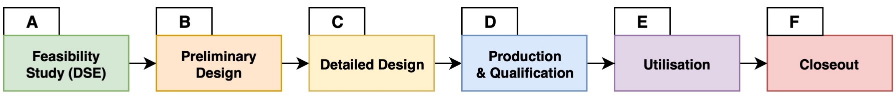

Figure 2: Main phases of the proposed project life cycle.

Business Case

In order to determine the financial feasibility of the SPS-2 Steps 1 and 2, the Business Case was elaborated upon. Overall, the conclusions are positive but nevertheless highly dependent on the demand present on the market. The SPS-1 is considered in terms of revenue per launch and is then compared to the SPS-2 FF. For an optimistic case, the revenue increases by a factor of 1.7. In a worse scenario, the factor of increase is 1.12. For Step 2, the profitability is highest. This allows for a feasible multi-step process overall.

1 INTRODUCTION

The original idea of providing access to space, via governmental institutions, has changed in the past years. Many commercial organisations have been established to provide access to space. Not only to provide this access to other companies, but also for governmental projects. An important driving factor for this change is rapid growth of the small satellite market for the past couple of years. One player, who wants to provide the small satellite market access to space is Airbus Defence & Space Netherlands (ADS NL). There is a need for a Secondary Payload Structure (SPS) that can detach from the primary payload and launcher and can act as a free flying structure, serving its own mission(s).

The objective of this report is to deliver a comprehensive and concise design of the concept chosen in the Midterm Review. A detailed product configuration and subsystem design is included in this document, in which a holistic sustainability approach has been used, and mission risk analysis has been conducted. It offers the client insight on the overall feasibility of an improved version of the SPS, and serves as baseline for the potential upcoming stages of the development of the upgraded product.

The first chapters of this document outline the context of the project. After the introduction of this chapter, chapter 2 presents the project objectives, chapter 3 gives an overview of the system requirements and constraints provided by the client and chapter 4 summarises the main outcomes of the concept trade-off performed in the previous design stage.

After this introductory part of the report, a technical introduction to the product is given and important design drivers are covered. Chapter 5 shows the general functional analysis of the product: the mission phases and the system functions to be performed within the established mission profile. The utilised risk management and sustainability assessment frameworks are presented in chapter 6. Chapter 7 gives an overview of the astrodynamic characteristics of the mission.

Next to that, the different subsystems of the spacecraft are discussed in depth, guiding the reader through their most important features an design rationale behind every subsystem of the spacecraft. The design of mission operations, communication subsystem and data handling subsystem of step 1 are presented in chapter 8, and updated in chapter 16 for step 2. The control and stability characteristics of the system are described in detail in chapter 9. The complete power generation, distribution and storage capabilities of the product are covered extensively in chapter 10. Chapter 11 includes the thermal control system of the spacecraft. The structural analysis and design of the SPS-2 FF is presented in chapter 12, followed by an overview of the spacecraft's configuration, including launcher integration, payload interfaces and service module distribution included in chapter 14. The manufacturing, assembly and testing of the product can be found in chapter 15.

After the detailed subsystem description, the last chapters of the report summarise the main outcomes of the presented product. An updated technical risk map is presented in chapter 22, while a business case exploring the commercial feasibility of the SPS-2 FF is included in chapter 25. The report concludes with a project development plan, which includes detailed activity flows for the next steps in the production of the SPS-2 FF (chapter 26). It also covers the main conclusions and further recommendations for the analysed spacecraft design, presented in chapter 27.

2
PROJECT OBJECTIVE

In a growing Space sector and a rapidly changing world, small satellites are set to be the future of in-orbit science and telecommunication missions. The objective of the group is to design a competitive European small satellite deployment and support platform that will act as a support structure for the main payload of the Arianespace Vega-C launchers. We hereby proudly present the pinnacle in small satellite support and deployment platforms: The SPS-2 Free-Flyer.

2.1. HERITAGE AND OVERVIEW OF SPS-2 FF

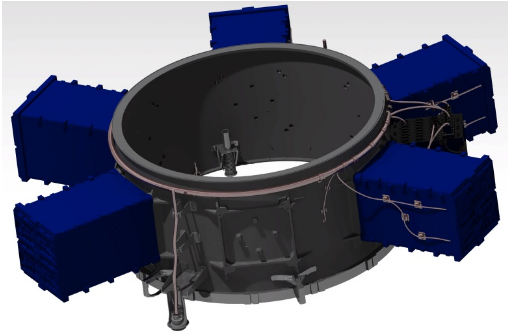

Figure 2.1: Render of the SPS-2 FF [10].

The first iteration of this concept, the SPS-1 (Secondary Payload Structure) is a payload carrier designed for the Vega-C with the capability to be a small satellite deployment platform, with integrated bays for CubeSats. Together with ADS NL, Group 15 has worked to make this platform a free-flying satellite in its own right, and thus the SPS-2 Free-Flyer was born. In order to assist ADS NL as much as possible, the design was worked out to the greatest degree of realism possible throughout the entire design phase. Instead of requiring an entire satellite design to use their instrument for important scientific measurement, customers can use the SPS-2 FF to power, stabilise and support a more demanding wide range of third-party payload at the lowest cost possible. This allows for organisations such as the European Space Agency (ESA) to focus on their instruments, while the SPS-2 FF provides all necessary support. For these reasons, the SPS can become a truly revolutionary platform, as it will be offering features that no other deployment system on the market will be able to provide.

The SPS-2 FF is expected to operate in an 850 by 350 km Sun-synchronous orbit, supporting up to 194 kg in payload mass and a total power supply requirement of 100 W. In terms of sizing, it has an internal diameter and height of 0.937 and 0.455 m respectively. This concept is sustainable by design: the purpose of it is to utilise space in the Vega-C launcher that would not be used otherwise, thus lowering cost and maximising the amount of payload in space without supplementary launch equipment. The group has worked on the complete conceptual design of the SPS for the entire duration of the project and has designed all subsystems, analysed costs, risk and sustainability to assist ADS NL in the design of the SPS-2 FF. Several concepts are traded off and the concept shown in Figure 2.1 is selected for its robustness during the trade-off process. The detailed design of this concept is presented in this report.

2.2. STEPWISE APPROACH

The three-Step approach is a design methodology that has been used throughout the design of the SPS-2 FF. Suggested by Airbus Defence and Space, the approach consists of several key considerations.

Firstly, the Steps themselves are considered to be three distinct versions of the design. Step 1 is a simple Sun-pointing design that must cater for 50 W of payload power. Step 2 changes the pointing requirement to Earth-pointing with a higher pointing accuracy, and an increased payload power of 70 W. Step 3 retains the Earth-pointing regime but drastically increases the pointing accuracy required and payload power to 100 W.

The first two Steps are worked out in detail, to the extent of component selection and sizing. For Step 3, the differences in power, mass and cost with respect to Step 2 are analysed in order to assess the feasibility of this final Step.

The main requirement behind the three-Step approach is the fact that the 'Delta' (investment and complexity difference) between steps must be actively minimised: the SPS-2 FF is considered a program, and investments are broken up into segments in order to maximise the potential success of the product. The low Delta between steps thus maximises the success probability of the system.

3
SYSTEM REQUIREMENTS

This chapter contains all the user requirements, constraints and sub-system requirements of the SPS-2-FF which the design needs to adhere to. All requirements are assigned an ID and a means of compliance. Green is used for compliant requirements, yellow for requirements which have been altered and red for requirements to which the current design is not compliant.

Compliance matrix part 1

ID	system	Description	Means of compliance	Compliant?
Internal Stakeholders				
SPS-2-MEMB-1	members	The project shall provide ample learning opportunities for all group members by going through all design phases	Experience	Yes
SPS-2-MEMB-2	members	The project shall provide a learning experience for both technical and organisational roles within a group project	Experience	Yes
SPS-2-MEMB-3	members	The design of the system shall result in a sufficient grade for the design synthesis exercise for all group members	Inspection	Cannot be assesed
SPS-2-TUTO-1	Tutors	The project shall end in a positive learning experience and aid in experience with tutoring a group of students	Experience	Cannot be assesed
SPS-2-CLIE-1	Client	The project shall provide an organised overview as to whether the project is economically feasible	Inspection	Yes
S-2-CLIE-2	client	The project outcome shall be a cost effective system	Inspection	Yes
SPS-2-PMSE-1	PMSE Lecturers	The design shall be done in accordance with methods taught in the project management/systems engineering lectures	Inspection	Yes
SPS-2-PMSE-2	PMSE Lecturers	The design process shall actively employ the project management/systems engineering principles and methods	Inspection	Yes
Connected Stakeholders				
SPS-2-TUDE-1	TU Delft	The system shall be designed in accordance to TU Delft's standards	Inspection	Yes
SPS-2-TUDE-2	TU Delft	The system design process shall increase the knowledge and research pool available to the TU and its students	Experience	Yes
SPS-2-TUDE-3	TU Delft	The system design shall demonstrate the technical and organisational capabilities of the students of the TU Delft	Inspection	Yes
SPS-2-TUDE-4	TU Delft	he system design shall demonstrate the success of the academic methods used at TU Delft	Inspection	Yes
SPS-2-ESA-1	ESA	The system shall be able to host a range of ESA's in-orbit-demonstration missions	Analysis	Yes
SPS-2-ESA-2	ESA	The system shall be available for use by ESA at all times	Analysis	Yes
SPS-2-SSM-1	small sattelite market	The system shall provide the opportunity for small satellites to be launched in the near future	Analysis	Yes
SPS-2-SSM-2	small sattelite market	The system shall aid in providing more access to space for small satellites	Analysis	It is able to host both quadpacks and IOD payload thus an entry to the smallsat market is given
SPS-2-SSM-3	small sattelite market	The system shall increase the capabilities expected from LEO ride-share services	Analysis	Yes
SPS-2-ABDS-1	Airbus Defence and Space	The system shall be ready to launch in 2022	Analysis	Not reasonable
SPS-2-ABDS-2	Airbus Defence and Space	The system shall promote the in-orbit deployment capabilities through demonstration	Analysis	Yes
SPS-2-ITU-1	International Telecommunications Union	The system shall not interfere with other satellite communication systems	Analysis	Yes
SPS-2-SUPPLY-1	Suppliers	The system shall feature COTS solutions as long this does not conflict with the cost requirement	Inspection	Yes
SPS-2-EU-1	European Union	The system shall be able to host missions for ESA and other agencies	Inspection	Yes
SPS-2-EU-2	European Union	The system shall demonstrate the design capabilities in the aerospace sector in Europe	Inspection	Yes
SPS-2-EU-3	European Union	The system shall guarantee streamlined space LEO access to key European small satellites	Analysis	Yes
SPS-2-ABSH-1	Airbus Stakeholders	The system deployment and programme shall be profitable	Analysis	Yes
SPS-2-ABSH-2	Airbus Stakeholders	The system shall secure a government research contract	Analysis	The system has been designed to suit ESA's IOD mission contracts
SPS-2-ABSH-3	Airbus Stakeholders	The system shall provide a viable entry in the small satellite market	Analysis	Yes
SPS-2-ABEM-1	Airbus Defence and Space NL Employees	The system shall aid in the research and development of the final SPS-2 FF	Inspection	Yes
SPS-2-ABEM-2	Airbus Defence and Space NL Employees	The designed system shall aid in financial feasibility assessment	INspection	Yes
SPS-2-SUIN-1	Instrument suppliers	The system shall be usable as a technology demonstrator platform	Analysis	Yes
SPS-2-SUIN-2	Instrument suppliers	The system shall be compatible with a wide range of instrument interfaces	INspection	Yes
External Stakeholders				
SPS-2-MEDI-1	Media	The project shall result in content for press coverage	Analysis	No
SPS-2-SC-1	Scientific Community	The system shall be able to host scientific payload on board	Analysis	Yes, it can host payload and thus also scientific payload
SPS-2-SC-2.1	Scientific Community	The system shall allow for space research at a lower cost for researchers and research institutes	Analysis	Yes
SPS-2-CUBE-1	Cubesat	The system shall demonstrate the capabilities of the CubeSat platform	Inspection of reports	The opportunities of the SPS-2 to cheaply and reliably deploy a multitude of cubesats without a dedicated launcher are illustrated
SPS-2-SPET-1.1	Space Enthusiasts	The entire design process of the system shall be documented in LaTeX	Inspection	Yes
SPS-2-SPET-2	Space Enthusiasts	The system shall share data of interest with space enthusiasts	Inspection	No
SPS-2-LEID-1	Leiden	The production of the system shall not impose problems on the city	Inspection	Yes
SPS-2-LEID-2	Leiden	The production of the system shall sustain employment in the Leiden area	Inspection	Yes
SPS-2-OSA-1	Other Space Agencies	The system shall not interfere with the orbit of other satellites	Analysis, Inspection	The SPS-2-FF is not placed in an already active orbit
SPS-2-OSA-2	Other Space Agencies	The system shall not create space debris	Analysis	The SPS-2-FF and all objects released from it shall deorbit either through decay orbits or propulsive methods
SPS-2-RELS-1	Relatives of Group members	The presentation of the system shall provide an overview of what the group has worked on the past 10 weeks	Inspection	Yes
SPS-2-CLIM-1	Climate Enthusiasts	The system shall be able to host atmosphere scanning payload	Analysis	Yes it can host payload and thus also an atmosphere scanning payload
SPS-2-CLIM-2	Climate Enthusiasts	The system shall have a limited footprint on the climate	Analysis	Sustainability has been taken into account on a material and structure level as to minimize the ecological footprint
SPS-2-MEAF-1	Ministry of economic affairs	The system shall aid in the advancement of the local space sector	Analysis	Yes
SPS-2-MEAF-2	Ministry of economic affairs	The system shall improve the market position of the Dutch space sector	Inspection	Yes
SPS-2-REGS-1	Regulatory authorities	The system shall not violate any international regulations regarding the operations of satellites		No known laws are breached
Step 0 cost requirements.				
SPS-2-CS-1	Cost	The economical feasibility of the conceptual designs shall be a criteria in the design trade-off process	Inspection of reports	It was only a part of the technical and effective feasibility, not its own separate part
SPS-2-CS-2	Cost	Cost assessment shall be a part of the design trade-off	Inspection of reports	Within TRL & Market acc
SPS-2-CS-3	Cost	Cost assessment shall be a part of the design conception	Inspection of reports	Within concept generation's TRL & Market acc
SPS-2-CS-4	Cost	The design shall incorporate minimised risks but not at the expense of cost	Inspection of reports	Seen in the ranking of trade-off criteria of risk and TRL and effectivenes (costs hidden in this)
SPS-2-CS-PC-1	Production Cost	Production cost shall not exceed € <2,000,000> (FY2019)	Inspection of reports	The maximum production cost requirement was not further determined
SPS-2-CS-CE-1	Cost effectiveness	The cost of the SPS-2 FF shall be monitored and reported at every stage of the design process		Yes
SPS-2-CS-CE-2	Cost effectiveness	The total unit deployment cost per kilogram in a 6 QuadPack configuration shall not exceed 60,500 \$/kg (FY2019)		Working with 50k$/kg for the cubesats
SPS-2-CS-CE-3	Cost effectiveness	Return On Investment shall be greater than € <TBD> (FY2019)		Has not been further specified
SPS-2-CS-CE-4	Cost effectiveness	Recurring platform cost of the SPS-2 FF shall be less than €2 million (FY2019)	Analysis	Not compliant: recurring costs are €2.76 million (FY2019) including production, operations and program.
SPS-2-CS-CE-5	Cost effectiveness	Launch operation cost of the SPS-2 FF shall be less €2 million (FY2019)		Compliant: Launch operation costs are €0.75 million (FY2019)
SPS-2-CS-CE-6	Cost effectiveness	The SPS-2 FF shall have a ROI of at least 1.15 [-]	Analysis	Has not been further specified
SPS-2-CS-OC-1	Operational Cost	Operational cost shall be competitive compared to launches in the small satellite market	Analysis	Has not been further specified
SPS-2-CS-BUD-1.2	Budgetary	The total mission development of the SPS-2 FF shall have a budget of € 10 million (FY2019)		Not compliant: Investment of the SPS-2-FF is estimated to be € 17.2 million (FY2019)
Step 0 launch procedure requirements.				
SPS-2-LPC-TL-1	Transport and Logistics	The transportation of the SPS-2 FF shall not cause damage to the system	Inspection	The transportation loads were concluded to be insignificant as compared to the launch-induced loads
SPS-2-LPC-TL-2	Transport and Logistics	The transportation of the SPS-2 FF shall be done by conventional means of transportation	Inspection	the size of the SPS-2 is not significant compared to a train, bus or airplane, and thus it can be transported using these methods
SPS-2-LPC-SAR-1	Stage Assembly Requirements	The integration of tertiary payloads with the SPS-2 FF shall be done by Airbus DS NL	Inspection	Yes
SPS-2-LPC-PLPP-1	Pre-launch Procedude Performance	The Pre-launch procedure shall comply with the nominal ESA procedures	Inspection	Yes
SPS-2-LPC-IFP-1	In Flight Procedures	The in-flight procedure shall comply with the nominal ESA procedures	Inspection	Yes
Step 0 launcher environment requirements.				
SPS-2-LEI-PPLA-1	Primary payload attachment	The SPS-2 FF shall be able to host the marman clamp for the primary payload after primary payload separation	Analysis	Yes, see chapter 12: Structural Design
SPS-2-LEI-LATT-1	Launcher Attachment	he SPS-2 FF shall be separable from the launch vehicle	Analysis	Yes, see chapter 12: Structural Design
SPS-2-LEI-LATT-2	Launcher Attachment	The SPS-2 FF shall be separated from the launch vehicle after the release of the PPL	Analysis	Yes, see chapter 12: Structural Design
SPS-2-LEI-ASSEM-1	Assembly	The SPS-2 FF shall be able to be integrated to the PPL and launch vehicle by external launch providers	Inspection	Yes, standard procedures for the marman clamp exist, the SPS-2-FF imposes no negative effects upon this
SPS-2-LEI-MASS-1.2	Mass	The maximum dry mass of the SPS-2 FF shall be less than 250 [kg] in launch state	Inspection	original wet mass was added as extra to dry mass. This allows the satellite to fit in the mass budget
SPS-2-LEI-MASS-2	Mass	The maximum wet mass of the SPS-2 FF shall be less than 250 [kg] in launch state	Inspection	No wet mass
SPS-2-LEI-MASS-3	Mass	The SPS-2 FF shall be able to support a maximum PPL mass of 1500 [kg] during rocket payload assembly	Analysis	The structure is designed to be able to hold the loads induced during launch, so it should be able to carry a PPL mass of 1500 kg
SPS-2-LEI-MASS-4	Mass	The SPS-2 FF shall be able to support a maximum PPL mass of 1500 [kg] during launch	Analysis	Yes, see chapter 12: Structural Design
SPS-2-LEI-VOL-1	Volume	The SPS-2 shall fit in the payload fairing of the Vega-C launcher	Inspection	Yes, the same height as the SPS-1 is used
SPS-2-LEI-SIZE-1	Size	The system's diameter shall not exceed 3050 [mm]	Inspection	Yes, its diameter is 937 mm
SPS-2-LEI-SIZE-2	Size	The system's height shall not exceed 500 [mm]	inspection	The height of the SPS-2 FF is currently 455mm. Confirmation of height from client necessary
SPS-2-LEI-SIZE-3	Size	The Moment of Inertia of the SPS-2 shall be to ESA's	inspection	Not compliant. No attention was payed to this requirement
SPS-2-LEI-PDO-1	Predetermined orbit	The SPS-2 FF shall have an orbit inclination between 98 and 108 [deg]	Analysis	Not compliant: inclination is 97.8 and 97.2 respectively. Deemed to have neglible effect
SPS-2-LEI-PDO-2.2	Predetermined orbit	The SPS-2 FF shall be in an orbit altitude between 350 and 850 [km] with respect to Earth's surface	Analysis	step 1&2: 350x850, step 3: 450
SPS-2-LEI-PDO-3	Predetermined orbit	The SPS-2 FF shall be released into a different orbit than that of the PPL	Analysis, Inspection	PPL: 850. step 1&2: 350x850, step 3: 450
Step 1 spacecraft performance requirements.				
SPS-2-PERF-1	Spacecraft Performance	The technical feasibility of the conceptual designs shall be a criteria in the design trade-off	Inspection Midterm Report	Yes
SPS-2-PERF-2	Spacecraft Performance	The SPS-2A-1 FF shall provide structural support for the PPL until release of the PPL	Analysis	Yes, see chapter 12: Structural Design
SPS-2-PERF-3	Spacecraft Performance	The SPS-2A-1 FF shall provide telemetry during all stages in flight	Analysis	Should cover all directions, detailed analysis needed
SPS-2-PERF-4.2	Spacecraft Performance	The SPS-2A-1 FF system shall be capable of separation from the primary payload	Test	Yes
SPS-2-PERF-5	Spacecraft Performance	The SPS-2A-1 FF system shall be capable of fourth stage separation	Inspection	The SPS-2 FF uses a 937S marman clamp from Ruag Space to separate itself from the payload adapter
SPS-2-PERF-6	Spacecraft Performance	The SPS-2A-1 FF system shall be capable of simple IOD hosting	Analysis	Yes
SPS-2-PERF-7	Spacecraft Performance	he SPS-2A-1 FF system shall be capable of coarse Sun-pointin	Analysis	Quite accurate sun pointing (0.5 deg from sensors)
SPS-2-PERF-8	Spacecraft Performance	The SPS-2A-1 FF system shall be capable of coarse Sun-pointing for power generation	Analysis	This is done by analysis in the ADCS section

SPS-2-PERF-OBP-1	On board processing	The SPS-2A-1 FF shall be able to perform on board processing	Test	Yes
SPS-2-PERF-OBP-2.2	On board processing	The SPS-2A-1 FF shall provide a minimum data storage of 5.5 [GB]	Test	4.35 Gbits per orbit, *10 orbits, /8 to bet GB
SPS-2-PERF-OBP-3.2	On board processing	The SPS-2 FF shall provide a link budget margin bigger than or equal to 3 [dB] during all communication.	Analysis	client requested this, communication rather than on board processing
SPS-2-PERF-ADCS-1	Attitude determination and Control systems	The SPS-2A-1 FF shall have a system that can provide three axis stabilisation	Inspection	Yes
SPS-2-PERF-ADCS-2	Attitude determination and Control systems	The ADCS shall be able to provide a stability accuracy no more than <TBD> [rad/s] in all three axis to the instruments in flight	Analysis	This was never specified and not designed for, important in step 3
SPS-2-PERF-ADCS-3	Attitude determination and Control systems	The ADCS shall be able to determine its rotational velocity vector up to <TBD> [rad/s]	Analysis	Yes, up to 100 deg/s (https://www.systron.com/gyroscopes/qrs116-single-axis-tactical-grade-analog-gyroscope-non-itar)
SPS-2-PERF-ADCS-4	Attitude determination and Control systems	The ADCS shall be able to provide a pointing accuracy no more than <TBD> [rad] in all three axis to the instruments in flight	Analysis	Accounted for in every step
SPS-2-PERF-ADCS-5	Attitude determination and Control systems	The ADCS shall be able to counteract the deflection caused by the aerodynamic effects.	Analysis	Yes
SPS-2-PERF-ODCS-1	Orbit determination and control systems	The SPS-2A-1 FF shall be able to control its orbit	Analysis	NO, not necessary
SPS-2-PERF-ODCS-2.2	Orbit determination and control systems	The SPS-2 FF shall be able to determine its orbital altitude with an accuracy of 6 [km]	Inspection	6km position error with 24 hour propagation time
SPS-2-PERF-ODCS-3	Orbit determination and control systems	The SPS-2A-1 FF shall be able to control its orbital altitude with an accuracy of <TBD> [m]	Analysis	No control necessary
SPS-2-PERF-ODCS-4	Orbit determination and control systems	The SPS-2A-1 FF shall be able to control its orbital altitude with a velocity of <TBD> [m/s]	Analysis	No propulsion or drag shields
SPS-2-PERF-ODCS-5.2	Orbit determination and control systems	The SPS-2A-1 FF shall be able to determine its orbital inclination with an accuracy of 0.1 [deg]	Analysis	Yes: inclination accuracy due to GNSS position error = 0.05 deg.
SPS-2-PERF-ODCS-6	Orbit determination and control systems	The SPS-2A-1 FF shall be able to control its orbital inclination with an accuracy of <TBD> [rad]	Analysis	No propulsion subsystem for changing inclination
SPS-2-PERF-ODCS-7	Orbit determination and control systems	The SPS-2A-1 FF shall be able to control its orbital inclination with an angular velocity of <TBD> [rad/s	Analysis	No propulsion subsystem for changing inclination
SPS-2-PERF-ELEC-1	Electronic	The electronics shall be easily reconfigurable to service the payload optimally (if necessary)	Analysis, Testing	Yes: a custom power converter and switch network allow for this
SPS-2-PERF-ELEC-2	Electronic	The electronic subsystems shall have no single point of failure	Analysis, Testing	Yes: redundant mechanisms are to be implemented later
SPS-2-PERF-ELEC-3.2	Electronic	The electronic subsystems shall always provide optimal power transfer (load matching, minimum losses)	Analysis	This was too ambitious, cannot check
SPS-2-PERF-ELEC-4	Electronic	The electronic system shall be able to provide <TBD> [W] of power to instruments in flight	Analysis	Matched values in report
SPS-2-PERF-ENV-1	Environment	The SPS-2A-1 FF shall be able to operate while being exposed to a Total Ionizing Dose (TID) rate of <TBD> [mgy/day] during its mission lifetime	Consultancy by experts	Confirmed by Airbus that it will not be a problem for Aluminium
SPS-2-PERF-ENV-2	Environment	The SPS-2A-1 FF shall be able to withstand a solar flux of <TBD> [W/m^2] without structural failure	Consultancy by experts	Confirmed by Airbus that it will not be a problem for Aluminium
SPS-2-PERF-ENV-3	Environment	The SPS-2A-1 FF shall be able to withstand aerodynamic drag effects without structural failure	Analysis	Yes
SPS-2-PERF-ENV-4.2	Environment	The maximum imposed deflection of the SPS-2A-1 FF due to aerodynamic and J2 effects shall not exceed 2×10−7 [rad/s]	Analysis	Only aerodynamic preferred decay and deflection due to J2 is 1.99×10−7 rad/s for Sun-Synchronous
SPS-2-PERF-ENV-5.2	Environment	The SPS-2A-1 FF Service Module temperature shall be kept in the range of 253.5K and 333.3K		changed
SPS-2-PERF-ENV-5.1.2	Environment	The mounting ring structure shall be kept within 193.5K and 373.5K		changed
SPS-2-PERF-ENV-5.2				
SPS-2-PERF-STRUC-1	Structures	The SPS-2A-1 FF shall be able to support a PPL of 1500 [kg] (TBC) during all stages in-flight	Analysis	Yes, see chapter 12.1: Load cases during launch
SPS-2-PERF-STRUC-2	Structures	The SPS-2A-1 FF shall be able to withstand the vibration testing compliant with the Vega-C	Analysis	Yes, frequency calculation is done on the SPS-2
SPS-2-PERF-STRUC-3	Structures	The SPS-2A-1 FF shall be able to withstand the shock loading presented by the Primary Payload Separation without structural failure	Analysis	No analysis done
SPS-2-PERF-STRUC-4	Structures	The SPS-2A-1 FF shall be able to withstand the shock loading presented by the Payload Structure Separation without structural failure	Analysis	No analysis done
SPS-2-PERF-STRUC-5	Structures	The SPS-2A-1 FF shall exhibit lateral natural frequencies $\geq$ 20 [Hz] when attached to the Vega-C	Analysis	Yes, frequency calculation is done on the SPS-2
SPS-2-PERF-STRUC-6	Structures	The SPS-2A-1 FF shall exhibit longitudinal natural frequencies $\geq$ 75 [Hz] when attached to the Vega-C	Analysis	Yes, frequency calculation is done on the SPS-2
Step 1 reliability and safety requirements.				
SPS-2-RS-1	Risk	The SPS-2 FF system shall have a reliability greater or equal to <TBD> [-]	Analysis	Could not be further analysed
SPS-2-RS-2	Risk	Safety shall be considered in the design trade-off process	Inspection of reports	Considered in sustainability and technology readiness level
SPS-2-RS-3.2	Risk	Reliability shall be considered in the design trade-off process	Inspection of reports	Within risk and trl, CHANGED: no criteria, but considered
SPS-2-RS-SH-1	Safety handling	The personnel involved in testing of the SPS-2 FF shall not be exposed to serious danger	Inspection	The materials have been selected to be non-toxic, and the separation system has failsafes to prevent separation during integration
SPS-2-RS-SH-2	Safety handling	The personnel involved in integrating the SPS-2 FF design shall not be exposed to serious danger	Inspection	The materials have been selected to be non-toxic, and the separation system has failsafes to prevent separation during integration
SPS-2-RS-SH-3	Safety handling	The personnel involved in operation of the SPS-2 FF shall not be exposed to serious danger	Inspection	Yes
SPS-2-RS-SEPS-1	Separation system	The SPS-2 FF system shall have a reliability of <TBD> for successful main payload release	Analysis	Could not be further analysed
SPS-2-RS-SEPS-2	Separation system	The SPS-2 FF system shall have a reliability of <TBD> for successful AVUM release	Analysis	Could not be further analysed
Step 1 flexibility/adaptability requirements.				
SPS-2-FA-1	Flexibility/ adaptability	The SPS-2 FF shall allow for integration of multiple tertiary payloads without significant redesign and verification	Inspection, Analysis	Yes
SPS-2-FA-2	Flexibility/ adaptability	The first operation of the SPS-2 FF shall take place in 2022	Analysis, Inspection reports	Was found not to be realistic
SPS-2-FA-3	Flexibility/ adaptability	Reliability shall be a criteria in the design trade-off proces	Inspection of reports	Yes
SPS-2-FA-SSS-1	Satellite support system	he SPS-2 shall feature support systems for tertiary payloads if required		Not necessary, TPL's will be independent
SPS-2-FA-SIR-1	Satellite integration	The SPS-2 FF shall be easily converted between mission support and CubeSat deployment mode		No different mission operation modes
SPS-2-FA-SIR-2	Satellite integration	The PPL shall be able to cover the entire top part of a fairing the size of a Vega-C launcher fairing.	Inspection	Yes
SPS-2-FA-SCR-1.2	Spacecraft reliability	The SPS-2 shall have 5 different tertiary payload mounting configurations	Inspection	Yes
Step 1 sustainability requirements.				
SPS-2-SUS-1	Sustainability	Sustainability shall be a criterion in the design trade-off process	Inspection	Yes, see the trade-offs in chapter 12: structures for the materials used and for the service module concept
SPS-2-SUS-2	Sustainability	The environment shall not be exposed to toxic materials from the SPS-2 FF for all possible scenarios during and after the mission	analysis	The materials that are selected are considered non-toxic to the environment
SPS-2-SUS-UOR-1	Use of resources	The type of manufacturing method (COTS, Production line) shall be an important factor in the design trade off	Inspection	Sustainability has been taken into account for every subsection
SPS-2-SUS-EOL-1	End of Life	The SPS-2 FF shall de-orbit within 25 years	Analysis	Yes: step 1 4.8-7.0, step 2 4.8, step 3 3.6 years
SPS-2-SUS-EOL-2	End of Life	The SPS-2 FF shall disintegrate fully into the atmosphere	Analysis, experience	Yes
SPS-2-SUS-REUSE-1	Reusability	The SPS-2 FF design shall be used for a minimum of 10 launches	Analysis	The service module has been designed to offer flexibility for the upcoming changes to the design.
SPS-2-SUS-REUSE-2	Reusability	The total mission lifetime of the SPS2-FF shall be equal to 0.5 years	Analysis	Yes
Step 2 IOD hosting and Sun Pointing requirements.				
SPS-2-LT-1	Lifetime	The SPS-2A-2 FF shall be capable of operating for a lifetime of 6 months	Analysis	Step 2: 4.8 years
SPS-2-LT-2	Lifetime	The SPS-2A-2 FF shall provide a minimum life time of 6 months to the Methane IOD payload	Analysis	No methane IOD on step 2, but 6 months is well within capability
SPS-2-POINT-1.2	pointing accuracy	The SPS-2A-2 FF shall be capable of 0.5 [deg] of sun pointing accuracy	Analysis	Changed from 0.2 to 0.5 as that is right. 0.25 is the capability of the SPS
SPS-2-COMM-1	Communications	The SPS-2A-2 FF shall be able to communicate with the tertiary payloads	Analysis	No connection anymore
SPS-2-COMM-2	Communications	The SPS-2A-2 FF shall have a data rate of at most 1 [kpbs] with the tertiary payloads	Analysis	No connection anymore
SPS-2-COMM-3.2	Communications	The SPS-2A-2 shall have a minimum data rate of 5.15 [Mbps] with the ground stations	Analysis	changed
SPS-2-COMM-4.2	Communications	The SPS-2A-2 FF shall be able to receive data from the payload with a minimum total rate of 500 [kbps]	Analysis	changed
SPS-2-SEP-1.2	Tom	The SPS-2A-2 shall attenuate the rotational velocity of 1 [deg/s] after separation	Analysis	The tip off rate was defined as 1.5 about the xy axis and 1.75 deg/s about the z axis
SPS-2-POW-1	Payload Power	The SPS-2A-2 FF shall be able to distribute <TBD> [W] of power to each of the attached payloads at all times	Test	The distribution system will not change and will be albe to provide this for all steps
SPS-2-TPL-1}	Tertiary payloads	The SPS-2A-2 FF shall provide the capability of deploying tertiary payloads	Test	In place of the IOD payloads tertiary payloads can be hosted
SPS-2-TPL-1.2	Tertiary payloads	The SPS-2A-2 FF shall attenuate the rotational velocities introduced from deploying a tertiary payload	Analysis	Not designed for, though it is able to do it
SPS-2-ATT-1.2	Attitude	The SPS-2A-2 FF shall be able to determine its orbital height to a 6 [km]	Analysis	6 km error location, thus 6 km error in altitude
SPS-2-ATT-2.2	Attitude	The SPS-2A-2 FF shall be able to determine its inclination position to a 0.1 [deg]	Analysis	Yes: inclination accuracy due to GNSS position error = 0.05 deg.
SPS-2-ATT-2.2	Attitude	The SPS-2A-2 FF shall be able to determine its orbital velocity relative to the earth to a <TBD> [m/s]	Analysis	No values could be obtained for the accuracy of the GNSS receiver
Step 3: Methane Mission \& Earth Pointing				
SPS-2-MM-1	Methane mission	The first mission of the SPS-2A-3 FF shall measure methane in the atmosphere	Analysis	Designed the spacecraft such that it is possible
SPS-2-MM-2	Methane mission	The methane mission lifetime of the SPS-2A-3 FF shall be at least 3 years	Analysis	Yes: step 3 3.6 years orbital lifetime
SPS-2-MM-3	Methane mission	The SPS-2A-3 FF system shall have a reliability greater or equal to <TBD> [-]	Analysis	Could not be further analysed
SPS-2-MM-ATT-1	Attitude control	The SPS-2A-2 FF shall have an attitude control capability of at most 0.03 [deg]	Analysis	Step 3 specific, so not designed for
SPS-2-MM-ATT-2	Attitude control	The SPS-2A-2 FF shall have an attitude knowledge capability of at most 0.6 [deg]	Analysis	Yes, star tracker
{SPS-2-MM-ATT-3	Attitude control	The SPS-2A-2 FF shall provide an attitude instantaneous acceleration no less than 0.9 [deg/s/s]	Analysis	Step 3 specific, so not designed for
SPS-2-MM-ATT-4	Attitude control	The SPS-2A-2 FF shall provide an attitude jitter no less than 100 [arcsec/s]	Analysis	Step 3 specific, so not designed for
SPS-2-MM-ATT-5	Attitude control	The SPS-2A-2 FF shall provide an attitude slew rate no less than 1.2 [deg/s]	Analysis	Step 3 specific, so not designed for
SPS-2-MM-INSTR-1	Methane mission Instrument	The methane instrument(s) shall be pointed in nadir direction in flight	Analysis	Step 2 already
SPS-2-MM-INSTR-2	Methane mission Instrument	The methane instrument(s) shall not have moving parts in flight	Analysis	Step 3 specific, so not designed for
SPS-2-MM-INSTR-3	Methane mission Instrument	The coarse width swath of the SPS-2A-3 FF shall have an accuracy less or equal to 100 km	Analysis	Step 3 specific, so not designed for
SPS-2-MM-INSTR-4	Methane mission Instrument	The fine small swath of the SPS-2A-3 FF shall have an accuracy between 5 and 10 km	Analysis	Step 3 specific, so not designed for
SPS-2-MM-INSTR-5	Methane mission Instrument	The instrument complexity shall be integrated in the instrument design trade-off	Inspection of reports	Step 3 specific, so not designed for
SPS-2-MM-MIS-1	Mission requirements	The methane mission payload volume shall not exceed 70x70x70 [cm^3]	Analysis	Payload defined by Airbus Defence and space
SPS-2-MM-MIS-2	Mission requirements	The methane mission payload mass shall not exceed 50 [kg]	Inspection	Payload defined by Airbus Defence and space
SPS-2-MM-MIS-3	Mission requirements	The methane mission payload shall be provided with a data storage and handling solution	Inspection	Yes
SPS-2-MM-MIS-4	Mission requirements	The main payload shall have a orbit average/peak power of 100 [W] during nominal operation	Analysis	Analysis could not determine definitively wether this is obtainable
SPS-2-MM-MIS-5	Mission requirements	The main payload shall be provided with a survival power of 20 [W] after the mission lifetime.	Analysis	Verified, it can do it
SPS-2-MM-MIS-6.2	Mission requirements	The average orbit data rate to the ground stations shall be no less than 10 [Mbps].	Analysis	changed
SPS-2-MM-MIS-7	Mission requirements	Data collection with the instrument shall be done using spot-track and push-broom scanning methods	Test	Instrument to be used defined by airbus
SPS-2-MM-MIS-8	Mission requirements	Measurements shall be made during 'in sun' period	Analysis	Step 3 specific, so not designed for
SPS-2-MM-MIS-9	Mission requirements	Instrument reset shall occur in eclipse	Analysis	Step 3 specific, so not designed for

4
Trade-Off Summary

In the previous phase of the design a trade-off was made to select a concept. This is documented in the midterm report [7]. All concepts can be found within, along with a performance analysis of those concepts. This allows for the generation of a trade-off matrix, which can be seen in Table 4.1. This matrix can be used to select a concept, which is developed in detail within this report.

Table 4.1: Conceptual Design Trade-off Table.

Concept	TRL& MRL	Design Eff.	Adaptability	Market Acc.	Rel.& Risks	Sus.
Armadillo	4 O	8 G	7 B	4.5 O	4 O	6 B
Bat Beam	2 R	5 O	7 B	6 B	5 O	5 O
Workhorse	5.5 O	7 B	8 G	8 G	8 G	8 G
Vipre	2 R	3 R	5 O	3.5 R	2 R	4 O

Four concepts were described and considered[7]. From these the Workhorse concept was chosen as the winner, and was taken into the detailed design. This is due to the fact “that the Workhorse Concept clearly outperforms the rest of the concepts. The Workhorse Concept turns out to be dominant in Technology Readiness Level, Adaptability, Market Accessibility, Reliability and Sustainability, being only overcome by the Armadillo Concept in Design Effectiveness. The Bat Beam, Armadillo and Workhorse can all be compared in terms of Adaptability. The two latter have also a similar score in Design Effectiveness. However, despite the resemblance of their scores in some major criteria, the huge difference of performance in Reliability and Sustainability make the Bat Beam and Armadillo concepts less attractive options. It can be concluded that the Vipre Concept is an option that fails to fit within the established criteria and that the Workhorse Concept is the most recommendable selection based on the trade-off scores.” [7]

“In addition to being the highest ranking in the trade-off and favoured by the trade-off model, as established in the sensitivity analysis, there are other factors that indicate the Workhorse concept as the most ideal to select. These include its simplicity which fosters modularity and reduces the severity and amount of risks related to interface complexity, as well as its similarity to the previous SPS-2 FF concept developed by Airbus. More specifically, due to the previous research conducted by Airbus into a concept similar to the Workhorse there exists documentation and reference material which can be built upon during the detailed design phase. This will accelerate the definition of the V&V [Verification & Validation] procedures, a manufacturing plan and the development process in general.” [7]

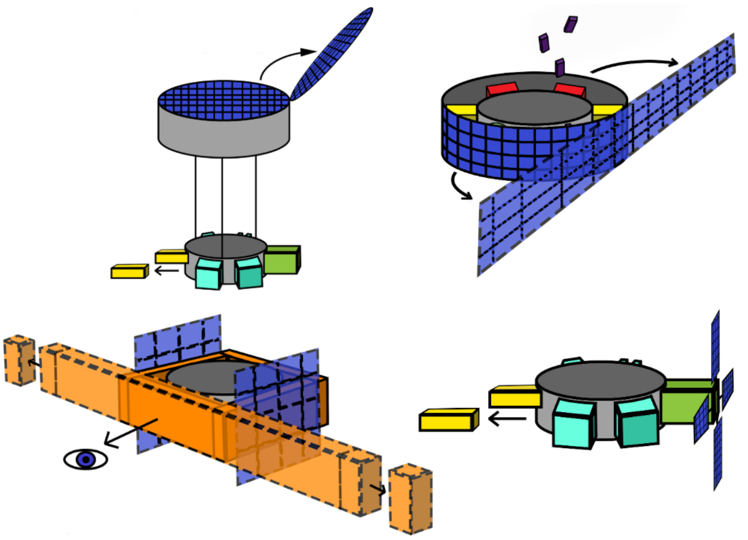

Figure 4.1: The four concepts that were used in the trade off. Top left: Vipre Concept, top right: Armadillo concept, bottom left: Bat Beam concept, bottom right: Workhorse Concept

5
FUNCTIONAL ANALYSIS

The functional analysis implemented in the design of the SPS-2 FF is presented in this chapter. The information included in this chapter is an updated version from the content presented in the past Baseline Review Report. Two functional design tools are used for the design of the spacecraft and presented in the following sections: the Functional Flow Diagram (FFD) and the Functional Breakdown Structure (FBS). The phases will be described in terms of these two functional tools.

5.1. MISSION PROFILE

To better understand the functional analysis developed throughout this chapter, the mission profile of the SPS-2 FF using the Vega Launcher is shown in Figure 5.1. The astrodynamic characteristics of the mission are covered in detail in chapter 7. Five phases form the mission profile: pre-launch operations (F1), orbit insertion (F2), deployment (F3), the on-board mission itself (F4) and end-of-life operations (F5).

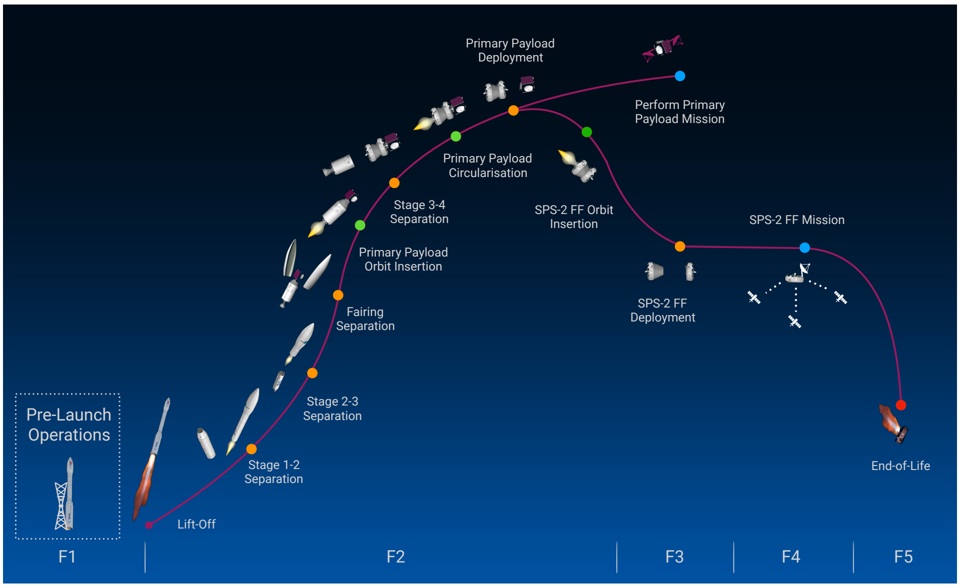

Figure 5.1: Overview of a typical SPS-2 FF Mission Profile [1].

5.2. FUNCTIONAL FLOW DIAGRAM

The Functional Flow Diagram visualises the function sequence the system is designed to perform. The blocks are connected in logical order by arrows showing the functional path followed by the system throughout the different mission stages. The first level of the SPS-2 FF functional flow diagram is presented in Figure 5.2. The colour codes implemented in the following sections are selected such that functions with equivalent level have the same colour.

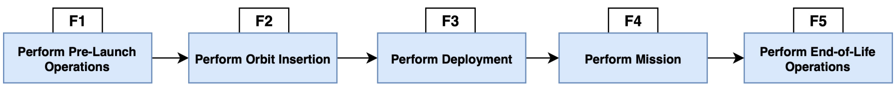

Figure 5.2: Top level of the SPS-2 FF functional flow diagram.

[1] URL:http://www.esa.int/spaceinimages/Images/2004/06/Synoptic_view_of_a_typical_mission_of_ESA_s_Vega_small_satellite_launcher [cited 2nd of May 2019]

5.3. FUNCTIONAL BREAKDOWN STRUCTURE

The Functional Breakdown summarises the functions performed by the system. Function groups are created based on the main phases of the mission. It includes functions not presented in the functional flow, which are difficult to include in a time-dependent flow. The first functional breakdown level of the system is presented in Figure 5.3.

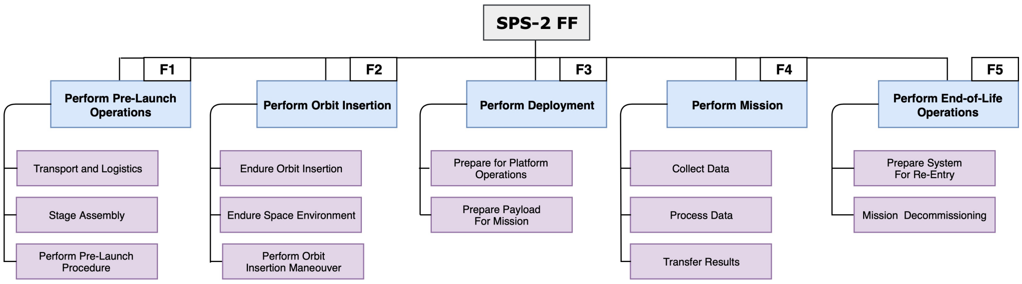

Figure 5.3: Top level of the SPS-2 FF functional Breakdown Structure.

5.4. MISSION PHASE PLANNING

The detailed functional flow diagrams and the functional breakdown structures at detailed level are presented in this section. The procedure and routines performed at a more detailed subsystem level can be found throughout the subsystem design chapters of this report.

F1: Pre-launch Operations

This phase includes all the activities related to the final assembly of the product, transport to the launch site and the system integration. It also covers the mission's logistics in general. Section 5.4 shows the functional flow and functional breakdown of this phase, labelled by F1.

F2: Orbit Insertion

After its deployment, the spacecraft goes through a detumbling process, enters its operational attitude mode and the initialisation of the rest of subsystems is performed to prepare the spacecraft for its mission. The functional flow and functional breakdown diagram of this phase are depicted in section 5.4, and are labelled F2.

F3: Deployment

After the successful deployment and stabilisation of the SPS-2 FF, the system is prepared for nominal operations, including the communications of full system health telemetry and mission progress tracking. The complete availability of the subsystem functions is checked and the payload mission requirements are fulfilled. After the confirmation of payload deployment, the control and maintenance of the payload's mission is handed over to the appropriate client or user and the procedure for hosting the in-orbit demonstration activities are initiated. Section 5.4 shows the functional flow and functional breakdown of this phase, depicted by blocks labelled with F3.

F4: Mission

Section 5.4 shows the functional flow and functional breakdown of the mission phase. The data gathered during each mission cycle is then processed and prepared for the scheduled data downlink contact passes or on-board maintenance activities. The functional flow and functional breakdown of mission phase are depicted with a block labelled F4.

F5: End-of-Life Operations

Section 5.4 also shows the functional flow and functional breakdown of the spacecraft once it has reached its maximum operational life time. These are depicted by starting with a block labelled F5.

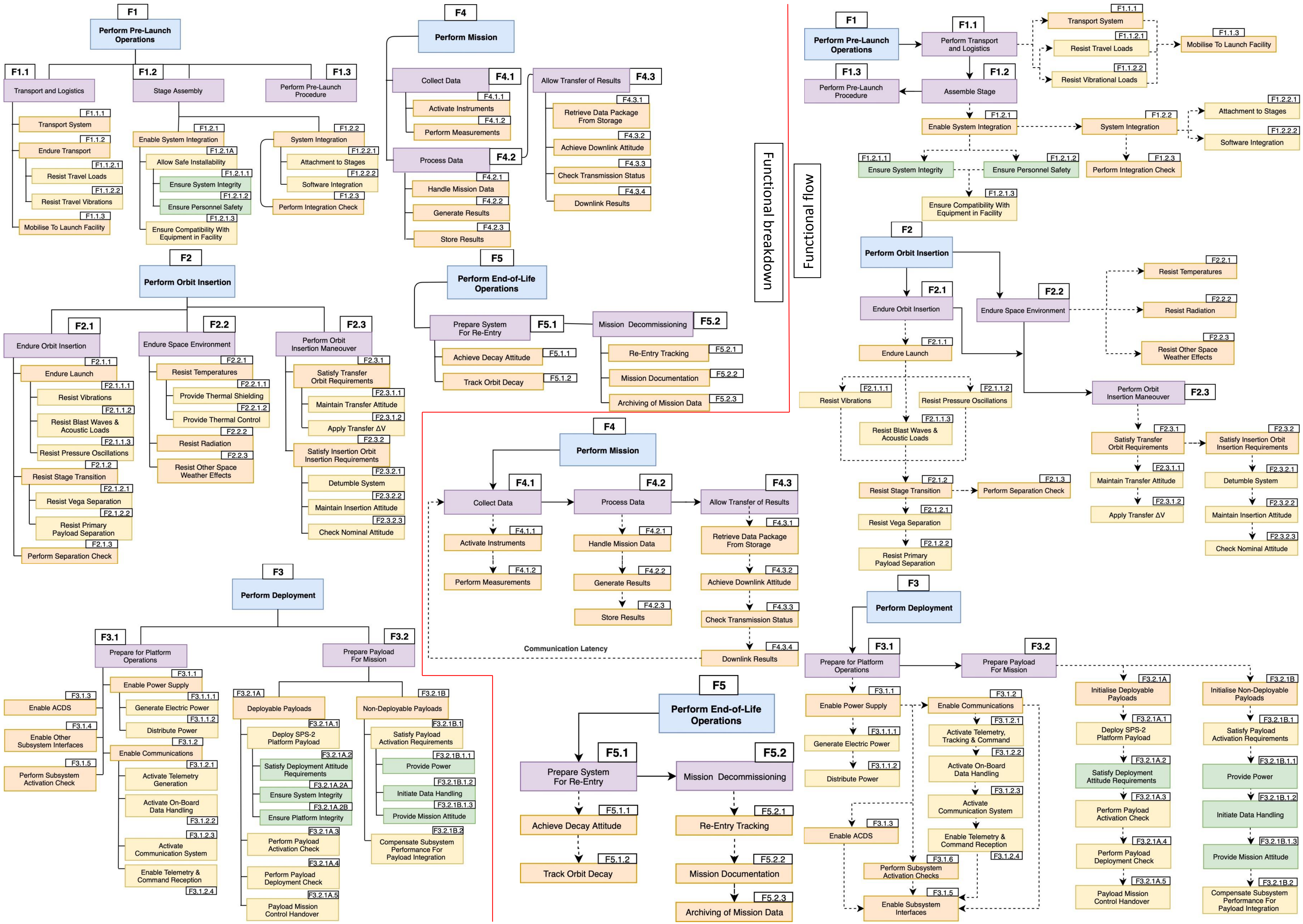

Work Breakdown and Work Flow Diagrams.

6
Risk & Sustainability Framework

Each chapter presents a section on risk and sustainability. It shows how these topics are entailed within the design. The groundwork of this framework can be found in the Baseline Report [11]. The most important aspects are repeated in this chapter.

6.1. Risk Approach

Each subsection will discuss its own risks, and the mitigation applied. Towards the end of the report, there is a chapter (chapter 22) listing all the risks and presenting them in a risk map.

6.2. Risk Scales

The scales used in this report for the risk assessment are explained below. They originated from the baseline report [11]. The scales for the probability range from rare to very likely. "The scales are selected in such a way that the reader has a clear estimate of the likelihood of the event happening in a lifetime of maximum 15-25 years.

- Negligible: No impact on mission or inconvenience
- Minor: Small reduction in technical performance, minor delay in mission plan.
- Significant: Partial reduction of technical performance, delay in mission plan.
- Critical: Questionable mission success, major reduction of technical performance.
- Fatal: Mission failure, complete reduction of technical performance." [11]

6.3. Sustainability Framework

To implement sustainability on subsystem design level, the sustainability criteria framework given in the baseline report will be used [11]. Information about the given components in a subsystem will be used as input for this framework. For the structure of the ring for example (Table 12.9), sustainability is to be implemented in its material trade-off. From the framework, it can be obtained that Emissions, Disposal Method and Energy used to produce the part are the most relevant criteria for this example. From *CES EduPack* information about all kinds of materials can be found [12]. These are, if the material is toxic to the environment/workforce or how much emissions and energy it cost to produce that material. This information can then be used in the material trade-off.

7
Astrodynamics Step 1 and 2

As for any satellite, knowledge and design of the orbits to be used by the SPS-2-FF is crucial to the success of its mission, as it is the deciding factor for where the satellite will be, at a given time and also determines what it will be exposed to. This will in turn be a governing factor for possible power generation, payload possibilities, communication, lifetime, propulsion and environmental considerations. Therefore this chapter will discuss the design of the orbits under consideration, the chosen orbits for the 3-step approach, their orbital parameters and their respective consequences for the design of the SPS-2-FF. The general mission profile of the SPS-2-FF is be discussed in section 5.1. Now, the chosen orbits will be presented and elaborated upon in subsection 7.1.1 and section 21.1. Thirdly, the resulting parameters and considerations are discussed in subsection 21.1.1. Finally the space environment and its effects and considerations on the SPS-2-FF for these orbits will be considered in section 12.7.

7.1. Orbits

In the midterm report on the SPS-2-FF an orbit trade-off was made to determine the orbit to be used per step. The four considered orbits in this trade-off were:

1. 850 km circular orbit (PPL orbit)
2. 450x450 km circular orbit(obtained by a ΔV expenditure by the SPS-2)
3. 450x450 km circular orbit(obtained by a ΔV expenditure by the AVUM stage)
4. 850x350 km orbit (AVUM+ orbit post PPL separation)

The orbits were trade off based on the following criteria: ΔV budget, Instrument compatibility, Design Complexity and Environment. The result from this trade-off is as follows: For step 1 and 2 a Sun-synchronous polar elliptical orbit of 350 by 850 km altitude is chosen, while step 3 will be placed by the AVUM+ in a Sun-synchronous polar circular orbit of 450 km altitude. The choice for a different orbit in step 3 is based on the methane mission orbital altitude requirement, which states an altitude 0f 450 km.

7.1.1. Step 1 and 2

For step 1 and 2, the elliptical 350 by 850 km orbit provided by the AVUM+ deorbiting after PPL separation is used. The general mission profile can be seen in Figure 5.1. After PPL separation at 850 km altitude the AVUM+ will deorbit itself to a 350 km altitude, after which the SPS-2-FF will be separated, placing the SPS-2-FF in an elliptical orbit as can be seen in Figure 7.1.

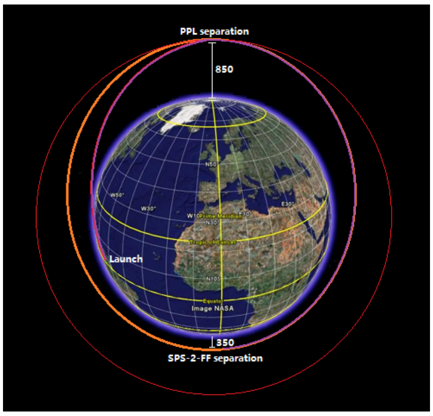

Figure 7.1: The orbit insertion profile of the SPS-2-FF (not to scale, arbitrary orbit orientation). Purple: Vega-C and Avum+. Red: PPL. Orange: SPS-2-FF.

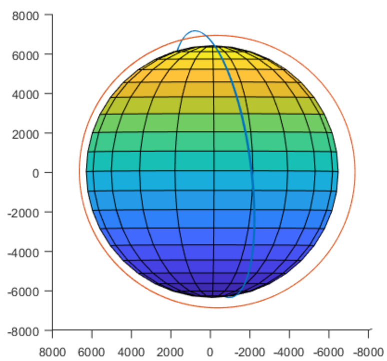

Figure 7.2: SGP4 model of the initial (orange) and final (blue) orbit of the SPS-2 FF in the 350-850 elliptical orbit.

The lifetime and behaviour of this elliptical orbit was simulated with the collection of Simplified General Perturbation models(SGP4) orbit propagation tool. This resulted in a lifetime of 4.6 years due to passive deorbiting. In Figure 7.2 the initial orbit, with arbitrary orientation, can be seen together with the final orbit. The flow diagram for the use of the SGP4 orbit propagation model can be seen in Figure 7.3.

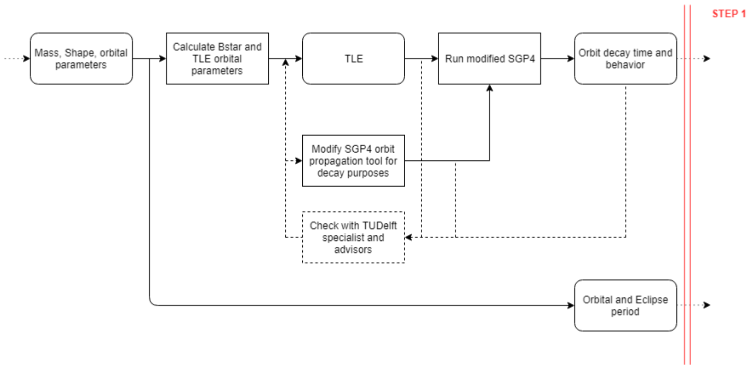

Figure 7.3: Functional flow of the SGP4 orbit propagation tool.

For a 350 by 850 km elliptical orbit, the initial orbital period and eclipse are:

$$T = 2\pi \cdot \sqrt{\frac{a^3}{\mu}} = 5792s = 97min. \tag{7.1}$$

$$\theta = \arcsin\left(\frac{Re}{r}\right) \tag{7.2}$$

$$T_{eclipse} = T \cdot \frac{\theta}{\pi} = 2126s = 35min. \tag{7.3}$$

Where a circularised orbit is used for the calculation of the eclipse period, as seen in Figure 7.4. Furthermore, in order to adhere to the requirement **SPS-2-SUS-EOL** (chapter 3) the orbital lifetime may be no more than 25 years. A custom two-line element is made for the SPS-2-FF and it is used with the SGP4 orbit propagation MATLAB model in order to calculate the orbit decay. For step 1, where due to the sun-pointing nature of the SPS-2-FF step 1 configuration the area perpendicular to the velocity is not constant, this gave a lifetime range of 4.8-7.0 years. For step 2 however, the SPS-2-FF will be earth pointing, causing the entire side to constantly be the area perpendicular to the velocity, which is the biggest exposed surface possible. This results in an orbital lifetime of 4.8 years. The assumption for both of these is that the satellite has all 5 CubeSat QuadPack deployers and the service module attached to the structure. This analysis is conducted for the scenario previous to CubeSat deployment and thus the maximum mass of the system. For step 1 for the worst case scenario, where the top of the SPS-2-FF is perpendicular to the velocity and only 1 payload and the service module is attached, the orbital lifetime is 7.6 years. This is however not realistic as the top will not remain constantly perpendicular to the flow direction and therefore the lifetime will be quite a bit shorter. For the step 2 orbit the ballistic coefficient is the same for the minimal QuadPacks attached as it is for the maximum. Between there it only decreases somewhat, resulting in slightly lower orbital lifetimes than the aforementioned 4.8 years.

Figure 7.4: Depiction of the worst case eclipse scenario (not to scale).

The orbit is required to be sun-synchronous and polar, with an inclination range between 98° to 108°. To achieve a sun-synchronous orbit, a precession rate ρ of 360° per sidereal year is required. Using the relation for angular precession per orbit for an orbit around an oblate planet:

$$\Delta\Omega = -3\pi \frac{J_2 R_e^2}{p^2} \cdot \cos(i) \tag{7.4}$$

The necessary relation between the inclination and semi-major axis can be found:

$$\cos(i) = -\frac{2\rho}{3J_2 R_e^2 \sqrt{\mu}} a^{\frac{7}{2}} = -\left(\frac{a}{12352\,km}\right)^{\frac{7}{2}} \tag{7.5}$$

The required inclination for this is 97.8°. This is slightly outside of the 98° to 108° polar orbit range required by ADS NL. The difference however is deemed to be negligible enough to be accepted, as to be precisely sun-synchronous was decided to have a higher importance than to fit exactly in the 108° to 108° range. Thus, the orbital inclination for step 1 and 2 will be 97.8°.

7.1.2. ORBIT PARAMETERS

The resulting parameters of the orbit design for step 1 and 2 can be seen in Table 21.1.

Table 7.1: Orbital parameters for all three steps.

Parameter	Step 1	Step 2
altitude (km)	350x850	350x850
semi-major axis (km.)	6971	6971
eccentricity (-)	0.04	0.04
orbital period (min.)	97	97
eclipse period (min.)	35	35
inclination (deg.)	97.8°	97.8°
lifetime all quadpacks attached (yrs)	4.8-7.0	4.8

7.1.3. FURTHER CONSIDERATIONS

Risk-wise, there is a some uncertainty of the exact ballistic coefficient that will be experienced by the SPS-2-FF while it orbits through the upper layers of the atmosphere for step 1. This is due to the varying exposed surface area perpendicular to the direction of velocity and induces an uncertainty in the orbit decay time of the SPS-2-FF for step 1. The probability of this is likely, but the impact of this risk is negligible, as the required lifetime for step 1 is lower than the range of orbital lifetimes while that range is still under the 25 year maximum.

8
Mission Operations Step 1

This chapter includes the design of the operational model used during the first mission of the SPS-2 FF, which is the Step 1 of the design development. This chapter also covers the detailed design of the Communication System and Data Handling System of the spacecraft. It was considered to group the design of these subsystems, given their high degree of interdependence. The logic behind the design process is described in more detail in section 8.1.

8.1. Subsystem Design Flow

The subsystem design flow that has been used for the results presented in this chapter is described graphically in Figure 8.1. The flow is convenient to combine the constraints imposed by each subsystem in a way that improves the traceability of design choices, assessment of design changes and iterations between Step 1 and Step 2.

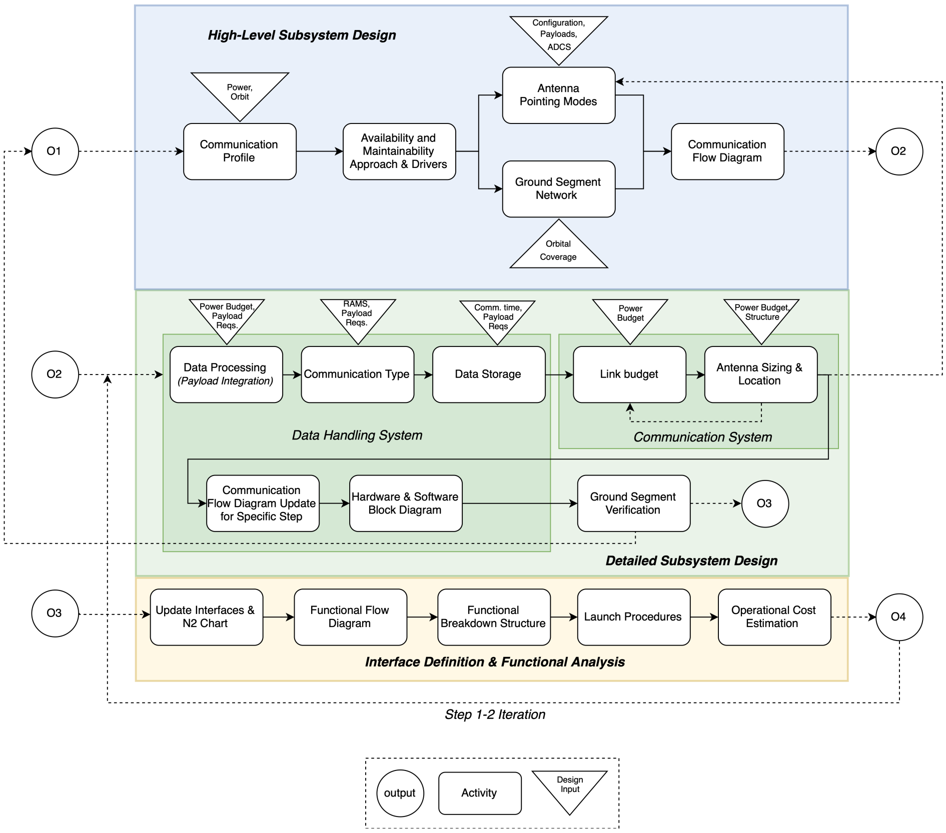

Figure 8.1: Work-flow diagram for the mission operations, communications and data handling design.

High-Level Subsystem Design

The High-Level Subsystem Design offers a deeper analysis and update of relevant system requirements. It includes the initial detailed calculations needed to generate accurate subsystem performance constraints. Its outcome will determine the drivers of the Detailed Subsystem Design. Most of this information will be reiterated if conflicting detailed requirements are found during the on-board data handling or communications subsystem design.

Detailed Subsystem Design

This is the most detailed design of the components included in the Communications System and Data Handling System. It uses the subsystem performance analysis of the High-Level Subsystem Design and translates it into final subsystem designs, in which the design constraints and drivers of the previous stage are combined. The calculations and assumptions used throughout this process are verified and later validated before entering the last design block.

Interface Definition & Functional Analysis

Despite not being depicted in Figure 8.1, this last segment depends to a considerable extent on other subsystems. It will offer a formal overview of the system's functionality and a detailed description of the subsystem's interfaces. It also includes an estimation of the costs associated to the manufacturing of the on-board data handling and communication systems, as well as to the operation and maintenance of the spacecraft.

8.2. OPERATIONS FRAMEWORK

The approach presented in this section has been already covered to some extent in the midterm report [7], and envisions an expandable operations model able to adapt to a fast-growing market, in which scalability is essential to efficiently cope with sudden increases in demand and competition. The framework, shown in detail in Figure 8.2, is formed by the Space Segment, the Ground Station Network and the Ground Operations Model (GOM). It was decided to implement such a framework given the possible advantages it offers for the development, deployment and maintenance of mission operations infrastructure [13]:

- Inter-operability between agencies, specially for ground-segment infrastructure
- Standardisation of operational interfaces for spacecraft from different manufacturers
- Competition in the provision of commercial tools, leading to cost reduction and vendor independence
- Long-term maintainability and system evolution over the mission lifetime through infrastructure replacement
- Standardisation of infrastructure interfaces, even within agencies, leading to reuse between missions and the ability to establish common multi-mission infrastructure

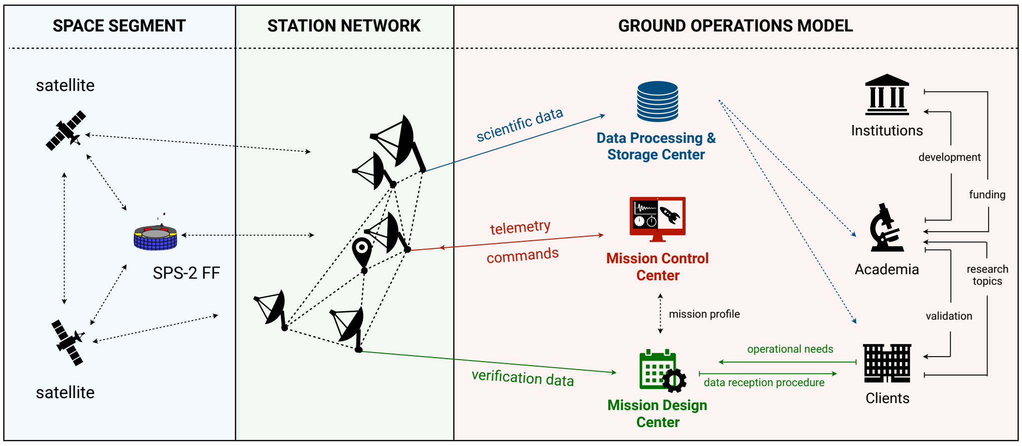

Figure 8.2: SPS-2 FF Mission Logistics & Operations Framework.

There are three principal actors in the GOM: the Data Processing & Storage Centre (DP&SC), the Mission Control Centre (MCC) and the Mission Design Centre (MDC). The MCC keeps track of the telemetry data of the mission, as well as being the coordinator of the uplink commands transmission. It is responsible for monitoring the correct development of the mission profile, which is provided by the MDC, which provides dynamic analytical support to the MCC and is the direct point of contact with the clients. It is responsible for the translation of operational needs expressed by the clients into missions profiles executable by the SPS-2. This includes assuring the compatibility of the mission with the SPS-2 FF capabilities and also with the mission requirements of the rest of payloads that will be included in a specific launch. The MDC has constant access to the data provided by the ground station network for the design and coordination of future sets of payload missions. The MDC is also in charge of providing the MCC with refined calibration data, improvement of orbital and subsystem performance models, software updates and modifications of the mission profile based on requirements expressed by the clients. For security reasons and the sake of functionality, the storage of data generated by the SPS-2 FF and its payloads is directly stored (and processed if required) in the DP&SC. This centre ensure the adequate maintenance, safety and availability of current and past mission data, which might be used for posterior statistical studies or used as reference data for the optimisation of future versions of the SPS-2 FF. As mentioned before, the clients will be able to access their data through the DP&SC, which acts as a data hub for the end user network depicted at the right extreme of Figure 8.2.

8.2.1. GROUND STATION NETWORK

Due to the close commercial relationship between the client and the European Space Agency (ESA), it was agreed to consider ESA's ground station network in the communications design. The candidate ground stations are shown in Figure 8.3. It includes the Core ESA Network (except the deep space stations), the Augmented Network and part of the Cooperative Network [1]. Detailed information about the considered stations can be found in Table 8.1.

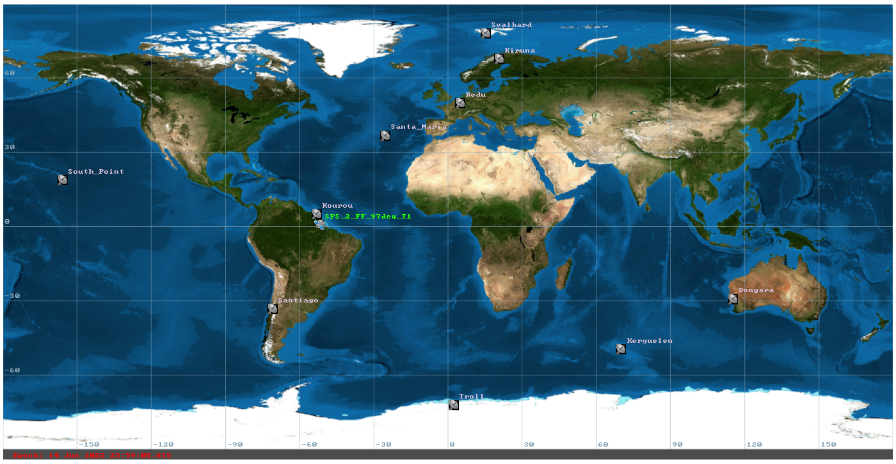

Figure 8.3: SPS-2 FF ground station network [14].

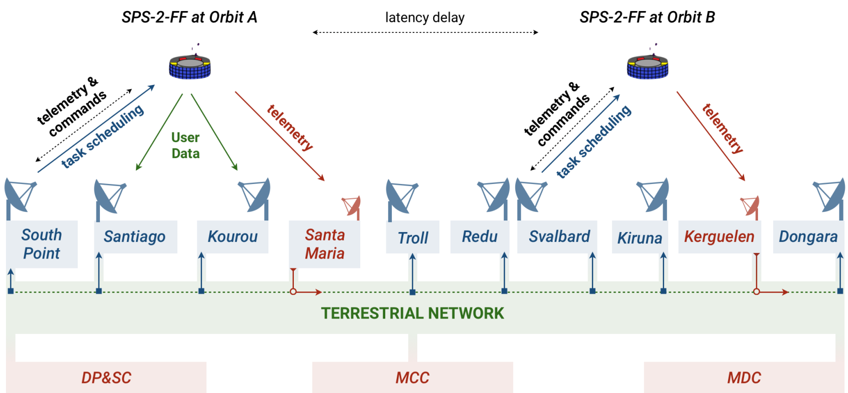

Figure 8.4: Example of data relay model based on the Augmented ESA Ground Station Network.

Covered in Table 8.1 is the detailed station information used in the communications analysis. As mentioned in section 8.2, the high level of cooperation between agencies and private station owners has lead to a substantial standardisation of ground segment infrastructure. These stations use common frequency ranges, which are reserved for specific purposes [15]. All the presented stations offer tracking, telemetry, telecommand and radiometric measurements in S-band: transmission lies between 2.2 and 2.4 GHz, while reception is performed between 2.025 and 2.15 GHz, which is the standard for LEO satellite telemetry, tracking and command communications [16]. It has to be noted that no reliable information regarding the uplink capabilities of Santa Maria station could be found, being normally used for launch tracking. Similarly, Kerguelen station is normally used as a downlink telemetry, tracking and command station for the tracking of launch vehicles. These two stations depend therefore on information relay infrastructure, capable of performing station handover for synchronised sets of passes by transmitting the gathered data by terrestrial radio systems or other means of communication. An example of such a data relay model is depicted in Figure 8.4.

[1]URL: "https://www.esa.int/Our_Activities/Operations/Estrack/Estrack_ground_stations" cited on [19th of June 2019]

In the near future, more advanced relay networks, such as the European Data Relay System (EDRS), might be used to ensure the continuous visibility of the SPS-2 FF. When fully operational at the beginning of the next decade, the EDRS will make visibility requirements less strict for LEO missions [2]. This is of special interest for further versions of the SPS-2 FF, in which larger data volumes need to be transferred to earth. By reducing the size and complexity of the ground station network needed to fulfil the mission requirements, the EDRS offers the possibility of reducing operational costs. This can be achieved by centralising the data relay in a unique data coordination centre supported by a geostationary constellation. However, the implementation of such infrastructure improvements are to be considered only in future versions of the product.

Table 8.1: Detailed ground station information[3].

Station (*Country*)	Lat. (°N) / Long. (°E)	Altitude (m)	Diameter (m)	Reception Band	Transmission Band	Comm. Type
Dongara (*Australia*)	-29.05°N, 115.35°E	250	13.5	S-band, X-band, Ku-band, Ka-band	S-band, X-band, Ku-band, Ka-band	TT&C (Uplink & Downlink)
Kerguelen (*France*)	-49.35°N, 70.26°E	50	10	S-band	Ground Relay	TT&C
Kiruna (*Sweden*)	67.86°N, 20.97°E	402	13 / 15	S-band, X-band	S-band	TT&C (Uplink & Downlink)
Kourou (*French Guiana*)	5.25°N, 307.20°E	-14.7	15	S-band, X-band	S-band, X-band	TT&C (Uplink & Downlink)
Redu (*Belgium*)	50.00°N, 5.15°E	387	2.4 / 13 / 15	S-band, Ka-band	S-band, Ka-band	TT&C (Uplink & Downlink)
Santa María (*Portugal*)	36.99°N, 334.86°E	276	5.5	S-band	Ground Relay	TT&C
Santiago (*Chile*)	-33.13°N, 289.33°E	723	9 / 12 / 13	L-band, S-band, X-band	S-band	TT&C (Uplink & Downlink)
South Point (*USA*)	19.02°N, 204.35°E	367	13	S-band, X-band, Ku-band	S-band, X-band, Ku-band	TT&C (Uplink & Downlink)
Svalbard (*Norway*)	78.22°N, 15.38°E	248	13	S-band, X-band	S-band	TT&C (Uplink & Downlink)
Troll (*Antartica*)	-72.01°N, 2.53°E	1270	7.3	S-band, X-band	S-band	TT&C (Uplink & Downlink)

The stations located in the Azores (Santa Maria) and in the Kerguelen Islands (Kerguelen) are not taken into account for the communication system sizing, but can be included in a back-up station network. This decision has been based on the fact that these are unable to partake in the mission data uplink and their trivial contribution to the ground communication profile (see section 8.3). These stations can be used if additional coverage is needed during the in-orbit maintenance activities covered in section 8.4, or for future design versions of the product in case that the downlink of scientific data has become more critical.

8.3. ORBITAL CONSIDERATIONS

General Mission Analysis Tool (GMAT) is open source orbit propagation software distributed by the Goddard Space Flight Center [14]. It has been used during the analysis of contact times with the ground station network. The mission has not been assigned an official launch date yet. For the sake of practicality, given that the only requirement expressed by the client is the need of launching in the year 2022, it has been decided to use June 15th 2022, (00:00:00 UTC) as the initial epoch of the mission. This refers to the instant in which the SPS-2 FF becomes completely independent from the AVUM+ module. The product depends on the ascent trajectory of the main payload, which might vary from launch to launch. Hence, the results covered in this section represent the communication capabilities of the SPS-2 FF after its successful orbit insertion as specified in chapter 7. The reference epoch is the start reference time for all the simulations performed during the design of the system, including the orbit propagation analysis presented in this chapter, as well as the influence of solar pressure and magnetic fields disturbances in the system's attitude control system. The latter two are explained in detail in chapter 9.

Analysis Cycle

As expressed by the client, the maximum expected life-time of the SPS-2 FF is of one year, preferably lying in the range of 3-6 months. The analysis of data obtained from simulations of orbit propagation for such time periods was

[2]URL:"https://www.esa.int/Our_Activities/Telecommunications_Integrated_Applications/EDRS/Infrastructure" cited on [19th of June 2019]
[3]URL: "https://www.esa.int/Our_Activities/Operations/Estrack/Estrack_ground_stations" cited on [19th of June 2019]

found rather impractical, given the iterative subsystem design purpose of the current design stage and the absence of a definitive launch date and orbit insertion profile. With the currently available information, it is not possible to determine the first perigee and apogee epochs nor over which ground surface points these will occur. Therefore, it was decided to use an approximated ground track repeating cycle for the simulation of contact times, with which to evaluate the specifications of available off-the-shelf products.

GMAT is used to find a cycle of 15.0010834 days. The resulting ground track for such cycle is shown in Figure 8.5. After this time interval, the spacecraft returns to the initial position of the simulation with 0.0548 degrees longitude deviation. When comparing the repeating cycle value with the theoretical orbital period of the mission, it corresponds to 223.76 orbits. This discrepancy is occasioned by the precise earth radius, gravity and atmospheric models incorporated in GMAT, which make the orbital period to decrease after each orbit. During the remaining calculations shown in this chapter, a reference value of 224 orbits per cycle has been used.

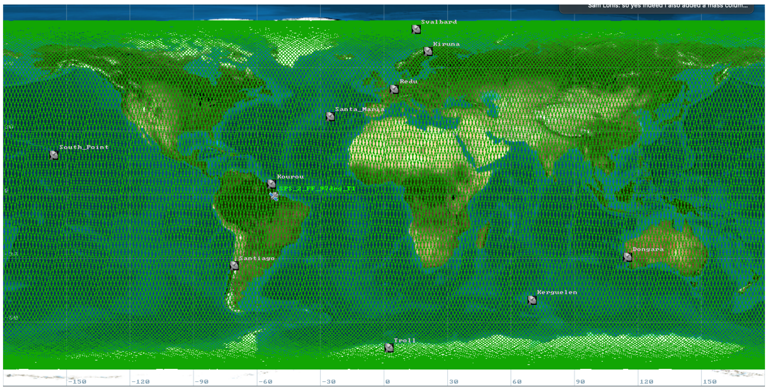

Figure 8.5: SPS-2 FF ground track cycle after 224 orbits [14].

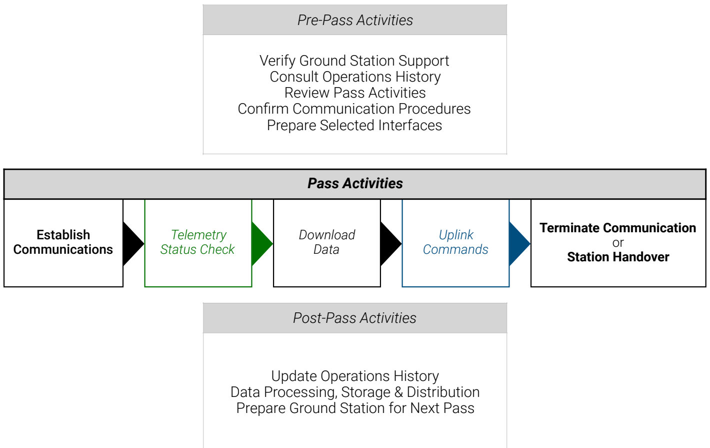

Figure 8.6: Standard ground station pass procedure.

8.4. ORBITAL AVAILABILITY & MAINTAINABILITY

Thoughtful examination of the impact of design decisions on the spacecraft's availability and maintainability are crucial for the successful operation of the SPS 2-FF. The positive impact of a carefully considered operational constraint mitigation plan on the system's performance is considerable. Therefore, the inclusion of in-orbit maintenance activities and procedures to the design of the communication system and ground segment is covered in this section. The standard communication procedure that will be used during the passes of the SPS-2 FF is shown in Figure 8.6, which includes the typical elements of a ground station pass profile [17]. This is the general case, that shows the steps to be performed in every planned pass, which are covered extensively in further sections of this chapter. After the ground station has completed the pre-pass activities and communication has been successfully established, a general subsystem status check is performed. When applicable to the current station, payload data is downloaded, if the telemetry check is nominal. Afterwards, the uplink commands are sent, which might range from profile correction commands to calibration data or software updates. The sequence is finished by the termination of communications or the initiation of task scheduling to prepare the system for ground station handover. The pass procedure is finalised by a set of post-pass activities involving the possible processing and distribution of downloaded data, communication with dependent relay stations and the archiving of the performance data gathered during the contact.

General Troubleshooting

In-orbit maintenance results in reduced availability due to unexpected communication delays. The maintenance activities consume contact time and prevent the system from performing its mission during determined periods of time. Shown in Figure 8.7 is the incident resolution procedure, which reflects the impact of unexpected maintenance activities. It provides a base for the estimation of communication time margins that will be applied in the scheduling of maintenance activities. Considering these procedures from the beginning of the design leads to more accurate contingencies, while ensuring the evaluation of all design constraints. Instead of applying only statistically derived or literature based margins after every iteration, a realistic operational environment is taken into account throughout the whole design process. This reduces the risk of delivering an unnecessarily over-designed subsystem.

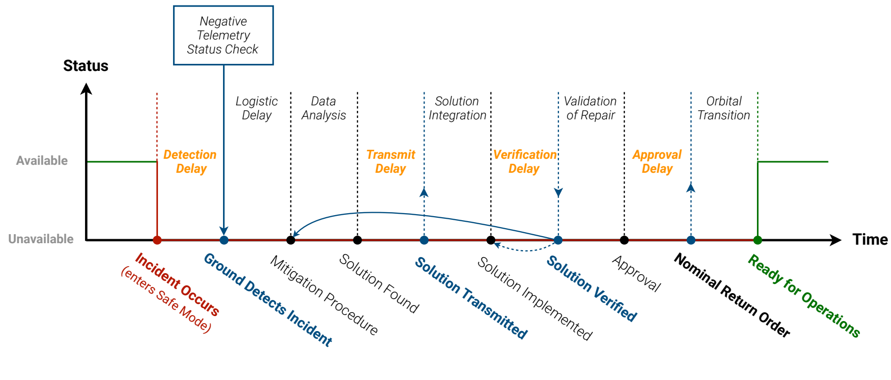

Figure 8.7: Incident mitigation procedure for general troubleshooting.

On-Board Troubleshooting

Despite the risks its entails, there are numerous advantages that the use of new technologies, such as machine learning and data mining, can bring to the space sector. The unavoidable automation revolution that the industry is undergoing is bringing the concept of autonomous spacecraft closer to reality. Artificial intelligence for space applications will provide safer and more reliable spacecraft in the near future. Improved self-awareness of space systems allows for automated on-board decision making, reducing the high level of dependence on the ground segment [4]. Current space missions require extensive number of experts to constantly monitor the status of space missions by means of costly space to ground infrastructure. The implementation of on-board predictive maintenance allows to reduce the impact of maintenance activities in satellite operations, reducing costs and improving performance [5] [18]. The effectiveness of these maintenance approach is shown in Figure 8.8. Incidents might be resolved during latency and maintenance reports are sent to ground during the next pass.

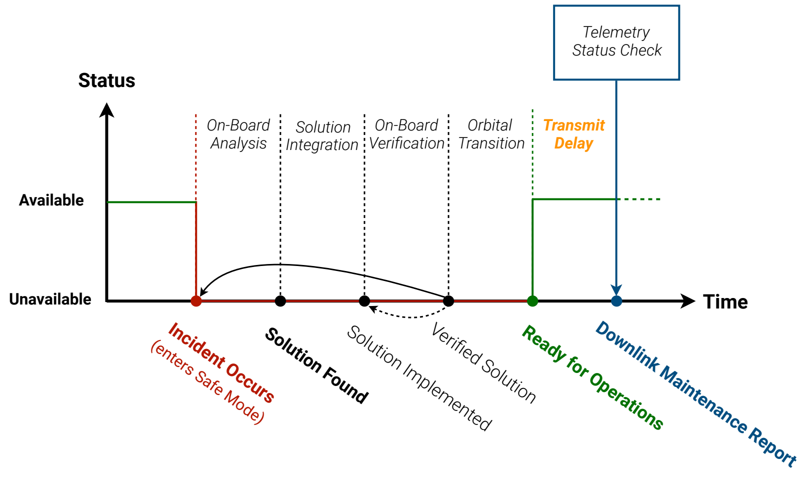

Figure 8.8: On-board incident mitigation procedure.

System Calibration & Software Updates

It is important to ensure that the spacecraft availability is sufficient for implementing software updates and refining the on-board positioning and control models with updated calibrated data from the ground. These type of maintenance activities follows the procedure for presented in subsection 8.8.1. Depending on the size and criticality of the software upgrade or data calibration command, the right combination of ground station passes needs to be chosen to ensure the correct implementation and verification of the on-board system update.

[4] URL:"https://www.esa.int/gsp/ACT/doc/AI/pub/ACT-RPR-AI-2007-ArtificialIntelligenceForSpaceApplications.pdf" cited on [19th of June]
[5] URL:"http://chaire-sirius.eu/wp-content/uploads/2016/10/Krishna-et-al.-2016-In-Orbit-maintenance-the-future-of-the-satellite-industry-Unknown.pdf" cited on [19th of June]

This is shown in Figure 8.9, and is closely related to the fault detection and resolution capabilities described in the communication flow diagram of section 8.7 and the software cost estimation of subsection 8.8.1.

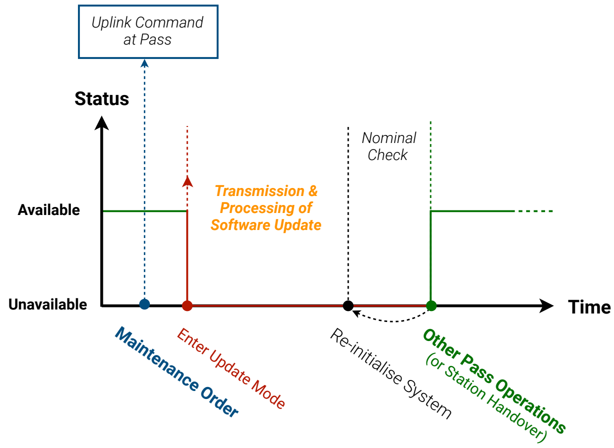

Figure 8.9: Software update and data calibration procedure procedure.

8.4.1. MAINTENANCE SCHEDULING

Optimal planning of maintenance activities is beneficial for cost reduction and increased client satisfaction. An overview of the simulated contacts times for the 224 orbital cycle is shown in Figure 8.10. The most available stations for the given mission geometry can be seen in this figure. The complete link budget calculations are covered extensively in subsection 8.7.2, but a brief overview of its results will be mentioned in this section to present the rationale behind the distribution of maintenance activities and types of communication.

Figure 8.10: Overview of passes for all ground stations during the 224 orbit period.

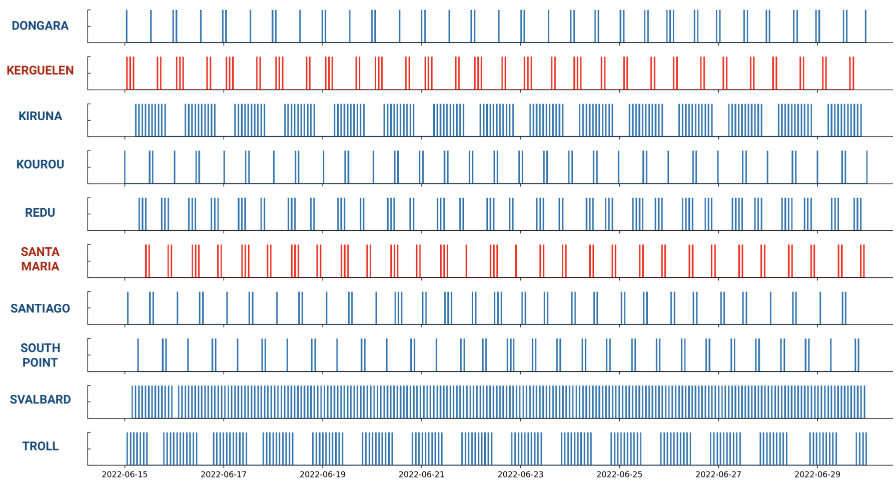

For the first step of the SPS-2 FF not all stations need to be used. Svalbard (Norway) is the most available ground station, being the station with the most regular contact cycle and the highest contact frequency, directly followed by Kiruna (Sweden) and Troll (Antartica). This is not surprising for stations located at such extreme longitudes and the highly inclined orbit of the mission. Furthermore, a detailed summary of the data obtained from the simulated orbit propagation can be found in Table 8.2.

Table 8.2: Predicted number of ground station passes and contact times for 224 orbits.

Station Name	Passes Per Cycle (224 Orbits)	Average Contact Time
Dongara (*Australia*)	52	464 s
Kerguelen (*France*)	70	453 s
Kiruna (*Sweden*)	158	571 s
Kourou (*French Guiana*)	50	488 s
Redu (*Belgium*)	87	523 s
Santa María (*Portugal*)	65	525 s
Santiago (*Chile*)	55	459 s
South Point (*USA*)	53	516 s
Svalbard (*Norway*)	221	558 s
Troll (*Antartica*)	151	462 s

Based on the link budget analysis of subsection 8.7.2, the use of one station is sufficient for successful communication throughout the spacecraft life time. Svalbard (Norway) station will be therefore used as the main payload data downlink point. The rest of the stations are still available for telemetry and tracking, but the mission does not depend on them to operate consistently. The amount of additional stations to be included in the mission ground network will depend on the degree of availability required by the on-board payload clients. Another aspect to be considered is the direct effect of growing the ground network supporting the SPS-2 FF and its operational costs, which is covered in subsection 8.8.1. Lastly, station handover can be a factor in the election of a ground station network. It can be convenient to combine different passes when two or more ground stations are located relatively close to each other. This is the case for initial tracking, orbit calibration or eventual software updates. An example of such a station handover chain is Svalbard (Norway), Kiruna(Sweden) and Redu (Belgium). The latter two might be used during these merged station passes, as their contact epochs tend to coincide sequentially. Implementing these sequential passes is not required, but is an available option to be considered during the operation of the system.

8.5. PRODUCT SELECTION

As described by the requirements imposed by the client, the design of the different subsystems of the SPS-2 FF will be based on off-the-shelf products. This section presents the chosen products that will compose the communications and data handling systems. Products from a wide range of suppliers are considered: Pumpkin Space Systems, Innovative Solutions In Space B.V., Gomspace, Nano Avionics, ENDUROSAT and IQ Spacecom. The link budget calculations presented in subsection 8.7.2 are performed for the different products, which had direct influence in the product selection. A set of products by Gomspace has been selected due to their unrivalled antenna power, gain performance, range of integration interfaces and design modularity. The following subsections present the most important specifications of the chosen elements. The exact internal layout of these components is covered in section 8.6, where the Data Handling System is presented in detail. NanoCom SDR stands for Software Designed Radio. This product consists of three separate components capable of centralising the data and communication processing functions of a satellite [19]. The default version of the NanoCom SDR includes a powerful processing module (NanoCom Z7000), a transceiver (NanoCom TR-600) and a board carrier (NanoDock SDR). Furthermore, this includes software packages for the products. Only one of these will be used, choosing a safe-life approach.

The NanoDock SDR is a modular motherboard designed to connect data handling components, communication systems and payloads. It offers a great variety of interfaces for the integration of other spacecraft subsystem components. As a desire expressed by the client, the product includes different standardised bus interfaces to ensure the compatibility of payloads and future off-the-shelf components. Additionally, the expected performance increases when combined with other Gomspace products [2]. The on-board motherboard includes I^2C, CAN and LVDS channels. It offers additional ports with RS422 capabilities for cases in which personalised digital signalling is required.

This product is a powerful processing module. It can be used for a variety of advanced solutions, ranging from communication systems to signal and image processing [3]. Coming from one of the reference providers of satellite components, this is a highly reliable and flight proven on-board computer. It includes a 32GB data storage unit, which is found to be sufficient for the expected data generation rates covered in subsection 8.7.2.

The NanoCom TR-600 transceiver meets the communication requirements of the mission. It is design to operate between 70 MHz to 6 GHz signal ranges, including a tunable channel bandwidth from 200 kHz to 56 MHz. Integrated software ensures direct compatibility with the rest of the selected components antenna.

8.5.1. NANOCOM ANT2000 (ANTENNA)

This patch antenna has exceptional power and return loss performance, and its internal interface configuration ensures complete compatibility with the chosen transceiver, as well as flexible in-flight configuration with the rest of the communications and data handling subsystem components. A more accurate transmission model of this product is covered in subsection 8.7.4. This product is designed to receive signals in the 2025-2110 MHz range and to transmit in 2200-2290 MHz range, which coincides with the frequency requirements of the considered ground stations [6].

8.6. DATA HANDLING SYSTEM

This section presents the data flows between the components of the data handling systems. It provides a deeper view on the payload and on-board data processing requirements, as well as its effect on the communications subsystem.

8.6.1. DATA HANDLING BLOCK DIAGRAM

The diagram can be seen in Figure 8.11. It shows the on-board data handling subsystem and its components, along with the data flow within. The chosen products are visible within this diagram with the relevant internal components. The external aspects are the payload and the other subsystems as input of data. The data outputs towards the antennas along a build in frequency filter within the product.

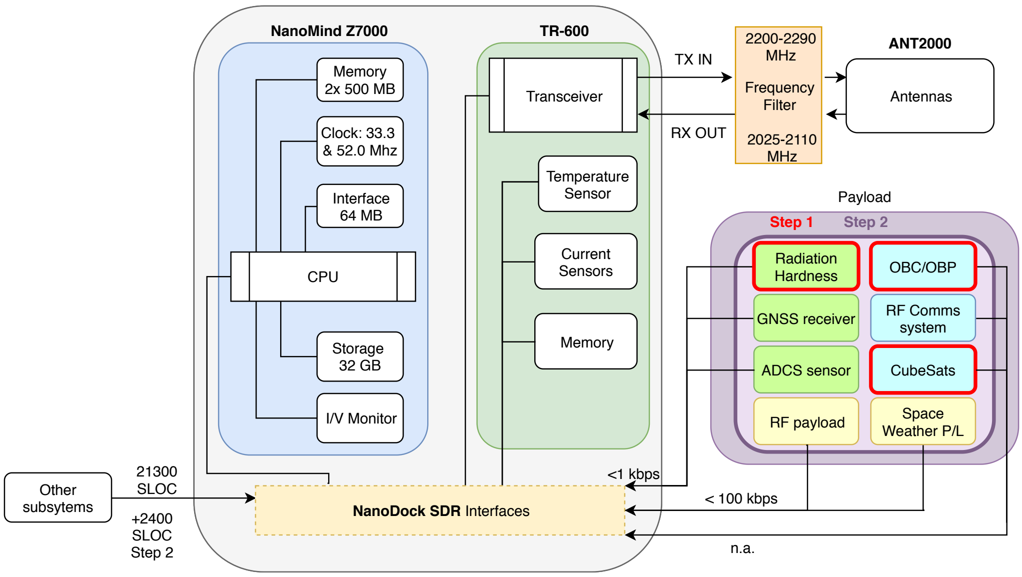

Figure 8.11: Data Handling Block Diagram for step 1 & 2.

8.6.2. DATA GENERATION

The data handling system depends on the data generated by the payload. This is shown in Table 8.3 for step 1 & 2. The worst case scenario is used in which five payloads are attached that produce the highest amount of data. This would lead to the following data generation for Step 1:

$$Data = (5 \cdot 1000 \cdot 1.5 + Service\ Module) \cdot 5792 = 49232000 bits = 49.232 Mbits, \tag{8.1}$$

using 5 payloads with a data generation of 1 *kbps*. This is multiplied by 1.5 to include overhead data as advised by the client. Additional data is generated by the service module, this is estimated to be 1 *kbps*. Finally, this is multiplied by the orbital period to get the data generated per orbit. This results in a data generation of 49.232 *Mbits* per orbit. Given that the chosen product has a data storage of 32 $GB = 256\ Gbits$, it will take $t = \frac{256 \cdot 10^9}{49.232 \cdot 10^6} = 5199.9\ orbits$ to fill up the storage, when ignoring the software storage needed for operations. The average communication time is 561.17 *s* for one pass, using the original data. This data is summarised in Table 8.2. This communication time is used to lower the cost and need for ground stations. As the data rate will be higher for step 2, it allows for a more efficient use of the antennas for step 1. This leads to a communication data rate of 87736.1 *bps* for step 1. A code rate of $\frac{1}{2}$ is used.[17] Therefore, this value is multiplied with 2, this leads to a data rate of 175472.2 *bps*. This is inputted for R in the link budget, which can be found in subsection 8.7.2.

Table 8.3: IOD requirement table, indicating the IODs for each step and their telemetry needs.[4]

	OBCs/ OBPs	RF Comms system	GNSS Receiver	ADCS sensor	Optical P/L	RF Payload	Space Weather P/L	Radiation Hardness	CubeSats
Step 1	x							x	
Telemetry needs	n.a.	n.a.	<1 kbps	<1 kbps	few GB per day	<100 kbps	<100 kbps	<1 kbps	n.a.

The analysis of the data generation requirements and the orbit propagation data leads to an initial set of communication characteristics summarised in Table 8.4. These values are used during the link budget design presented in subsection 8.7.2. Based on the orbital period and the aforementioned data generation rate, two cases for the required downlink rates have been calculated: using the average number of station passes and using only one station pass for communications.

8.7. COMMUNICATION SYSTEM

The main aspect of the communication subsystem are presented in this section. It includes an overview of the communication flow between the subsystems of the spacecraft, the link budget calculations ans the analysis of antenna coverage.

Average Passes Per Orbit	3.69
Data Generation Rate (kbps)	8.5
Orbit Storage (Mb/orbit)	49.24
Downlink Rate (kbps) ***(Average Passes / orbit)***	47.53
Downlink Rate (kbps) ***(1 Pass / orbit)***	175.47

Table 8.4: Overview of communication characteristics.

8.7.1. COMMUNICATION & HARDWARE FLOW DIAGRAM

The communication flow diagram seen in chapter 27 in the Appendix, is an updated version of the one from the baseline report [11]. It shows the communicational interaction between components and the type of information send. The diagram is elaborated to include the hardware within. Therefore, no separate hardware flow diagram is created as the communication between subsystems is already present in the diagram. The processing units in the subsystems are interface interactions that are performed by small electronic parts. This low level electronics interaction and signal processing has not been worked out in detail. Therefore, this is generally called processing unit. This diagram also includes the parts of step 2.

8.7.2. LINK BUDGET

Next, the link budget can be calculated. The equation can be seen in Equation 8.2. [20] The parameters in orange represent the parameters that are determined by the chosen product. The parameters in blue are affected by the chosen product. The SNR, signal to noise ratio, needs to be at least 3 dB in order to close the link as specified by the client and the TU Delft. [21]

$$\begin{aligned} SNR &= \frac{P \cdot L_l \cdot G_t \cdot L_s \cdot L_a \cdot L_{pr} \cdot G_r \cdot L_r}{R \cdot k \cdot T_s} \\ SNR[\text{dB}] &= P + L_l + G_t + L_s + L_a + L_{pr} + G_r + L_r - 10\log_{10} R + 228.6 - 10\log_{10} T_s \end{aligned} \tag{8.2}$$

All values below are the final values generated by using the ANT2000 antenna from GomSpace. [6] This is the case for any values listed related to the SNR later in this report. The SNR is also calculated for the other considered products. However, as these products are not selected, their results are not documented in this report.

- P = power by transmitter, equal to 8.9 W = 9.5 dBW.
- L_l = loss from transmitter, equal to 0 dB, as the loss is included in the gain.
- G_t = gain from transmitter, this value depends on the pointing of the antenna with respect to the ground station. This values ranges from -8 to 8 dBi. This is discussed in subsection 8.7.4.
- L_s = space loss, equal to -155.7 dB.

Space loss can be calculated using Equation 8.3, where λ (0.7 m) is the wavelength.[21] This can be found from the frequency which is determined by the chosen product. S is the distance between the SPS-2 FF and the ground station at zero elevation (worst case), given by $S = \sqrt{(R_E + h)^2 - R_E^2}$ (3399km). [21] With R_E as the Earth radius and h the altitude of the spacecraft (850 km in worst case).

$$L_s = \left(\frac{\lambda}{4\pi S}\right)^2 \tag{8.3}$$

- L_a = transmission path losses, mainly atmosphere and rain attenuation, equal to -14.3 dB

This factor can be estimated using figures from SMAD.[22]

- L_{pr} = antenna pointing loss, equal to -0.13 dB

This can be calculated using Equation 8.4, where e_t = pointing offset angle [deg] and $\alpha_{1/2}$. = antenna half-power beam width. For the SPS-2 FF, the former is determined by the ADCS system, the latter by the chosen product. The selected sensor from ADCS has an accuracy of 0.5°. The ADCS model (SPENVIS, see subsection 9.3.1) can output the angle between the Sun and the Earth. Therefore, e_t can be set equal to the accuracy of the sensor, two degrees are added to account for possible mistakes in the model. The chosen product provides the value of $\alpha_{1/2}$. For the ground station, e_t can be estimated to be 10% of $\alpha_{1/2}$.[21]

$$L_{pr}[\text{dB}] = -12 \cdot \left(\frac{e_t}{\alpha_{1/2}}\right)^2 \tag{8.4}$$

- G_r = gain receiver, equal to 18 dB, for a diameter of 2.4 m and 25.3 dB, for a diameter of 5.5 m. It is explained below how this is calculated. However, these calculations underestimate the gain. For example, it gives a gain of 33 dB for the ground station Redu-2 (13.5 m diameter),while it has a gain of 65 dBi. [1]

This can be calculated with Equation 8.5 [20], with η_{ant} = antenna efficiency (typically 0.55 for parabolic antennas)[23], λ = wavelength, D_r = receiving antenna diameter.

$$G_r = \eta_{ant}\left(\frac{4\pi}{\lambda^2}\right)A = \eta_{ant}\frac{\pi^2 \cdot D_r^2}{\lambda^2} \tag{8.5}$$

- L_r = loss receiver, equal to -0.46 dB using an efficiency of 0.9.
- R = data rate [bit/s], equal to 175.5 $kbits/s$ = 52.4 dB
- k = Boltzmann's constant = $1.38 \cdot 10^{-23}$ $\frac{J}{K}$ = -228.6 dB
- T_s = system noise temperature, equal to 135 K = 21.3 dB for downlink.

This last value is determined by using a table from the lecture slides [20].

It is assumed that the downlink is the driving limiting condition, as for uplink the transmission power and gain of the ground station can compensate the increased system noise temperature and the lower performance of the SPS-2 FF receiver by far. Lastly, the SNR is found to be 19.8 dB for the 2.4 m diameter of the Redu station. This is the smallest diameter to be used. Therefore, it is clear that the link closes as the SNR is bigger than 3 dB. This is over designed, but this is due to the higher requirements of step 2 that are already taken into account at this stage. The SNR is also analysed when the antenna is radiating under an angle of 90°. This is to check the usefulness of the omnidirectional aspect of the antenna. The gain of the antenna is equal to -8 dBi under this condition. Even under this worst case condition, the link budget still closes for the 2.4 m diameter (SNR of 3.8).

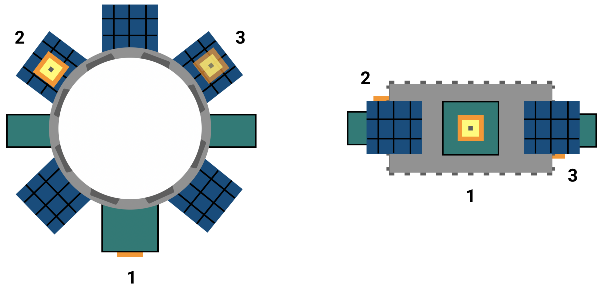

Figure 8.12: Schematic distribution of the three patch antennas ob-board the SPS-2 FF.

8.7.3. ANTENNA CONFIGURATION

The SPS-2 FF will count with three patch antennas arranged as shown in Figure 8.12. The first antenna is located in the exterior of the service module, while the other two are located in the bottom and the top of two of the payload quadpacks. This redundant configuration allows for constant omnidirectional signal transmission. It also reduces the risk of complete subsystem failure. This increases the overall availability of the system and improves considerably the reliability of the communications subsystem.

8.7.4. ANTENNA COVERAGE

To further validate the calculations shown in subsection 8.7.2, MATLAB is used to create a radiation model comparable to the gain distribution of the actual antenna. These two are shown in Figure 8.13 and Figure 8.14. The manufacturer of the patch antenna provides extensive information in the product's data sheet [6]. This allowed the reproduction of the antenna's performance. However, the model does not include ground plane features or electric components like the resistor and capacitor layout. Properties of the dielectric materials used in the antenna have been also omitted, despite being available as input parameters in the design tool used. The effect of neglecting these properties has an influence on the reliability of the analysis and should be improved in the future. This model is nonetheless considered sufficient to estimate the communication coverage, given the exploratory nature of the calculations in this feasibility design stage.

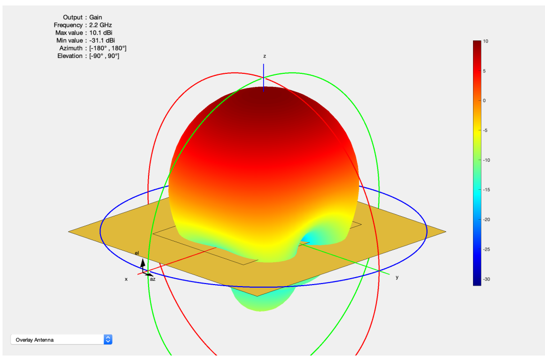

Figure 8.13: MATLAB antenna model to verify ground coverage.

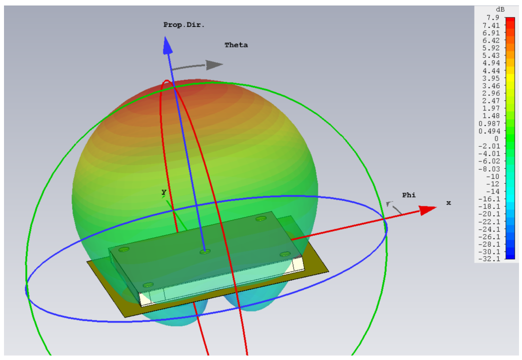

Figure 8.14: Reference antenna model from manufacturer [6].

The antenna radiation model is used to assess the range and magnitude of the signal strength over the regions surrounding the most visible ground stations. As discussed in subsection 8.4.1, the spacecraft will be mostly visible through polar ground stations, i.e. Svalbard and Troll stations. Figure 8.17 to Figure 8.18 show the power distribution of the downlink signal at the moment in which the spacecraft passes exactly over these two stations. Similarly to the antenna design, the detailed assessment of complex variables within the signal propagation model have not been carried out. Parameters such as atmospheric refractivity, conductivity or ground permittivity are set to the default values recommended by the software provider. Deeper insight in the effect of these variables is recommended for more detailed versions of the design, as they depend on the specific atmospheric conditions of each station throughout the year. However, their effect on the feasibility verification of the design is negligible.

The analysis of antenna coverage is performed under two limiting conditions of signal incidence angle: $\phi = 0$ degrees and $\phi = 90$ degrees, representing antenna pointing in the station direction and perpendicular alignment of the radiation plane with respect to the station direction, respectively. This angle is defined in Figure 8.15. Given the sun-pointing attitude control of the spacecraft, the chosen antenna configuration is designed to ensure sufficient transmission and reception signal strength at all times. In order to successfully communicate with the ground stations at any available pass, the antenna with the best reception or transmission angle will be used. The optimal antenna, i.e., the antenna with the lowest ϕ, is determined based on the data produced by the on-board attitude control. The polar coverage and signal intensity propagation is evaluated at perigee and apogee altitudes. This is performed to compare the expected signal power to be received by the ground stations with typical LEO mission signal reception thresholds found in literature.

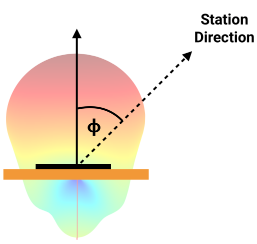

Figure 8.15: Graphic description of the signal incidence angle ϕ relative to ground station direction.

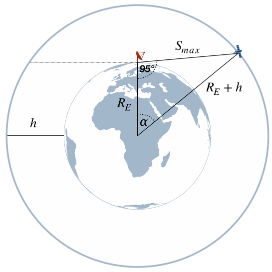

Figure 8.16: Geometrical definition of angles and distances for communication coverage.

The consulted literature shows similar ranges for the typical values of signal power reaching earth surface from satellite missions: small LEO satellite signals oscillating between -80dBm and -105 dBm [24], and another data set showing successful recorded values ranging from -120 dBm to -95 dBm [25]. The results generated for the SPS-2FF show ground signal reception levels ranging from -70 dBm to -100 dBm, which falls within the expected range. It is worth noting, that the signal amplification capacity of the proposed ground station network (subsection 8.2.1), is more powerful than the ones used during the experiments shown in literature, leaving additional margin for the required signal strength. For instance, the TMS-1 antenna located in Redu Station (Belgium) is able to receive signal with a flux as low as -127 dBW/m^2 [1]. It has been assumed that the rest of the stations are prepared to support LEO missions with comparable signal strength levels, due to the high number of similarities found between all the considered ground stations. This value is compared with the estimated intensity of the signal received by the ground. These results have been generated taking into account the geometrical contact constraints of the stations for a minimum elevation angle of 5 degrees. The altitude of the ground stations above sea level has a negligible effect on the calculations and were therefore omitted from the equations included in this report. The radius of the antenna coverage is calculated with Equation 8.6 and Equation 8.7.

$$\alpha = 85 - arcsin\left(\frac{R_E}{R_E + h} \cdot sin(90+5)\right) \tag{8.6}$$

$$R_{cont} = \frac{\pi \cdot \alpha}{180} \cdot R_E \tag{8.7}$$

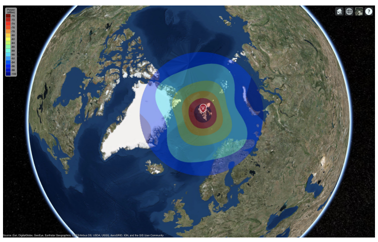

(a) h = 350 km and ϕ = 0 deg.

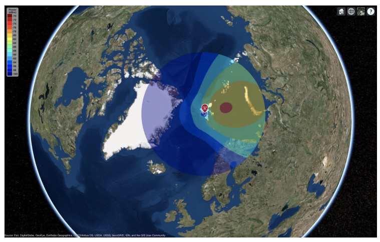

(b) h = 350 km and ϕ = 90 deg.

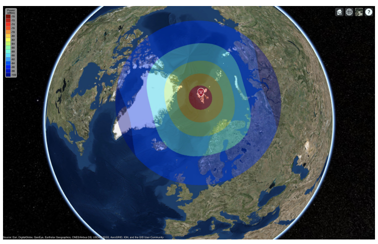

(c) h = 850 km and ϕ = 0 deg.

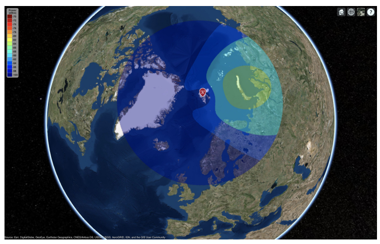

(d) h = 850 km and ϕ = 90 deg.

Figure 8.17: Downlink SPS-2-FF coverage to Svalbard (Norway) ground station at perigee, apogee and the two limiting transmission angles [14].

Figure 8.16 shows the geometrical parameters from which the mathematical expressions have been derived. Equation (8.6) and Equation 8.7 yields in a maximum visibility range of 2612 km at apogee (850 km altitude) and 1580 km at perigee (350 km altitude), which is the radius of the coverage regions presented before. The actual signal range trespasses the defined circle. However, not further insight on the system capabilities is gained by studying further regions due to the extremely low signal levels found beyond the established contact threshold.

$$S_{max} = \frac{sin(\alpha)}{sin(90+5)} \cdot (R_E + h) \tag{8.8}$$

In order to confirm that the available type of ground antenna is able to detect and process the spacecraft's signals, the minimum Effective Isotropic Radiated Power (EIRP) of the spacecraft is determined. This critical value is found at apogee altitude and where the distance between the spacecraft and the ground station for contact is maximum. This distance is represented as S in Figure 8.16 and calculated using Equation 8.8. This leads to a maximum distance of 2888.788 km. The EIRP is computed with Equation 8.9, where P is the on-board transmitter power and G_t the transmitter antenna gain. This yields a value of -120,88 dBW/m^2, which corresponds to a 6.12 dB margin for signal flux at the receiver end with respect to the signal flux threshold of the ground station antennas.

$$EIRP = \frac{P \cdot G_t}{4\pi \cdot S^2} \tag{8.9}$$

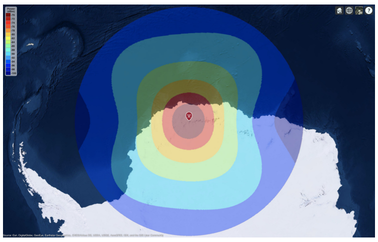

(a) h = 350 km and ϕ = 0 deg.

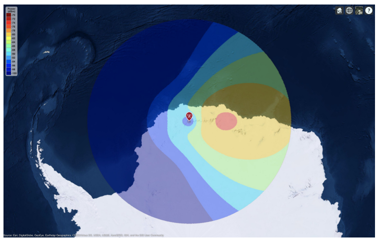

(b) h = 350 km and ϕ = 90 deg.

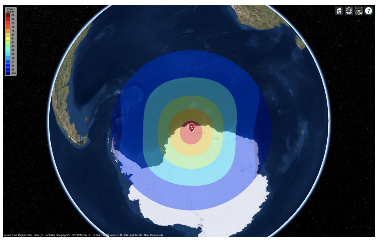

(c) h = 850 km and ϕ = 0 deg.

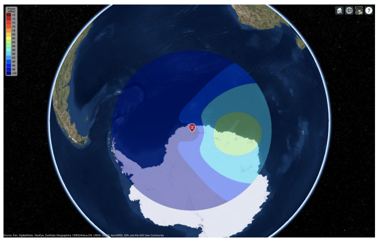

(d) h = 850 km and ϕ = 90 deg.

Figure 8.18: Downlink SPS-2-FF coverage to Troll (Antartica) ground station at perigee, apogee and the two limiting transmission angles [14].

8.8. Cost Breakdown

This section provides a brief overview of the data handling and communication hardware costs, as well as the costs generated by the manpower and maintenance of facilities for the successful operation of the SPS-2 FF.

8.8.1. Operational Costs

There are many aspects that contribute to the operational costs of a space mission. The following are the identified sources of costs related to the operation of the SPS-2 FF:

- Mission Control Facilities: It is assumed that the mission analysis and control is performed by already existing centres, as the product is a secondary payload, that will travel in predetermined launches. Therefore, the costs for the development of Ground Command & Control is covered by other mission stakeholders.
- Ground Station Network: No development of this is required for the SPS-2 FF as only existing ground stations will be used. The main source of cost is the scheduling of ground station usage.
- Ground Operations Support: costs associated to pre-launch operations, the preparation of the launch site and the integration of the spacecraft and launcher. It includes yearly missions maintenance costs.
- Software Development: one of the most costly elements of a space mission. The software costs are based on the information gathered in the on-board data handling system (section 8.6).

- Project Management & Assurance: This includes the business and administrative coordination, quality control procedures and the technical organisation behind the integration of complex subsystem with very sensitive and restrictive requirements. It also takes into account the labour costs of the personnel required for ground support activities. Such a detailed analysis is not included in this feasibility study, but should be considered in future project budgets during post-DSE project definition stages.

Ground Operations Support

It is challenging to provide an accurate evaluation of the complete operational costs a mission like the SPS-2 FF entails. However, parametric cost estimations methods are commonly used to estimate some of the aforementioned cost sources. Based on the cost estimating relationships model provided in SMAD [17] and shown in Figure 8.19, the mission will have a yearly ground segment and operations cost of 2.64 million €.

Software Development

The average cost per source lines of code (SLOC) for unmanned spacecraft is FY2010 550$, or 566,83€ when converted and adjusted to inflation. The estimated total number of SLOC is derived from the communication flow diagram (chapter 27). Based on the SLOC allocation, the flight software of Step 1 of SPS-2 FF will have 47000 SLOC, which includes the central on-board data handling, system maintenance and the software integration of all the chosen COTS products. However, many of the selected components offer integrated software with high degree of customisation, such as the Software Defined Radio and the GNSS receiver. Omitting these contributions would bring down the initial SLOC estimation to 40000. Moreover, this estimate includes automated on-board fault identification and correction. Removing this feature from the design would reduce the number of SLOC to 32000, thus decreasing the software development costs by around 4 million €. Nonetheless, as discussed section 8.4, this could create additional ground segment costs, due to the increased personnel and system availability required to monitor the spacecraft's health and well as the increased communication time needed for incident resolution.

The SLOC values shown in subsection 8.7.1 do not represent the influence of more recent technologies implemented in the chosen COTS products. Also, the heritage software available to the client from similar projects can not be taken into account in this cost analysis for the current design stage. Therefore, only the cost of source code related to the main on-board data handling of the system is included in the final cost estimation, i.e., on-board fault detection and on-board utilities. This brings down the initial number of SLOC to 17200, which entails a **direct development cost of 9.75 million €**. In addition, compatible ground software is to be generated to support the mission. As the ground facilities used for the SPS-2 FF form part of an established ground network, it is assumed that the software cost related to the ground equipment is negligible for the current feasibility phase of the design.

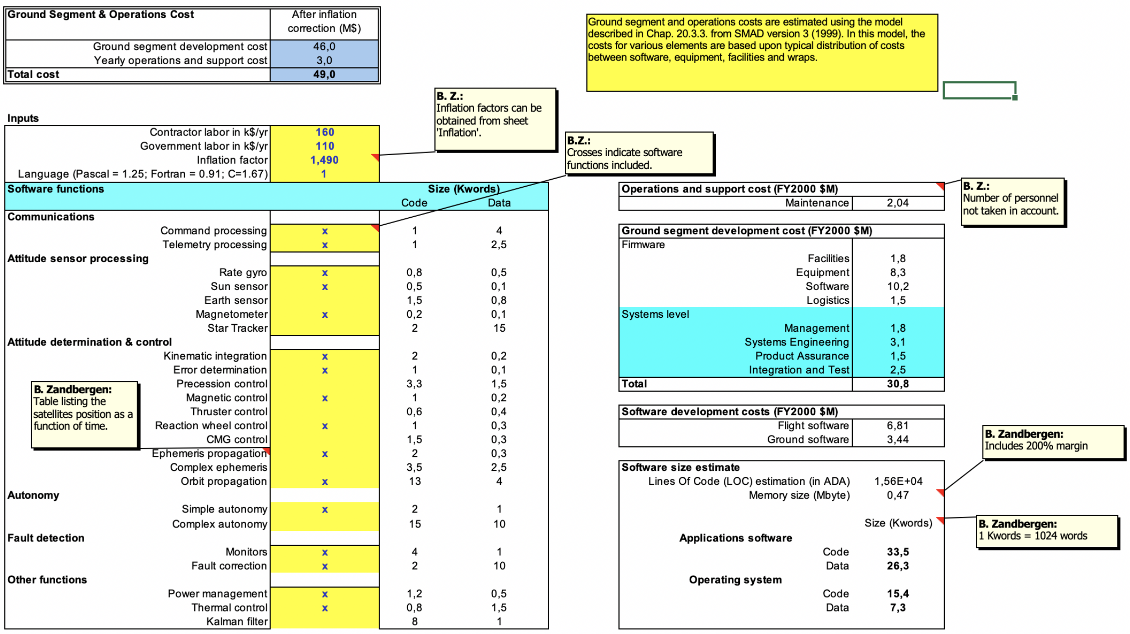

Figure 8.19: Parametric estimation of the ground segment costs for the SPS-2 FF.

8.9. OPERATIONAL RISKS

The operational risks are discussed in this section. First assessing the risks and afterwards, mitigating those risks.

8.9.1. RISK ASSESSMENT

- OP-1: Computer program GMAT mistakes, causing communication issues: The probability is *unlikely* as the program is made by NASA. They made and manage the software, which makes it a reliable source of information. The impact is *significant*, as the communication plan needs to be redone and errors will arise. This could lead to less communication time.
- HW-1: Hardware failure: the probability is considered *rare* as all components except the antennas have been flight proven. [2, 3, 5] However, the antennas are designed to work with the chosen transceiver. [6] The impact is *fatal*, no retrieval of payload data is possible and it leads to mission end.
- GC-1: No data downlink possible for a long period of time: The probability of this happening is *unlikely* as many ground station are available from existing partners. The impact is considered *significant* as data is lost and measurements might have to be repeated.

8.9.2. RISK MITIGATION

The mitigation techniques listed below are implemented during the design. Therefore, no clear specific actions are present that show the mitigation techniques. However, they are included within other aspects such as product selection.

- OP-1: Safety factors and a conservative approach reduces both the probability (to *rare*) and the impact (to *minor*). This allows the system to perform the communication in a different procedure than planned.
- HW-1: Redundancy can be applied to lower the impact to *critical*.
- GC-1: This risk can be mitigated by having more on-board data storage. This reduces the impact *minor*.

This risk mitigation is implemented within the design iterations. For OP-1, this can be seen in the fact that the average communication time used, is the average communication time with only one station (during one orbit). This is not the case as more ground stations will be available. HW-1 is taken into account during the product selection, for example three antenna's are chosen to ensure communication at all time. Furthermore, the majority of the products are flight proven. This is taken into account during the product selection as it lowers the risk. The GC-1 risk is also taken into account during the product selection. Therefore, a product is chosen with 32 GB of storage.

8.10. OPERATIONAL SUSTAINABILITY

All the selected products have been manufactured with material based on glass/polyimide. This material combination can not be recycled. The antenna also includes the Rogers RO4003C material. This is lead-free process compatible, which allows the implementation of more environmentally friendly production methods. As the SPS-2 FF will fly multiple times, different versions of the same product will be used and produced. This improves the efficiency of the production. Furthermore, the supplier of components for this subsystem is Gomspace, an aerospace manufacturer based in Denmark. Assuming that the SPS-2 FF will be assembled in the west of Europe, the geographical proximity of the supplier permits limiting the transportation period needed. Applying this type of policies for long-term space projects with a high number of suppliers can have considerable effects in terms of production sustainability during years of development and production.

8.11. SENSITIVITY ANALYSIS

For the link budget, the communication data rate and the transmitter antenna gain are the most sensitive parts. The former depends on the data generation and the number of contacts within an orbit (including time of contacts). The data generation rate will not change, but the number of contact might. This highly affects the communication rate as now twice the amount of data needs to be sent the next time. This extra data can be sent in one pass or spread out over multiple. However, the design is able to handle this as it can increase the number of contact within an orbit and it has sufficient data storage.

The transmitter antenna gain depends on the angle at which the data is transmitted to the ground station. The gain ranges from -8 dBi for an angle of 90 deg to 8 dBi for perfect pointing towards the ground station. These values are retrieved from Figure 8.13 and Figure 8.15. This is taken into account in the design, allowing the communication to work during worst case. Furthermore, the number of contacts can again be increased if the link budget fails to close during the worst case scenario.

9
Guidance, Navigation & Control Step 1

It is important for the satellite and its operations to know where it is and how it is pointed. The design of this Orbital Determination and Control System (ODCS) and Attitude Determination and Control System (ADCS) is described in this chapter.

Firstly, the implementation of the ODCS is explained in section 9.1. Secondly, it is explained how the ADCS has been designed in section 9.2. Next, the database, coordinate transformations and disturbance torque models are explained in section 9.3. Afterwards, the ADCS architecture and its components are designed and the attitude sensors are selected in section 9.4. Then, it is described how the selected components work together in the mission operations, see section 9.5. After that, the magnetorquers are analysed and selected in section 9.6 and the same goes for the reaction wheels in section 9.7. Next, the attitude control after eclipse is analysed with the implemented sensors and actuators in section 9.8. Then, the cost, risk and sustainability for the ADCS is explained in section 9.9. After that, an overview of the code used for the ADCS design is shown in section 9.10. Lastly, the recommendations for further investigation is given in section 9.11.

9.1. ODCS

In the midterm report the choice was made to use a Global Navigation Satellite System (GNSS) receiver for orbit determination. However, it had been decided to explore the possibility of satellite laser ranging as well. As the advantages of a light GNSS module would also hold for ranging, where a light reflector would be used, and thus both would not create a big physical delta on the SPS-2-FF.

However, using laser ranging would require a manned tracking station on Earth. It is possible to combine this with the manned stations for the data-link between the satellite and the ground station, which has contact once every orbit. However, this would impose extra tasks and complexity upon this station. Thus, it would increase the costs of these operations, which will be the case for as long as the satellite remains in orbit.

Furthermore, the possibility and accuracy of laser ranging is dependent on the weather conditions, which brings in the risk of having inaccurate orbit measurements for periods of bad weather over the ground station. Meanwhile, the GNSS receiver does not require a manned tracking station. Therefore, it imposes a cheaper solution for the costs during the orbit's lifetime, as one only has to pay for the use of a GNSS network, while not requiring active labour.

Finally, laser ranging would require a reflector to be pointed towards the Earth, which is not possible in step 1 unless a specific mechanism would be developed to correct for the Sun-pointing, or multiple reflectors would be necessary. The GNSS receiver only needs to be present and given sufficient power, its location and attitude do not matter as much as that of the reflector.

For these reasons it was decided to uphold the decision of using a GNSS receiver as the method of orbit determination. The receiver used will be a COTS GNSS receiver board, the CubeSat Kit™ GPSRM 1 GPS Receiver Module [1]. This will use the Vinti orbit propagation model to deliver all necessary orbital parameters based on double-precision GNSS position and velocity.

9.2. ADCS Design for Step 1

The ADCS in step 1 has been designed according to a flow, shown Figure 9.1. A literature study has been performed, the detumbling motion has been analysed, the disturbance torques have been calculated and sensors and actuators have been traded-off. This has been iterated after design changes happened in, for example the PG&D subsystem. This ensured the requirements from the customer as well as from other subsystems are met.

[1] URL: http://www.pumpkininc.com/space/datasheet/710-00908-D_DS_GPSRM_1.pdf [cited on 24th of June]

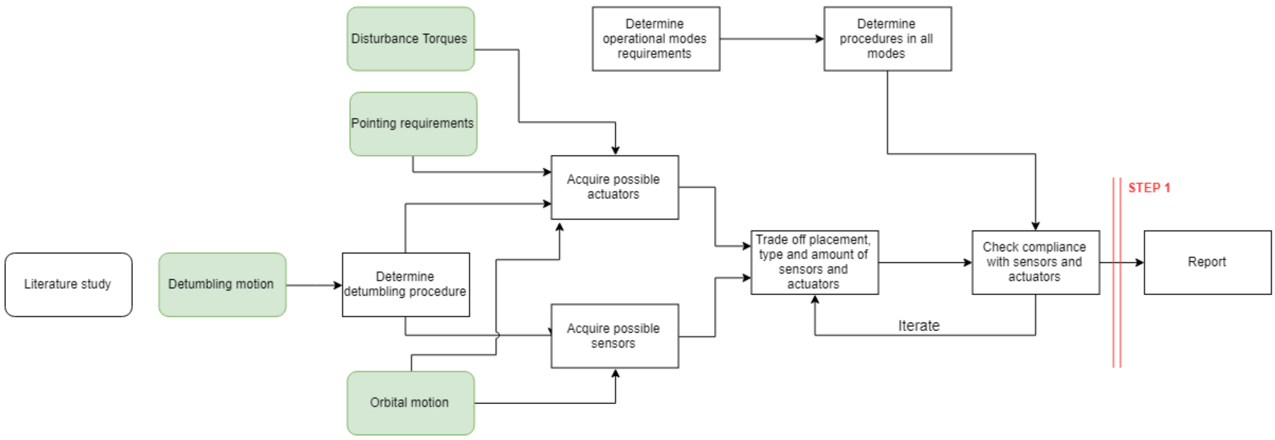

Figure 9.1: ADCS design flow.

9.3. DATABASE & MODELS

In order to analyse what attitude sensors and actuators should be implemented, it is important to know the environment the spacecraft is operating in. This section explains all the data sets and models that are used and how they are implemented.

Firstly, the database is explained in subsection 9.3.1. Secondly, the data and disturbance torque models for aerodynamics, magnetic field and gravitational field are explained subsection 9.3.2, subsection 9.3.3 and subsection 9.3.4, respectively. Lastly, the total disturbance torques are analysed in subsection 9.3.5.

9.3.1. DATABASE

The Database was a requirement to obtain the necessary values for creating the disturbance torque models and modelling the spacecraft motion. These sort of values include:

- Location of the spacecraft at every time interval
- Orbit propagation of the spacecraft
- Velocity components of the spacecraft at every time interval
- Atmospheric density at every relevant orbital position
- Magnetic field flux components at every relevant orbital position
- Direction of the Earth with respect to the Sun at every time interval

SPENVIS[2] has been used for the acquisition of these values. It is a tool created by ESA to model the space environment and its effects. Note that the solar intensity has not been included in step 1, as the solar radiation disturbance torque has little to no effect on the spacecraft's attitude, due to the Sun-pointing requirements. All other assumptions regarding the models can be found on SPENVIS[2], as well.

ORBIT GENERATOR

The first model used in SPENVIS is the orbit generator, a tool created by the European Space Operations Centre. It allows the user to enter all necessary values to model the orbit and its propagation. The orbit start has been set on the 15th of June 2022 at 00:00:00, as during this period the highest angular momentum build-up occurs for the SPS-2 FF [26]. All models use this launch moment, not only to model the ADCS, but also the communication system, for example. This ensures all external and orbit parameters are the same to most effectively model the situation for the whole system. The orbit is modelled for 30 days, as that is the longest period it can be modelled in SPENVIS. The other orbital parameters used can be found in Figure A.1 and Figure A.2, as calculated in section 7.1. The orbit propagation on the first day of the mission has been visualised in Figure 9.2.

The orbit generator takes the variations in the gravitation field of the Earth and the corresponding drift of the orbital plane into account. How

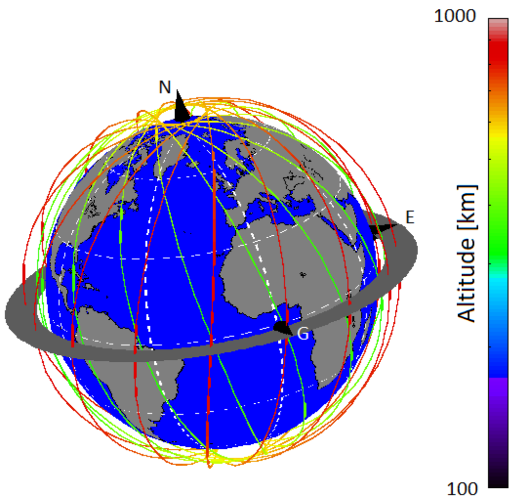

Figure 9.2: Orbit propagation of the SPS-2 FF on the first day after launch[2].

[2] URL: https://www.spenvis.oma.be/intro.php [cited on 13th of June]

solar radiation pressure and atmospheric drag have been implemented into the SPENVIS model could not be retrieved and thus the effects are not verifiable with the other models used and created. These settings have therefore not been implemented in the orbit propagation. The values resulting from the orbit generator have been used as an input for other simulations in SPENVIS.

SPENVIS COORDINATE FRAMES

All disturbance torques will be modelled in the P-frame in order to model the control torques and dynamics of the system. The data from SPENVIS is not output in consistent frames. All coordinate transformations will be explained in order to get from the SPENVIS output to the P-frame later. An overview of the data sets and in which frame they are represented is shown in Table 9.1. The reference frames are depicted in Figure 9.4-Figure 9.7.

Table 9.1: Overview of data sets and their original reference frame.

Data set	Original reference frame
Spacecraft coordinates	C-frame
Spacecraft velocity	I-frame
Sun position	I-frame
Magnetic field	E-frame
Aerodynamic data	Independent

The output of the orbit generator consists of two data sets: one for the coordinates containing the spacecraft's relevant altitude, latitude, longitude and time in Modified Julian Date (MJD), expressed in the Geographic (GEO) coordinate- or C-frame. The other data set contains the attitude, velocity and Sun position vectors expressed in the Geocentric Equatorial Inertial (GEI) coordinate- or I-frame. The magnetic field is expressed in spherical coordinates in the E-frame, see Figure 9.3. The aerodynamic data does not contain any vectors or coordinates, but the general aerodynamic environment at the location of the spacecraft modelled in the orbit generator. More information about the specific models and their inputs will be presented once the data from those models will be implemented after this subsection. First the coordinate transformations between reference frames will be explained.

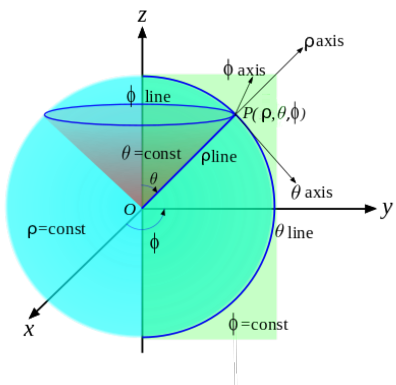

Figure 9.3: Elements of spherical coordinates: surfaces, lines and axes[3].

COORDINATE FRAME TRANSFORMATIONS

It is important to write the data from one coordinate frame to another. In this case from general coordinate frames about the Earth to a spacecraft coordinate frame. From that the forces on the spacecraft can be calculated to design the ADCS. If any assumptions have been made they are stated, other assumptions for the coordinate frames and their transformations can be found in [27].

The Earth-centred inertial reference frame (I-frame) is defined in a way where the x-axis crosses the vernal equinox and the Earth's equatorial plane, the z-axis points north and the y-axis makes the frame right-handed, see Figure 9.4. The Earth-centered, Earth-fixed reference frame (C-frame), Figure 9.5, also takes the rotation of the Earth into account. The Vehicle carried normal Earth reference frame for a spherical Earth (E-frame) is defined such that the z-axis points toward the centre of the Earth, the x-axis points north and the y-axis in eastern direction, see Figure 9.6. Lastly, the Body-fixed geometric reference frame (P-frame) is similar to the body-fixed reference frame (B-frame), except that centre of the P-frame is located at the geometric centre of the SPS ring, while the B-frame is located in the CG location. In the P-frame the z-axis points upwards, the x-axis through the service module and the y-axis makes the frame right-handed, see Figure 9.7.

[3] URL: https://www.spenvis.oma.be/forum/viewtopic.php?f=13&t=3 [cited on 19th of June 2019]

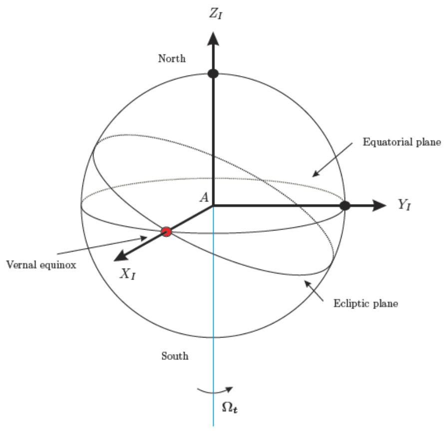

Figure 9.4: Earth-centred inertial reference frame (I-frame) [27]

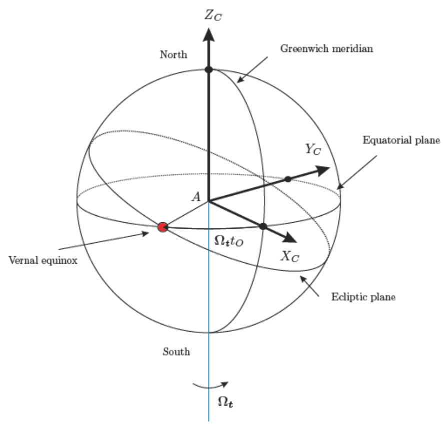

Figure 9.5: Earth-centered, Earth-fixed reference frame (C-frame) [27]

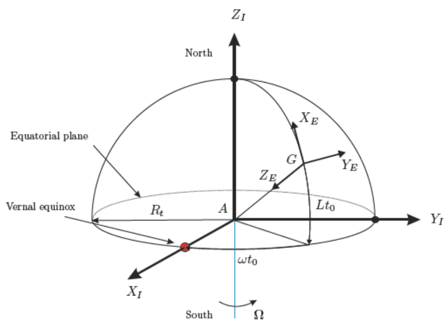

Figure 9.6: Vehicle carried normal Earth reference frame for a spherical Earth (E-frame) [27]

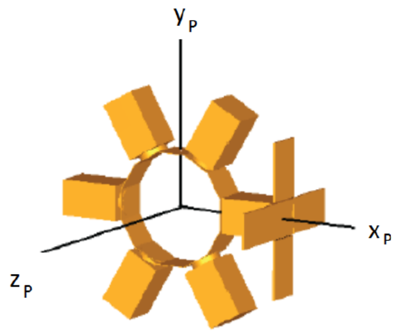

Figure 9.7: Body-fixed geometric reference frame (P-frame) [28]

Now for the transformations between the frames: The C-frame in SPENVIS differs from the I-frame by the Earth's rotation around the z-axis measured from 00:00 UT on November 17, 1858, which is depicted by the Greenwich mean sidereal time and can be calculated using Equation 9.1[4]:

$$\theta = 100.461 + 36000.770 \cdot T_0 + 15.04107 \cdot UT \tag{9.1}$$

where

$$T_0 = \frac{MJD - 51544.5}{36525.0} \tag{9.2}$$

Where θ $[rad]$ is the Greenwich mean sidereal time, T_0 $[a]$ the time in Julian centuries (100a), UT $[hrs.:min.:sec.]$ the Universal Time and MJD $[days]$ the Modified Julian Date. So, that the transformation matrix to go from the I- to the C-frame equals [27]:

$$\boldsymbol{T_{CI}} = \begin{bmatrix} \cos\theta & \sin\theta & 0 \\ -\sin\theta & \cos\theta & 0 \\ 0 & 0 & 1 \end{bmatrix} \tag{9.3}$$

Where $\boldsymbol{T_{CI}}$ $[-]$ is the I- to C-frame transformation matrix.

Now that the data can be transformed to the C-frame, it is important to have all the SPENVIS data in the C-frame consistent. The coordinate data in SPENVIS is output in ellipsoidal coordinates. This can be transformed to Cartesian coordinates with the following equations[4]:

$$\begin{aligned} x_C &= (N+h) \cdot cos\,\phi \cdot cos\,\lambda \\ y_C &= (N+h) \cdot cos\,\phi \cdot sin\,\lambda \\ z_C &= [N \cdot (1-e^2) + h] \cdot sin\,\phi \end{aligned} \tag{9.4}$$

[4] URL: https://www.spenvis.oma.be/help/background/coortran/coortran.html [cited on 19th of June 2019]

where

$$
\begin{aligned}
N &= a \cdot [1 - f \cdot (2 - f) \cdot \sin^2 \phi]^{-1/2} \\
e &= \frac{(a^2 - b^2)^{-1/2}}{a} \\
f &= \frac{a - b}{a}
\end{aligned}
\tag{9.5}
$$

Where x_C, y_C and z_C $[m]$ is the distance in x-, y- and z-direction in the C-frame, respectively, N $[m]$ the radius of curvature in the prime vertical, h $[m]$ the altitude, ϕ $[rad]$ the latitude, λ $[rad]$ the longitude, e $[-]$ the first eccentricity, a $[m]$ the semi-major axis, which equals $6,378,160$ m and f $[-]$ is the flattening of the Earth and equals 298.25, both from the IAU (1964) reference ellipsoid used in SPENVIS[4]. Lastly, b $[m]$, is the semi-minor axis.

Equation 9.4 can be written as transformation matrix as:

$$
\boldsymbol{T_{C,elli}} = \begin{bmatrix} (N+h) \cdot cos\,\phi \cdot cos\,\lambda & 0 & 0 \\ 0 & (N+h) \cdot cos\,\phi \cdot sin\,\lambda & 0 \\ 0 & 0 & [N \cdot (1-e^2) + h] \cdot sin\,\phi \end{bmatrix}
\tag{9.6}
$$

Where $\boldsymbol{T_{C,elli}}$ $[-]$ is the ellipsoidal to C-frame transformation matrix.

All data can now be transformed to the C-frame. In order to get to the P-frame the data first has to be transformed to the E-frame. This can be done using Equation 9.7 [27]:

$$
\boldsymbol{T_{EC}} = \begin{bmatrix} -\sin\phi \cdot \cos\lambda & -\sin\phi \cdot \sin\lambda & \cos\phi \\ -\sin\lambda & \cos\lambda & 0 \\ -\cos\phi \cdot \cos\lambda & -\sin\phi \cdot \sin\lambda & -\sin\phi \end{bmatrix}
\tag{9.7}
$$

Where $\boldsymbol{T_{EC}}$ $[-]$ is the C- to E-frame transformation matrix.

The magnetic field date in SPENVIS is output in spherical coordinates (ρ, θ, ϕ) in the E-frame, see Figure 9.3. To have it point in the right direction in the E-frame the ρ and θ-axis have to be inverted.

Now, the data can be transformed into the P-frame. In step 1 the z-axis of the P-frame points towards the Sun due to the Sun-pointing requirements. By using the difference between the normalised Sun vector ($\mathbf{S_E}$) and the E-frame, the attitude angles with respect to the P-frame can be calculated.

The E-frame will first be rotated around the x_E-axis at an angle α and afterwards around the y_E-axis at an angle β, see Figure 9.8 and Figure 9.9:

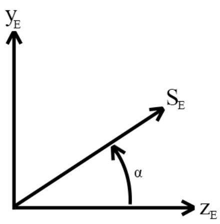

Figure 9.8: Angle between the normalised Sun vector and the E-frame in the (z, y)-plane

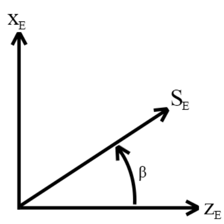

Figure 9.9: Angle between the normalised Sun vector and the E-frame in the (z, x)-plane

For both angles the Sun vector is projected on the plane in which the angle is computed. These rotations can be gathered in the following transformation matrix:

$$
\begin{aligned}
\boldsymbol{T_{PE}} &= \boldsymbol{T_{PE'}} \cdot \boldsymbol{T_{E'E}} \\
&= \begin{bmatrix} \cos\beta & 0 & \sin\beta \\ 0 & 1 & 0 \\ -\sin\beta & 0 & \cos\beta \end{bmatrix} \cdot \begin{bmatrix} 1 & 0 & 0 \\ 0 & \cos\alpha & -\sin\alpha \\ 0 & \sin\alpha & \cos\alpha \end{bmatrix} \\
&= \begin{bmatrix} \cos\beta & \sin\beta \cdot \sin\alpha & \sin\beta \cdot \cos\alpha \\ 0 & \cos\alpha & -\sin\alpha \\ -\sin\beta & \cos\beta \cdot \sin\alpha & \cos\beta \cdot cos\,\alpha \end{bmatrix}
\end{aligned}
\tag{9.8}
$$

Where $\boldsymbol{T_{PE}}$ $[-]$ is the E- to P-frame transformation matrix, $\boldsymbol{T_{PE'}}$ $[-]$ the E'- to P-frame transformation matrix and $\boldsymbol{T_{E'E}}$ $[-]$ the E- to E'-frame transformation matrix.

These rotations will align the z_E-axis with $\mathbf{S_E}$ so that the z_P-axis of the spacecraft is pointed at the Sun. Note that is has not been rotated around the z_E-axis. In step 1 the spacecraft's service module (SVM) is pointing in positive z_C-direction during science mode. From $\mathbf{S_E}$ the required rotation around the z_E-axis to have the spacecraft's SVM point in positive z_C-direction cannot be retrieved. Therefore, a reference vector in the C-frame will be used to compare the orientation of the spacecraft in the P-frame and rotate the spacecraft for one last time to the correct the attitude. To make sure the reference vector still points up in the P-frame after all the transformations, it must be (close to) infinity. Unfortunately, this is not possible while coding the system in Python, so the largest vector possible has been used[5]. The reference vector equals: $\boldsymbol{z_{ref_C}} = [0, 0, 10^{308}]^T$. This vector will be transformed to the P-frame [27]:

[5] URL: https://stackoverflow.com/questions/3477283/what-is-the-maximum-float-in-python [cited on 20th of June]

$$z_{ref_P} = T_{PE}\ T_{EC}\ z_{ref_C} \tag{9.9}$$

Now that the reference vector is defined in the P-frame, the rotation angle γ can be computed. It is the angle between the z_P-axis of the spacecraft and the projection of $\boldsymbol{z_{ref_P}}$ on the (x, y)-plane in the P-frame, see Figure 9.10:

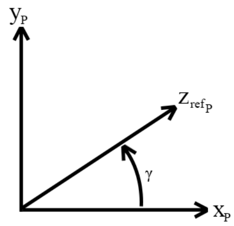

Figure 9.10: Angle between the reference vector and the P-frame in the (x, y)-plane

Again, a transformation matrix can be defined to rotate from the P-frame to the frame in which the x-axis points in positive z_C-direction, defined as the P*-frame:

$$\boldsymbol{T_{P*P}} = \begin{bmatrix} \cos\gamma & \sin\gamma & 0 \\ -\sin\gamma & \cos\gamma & 0 \\ 0 & 0 & 1 \end{bmatrix} \tag{9.10}$$

At last, all data can be expressed in the correct coordinate frame, the P*-frame, which is the actual orientation of the spacecraft during the mission. The transformations can be used for every data point retrieved from SPENVIS to model the spacecraft environment in the P*-frame, as explained in [26] [27] [28]. How the specific models are used and how the disturbance and control torques are calculated is explained next.

9.3.2. ATMOSPHERIC AND AERODYNAMIC DISTURBANCE TORQUE MODELS

The atmospheric and ionospheric models used for the aerodynamic disturbance torque computations will be discussed in this subsection. Following from that, the geometric model from which the disturbance torques can be computed will be outlined.

ATMOSPHERIC AND IONOSPHERIC MODELS

The atmosphere and ionosphere have been modelled using the NRLMSISE-00 model, which is included in SPENVIS. This has been developed by NASA and the U.S. Naval Research Laboratory. It models the aerodynamic density and fluxes at every interval in the orbit. The atmosphere/ionosphere constituent in the model has been set to cover all particles present to model the full atmospheric effects. This and other parameters can be found in Figure A.3. Standard values used have been retrieved from[6]. The total mass density $[g \cdot cm^{-3}]$ is shown in Figure 9.11. As one can see, the density changes over time. This is dependent on the altitude of the satellite and eclipses but the large fluctuation over time is a result from changes in solar intensity.

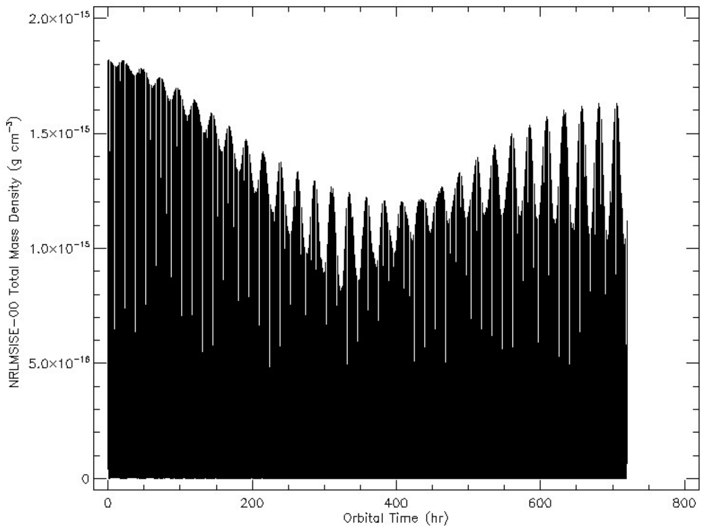

Figure 9.11: Variation of the Total Mass Density (TMD) over the 30 day simulation range[2].

AERODYNAMIC DISTURBANCE TORQUE MODEL

A cylinder is used to represent the SPS-2 FF, which is verified in [28]. An assumed drag coefficient C_D [-] of 2 has been agreed on together with the client: this is relatively a high value, but it provides an additional safety factor for the design due to it being an overestimation. It is sufficient at this time, given that a detailed model would simply require a surplus amount of time. Note that the equations are used for the entire range of data points generated from the Database: this is a total of 43201 points. When possible, for-loops are avoided in the Python script. However, loops are indispensable for some code sections, such as the vector product in Equation 9.16 and Equation 9.15. Note that all vectorial quantities relevant to the analysis can be seen in Figure 9.12.

To begin the analysis, the "Plate" and "Wall" forces F_{plate} [N] and F_{wall} [N] [28] as seen in Figure 9.12 are required. They are computed for every data point through the following equations:

$$\boldsymbol{F}_{plate} = \frac{1}{2}\rho C_D(\pi r_{SPS}^2)V^2\boldsymbol{V}^P \tag{9.11}$$

[6] URL: http://www.lizard-tail.com/isana/lab/orbital_decay/ [cited on 13th of June]

$$\boldsymbol{F}_{wall} = -\frac{1}{2}\rho C_D(2\pi r_{sps}h_{sps})V^2\boldsymbol{V}^P sin(\beta) \tag{9.12}$$

Here, V $[m/s]$ is the scalar velocity, $\boldsymbol{V}^P$ $[m/s]$ is the unit direction vector of the velocity given in the P*-frame. Other necessary values are the total mass density (given as "TMD" in Spenvis), ρ $[kg/m^3]$, $C_D[-]$, which is the drag coefficient and h_{sps} $[m]$ of 0.45 and r_{sps} $[m]$ of 0.4685, which are the height and radius of the SPS-2 FF, respectively. Now that the forces have been computed, additional geometric parameters need to be computed. These are vectorial quantities, which are generated as follows [28]:

$$\boldsymbol{r}_{plate} = (0, 0, 0.5 \cdot h_{sps}) \tag{9.13}$$

$$\boldsymbol{r}_{wall} = (r_{sps}\boldsymbol{V}_x, r_{sps}\boldsymbol{V}_y, 0) \tag{9.14}$$

The vector $\boldsymbol{r}_{plate}[m]$ pertains to the location of the plate centre of pressure with respect to the body-centered P-frame and $\boldsymbol{r}_{wall}[m]$ is an analogous quantity in but for the wall surface centre of pressure.

The aerodynamic moments $\boldsymbol{M}_{plate}$ [Nm] and $\boldsymbol{M}_{wall}$ [Nm] are computed as follows [28]:

$$\boldsymbol{M}_{plate} = (\boldsymbol{r}_{plate} - \boldsymbol{r}_{com}) \times \boldsymbol{F}_{plate} \tag{9.15}$$

$$\boldsymbol{M}_{wall} = (\boldsymbol{r}_{wall} - \boldsymbol{r}_{com}) \times \boldsymbol{F}_{wall} \tag{9.16}$$

A quantity that is required is $\boldsymbol{r}_{com}$ $[m]$, which is the centre of mass with respect to the centred body axis system. This allows for the moments to be computed about the centre of mass. This value has been specified in [8] and is set to 15 mm. Note that in this analysis no payload is deployed from the satellite. If payload is deployed the CG location will deviate more and the effect of it should be analysed in further research. The schematic of the vectors looks as follows:

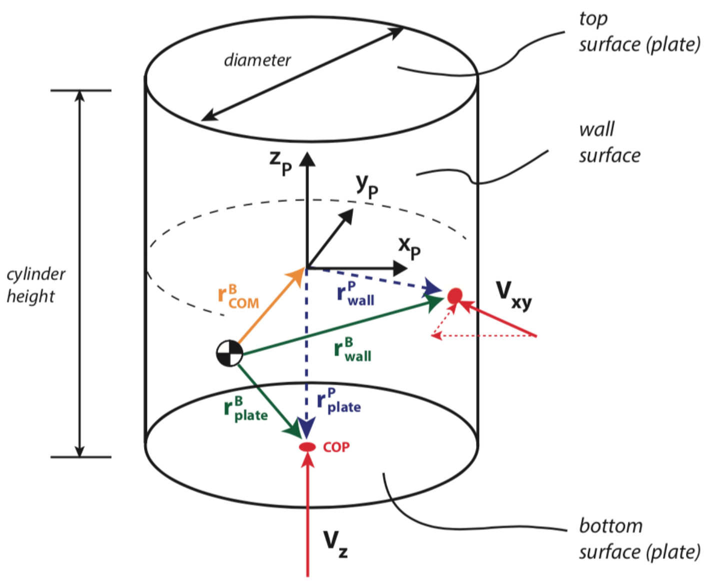

Figure 9.12: Geometry of Aerodynamic Model [28].

Note that the conversion of the position vectors from the P*- to the B-frame is simply done by subtracting $\boldsymbol{r}_{com}$ from $\boldsymbol{r}_{plate}$ and $\boldsymbol{r}_{wall}$, as seen in Equation 9.16 and Equation 9.15.

9.3.3. MAGNETIC FIELD DISTURBANCE TORQUE MODEL

In order to model the magnetic field SPENVIS' internal IRGF 2000 model has been used. The magnetic field changes over time, but this model from the year 2000 is the most recent model that can be implemented in SPENVIS. A representation of the magnetic field as visualisation is shown in Figure 9.13.

This data can be used to model the disturbance torque resulting from the Earth's magnetic field and the passive residual dipole moment in the satellite. The residual dipole moment in a satellite consists of two parts, an active and a passive residual dipole moment [17]. The passive residual dipole moment results from internal currents and batteries in the satellite. The active part can be generated from magnetorquers installed in the satellite and is therefore not a disturbance torque. The passive disturbance torque can be calculated with Equation 9.17:

$$\mathbf{M^{P*}} = \mathbf{B^{P*}} \times \mathbf{m^{P*}} \tag{9.17}$$

Where $\mathbf{M^{P*}}$ $[Nm]$ is the magnetic field disturbance moment vector, $\mathbf{B^{P*}}$ $[T]$ the magnetic field vector in the P frame, $\mathbf{m^{P*}}$ $[Am^2]$. All these vectors are expressed in the P-frame. After consulting the client the passive residual is estimated to be 0.2 Am^2 on each axis, just as in [28]. Again, this disturbance torque can be calculated for every data point retrieved from SPENVIS.

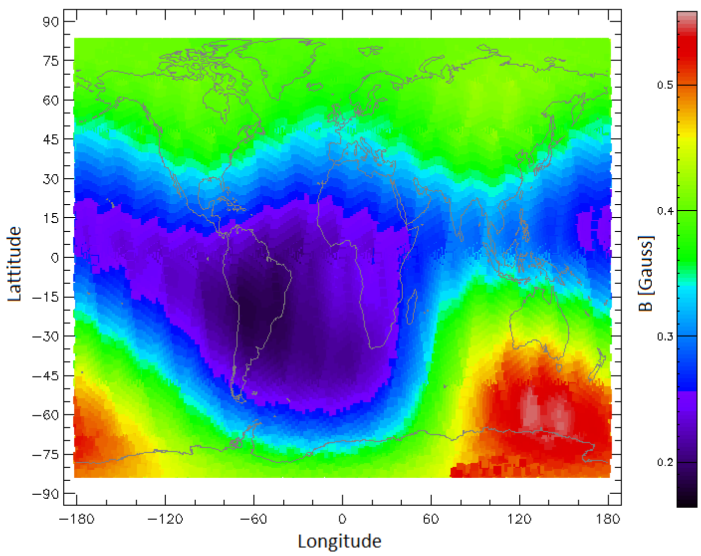

Figure 9.13: Visualisation of the magnetic field strength in the orbital track[2].

9.3.4. GRAVITATIONAL DISTURBANCE TORQUE MODEL

The last disturbance torque considered in step 1 is the gravitational disturbance torque. It can also be modeled for every point of the data set. It can be calculated by [29]:

$$\boldsymbol{M}^{\boldsymbol{P}*} = \frac{3\mu}{|\, r\,|^3}\hat{\boldsymbol{r}}^{\boldsymbol{P}*} \times \boldsymbol{J}\hat{\boldsymbol{r}}^{\boldsymbol{P}*} \tag{9.18}$$

$$\hat{\boldsymbol{r}}^{\boldsymbol{P}*} = -\frac{\boldsymbol{r}^{\boldsymbol{P}*}}{|\,\boldsymbol{r}^{\boldsymbol{P}*}|}$$
$$\boldsymbol{J} = \begin{bmatrix} I_{xx} & 0 & 0 \\ 0 & I_{yy} & 0 \\ 0 & 0 & I_{zz} \end{bmatrix} = \begin{bmatrix} 45.9621 & 0 & 0 \\ 0 & 45.9621 & 0 \\ 0 & 0 & 83.2981 \end{bmatrix} \tag{9.19}$$

Where, $\hat{\boldsymbol{r}}^{\boldsymbol{P}*}$ $[Nm]$ is the gravitation disturbance moment, μ $[m^3/s^2]$ Earth's standard gravitational parameter, r $[m]$ the distance of the satellite to the centre of the Earth, $\hat{\boldsymbol{r}}^{\boldsymbol{P}*}$ $[-]$ the normalised distance vector in the P-frame, $\boldsymbol{J}$ $[kgm^2]$ the Mass Moment of Inertia matrix and $\boldsymbol{r}^{\boldsymbol{P}*}$ $[m]$ the distance vector in the P-frame. The values for the Mass Moment of Inertia (MMOI) are retrieved from [7], where the SPS is assumed to be a hollow cylinder.

9.3.5. TOTAL DISTURBANCE TORQUE MODEL

Now that all significant disturbance torques can be analysed, they can be combined to calculate the full disturbance torque acting on the spacecraft. The average total disturbance torques in the 30 day simulation equal $[-3.72\cdot10^{-6}, -7.45\cdot10^{-6}, -9.16\cdot10^{-7}]^T$ Nm on the x-, y- and z-axis, respectively. The maximum total disturbance torques in the 30 day simulation equal $[1.07668\cdot10^{-4}, 9.11\cdot10^{-5}, 1.05\cdot10^{-5}]^T$ Nm on the x-, y- and z-axis, respectively. Now that the full disturbance torque environment is modelled, the actuators and sensors can be determined to operate the spacecraft in this environment.

9.4. ADCS ARCHITECTURE

There are many possible ADCS architectures available. The mission requirements guide the design of the architecture and how will be explained in this section. Firstly, the possible actuators will be chosen in subsection 9.4.1. Afterwards, the same will be done for the possible sensors in subsection 9.4.2. Next, the products that have been considered in the design are presented in subsection 9.4.3. Lastly, the considered sensors enter a trade-off in subsection 9.4.4.

9.4.1. ACTUATORS IMPLEMENTED

In [7] it was analysed that the maximum allowable mass of the SPS-2 FF of 250 kg is a driving requirement. As Control Moment Gyroscopes (CMGs) are heavy, expensive and their lifetime is limited [17], they have been omitted in the design.

If thrusters would be used, fuel tanks, piping and fuel should be added to the SPS. This is not beneficial in meeting the driving mass requirement [7]. On the other side, it can make detumbling a simple procedure. Furthermore, the propulsion system can be designed in such a way that the time needed for detumbling meets the requirements. More about detumbling can be found in section 9.6. The mass constraint is considered to be too stringent to implement a propulsion system in the design, as weight can be saved by using other actuators.

Control wheels are chosen to control the spacecraft's attitude and magnetorquers for momentum dumping. In step 1 coarse Sun-pointing is required and magnetorquers could take care of this as the spacecraft is in LEO [17]. However, due to the high inclination the spacecraft will fly over the Earth's magnetic poles. Due to the variation of the magnetic field at the poles control from magnetorquers is not possible [28]. This means that control wheels have to be added for continuous attitude control and that the magnetorquers can assist in desaturating the wheels. This setup also lowers the design delta to step 2 and 3, as the accuracy of momentum wheels can be high enough for the pointing requirements of step 2 and 3 [7] [17].

In this analysis the control wheels have been analysed as reaction wheels because of time constraints. In the analysis the wheels do not have an initial rotation, but constantly spin up or down due to the disturbance torques continuously acting on the spacecraft. So, essentially the wheels are spinning all the time just like momentum wheels. Only right after desaturation has occurred they are not spinning. A constant spin rate at which the wheels start their mission or end up in after momentum dumping and the corresponding effects have not been analysed.

9.4.2. SENSORS IMPLEMENTED

As the spacecraft has to direct itself towards the Sun in the first step, Sun sensors are implemented. Sun sensors are simple, relatively cheap, lightweight and easy to use [17]. Furthermore, they can measure the direct attitude with respect to the required attitude. 2 Sun sensors will be placed on the service module in positive z-direction, for redundancy. More sensors would not be necessary as the spacecraft is Sun-pointing in positive z-direction.

Star trackers are expensive and require a lot of data to operate with respect to other sensors [17]. They do have a high accuracy [17], which makes them a good choice for step 2 and 3, where higher accuracies are required [7]. For step 1, however, star sensors are too complicated and over-designed for the mission purpose and therefore not implemented in this step.

Horizon sensors do not measure the location of the Sun but that of the Earth. If the location of the satellite is known and the location of the Sun in some sort of catalog, the attitude can be determined with respect to the Sun with Earth sensors. However, that way the attitude determination would be over-complicated with respect to the possibilities of Sun sensors. Thus, horizon sensors are also omitted from the design.

The magnetometers are required to measure the local magnetic field, so that the magnetorquers can be controlled in the correct way. The magnetorquers need to be activated by a certain magnitude depending on the spacecraft's orientation and the local magnetic field strength and direction to control the spacecraft to a correct attitude. Magnetometers are thus a necessity in the ADCS architecture for the SPS2-FF.

A gyroscope is also a necessity. During detumbling knowledge of how much the spacecraft is rotating after separation from the AVUM+ stage is needed to control countering that rotation. Furthermore, with the selection of the current sensors the attitude of the spacecraft cannot be measured in eclipse, as the Sun sensors are regarded useless in eclipse. Also, the magnetometers cannot use a magnetic field and location database and their measurements above the magnetic poles, due to the variation, to create attitude knowledge. So, a gyro has to be added to measure the rotational deviation during eclipse to counter this. As the non-mechanical or optical gyroscopes are very durable, they are considered in the design.

9.4.3. CONSIDERED SENSOR & ACTUATOR PRODUCTS

A number of actuators and sensors have been gathered in a literature study to analyse which of them are best to implement in the design. The lists of considered sensors and actuators can be found in Appendix B. These options have been retrieved from [30], general vendor sites[7] and websites from specific vendors[8]. An analysis has been made to determine the actuators that best fit the design requirements. This analysis will be explained in section 9.6 for the magnetorquers and section 9.7 for the reaction wheels. After that analysis trade-off can be executed. The sensors can be traded off already and will be explained next.

9.4.4. SENSOR TRADE-OFFS

All attitude sensors considered for the design enter a trade-off. Due to a lack of time the sensors have not entered a performance analysis, but they have been ranked on their specifications and what requirement is most driving for that specific sensor.

Magnetometers

In Figure B.3 an overview of the magnetometers taken into consideration is shown. For important performance specification they have been ranked from best to worst performing magnetometer. This ranking is shown in Table 9.2. Note that price of the component was not included in the trade-off, as at this stage not all unit prices are known. The mass and size are considered the driving requirements and should preferably be as low as possible. The accuracies lie close for all magnetometers and the range of all magnetometers is able to measure the magnetic field and therefore, those specifications are considered less important in the trade-off. From this the the magnetometer NMRM-001-485[9], with ID MM-04 is considered the preferred magnetometer used in the SPS-2.

Table 9.2: Ranking of the magnetometers considered for the SPS-2 FF.

ID	Size	Mass	Accuracy	Range	Power
MM-01	3	2	2	1	1
MM-02	2	3	1	1	4
MM-03	4	4	3	1	2
MM-04	1	1	3	2	3

[7] URL: https://www.cubesatshop.com/ [cited on 21th of June 2019]
[8] URL: https://www.bluecanyontech.com/ [cited on 21th of June 2019]
[9] URL: https://www.cubesatshop.com/product/nss-magnetometer/ [cited on 23rd of June]

Gyroscope

As explained in section 9.4 a gyroscope is needed for detumbling and drift during eclipse. Two gyroscopes were considered during the trade-off and can be found in Figure B.4. Both gyroscopes have roughly the same dimensions and mass. Furthermore, the bias stability is both small enough, so that after eclipse the spacecraft does not have to correct its altitude much., e.g. 1.5° for the QRS116 gyroscope. So, the gyroscopes have been ranked on their respective power consumption. As the QRS116 only needs 0.3 W for three gyroscopes and the ButterflyGyro STIM210 4.5 W, the QRS116[12] has been chosen to be included in the SPS-2.

Sun Sensors

The Sun sensors shown in Figure B.5 have been ranked as well. Again, their respective volume and power were important as some Sun sensors were too large and used too much power for their function. All accuracies were higher then expected from [17] and was a less stringent trade-off criteria. The FOV was an important criteria, but from later analysis it was shown that all Sun sensors met the criteria. The overview is shown in Table 9.3

From this overview the Sun sensors with ID SS-01 and SS-02 came out with the best score. Based on the other specifications such as mass, voltage and temperature range and the amount of information available, the SS-02[10] has been chosen to implement in the SPS-2.

Table 9.3: Ranking of the Sun sensors considered for the SPS-2 FF.

ID	Size	Accuracy	FOV	Power
SS-01	1	2	2	4
SS-02	2	2	3	1
SS-03	3	2	3	2
SS-04	4	1	3	3
SS-05	5	1	3	6
SS-06	6	1	1	5

9.5. MISSION OPERATIONS

Now that the sensors and actuators has been decided on, the way they are functioning during the mission can be determined. The different states of the spacecraft have been visualised in Figure 9.14. As one can see, after separation the spacecraft will enter detumbling mode (DT). In this mode the gyroscope, magnetorquers and magnetometers will be active. Why this is the case is explained in section 9.6. If the spacecraft manages to rate damp and get its rotational velocity below, 0.5°/deg, see section 9.6 the spacecraft will enter the Sun Acquisition mode (SA). If the spacecraft is not able to detumble, it will be catastrophic for the mission.

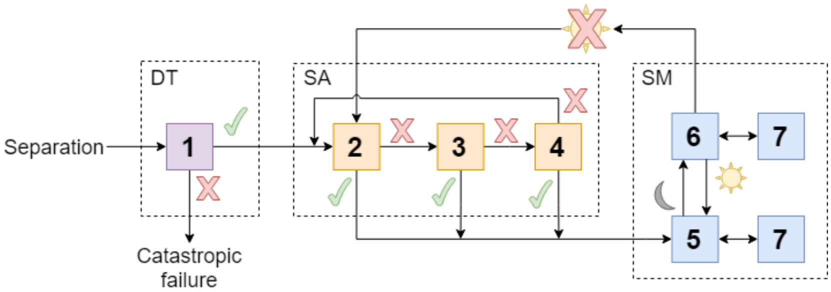

Figure 9.14: Mode switching diagram of step 1. DT = Detubmling mode, SA = Sun Acquisition mode, SM = Science Mode.

In SA mode, the spacecraft will look for a Sun-pointing orientation. In this mode the Sun sensors, reaction wheels and gyroscope are active. The spacecraft will make a 360° rotation around its x-axis (block 2), as that has, together with the y-axis, the lowest MMOI. If the Sun is acquired the spacecraft will enter the Science Mode (SM). If the sun has not been acquired the spacecraft will make another 360° rotation, but now around its y-axis and move on to the Science mode if successful Sun acquisition has occurred (block 3). Both these manoeuvres will mean some time is lost. The rotation about x and y axis will both take a maximum of 116 minutes. This is calculated using the maximum torque of the reaction wheels on the spacecraft. First it will accelerate until 180°, then decelerate to be stationary at the original position. If Sun-pointing is obtained before that, deceleration will happen sooner.

If after this Sun-pointing has not been achieved yet, the spacecraft will turn 45° around the x-axis and then 360° around the y-axis (block 4), requiring 158 minutes. If this is still not successful the spacecraft will go back to block 2. If it is, the spacecraft will enter the Science Mode.

In SM the spacecraft will keep its Sun-pointing orientation. The Sun-sensors, reaction wheels and gyroscope are always active, while the magnetorquers and magnetometers are only active during momentum dumping (block 7). The difference in block 5 and block 6 is the presence of Sun light on the Sun sensors. This can be absent in e.g.

[10] URL: https://www.cubesatshop.com/product/nano-ssoc-a60-analog-sun-sensor/ [cited on 23rd of June]

eclipse or if the spacecraft is in a wrong attitude. In block 5 the spacecraft can rely on its Sun sensors and gyroscope for attitude control, while in block 6 only the gyroscope can be used for attitude determination. If the Sun sensors do not measure Sun light for at least 70 minutes, which is twice the eclipse time, the spacecraft will enter SA again. This safety factor ensures that a wrong Sun sensor measurement does not immediately implement SA mode.

9.6. MAGNETORQUER ANALYSIS

In this section, the detumbling modes will be described and verified. Also the magnetorquer that suits the requirements best will be analysed. Firstly, the detumbling strategy is explained in subsection 9.6.1. Secondly, detumbling using magnetorquers is analysed in subsection 9.6.2. After that the detubmling strategy using magnetorquers and reaction wheels is explained in subsection 9.6.3. Lastly, a sensitivity analysis is performed on the detumbling strategy for magnetorquers in subsection 9.6.4.

9.6.1. DETUMBLING STRATEGY

As analysed in [7], the SPS-2 FF system possesses stringent detumbling requirements. From [8], these are as follows:

Three-axis stabilised mode:

- Geometrical axis depointing ≤ 1.5 deg;
- Angular tip-off rates along longitudinal axis ≤ 1.75 deg/s;
- Angular tip-off rates along transversal axes ≤ 1.5 deg/s.

These specifications are valid for a 2.0 ton class spacecraft. Note that a basic detumbling strategy has already been analysed in [7], but a precise detumbling mode needs to be designed for in the detailed design. In essence, the spacecraft will have residual angular velocity components about several axes. Therefore, there is angular momentum, which must be nullified before sun-pointing can be achieved. This angular momentum is expressed as in Figure 9.15.

$$\mathbf{H} = \begin{bmatrix} I_{xx}\omega_u \\ I_{yy}\omega_v \\ I_{zz}\omega_w \end{bmatrix}$$

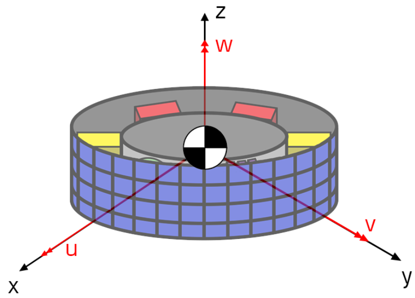

Figure 9.15: Body-Fixed Axis System for Detumbling Computations.

To recapitulate, the axis system that was used in [7] and will be used here is seen in Figure 9.15.

Note that this body-fixed axis system corresponds to that in Figure 9.12.

From [7], the equations below had been derived.

Around the u axis, the torque M_u [Nm] is given as:

$$M_u = I_{xx}\frac{\mathrm{d}}{\mathrm{d}t}\omega_u + \omega_v\omega_w(I_{zz} - I_{yy}) \tag{9.20}$$

For the v axis, the torque M_v [Nm] is:

$$M_v = I_{yy}\frac{\mathrm{d}}{\mathrm{d}t}\omega_v + \omega_u\omega_w(I_{xx} - I_{zz}) \tag{9.21}$$

Finally, for the w (yaw) axis, the torque M_w [Nm] is calculated with:

$$M_w = I_{zz}\frac{\mathrm{d}}{\mathrm{d}t}\omega_w + \omega_u\omega_v(I_{yy} - I_{xx}) \tag{9.22}$$

From the computations performed, the moments of inertia around the y-axis I_{yy} $[kg \cdot m^2]$ and around the x-axis I_{xx} $[kg \cdot m^2]$ are equivalent. Equation (9.22) changes as follows:

$$M_w = I_{zz}\frac{\mathrm{d}}{\mathrm{d}t}\omega_w$$

It has been analysed that a detumbling method, which is beneficial for simplicity and efficiency, is to first detumble around the vertical rotation axis w, which would yield $\omega_w = 0$. The additional efficiency in the detumbling of the other axes is obtained through the loss of gyroscopic stability due to the rotation around the w-axis. This would simplify Equation 9.20 and Equation 9.21 as follows:

$$M_u = I_{xx}\frac{\mathrm{d}}{\mathrm{d}t}\omega_u$$

$$M_v = I_{yy}\frac{\mathrm{d}}{\mathrm{d}t}\omega_v$$

The moments of inertias have been calculated in [7]: $I_{xx}, I_{yy} = 45.868\ [kgm^2]$ and $I_{zz} = 83.298\ [kgm^2]$. In general, the $\frac{d\omega}{dt}$ terms can be replaced with $\frac{\Delta\omega}{\Delta t}$ if the change in rotational velocity can be assumed to be linear: this is deemed reasonable given the time constraints faced. Now that the analytic framework has been set, the components that perform the detumbling will be chosen.

DETUMBLING WITH REACTION WHEELS

For reaction wheels, the instantaneous torque that can be generated is deemed to be independent of the spacecraft's attitude. This is strongly advantageous because the control algorithms do not depend on attitude and therefore both analysis and implementation can be simplified. The disadvantage of the reaction wheels is that they become saturated once a certain rotational speed is reached: in that sense, they exchange momentum with the spacecraft. This required desaturation will cost additional energy: magnetorquers will have to perform the desaturation manoeuvre such that the rotational velocity of the reaction wheels can be reduced.

From the equations seen in the previous section, it is clear that the detumbling time governs the average torque that must be applied. The maximum time that can be spent detumbling is dictated by the client's requirement, namely that the spacecraft must be detumbled within 1.5 orbits of the launch.

However, since the most efficient method requires sequential detumbling of the w- (yaw) axis and then the combined u- and v- (roll and pitch) axes, the time must be divided between these manoeuvres in the most efficient way possible. However, at this stage it is assumed that the total time will be split equally, due to time constraints.

Thus, the calculations for the required angular accelerations are as follows:

$$\frac{\Delta\omega_z}{\Delta t} = \frac{1.75\frac{\pi}{180}}{0.75\cdot 5119} = 7.96\times 10^{-6}\ \frac{rad}{s^2} \tag{9.23}$$

for the angular velocity around the z-axis, and for the combined x- and y-axis angular velocity:

$$\frac{\Delta\omega_{xy}}{\Delta t} = \frac{1.5\frac{\pi}{180}}{0.75\cdot 5119} = 6.82\times 10^{-6}\ \frac{rad}{s^2} \tag{9.24}$$

Now that these values have been computed, the average torques that must be produced are computed:

$$M_z = 83.298\cdot 7.96\times 10^{-6} = 6.627\times 10^{-4}\ Nm$$

$$M_{xy} = 45.868\cdot 6.82\times 10^{-6} = 3.128\times 10^{-4}\ Nm$$

Over the entire orbit, the momentum build-up will be:

$$H_z = M_z\cdot t_z = 6.627\times 10^{-4}\cdot\frac{5119}{2} = 1.7\ Nms \tag{9.25}$$

$$H_{xy} = M_{xy}\cdot t_{xy} = 3.128\times 10^{-4}\cdot\frac{5119}{2} = 0.8\ Nms \tag{9.26}$$

These quantities exceed the potential momentum storage capacity of the momentum wheels outlined in [31], which means that reaction wheels alone are not suitable for detumbling, as multiple desaturation procedures will be required. The wheels would reach their maximum rotational speed before detumbling would have been fully finished. They would then have to be desaturated by magnetorquers and detumble the spacecraft further. This would make it difficult to detumble the spacecraft within 1.5 orbit. Therefore, the use of reaction wheels has been discarded, the next option to be explored as a possibility for detumbling will be the use of magnetorquers.

9.6.2. DETUMBLING USING MAGNETORQUERS

For magnetorquer-only detumbling, it is clear that the non-uniformity of the magnetic field is an issue: this yields an attitude and position dependency for the instantaneous producible torque. Additionally, the positioning of the magnetometers alongside the magnetorquers only allows for measurement of the magnetic field when the torquers are inactive. For the main detumbling procedure, the use of magnetorquers holds the advantage of not requiring desaturation, which means that the system is ready to function without requiring any additional post-desaturation procedures. The equations that govern the torque that can be produced by magnetorquers are given below[32]. Firstly, the magnetic dipole moment $\boldsymbol{m}$ generated by a magnetorquer is given as

$$\boldsymbol{m} = n \cdot I_c \cdot \boldsymbol{A_c} \tag{9.27}$$

where n is the number of wire coils, I is the current fed to the coil and $\boldsymbol{A}$ is the vector coil area. The torque produced $\boldsymbol{\tau}$ is thus given as

$$\boldsymbol{\tau} = \boldsymbol{m} \times \boldsymbol{B} \tag{9.28}$$

where $\boldsymbol{B}$ is the magnetic field vector at the given point. The torque is averaged over one revolution. Assuming that current is regulated through the use of a feedback network, two maxima and minima are achieved per revolution, the force exerted by the magnetorquers to align with the magnetic field is scaled with the angle the magnetorquers has with respect to the magnetic field vector. Where the maximum torque will be exerted at an angle of 90° and the least torque is exerted when the vectors are aligned.

For the detumbling time analysis, it is assumed that the effect the rotation of the earth has on the magnetic field can be neglected. Furthermore, the SPS-2 is assumed a rigid body. The rotation of a rigid body can be described by Euler's rotation equations. Which, in matrix form is defined as Equation 9.29 [33].

$$\boldsymbol{M} = \boldsymbol{J}\dot{\omega} + \boldsymbol{J} \times \boldsymbol{J}\dot{\omega} \tag{9.29}$$

Where $\boldsymbol{M}$ depicts the moments acting on the spacecraft, $\dot{\omega}$ depicts the angular rate and $\boldsymbol{J}$ is the inertia matrix. For a principal-axis frame with a set of basis vectors, Euler's rotational equations of motion of a rigid body become similar to the earlier derived equations Equation 9.21, Equation 9.22 and Equation 9.20. These equations will be rewritten to calculate the angular acceleration, the resulting equations are depicted in Equation 9.30 - Equation 9.32.

$$\dot{\omega_x} = \frac{M_x + (J_{yy} - J_{zz}) \cdot \omega_y \cdot \omega_z}{J_{xx}} \tag{9.30}$$

$$\dot{\omega_y} = \frac{M_y + (J_{zz} - J_{xx}) \cdot \omega_z \cdot \omega_y}{J_{yy}} \tag{9.31}$$

$$\dot{\omega_z} = \frac{M_z + (J_{xx} - J_{yy}) \cdot \omega_x \cdot \omega_y}{J_{zz}} \tag{9.32}$$

In the case of the SPS-2, the moments acting on the spacecraft consist of the external disturbance torque and the internal torque due to the magnetometers. The external disturbance torques have been calculated in subsection 9.3.5 and the internal torque can be calculated using Equation 9.28. Using Equation 9.30 - Equation 9.32 the angular acceleration of the spacecraft can be calculated at every point in orbit. Starting with an initial rotational velocity, integrating this acceleration over time will result in a decreasing angular velocity. To make sure the magnetorquers are always outputting a magnetic field in the right direction, a control loop was added which checks in which direction the magnetorquer should produce the magnetic field. This is also done in actual operation to make sure the magnetorquers bring their own magnetic field in line with the magnetic field of the earth.

As the magnetorquers influence the measurements performed by magnetometers, the magnetorquers will periodically have to be turned off to be able to receive accurate measurements of the magnetic field. Turning the magnetorquers off for a prolonged period of time will increase the detumble time while having too little measurement time will result in an inaccurate depiction of the magnetic field, which will decrease the effectiveness of the magnetorquers as they will not always work to their full potential without knowledge of the magnetic field. It is therefore very important to have the best possible ratio, which, according to Airbus a measurement time of 1 *sec* will be sufficient [28]. This second where the magnetorquers are off during detumbling has been taken into account for the calculation of the detumble time. It is assumed that during this one second the spacecraft is left free to the influences of external torques. The desired result of detumbling is a spacecraft that has a rotational velocity of $< 0.5°/sec$, as defined for the IOD payloads used in step 1 in [7].

Detumbling after deployment

As all terms of Equation 9.29 are known except for the magnetic dipole, a simulation was performed for a number of dipole moments. The time it would take for detumbling, if possible at all was plotted and investigated. The results are depicted in Figure 9.16. As the required detumble time has been set to 1.5 orbit, which corresponds to 150 minutes. The results were a detumbling time of 99, 62 and 31 minutes for a dipole moments of 10, 15 and 30 Am^2 respectively.

It can be seen that from the available magnetorquers, only the ones with a dipole moment greater than 10 Am^2 are suitable. Looking at the possible options in this range of dipole moment and keeping in mind that to keep the desired delta between 'step 0' and step 1 a service module the size of one QuadPack is desired. This renders all magnetorquers with a length, width or height greater than 25 cm undesired, but not impossible as they can also be placed at an angle or on the outside of the service module in order to satisfy the spatial constraints . The only viable magnetorquers are the TQ-15 models, which require significantly more power than competitors but are able to fit in the defined space. The TQ-15 redundant wind was chosen as the geometrical constraints were deemed the driving constraint in the selection of a magnetorquer. The redundant version was chosen to improve reliability and sustainability of the spacecraft whilst also decreasing the risk.

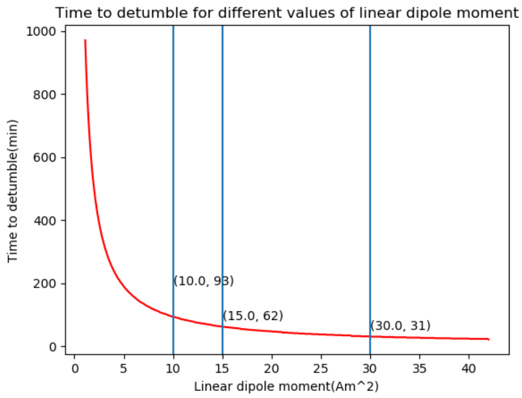

Figure 9.16: Detumble time plotted for several values of linear dipole moment, important points highlighted.

9.6.3. MIXED ACTUATOR DETUMBLING

Detumbling could also be performed through the simultaneous and coordinated use of both magnetorquers and reaction wheels. This, however, would require more extensive analysis than can be performed at this time. For this reason, the analysis will be left as a recommendation to the reader.

9.6.4. SENSITIVITY ANALYSIS

As the choice of magnetorquers has a great effect on the performance of the spacecraft, sensitivity analysis was performed on the method used to choose a magnetorquer. In addition to the linear dipole moment of the magnetorquer used, the magnetic field strength and the MMOI (and therefore configuration) of the spacecraft were identified as the biggest effectors of the detumble time.

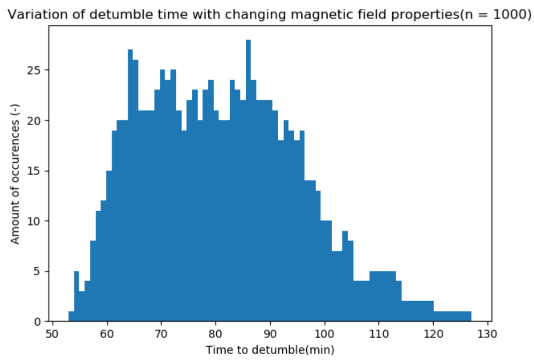

Figure 9.17: Sensitivity analysis of the detumble times with changing magnetic field properties (n = 1000).

As the torque provided by the magnetorquers depends highly on the magnetic field, the spacecraft will not have the same detumble times for different locations in orbit. In Figure 9.17 the sensitivity analysis with respect the strength of the magnetic field is shown. 1000 Simulations were performed where every simulation depicted a different cut-off from the AVUM+ stage, using the chosen magnetorquer ($\boldsymbol{m}$ = 15 Am^2) again the assumption was made that the tip off rate about the combined xy-axis was evenly distributed along these axes. The analysis resulted in a mean of 81 min, and a standard deviation of 14.8. It can be seen that the influence of the magnetic field is quite evident but will not influence the decision of magnetorquer as the detumbling requirement can still be met with the chosen magnetometer.

The effect of a changing configuration of the spacecraft was performed by changing the mass moments of inertia of the spacecraft. A variation in moment of inertia around the x-, y- and z-axis is separately plotted in Figure 9.18. The analysis was performed on the chosen magnetorquer ($\boldsymbol{m}$ = 15 Am^2) and at a time of release from the AVUM+ stage which leads to a detumble time of 62 minutes It can be seen that a variation in moment of inertia about the z-axis will have the greatest influence on the detumble time, whereas the variation about the x- and y-axis will only have a minimum effect of a few minutes difference. Changing the moment of inertia about the z-axis might increase or decrease the detumbling time by up to 20 minutes, but this does not influence the detumble times in such a manner that

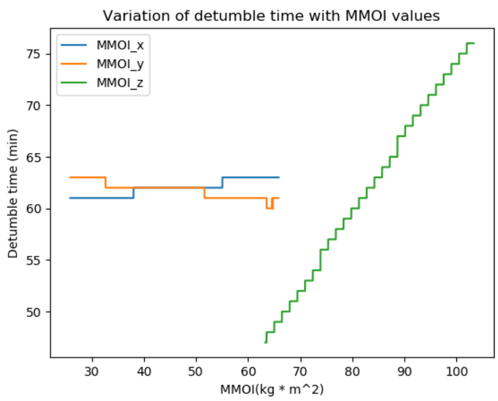

Figure 9.18: Sensitivity analysis of detumble times with changing MMOI of the spacecraft, ΔMMOI = 40 kgm^2.

the requirement is not met anymore.

9.7. REACTION WHEEL ANALYSIS

The main pointing accuracy of the spacecraft will be due to stabilisation obtained using reaction wheels. In this section first the reaction wheel architecture is discussed in subsection 9.7.1, as the orientation of the reaction wheels with respect to the spacecraft and themselves highly influences the effectivity of the reaction wheels. Afterwards, data is gathered to perform a trade-off on possible reaction wheels, as listed in Appendix B in subsection 9.7.2. When the proper reaction wheel has been chosen, the implications of this choice will be evaluated by analysing the time it takes to desaturate in subsection 9.7.3.

9.7.1. REACTION WHEEL ARCHITECTURE

As mentioned in section 9.4, reaction wheels will be used in the science mode during nominal use, as the magnetorquers cannot function properly above Earth's magnetic poles. At least three reaction wheels are needed to have full 3-axis control over the spacecraft [17]. However, if one of the wheels would fail, the spacecraft would lose its capability to control itself on all axes with possible catastrophic results for the mission. Consequently, 4 reaction wheels will be implemented in the spacecraft to account for redundancy.

The wheels will be placed in a pyramid shape, so that if one wheel fails the other three wheels can still control the spacecraft in all 3 axes, see Figure 9.19. The angle κ the wheels make with (x_{P^*}, y_{P^*})-plane changes how much of their capability is used in the x_{P^*}-, y_{P^*}- or z_{P^*}-axis. Note that even κ can differ for the reaction wheels on the x_{P^*}-axis with respect to the ones on the y_{P^*}-axis. Due to study-allocated time constraints, this analysis has not been executed. The wheels will be placed under an angle κ of 32° according research[11]. Note that the reaction wheels will be placed in the SVM and that the axes indicated in Figure 9.19 do not show the actual location of the reaction wheels with respect to the P-frame, but are used to help indicate inclination of the reaction wheels and about which axis they act.

9.7.2. REACTION WHEEL TRADE-OFF

Now that the way the reaction wheels are placed have been specified, the different wheels in Figure B.2 can be analysed. This analysis assumes the wheels have instantaneous torque, acceleration and deceleration. Firstly, the wheels will be analysed on two import characteristics: the maximum torque and the maximum momentum capacity. The maximum torque is important as the wheels need to be able to counter the maximum disturbance torque occurring during the mission about every axis. If the wheels are not able to counter the disturbance torques, the spacecraft will spin out of control. Also, if the maximum momentum capacity of the type of wheel is lower, desaturation will have to occur more times. This will increase the wear of the wheels and thus the reliability of the ADCS on longer missions.

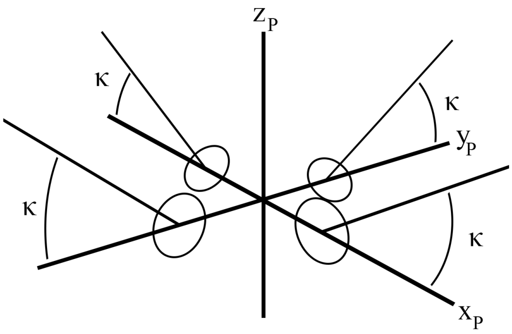

Figure 9.19: Reaction wheel architecture in the SPS-2 FF [11].

This maximum momentum capacity and torque of all the reaction wheels have been gathered in Figure B.2. To determine what the maximum required torque should be of a reaction wheel Equation 9.33 is used, which can be retrieved from Figure 9.19:

$$\begin{aligned} \tau_{max_x} &= 0.5 \cdot M_{max_x} \cdot \cos\kappa \\ \tau_{max_y} &= 0.5 \cdot M_{max_y} \cdot \cos\kappa \\ \tau_{max_z} &= 0.25 \cdot M_{max_z} \cdot \sin\kappa \end{aligned} \tag{9.33}$$

Where τ_{max_x}, τ_{max_y}, τ_{max_z} $[Nm]$ is the maximum required torque of the reaction wheel retrieved from the x-, y- and z-axis, respectively. M_{max_x}, M_{max_y}, M_{max_z} $[Nm]$ is the maximum disturbance torque on the x-, y- and z-axis, respectively. Note that the 0.5 comes from the fact that two reaction wheels exert torque on the x- and y-axis and the 0.25 from all four reaction wheels working in the z-axis as well.

The maximum torque occurring on each axis equals $[0.145, 0.147, 0.0178]^T$ $[Nm]$ on the x-, y- and z- axis, respectively. The maximum torque required from the disturbance torque equals 0.0625 Nm. This occurs on the y-axis and is higher than the x-axis, which equals 0.0613 Nm and the z-axis, which equals 0.002 Nm.

Of the list in Figure B.2, only the RW1 and the RWA-1000 reaction wheels are capable of handling this torque. The other reaction wheels are thereby omitted. Both reaction wheels have the same momentum capacity, but as the RW1 is lighter, smaller, as cheap and requires less power, the RW1 has been chosen to use in the SPS-2.

[11] URL: https://www.researchgate.net/profile/Abolfazl_Shirazi2/publication/276216468_Pyramidal_reaction_wheel_arrangement_optimization_of_satellite_attitude_control_subsystem_for_minimizing_power_consumption/links/566e4c6d08ae1a797e4061cc.pdf?origin=publication_list [cited on 23rd of June]

Now that the best reaction wheel from the list has been found, it is still important to look at its momentum capabilities to see if it is able to perform the mission. For this the external disturbance torque on each time instant in the mission has been integrated over the time step, which is 60 seconds. Then the momentum build up has been calculated to counter those torques and has been distributed over the correct wheels accounting for that. Using the maximum momentum capability of the RW1 of 1.1 Nms it can be calculated that in 30 days the reaction wheels have to be desaturated 14.83 times, so one time every 29.06 orbits, if the wheel is used to its full capacity. This has been calculated by dividing the maximum maximum momentum capacity of the wheels and the torque build up during each respective orbit of the 30-day simulation.

9.7.3. MOMENTUM DUMPING

After 29 orbits of operation the reaction wheels will be saturated. The magnetorquers will be used to desaturate the reaction wheels. For this calculation the magnetorquers are assumed to have instantaneous acceleration and deceleration. Furthermore, as for the detumbling analysis, the ratio of measuring using magnetometers and attitude control using magnetorquers has been taken into account. For the analysis a saturation level of momentum in the reaction wheels of 1 Nms on every axis was used. The used magnetorquers are 3 orthogonal placed TQ15 with a dipole moment of 15 Am^2. The result of the analysis is a desaturation time of 105 minutes, which is close to 1 orbit.

9.8. ATTITUDE CONTROL AFTER ECLIPSE

As sun pointing knowledge is gained by sun sensors, pointing knowledge will not be available during eclipse. Multiple strategies to keep a reasonable amount of sun-pointing time during non-eclipse have been considered:

- Use magnetorquers
- Use the gyroscope
- Use reaction wheels in combination with magnetorquers

These strategies all have their advantages and disadvantages, they will be considered in more detail here after to find a fitting strategy.

Normal Operation Form

One strategy is to use a magnetic field model on the OBC to predict the magnetic field. Together with measurements from the magnetometers the relative attitude of the spacecraft can be determined. As a result of these measurements the magnetorquers can be used to gain a new spacecraft attitude. Communication with the client lead to the conclusion that the technology readiness level(TRL) of this type of attitude control is too low and would take a considerable amount of time to analyze: this strategy was consequently discarded as a possibility.

Using the Gyroscope

When using the gyroscope during eclipse, the maximum angle the spacecraft will have with respect to its sun-pointing position will be about 1.5°, as the bias stability of the gyroscope implemented equals 3°/hrFigure B.4 and the eclipse takes 35 minutes. This angle could be reversed by using the reaction wheels. Analysis will be done if this is possible within reasonable time.A reasonable time was considered to be 12 minutes, as the time out of eclipse will be 65 minutes and it is desired to spend at least 80% of this time in sun pointing position.

Control Using Reaction Wheels

Attitude control after eclipse can be done by using the data of the gyroscope to counter rotation. If the spacecraft rotates a certain amount, it is logged by the gyro and the actuators can counter the rotation and rotate the spacecraft back to the position needed based on the last measurement from the Sun sensors before eclipse. Of course, the bias drift of the gyroscope should be taken into account, see section 9.4. If the bias drift of the gyroscope is too much during eclipse, the attitude spacecraft will still fall outside of the FOV of the Sun sensors with respect to the Sun. This should be avoided and therefore the bias drift of the gyroscope should be sufficiently small.

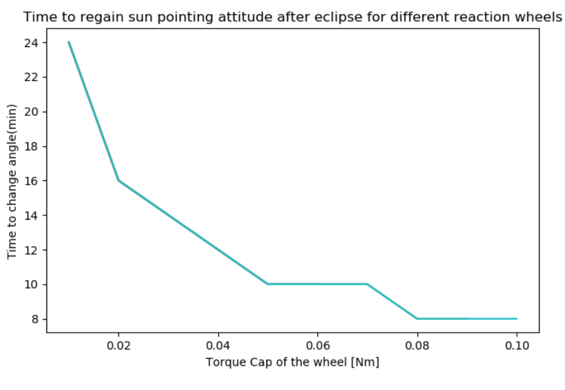

Figure 9.20: Time to regain sun pointing attitude after eclipse for different reaction wheels.

As the maximum offset after eclipse while using the gyroscope during eclipse is known to be 1.5°, as the bias stability of the QRS116

equals 3° per hour[12]. The time it takes for the reaction wheels to cover
this angle back to sun pointing was calculated. Using 4 reaction wheels in the configuration shown in Figure 9.19, the time it would take to get back to the initial orientation was calculated for different values for τ_{max} of the reaction wheels. The result is depicted in Figure 9.20.

The most important thing to note is that at a τ_{max} of 0.1 Nm, the time to cover the angle is 8 minutes. Which is deemed sufficient for the earlier set requirement. For reaction wheels with a lesser τ_{max}, this requirement will not be met, this will be taken into account for the trade-off.

Turn Off Magnetorquers

To save power, one could also turn down the magnetorquers during eclipse, leaving the SPS-2 free to the disturbance torques imposed by the environment. After eclipse the spacecraft will have to detumble. The amount of angular velocity obtained by the spacecraft in eclipse was calculated, and using the magnetorquer detumbling method described in subsection 9.6.1 the feasibility was checked. To check the feasibility, first the increase angular velocity as an effect of the disturbance torques was computed. The same equations were used as for the detumbling analysis, only in this case the torque due to magnetorquers was left out. It was found that the spacecraft, in these 35 minutes of being in eclipse, would rotate 11.8°, 7.7°and 6.3°about the x, y and z axis respectively. As the linear dipole was set to be 15 Am^2, the detumbling time could easily be calculated to be 0 minutes as the obtained rotational velocity did not exceed the requirement. As this angle will have to be rotated by the reaction wheels, the use of a gyroscope was deemed the better option due to the lower angle coming out of eclipse.

9.9. RISK & SUSTAINABILITY

This section will be focused on the rationale used for the risk and sustainability assessments. These are important to estimate at this stage, as they are a significant indicator of whether the design will meet specifications.

Firstly, the risks will be identified, analysed and mitigated in subsection 9.9.1. Then, a sustainability analysis is performed in subsection 9.9.2.

9.9.1. RISK ANALYSIS

The risk analysis for the ADCS subsystem will employ a similar approach to that seen in [7] and [11]. First, key risks will be identified for each sensor and actuator. Then, the mitigation strategy will be discussed.

RISK ASSESSMENT

- **S-1:** *Sun sensor failure*. The probability of this is *rare*, as the sun-sensors are tested and qualified for space use. The impact is considered *fatal* as the mission would be jeopardised.
- **R-1:** *Reaction Wheel Failure*. Here, the probability is *unlikely*: reaction wheels have, as only part, moving mechanical parts, and certain operational modes could cause premature failure and must be carefully considered when the controller is designed. The consequence of this is *fatal*, since you are no longer able to control the SPS-2 FF.
- **MM-1:** *Magnetometer Failure*. The probability of this is *rare*, as magnetometers are known for high reliability and the selected components filling this role are certified and tested. Furthermore, they are well-known aerospace instruments and have no inherent design complexity. The impact is *critical*, as a partial workaround could be found if one axis ceases to have measurements.
- **MT-1:** *Single Coil Magnetorquer Failure*. The failure associated with a single magnetorquer is *rare* as magnetorquers are in the upper tier of reliable components, but the impact would be *critical* as the mission performance would be reduced, but desaturation would be possible. It would just be less efficient.
- **G-1:** *Gyroscope Failure*. The probability of the gyroscope failing is *moderate* as it is a complex part with a lot of moving parts. Furthermore, historically speaking, they are known to fail. The impact of failure is *significant*, since more tumbling will occur during eclipse and the detumbling after release will go less quick.

SUGGESTED RISK MITIGATION PROCEDURES

For risk mitigation, effort had been made during the component selection and sizing to provide redundancy. For instance, the **R-1** reaction wheel failure has been lowered to *critical* impact due to a planned redundant fourth wheel inclusion.

[12] URL: https://www.systron.com/gyroscopes/qrs116-single-axis-tactical-grade-analog-gyroscope-non-itar [cited on 23rd of June]

The sun-sensor failure impact **S-1** can be significantly reduced to *critical*, by applying redundancy along with choosing components that are off-the-shelf with testing done by the manufacturer. Furthermore, the consequence of failure can be reduced further if, for instance, an emergency coarse sun-pointing mode is implemented using the solar panel instantaneous power distribution in tandem with the magnetometers as a reference for approximate attitude.

The mitigation applied to the magnetometers is redundancy. The magnetometers will still have to have an entire associated control and data handling adaptation system designed for them: additional care taken during the process can reduce the impact of failure of **MM-1** to *minor*. The magnetorquers can have their associated failure risks (**MT-1**) reduced through redundancy within the part (two coils instead of one) and additional post-integration tests, thus lowering their impact of occurrence to *significant*.

The gyroscopes have been chosen such that the risk allocated to them is reduced. This is due to the fact that it has no moving parts and it is a simple design[12]. This reduces the probability to *unlikely*.

9.9.2. SUSTAINABILITY ANALYSIS

The sustainability impact of the ADCS subsystem shall now be analyzed. This is done on the basis of Baseline Report [11] grading framework. Firstly, the *SUS-FW-1.1* Stakeholder sustainability requirements are met, therefore a 10 is given. For *SUS-FW-1.2* (Transport), the half of the ADCS subsystem components are from European partners, and therefore a score of 7 is awarded. The *SUS-FW-1.3* Health and Safety Criterion is a 10: COTS components do not pose a risk to the assembly team. *SUS-FW-1.4* cannot be accurately estimated, as the production/assembly methods are not defined yet, and some are simply not known as the components are COTS.

SUS-FW-1.5, *SUS-FW-1.6* and *SUS-FW-1.7* cannot be used at this stage due to a lack of knowledge about them. Regarding *SUS-FW-1.8*, jobs are not directly created but additional work is, which as a consequence may require additional jobs. The score given is a 7. *SUS-FW-1.9* is not dependent on the ADCS component selection: the exact differences between options in terms of overall material usage cannot be quantified. However, mostly solid-state components are used and hence an 8 is given.

For *SUS-FW-1.10*, most of the material in the assembly can be recycled but a 7 is given due to lack of knowledge about the assembly process. *SUS-FW-1.11* scores a 10: the tooling is minimal as all components are COTS. The *SUS-FW-1.12* criterion scores a 10: the assembly line can be strongly simplified due to, again, the use of exclusively COTS components. Regarding *SUS-FW-1.13*, the product must comply with all laws and regulations regardless of any other considerations: this is a priority and thus this scores a 10.

For *SUS-FW-1.14*, the impact on academic institutions and small businesses is positive: TU Delft can benefit strongly from the cooperation with Airbus Defence and Space, and small businesses may be required in the later development and production stages. A 10 is thus given. As for the Market Presence (*SUS-FW-1.15*), the local wage level may increase due to the potential success of the project and the additional commitments that some staff members will have to make to the project. An 8 is given here, as knowledge about the further development stages is limited. Also, the use of COTS components limits the on-site work needed for production and testing. *SUS-FW-1.17* (Market Share) shares a 9 with the previous section: a quick push into the market may prove successful and can potentially reinforce Airbus Defence and Space's position in it.

As for *SUS-FW-2.1*, the maintenance (pre-launch) is limited slightly by the use of ADCS components that are COTS: proprietary components are more maintainable and thus a 5 is given. The efficiency (*SUS-FW-2.2*) of the satellite is guaranteed as the optimal components have been chosen for the ADCS subsystem. This means that the overall efficiency is expected to be high, decreased only by the fact that non-COTS components could be optimized further: this is, however, a necessary trade-off as cost is a limiting factor. A 7 is given. *SUS-FW-2.3* gets an 8: the ADCS subsystem can change spacecraft orientation for quicker de-orbiting, if needed. This can be done by changing the exposed frontal area perpendicular to the orbital velocity. The overall grade is computed to be 8.53, which is high and deemed sufficient at this stage.

9.10. SOFTWARE BLOCK DIAGRAM

To get the models and to perform the simulations needed to size the ADCS components, software was made in python. As in input the data obtained from SPENVIS was used. This data was computed using the settings as depicted in Appendix A. The data was first reformatted using python to have it in a use-able format. After this the data will be transformed from the coordinate given by SPENVIS to the P*-frame, as discussed in subsection 9.3.1. When in the P*-frame, the data could be used to calculate all disturbance torques on the spacecraft, of which every disturbance torque has its own file. These disturbances, being aerodynamic, solar, gravity and magnetic disturbances were taken into account for the calculation of detumble time of the spacecraft as well as desaturation and saturation time of the reaction wheels.

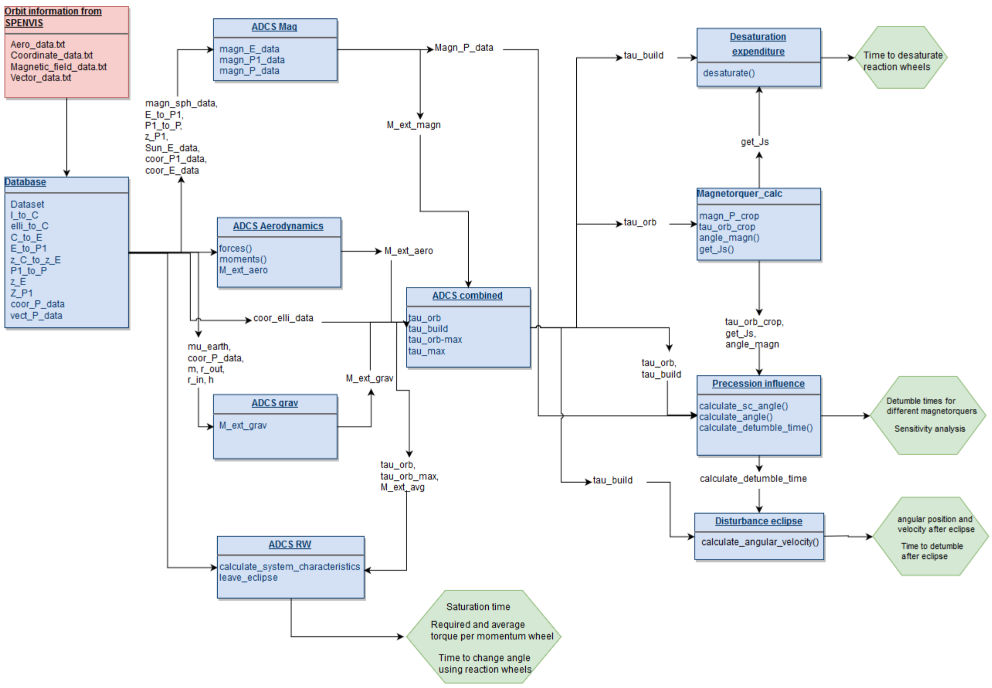

Figure 9.21: Software block diagram of the simulations used in the ADCS section.

9.11. RECOMMENDATIONS

The analysis of the ADCS subsystem has been performed to the most detailed extent possible, nevertheless, due to time or knowledge constraints a number of assumptions had to be made. Also some additional analysis which could improve models and predictions have been left open for further analysis. The most desired improvements to the analysis will be listed hereafter.

For the reaction wheels, the assumption of a pyramid layout was made. The efficiency of this layout has not been addressed and could therefore possibly not be most optimal. If further analysis leads to findings for a more efficient layout, this layout might be applied and time for saturation and desaturation might well decrease. Also, the time before momentum dumping has to be performed could increase. Also on the topic of the reaction wheels, the added stability offered by the rotation of the reaction wheels has not been addressed. Due to this rotation about an axis, the spacecraft will be less prone to disturbances about the other axis. This further analysis could lead to higher desaturation times as the reaction wheels will counteract the rotation induced by the magnetorquers. Positive effects could also be an increase in time before momentum dumping has to be performed due to resistance to the disturbance torques.

The best time in an orbit to desaturate the wheels should be investigated. This also includes the amount of RPM the wheels are at. If this can be reduced the wear of the reaction wheels will decrease and thus the reliability over a longer period will increase. It should be investigated when to desaturate the wheels from an operational perspective, but also a power perspective to find the most optimum time. The time the spacecraft is located above the magnetic poles should be investigated. At this time the magnetometers and magnetorquers cannot be used. This influences the detumbling and desaturation capabilities of the spacecraft. Also, more thought should be put into the detumbling procedure, mostly the on/off ratio of the magnetorquers to gain time for measurements. Literature could not be found about this topic and the value assumed now is just an estimate. Reducing the time for measurement will decrease the detumbling time. The Solar radiation pressure has not been implemented as it induces no disturbance torque during Science mode. However, it does affect the orbit propagation and disturbance torques during detumbling. Even though its effect is small [28], it should still be implemented for a higher accuracy.

Theoretically, the use of magnetorquers in combination with magnetometers and magnetic field date during eclipse might mean the spacecraft is sun-pointing after leaving eclipse. This is beneficial to the time available for measurements. A proper analysis could be done to get a better understanding of the feasibility and accuracy of this option. The effect of deploying payloads should be analysed in further research, as well. The MMOI and CG location will change. This will have an effect on the stability of the spacecraft and its disturbance torques. Also, a more recent model of the magnetic field can be used. The current model dates from the year 2000. A more recent model of the magnetic field will increase the effectiveness of the simulation.

10
Power Generation, Distribution & Storage Step 1

The Detailed Design of the Power Generation, Distribution and Storage (PGD&S) subsystem will be outlined in this section. Firstly, the work flow diagram for the detailed design of this subsystem will be presented. Then, the results of the midterm report will be summarised. Subsequently, the increase in depth of the detailed design will be made, for both Steps 1 and 2. The specifics of the system will be analysed, compiled and presented. Then, the power requirements from other subsystems will be used to compute the new required power values such that the required components such as the solar panels and batteries can be selected.

10.1. Work-flow & Design Outline

The following work flow diagram was generated for this subsystem design process:

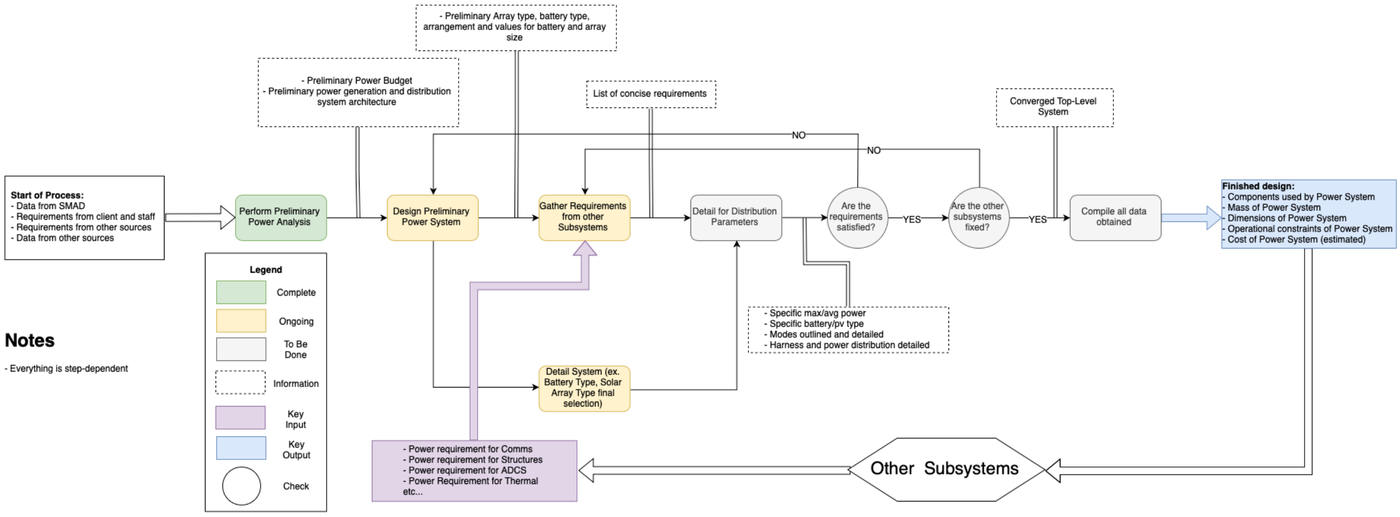

Figure 10.1: Work-flow diagram for power subsystem design.

10.2. Summary of Midterm Report Assumptions

Before the values obtained in the Midterm Report [7] can be re-iterated, the assumptions used to obtain them must be stated. These are as follows:

- The average Sun-pointing mode incidence angle θ was assumed to be a worst-case 10°
- The night/eclipse power is equal to 40% of the maximum day power
- The thermal coefficient for the solar panel efficiency is -0.00168 1/deg [34, 35]

The initial sizing had been performed based on the assumption that the spacecraft operates continuously on full power. In this phase of the design, this is no longer true and is altered in the detailing.

10.3. Step 1 Detailing

This section will be concerned with the Detailed Design detailing of the power subsystem for Step 1. Firstly, the power distribution itself will be modified to fit a more realistic set of operational modes. Then, the Step 1 payload power requirement will be modified, and a new power distribution and expected required solar panel area will be computed.

10.3.1. PRELIMINARY DEFINITION OF MODES AND THEIR POWER REQUIREMENTS

As mentioned in the previous sections, it can no longer be assumed that the system operates continuously at full power. This requires an expected power requirement breakdown per generic operational mode. The values here are assumed as at this stage, the instruments used are not known. If an iteration is possible withing the given time, it will be outlined later. An overview of estimated operational power requirements is given by Table 10.1. From Table 10.1, it can be obtained that the maximum average day power usage is 75% of the maximum power.

Table 10.1: Expected Generic Modes and Expected Power Usage.

Modes/Subsystems	PG&D (9%)	Structures (1%)	Thermal (5%)	Payload (46%)	ADCS (10%)	Propulsion (5%)	TT&C (12%)	OBP (12%)	Fraction of Total [%]
Detumbling	100% power	100% power	10% power	10% power	100% power	100% power	10% power	10% power	32.5%
Emergency	100% power	10% power	100% power	10% power	100% power	100% power	70% power	60% power	49.3%
Science	100% power	100% power	75% power	100% power	30% power	10% power	50% power	50% power	75%
Maintenance	100% power	100% power	75% power	50% power	20% power	10% power	100% power	70% power	59.65%

RE-ITERATION OF STEP 1 POWER WITH NEW INCREASED POWER

An important consideration was made: if the fist step allows for the placement of photo-voltaic panels on the top of every QuadPack, there is a surplus of power generated due to an area that is larger than required. This means that additional payload can be powered without significant complexity penalty. An enhanced Step 1 can yield a lower delta between steps as the power system will not require a heavy redesign, thus enhancing the business case feasibility despite a higher initial investment. The maximum allowable power for this step given that the solar panels were not allowed to be moved was computed to be 50W, and the values of the power requirements are recalculated. This leads to a re-iteration of the computations summarised in the previous section, which yields Table 10.2.

Table 10.2: Expected SPS-2 FF Maximum Power Distribution for Step 1.

Subsystem	**Power Fraction [% of Total Power]**	**Power Required [W]**
Payload	46 %	50
Structure and Mechanisms	1 %	1.1
Thermal Control	5 %	5.4
Power (incl. harness)	9 %	9.8
TT&C	12 %	13
On-Board Processing	12 %	13
ADCS	15 %	16.4
Propulsion	0 %	0
Total	100 %	109

Note that the Propulsion power requirement was set to be 0 W due to the fact that active propulsion is not utilised by the SPS-2 FF.

The required solar area for Step 1 was computed to be **0.55** m^2, using the following equations (Equation 10.1, Equation 10.2):

$$P_{sa} = \frac{\frac{P_e T_e}{X_e} + \frac{P_d T_d}{X_d}}{T_d} \tag{10.1}$$

and

$$A_{sa} = \frac{P_{sa}}{P_{eol}} \tag{10.2}$$

where P_{sa} [W] is the required solar array power, P_e, P_d [W] are the eclipse and day power required, T_e, T_d [s] are the eclipse and day periods, $X_e and X_d$ [-] are the day and night cumulative path efficiencies, $A_{sa}[m^2]$ is the solar array area required and $P_{eol}[W/M^2]$ is the specific end-of-life power. Note that thermal efficiency and lifetime degradation are taken into account for the computation of the end-of-life power. The value for X_e is assumed for an MPP tracking system, for which the reasoning for selection is given furhter in section 10.7. Note that this value is re-iterated upon again in the further sections: indeed, it must increase in order to charge the batteries to the level where desaturation can be performed in eclipse.

10.3.2. POWER REQUIREMENTS FROM OTHER SUBSYSTEMS

In this section, the power distribution will be re-computed based on power requirements from other subsystems. The modes and their power requirements are also reworked, along with the solar panel area and other sizing quantities.

POWER DISTRIBUTION FROM OTHER SUBSYSTEM REQUIREMENTS

Given that other subsystems (notably ADCS and OBDH) now have concrete selected parts, a more accurate power estimation can be performed. Firstly, a table of the required power per subsystem can be generated. Note that the subsystems for which precise power values will be indicated with italicised text. The other subsystems will be reconfigured in terms of power, if necessary. The new power fractions will also be provided in Table 10.3.

Table 10.3: Re-iterated Power Distribution Based on Other Subsystem Power Required.

Subsystem	Maximum Power Required [W]	Re-iterated Power Fraction [%]
Payload	50	44
Structure and Mech.	1.1	0.97
Power	9.8	8.63
TT&C	*10.7*	*9.4*
OBP	*3.3*	*2.9*
ADCS	*38.75*	*34.1*
Total	113.65	100

Several assumptions had to be made in order for this to be valid:

- The decrease in the OBP (On-Board Processing) power must be deemed reasonable, despite a steep decrease from 12 % down to 3 %.
- All ADCS components are assumed to function concurrently, even if in reality the magnetometers and magnetorquers cannot be operated at the same time.
- The ADCS is not functioning at its absolute rated maximum power: for instance, the reaction wheels each only operate at a maximum of 8 W instead of the rated "<9 W". This is a procedure to increase safety, as running actuators at full power can strongly increase failure rates and wear.
- The thermal subsystem is assumed to be entirely passive and all required power for components such as heaters, as per chapter 11.

With respect to the power distribution found in [7], the overall maximum required power is higher (114 W up from 109 W). This is mainly due to an ADCS power increase, and is not an issue as the system will be sized for average power: compliance to maximum power regimes is verified when the power distribution topology is finalised.

An important subsystem to define in detail is the ADCS. Since the components and the working modes were well-defined, some elaboration can be made on the power requirements of this subsystem. Three main modes of operation for the ADCS subsystem can be distinguished: *detumbling*, *nominal operations* and *desaturation*.

For **detumbling**, only the magnetorquers (3 units, 2.8 W each), gyroscopes (3 units, 0.1 W each) and magnetometers (3 units, 0.01 W each) are needed. This totals to **10.35 W**, assuming the magnetorquers and magnetometers operate simultaneously (which in principle cannot be the case as the actuation would interfere with the measurement) as a worst-case safety precaution. This represents both the average power and maximum power: the magnetorquers operate at full power for the entirety of the detumbling procedure.

Nominal Operations is a less defined mode for the ADCS subsystem: it is however assumed that on average, the power used will be equivalent to 4.5 W: the spooling-up of the wheels is assumed quasi-linear due to averaged external torques, and thus on average the power will be approximately half of the allowable maximum, which is taken to be 8 W. The additional 0.5 W are allocated as a safety for power used during idling. The magnetorquers are not needed and neither are the magnetometers, thus those are assumed to be idling at 10% of their maximum power: a value is assumed here as no specification is given. The sun-sensors and gyroscopes operate at full power. This yields an average power of 19.335 W.

The most stringent power requirement from the ADCS subsystem arises from **desaturation**. Here, the reaction wheels are brought from full momentum all the way down to idle. Thus, the maximum required power will begin at 8 W and decrease to idle, giving an average of 4.5 W over the desaturation procedure, again assuming a linear decrease in momentum and thus power. The magnetorquers and magnetometers, these operate at their maximum power. In reality, these alternate but for the sake of simplicity and the implementation of a safety margin they are assumed to operate simultaneously. The sun sensors are idling at 0.0066 W each, and the gyroscopes operate at full power. This yields a maximum of 38.75 W, with an average of 28.36 W.

RE-DEFINITION OF MODES AND THEIR POWER REQUIREMENTS

Since several precise subsystem power requirements are now known, it is necessary to re-compute the mode-specific power requirements. First, discussing the modes themselves is necessary:

- **Detumbling Mode:** it can be assumed that the PPGD&S, OBP and TT&C run on maximum power. The ADCS power value is specified in the previous section as 10.35 W: The rest of the systems are on standby.

- **Emergency Mode:** the objective of this mode is to recover the spacecraft using minimal power. All is on standby aside from the 100% power PGD&S subsystem, 100% power OBP and 75% ADCS. The TT&C does not run continuously but is required nonetheless, so is is deemed to run at 50% of its maximum required power.
- **Science Mode:** The objective of this mode is to provide all that is necessary for the instrument to measure at the specified performance. The Payload must run at 100% power, the ADCS must run at 60% power on average and the OBP also at 100%.
- **Maintenance Mode:** For this mode, the SPS either performs a software update or is in data downlink mode. This requires 100% PGD&S, OBP, TT&C and 60% ADCS.
- **Desaturation:** this mode has been explained previously. In terms of ADCS, it is the most demanding mode as reaction wheels and magnetorquers operate simultaneously at full power.

An important aspect to explain is the standby power: in general, the components for which the standby power requirements are known will use accurate values. Otherwise, 20% of the maximum power will be assumed to be the standby power. The table that results from this is such that the columns correspond to the subsystems, and rows correspond to operational modes. The percentages indicated in the subsystem cells correspond to the percentage of total maximum power needed. This can be seen in Table 10.4.

Table 10.4: Power Distribution Based on Other Subsystem Requirements.

Mode/Subsystem	PG&D	Structures	Payload	ADCS	TT&C	OBP	Total Power Req. [W]
Detumbling Power Req. [W]	9.8	1.1	10	10.35	2.14	3.3	36.69
Emergency Power Req. [W]	9.8	1.1	10	19.335	5.35	3.3	48.885
Science Power Req. [W]	9.8	1.1	50	19.335	2.14	3.3	85.675
Maintenance Power Req. [W]	9.8	1.1	20	19.335	10.7	3.3	64.235
Desaturation Power Req. [W]	9.8	1.1	10	28.3632	2.14	3.3	54.7

From this, it can be seen that the most stringent mode is the science mode, where the required continuous power is 86 W.

POWER DISSIPATION IS SERVICE MODULE

Considering the power dissipation within the Service Module, the payload power of 50 W is subtracted. This leaves a day power of 36 W in the service module, and approximately 40% of the day value. Thus, the day power dissipated is 36 W and the eclipse power dissipated is 14.4 W.

10.4. SELECTION OF SOLAR CELLS

In the Midterm Review, the triple-junction array type was selected due to its high efficiency, low degradation factor and reasonable thermal coefficient. However, a specific off-the-shelf model must now be selected for the detailed design. For triple-junction arrays, the options are the following:

1. AzurSpace Solar Power GMBH, 3C Series [1]
2. Solar Junction Triple Junction Solar Cell [2]
3. CESI CTJ30 [3]

There cells, while delivering similar performance levels, still possess some significant relative differences. A basic comparison must therefore be performed, and the results outlined. This comparison is a simplified trade-off, and must therefore lead to a winning option. This will be decided below.

10.4.1. OVERALL EFFICIENCY

In terms of efficiency, a higher value is always desired. From the sources mentioned above, general cell efficiencies border 40%, and implemented array efficiencies exceed 30%. The differences were so small that all options were deemed quasi-identical.

10.4.2. EASE OF IMPLEMENTATION

In terms of ease of implementation, the manufacturing was assumed to not vary between the different cells. The important factor was size: for a low delta for the further Steps, it was deemed necessary that the sizes of the cells be flexible. While a small size is always good, larger cells can also have their benefits, as less assembly needs to be done

[1]URL: http://www.azurspace.com/index.php/en/products/products-cpv/cpv-solar-cells [cited on 05-06-2019]
[2]URL: http://www.sj-solar.com/products/ [cited on 05-06-2019]
[3]URL: https://www.cesi.it/services/solar_cells/Documents/CTJ30-2015.pdf [cited on 05-06-2019]

for larger sections. Nevertheless, a small size is considered an advantage for the SPS-2 FF solar cells, as the surface area availability is low and space used must be maximized. Thus:

1. Solar Junction: 0.25 mm^2 to 4 cm^2
2. AzurSpace: 9 mm^2, 30.25 mm^2 and 100 mm^2 are available
3. CESI: 8 cm^2, 26.5 cm^2, 27.5 cm^2 and 30.15 cm^2 sizes available

Solar Junction is thus considered the winner here: however, a size as small as 0.25 mm^2 is not likely to be required, and thus the advantage over AzurSpace's offerings is considered small. CESI lags behind with only very large cell sizes.

10.4.3. Business and Logistics Considerations

In terms of business considerations, it must be noted that both CESI and AzurSpace are European companies: this facilitates logistics, is more sustainable due to the reduced need for transportation and enhances partnerships between European countries. AzurSpace is geographically closer due to its roots in Germany, and is already well established in the European space sector. Thus, the ranking is as follows:

1. AzurSpace
2. CESI
3. Solar Junction

Overall, the winner of this comparison is AzurSpace's range of triple junction cells. While it is not the easiest range of cells to implement due to a limited cell size range, it is located in a nearby country such that logistics and certification are made easier. Deepening on the solar panel architecture, which is not yet determined, several sizes are available to facilitate assembly and production.

10.5. Photo-Voltaic Power Generation: Preliminary Architecture

At this stage, a preliminary analysis of the architecture of the Photo-voltaic Power Generation System (PVPGS) can be made. This is done on two levels: the required geometric placement and number of solar panels needed along with their size, as well as the model selection for later design stage detailing possibility. These facets of the PVPGS will be discussed in the order indicated above.

10.5.1. Sizing and Placement

The sizing of the photo-voltaic panels and their subsequent placement is of great importance for a complete power system design. Due to required symmetry and the simplicity of integration, the top of each of the QuadPack modules is covered in photo-voltaics. With 6 QuadPacks, this allows for an area of $TopArea * NumberofQP$ = 0.272*0.391*6 = 0.628 m^2 [36], which is sufficient for Step 1. An orifice is allowed for the Sun-pointing IOD payloads and upper antenna. This means that one of the QuadPacks is only 40% covered. This yields $TopArea * NumberofQP$ = 0.272*0.391*5.4 = 0.5743 m^2, which is sufficient for the necessary 0.567 m^2 naturally, smaller folding panels as seen in [28] were also considered for Step 1: the size would have been sufficient and the hinges required readily available. While this could well be the case, the top-mounted stationary panels are such because of the inherent simplicity: no moving parts results in fewer points of failure. Another reason for which this as done was a possibility of greater power allowed for the payloads. This, of course, allows for the power system itself to avoid significant redesign due to a lower inter-step power increase.

10.5.2. Model Selection

For further analysis, the photo-voltaic panels will be modelled separately as the following circuit, seen in Figure 10.2.

The equations describing this can also be outlined. They are written as follows:

$$I_{pv} = I_{sc} - I_0 e^{\frac{q(V_{pv}+I_{pv})}{nkT_{cell}}} - \frac{V_{pv} + I_{pv}R_S}{R_P} \tag{10.3}$$

$$V_{oc} = \frac{nkT_{cell}}{q} ln(\frac{Isc}{I_o} + 1) \tag{10.4}$$

where the V_{oc} is the open-circuit voltage, I_{sc} is the short-circuit current, I_0 is the reverse saturation current, k is the Boltzmann constant, n is the diode ideality factor, q is the electron charge and T_{Cell}. The V_{oc} and I_0 are given for a certain irradiation and temperature, as can be seen in the IV curve depicted in Figure 10.3.

This can be all be used in the later design stages to model the PV cell performance, but is not utilized at this design stage.

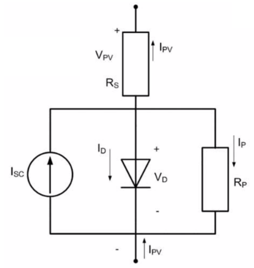

Figure 10.2: Equivalent Circuit for PV panel [37].

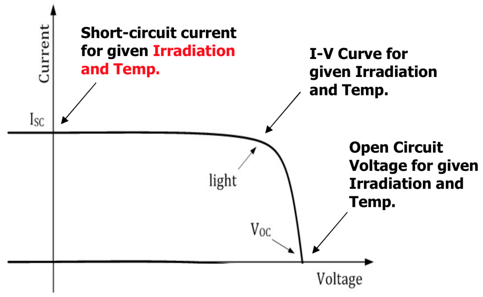

Figure 10.3: Example IV curve for given temperature and irradiation.

10.6. Battery Sizing & Type Selection

In the Midterm Report [7], the battery sizing was briefly discussed. However, it shall be detailed in this section. Firstly, the sizing will be performed. Secondly, relevant components will be selected.

10.6.1. Minimum Battery Capacity Required

The minimum required battery size per step was computed using the following equation:

$$E_{batt} = \frac{P_e T_e}{X_e} \tag{10.5}$$

However, in order for a sufficient fail-safe process to be designed, the operational conditions for the SPS-2 FF must be considered. For instance, one could consider the possibility of a recovery regime in which the satellite uses minimal power and runs exclusively from its batteries. This would require a larger amount of batteries than accounted for in Equation 10.5. In fact, taking a fail-safe of an entire functional day at reduced power emergency mode (50% of potential maximum power is used), the requirement becomes that:

Table 10.5: Minimum Battery Capacity Required Per Step, for Emergency Mode With Contingency.

Step	Battery Capacity Required [Wh]
Step 1	114
Step 2	151
Step 3	216

An important requirement to consider was the detumbling energy needs. Since sun-pointing and battery charging is impossible during the early detumbling stages, the batteries alone must be usable for detumbling. Knowing the requirement of the reaction wheels, magnetorquers and sun-sensors, the batteries can be sized for detumbling. For Step 1, detumbling is permitted to take 1.5 orbits. This means that a total worst-case detumbling time of 1.5*5136.65 seconds is allowed. A worst-case power requirement will be assumed to be equivalent to that in Table 10.4: the detumbling mode requires 36.69 W. With a cumulative path efficiency X_e of 0.667, as seen in [7] it is obtained that the battery capacity, worst-case, for Step 1 is:

$$C_{worst} = \frac{1.5 * T_{orbit} * P_{det_{worst}}}{X_e * 3600} = \frac{1.5 * 5136.65 * 36.69}{0.667 * 3600} = 117.73 Wh$$

This means that the Step 1 batteries must have at least a capacity of 117.73 Wh. Now that the required detumbling worst-case capacity is known, the desaturation must be analysed. For desaturation, it is known that:

- Desaturation must take place every 29 orbits as per chapter 9
- The procedure takes 1 orbit, as per chapter 9

Using the Python program developed for this solar power and battery sizing process, the following is implemented for the sizing:

- The batteries must be sufficient to power detumbling followed by a 1.5 orbit rotation towards the sun on their own
- The batteries must be sufficient to power one desaturation procedure that takes 1.5 orbits every 29 orbits

Using the software developed, the sizes are as follows:

- Required Battery Capacity: 191 Wh
- Required Array Area: 0.567 m^2
- Beginning-of-Life Array Power: 248.8 W
- End-of-life Array Power: 248.1 W

From this, the solar array sizing in section 10.5 is updated.

10.6.2. BATTERY SELECTION

Examining the Commercial Off-The-Shelf (COTS) market for battery systems, it is was rapidly concluded that the options available are plentiful and that a choice would have to be made on the basis of factors other than raw performance. As the mass budget was deemed to be an unreliable starting point for the design, due to being purely based on historical data, a trade-off in terms of power density $[Wh/kg]$ cannot be performed. Other methods were thus considered.

SUPPLIER SELECTION AND JUSTIFICATION

While a comprehensive list of manufacturers and models was researched, it was deemed best to go with a logistically convenient partner that operates outside of the USA, and thus Saft Groupe S.A. was selected as the supplier for COTS batteries for the SPS-2 FF. Note that a mass and volume safety factor of 1.2 was taken into account: the uncertainty with regards to the thermal necessities of the batteries at this design stage requires that additional mass is allocated to the potential inclusion of an insulation/active cooling mechanism for the battery pack. Thus, the *4s2p MP 176065 xlr XLSO* is a battery considered for the SPS-2 FF. Its specifications are found below:

- **Nominal Operational Capacity:** 198.5 Wh
- **Operational Temperatures:** -30° to 60° charge, -35° to 60° discharge
- **Mass:** 1.63 kg
- **Volume and Dimensions:** 1.49 l, 259 × 79 × 73 mm

A potential scalable alternative is the *MP 176065 xtd*. This is a smaller battery pack, and can be used in series to obtain the necessary capacity. A larger mass and volume safety factor of 1.5 is used for comparison as the connection and storage mechanism for this battery pack are heavier. The specifications are as follows:

- **Nominal Operational Capacity:** 20.4 Wh
- **Operational Temperatures:** -30° to 85° charge, -40° to 85° discharge
- **Mass:** 0.135 kg
- **Volume and Dimensions:** 0.077 l, 18.65 × 60.5 × 68.7 mm

While the first option only requires a single pack to fulfil all steps, the second one needs 10 for step 3. Comparing both implemented options directly, Table 10.6 is generated.

Table 10.6: Comparison of Mass and Volume Between Battery Options.

Quantity	xlr battery	xtd battery
Mass with safety [kg]	1.96	2.03
Volume [l]	1.79	1.15

More specifications and complete datasheets can be found on Saft's website [4].

It is clear that the second option is superior in terms of raw performance: the volumetiric power density is significantly higher, the temperature range is larger and these benefits does not come at a significant cost to mass. Additionally, the 10 battery packs can be distributed throughout the spacecraft, which allows for a mass fine-tuning with regards to CG position. Thus, the *MP 176065 xtd* is selected as the battery for the SPS-2 FF. The mass and volume requirements are state above in Table 10.6, and the nominal capacity of the 10 batteries is 204 Wh. On average, the specific price for Lithium-Ion batteries is 176$/$kWh$.[5], which means that the price here will be 0.204*176 = 36$. However, space-grade batteries, according to [6] near $6000 in costs. These have integrated temperature sensors while the Saft batteries do not: the additional integration will incur additional cost. The price of a single battery is thus taken to be $7000, as the capacity of the 176065 xtd is similar to that of the battery used as a reference.

10.7. POWER REGULATION

In this section, the Power Regulation Method for the SPS-2 FF will be chosen and subsequently outlined. These are crucial to delivering the power required to all components while maintaining a high efficiency throughout and preventing excess power delivery to components. While the detailing of a production-ready topology will need to be performed by specialists, the outline of the base technologies and methods is beneficial to increase the level of understanding with regards to the system.

10.7.1. COMPARISON AND SELECTION

In this section, the Power Point Tracking and Direct Energy Transfer methods will be presented, compared and the optimal method for the SPS-2 FF will be selected.

[4]URL: https://www.saftbatteries.com/products-solutions/products/mp-vl-batteries-launchers [cited on 11-06-2019]
[5]URL:https://about.bnef.com/blog/behind-scenes-take-lithium-ion-battery-prices/ [cited on 17-06-2019]
[6]URL:https://www.cubesatshop.com/product/ba0x-high-energy-density-battery-array/ [cited on 17-06-2019]

POWER POINT TRACKING AND DIRECT ENERGY TRANSFER

An important parameter to consider is the method used for power regulation and control. There are two possibilities, namely **Peak Power Tracking (PPT** and **Direct Energy Transfer (DET)** Systems. PPT uses a switching power converter to obtain the voltage necessary for the solar arrays to reach their Maximum Power Point (MPP), while DET transfers power directly to the load. The consequence of using DET is that the solar panels have a fixed and likely sub-optimal operational voltage, and while at its best the system is more efficient, usually the total power delivered will be greater when the MPP is attained through the use of a PPT system. Thus, the PPT approach is much more suitable in terms of power delivered by the solar panels and overall system implementation efficiency.

ADAPTABILITY DIFFERENCES

Additionally, the system requires a high adaptability (low delta) between steps: the PPT system is more adaptable for a range of different loads than a DET circuit, which will undergo heavier modification between steps in order to attain an optimal performance. This is due to the fact that the PPT switching circuit uses active components and digital system to regulate its power transfer characteristics, thus obtaining optimal transfer for a wide range of loads. Thus, PPT superior in terms of high adaptability/low delta. Therefore, PPT shall be utilised on the SPS-2 FF, as it is optimal for adaptability.

10.7.2. ORBITAL INFLUENCE ON BATTERY SIZING

A consideration that must be made at this stage is the possibility that some of the orbits that the SPS-2 FF may be launched into due to the AVUM+ module can be fully illuminated without any time spent in eclipse. This is not a reason to reduce battery size: as previously seen, the driving requirement for battery sizing is the possibility to detumble from battery power alone. Therefore, reducing battery size is deemed counter-productive to the design.

10.7.3. OUTLINE OF POWER REGULATION ARCHITECTURE

The power regulation system selected is designed to work as a switching circuit-based PPT. A set of bi-directional power converters will be used for this task. These converters will look as shown in Figure 10.4.

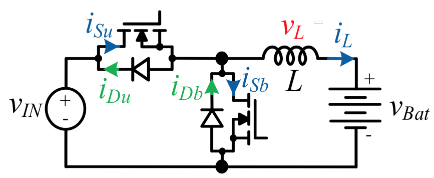

Figure 10.4: Bi-Directional Power Converter [37]

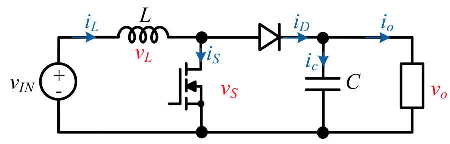

Figure 10.5: Equivalent Boost Converter [37]

As can be seen in the diagram, the main feature of the circuit is its use of active components. Capacitors allow for DC transfer, and digital-system controlled transistors ensure that current passes when required. As for the conduction modes, the Continuous Conduction Mode (CCM) is necessary for correct operation. When working to boost voltage, the circuit is equivalent to Figure 10.5.

The CCM condition is described by the following equation [37]:

$$\Delta I_L < 2 I_{IN,avg} \tag{10.6}$$

$$\Delta I_L = \frac{V_{IN} D T_s}{L}$$

$$I_{IN,avg} = \frac{I_o}{1-D}$$

For these equations, ΔI_L is the ripple current at the inductor, D is the duty cycle of the system (T_{active}/T_{total}) and the I_o represents the output current, equal to I_L in this configuration. Once the precise requirements from other subsystems have been gathered, the values here can be determined and the topology design of each of the power converters and harness can be done.

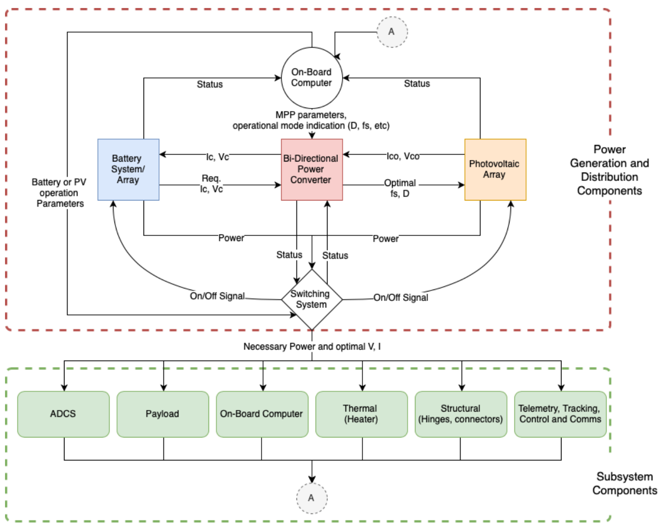

Figure 10.6: Power System Block Diagram

10.8. Power Generation, Distribution & Storage Block Diagram

The PG&D subsystem relations between all elements have been considered, the generated diagram is depicted in Figure 10.6. Note that the switching system block is more complex than it may appear on the diagram, as it houses several power converters such that each of the payloads is provided with sufficient power but optimal voltage and current for an increased overall system efficiency. This is guaranteed by the computer and MPP tracker system, as shown in the diagram. Note that this is prone to change if the final architecture is to differ with respect to the one indicated here.

10.9. Cost, Risk & Sustainability

This section will discuss the estimated cost of the power subsystem, predicted associated risk and its compliance to the sustainability criteria. This will be done for all components of the subsystem when possible.

In order to obtain an accurate idea of the feasibility of the SPS-2 FF, the cost must be estimated at a subsystem level. For the power subsystem, no exact cost values for any of the components chosen could be obtained. However, an estimation was made regardless, using some assumptions which are detailed below.

Estimated Component Costs

The estimated component costs are outlined below in Table 10.7.

Table 10.7: Power Subsystem: Preliminary Cost Estimation

Component and (Quantity)	Unit Cost [$]	Quantity [-]	Total Cost[$]
Batteries: Saft MP 176065 xtd	7,000	10	70,000
Solar Array Assembly	125,000	1	125,000
Harness, Power Conversion and PPT mechanism	100,000	1	100,000
Total Subsystem Cost			295,000

Assumptions, Justification and Reasoning

It is clear that the batteries are the least expensive sub-component of the PGD&S subsystem. If the cost needs to be reduced, some can be removed from the design as only 6 batteries would be sufficient for nominal operation. The cost for the batteries was estimated on the basis of [7], which shows that a high-density battery amounts to near $6000 in costs. These have integrated temperature sensors while the Saft batteries do not: the additional integration will incur additional cost. The price of a single battery is thus taken to be $7000, as the capacity of the 176065 xtd is similar to that of the battery used as a reference.

It is estimated that the power subsystem will incur 17.5% of the total cost of the system: this amounts to a maximum of €350,000 ($398,791) for the PGD&S subsystem, and since the subsystem is expected to cost $295,000 for Step 1, a large margin is left for the development of later steps. The cost of the AzurSpace solar cell assembly is coarsely estimated based on [8]: the worst-case scenario will require $8,500 per 6U panel: the SPS-2 FF geometry will require a maximum of 12 of these. This amounts to a total cost of 12*8,500 = $102,000. A safety margin of $23,000 is allowed for assembly and acceptance testing, if necessary, totalling the cost at $125,000. The harness, power conversion and PPT mechanism constitute the second-most expensive set of sub-components as a topology optimised for the SPS-2 power distribution is recommended: this requires design and certification work. The leftover budget for the Step 1 subsystem is allocated to this set of components: this leaves a budget of $100,000. It is important to note that the costs estimated here are the worst-case costs, with large margins taken into account: the overall SPS-2 FF is not allowed to exceed 2 million Euro in unit costs, and an over-estimation of component cost at this stage is beneficial as it can lower the overall once production is reached.

10.9.1. Risk Quantification for PGD&S

For a successful implementation of the PGD&S subsystem, the risks must be researched and quantified. The approach to risk will follow that used in the Midterm Report [7].

Risks Associated with Batteries

- **B-1:** *Batteries cease working prematurely.* The probability of this is *unlikely*, as batteries are often used for space applications and are well known. The impact of this is *fatal*: possible loss of eclipse power is threatening to the mission's feasibility.

[7] URL: *https://www.cubesatshop.com/product/ba0x-high-energy-density-battery-array/* [cited on 17th of June]
[8] URL: *https://www.cubesatshop.com/product/single-cubesat-solar-panels/* [cited on 17th of June]

- **B-2:** *Batteries experience a wiring issue:* The probability of this is *moderate*, but is higher than for **B-1** as the wiring and protection circuitry needs to be taken into account, as it will be SPS-2 FF specific. This is not expected to affect all batteries, as that would fall under **B-1**, and thus the *critical*.
- **B-3:** *Supplier refuses to source batteries at given price:* Given the certifications that the supplier will need to provide and the general trend that space products are expensive, the probability of the batteries not being sourced at the price indicated is *moderate*. The impact at this stage of the design is *significant*: new batteries will have to be selected and there will be design setbacks, however the impact will not threaten the project.

RISKS ASSOCIATED WITH PHOTO-VOLTAIC PANELS

- **P-1:** *The solar panels fail prematurely.* This is *unlikely*, as solar cells are normally certified and tested. The probability is increased by the need to assemble the panels. The impact is *fatal*, as no power generation is present if all solar panels fail.
- **P-2:** *Supplier refuses to source cells/assemble panels at given price.* The probability here is *moderate*: the same reasoning as for **B-3**. The impact is *significant*, but not critical as other manufacturers are present on the market and similar products can be obtained at minimal cost increase.

SUGGESTED RISK MITIGATION PROCEDURES

The risk mitigation procedures are done on a per-component basis. This allows for a simplified definition of the risk mitigation procedure during design, testing and production to be clearly outlined for each component. For the batteries, a risk mitigation procedure can be to select products from a large and reputable vendor, as they test and certify the products. This can be done by contacting Saft as soon as possible with regards to their product performance and component pricing: if the business proposition is clearly thought out, the probability of **B-3** can be reduced to *unlikely*. Especially as a safety factor has already been applied on the cost estimation. Additional test-bench stress testing of the battery integration system is another possible measure, which would reduce **B-2** (new probability is *unlikely*) and subsequently also **B-1** (new probability is *rare*). The photo-voltaic panel associated risks can also be mitigated through the selection of a reliable partner with flight heritage products. Additional on-site testing can also be performed lowering the probability of **P-1** from unlikely to *rare* with additional testing. The measures for **P-2** probability reduction are ensured by selecting products from AzurSpace, which is a respectable company in the aerospace industry. They have a lot of experience and flight heritage. Therefore, they are able to charge a reasonable price for their services and the risk probability reduces to *unlikely*.

10.9.2. SUSTAINABILITY QUANTIFICATION

Now that the costs and risks have been analysed, the sustainability metrics set in [11] will be used to evaluate the performance of the power subsystem with respect to sustainability. With respect to *SUS-FW-1.1*, the power subsystem does not conflict with stakeholder sustainability requirements at all and is therefore given a score of 10. The transportation of the components is simple, as European partners have been chosen to minimise waste. No avoidable flaws are present, and therefore *SUS-FW-1.2* is also given a score of 10.

The *SUS-FW-1.3* criterion regarding health and safety cannot be accurately estimated, but the high-power testing that will have to be performed and the sharp additional assembly steps constitute a small risk to personnel. Thus, a 9 is awarded. The Emissions (*SUS-FW-1.4*) have not been considered during the design, as the SPS is not mass-produced and a decrease in emissions will not significantly impact the global sustainability issues. No accurate emissions rating can be given due to lack of knowledge about the production and assembly methods. *SUS-FW-1.5*, *SUS-FW-1.6* and *SUS-FW-1.7* are not applicable to the subsystem due to the lack of detail about these aspects.

The impact on jobs created (*SUS-FW-1.8*) is deemed to be positive as design, manufacturing and testing is necessary: a 7 is awarded as there is no direct creation component but an increase in overall work is required. *SUS-FW-1.9* is a 10: the use of materials is minimised as compact solid-state components are used. For *SUS-FW-1.10*, the production method itself has not been designed but is not expected to pose significant difficulty or require supplementary equipment: GaAs and Aluminium can be recycled. Thus, a 7 is given as precise production and assembly methods are not known. *SUS-FW-1.11* is a 10: the tooling required is minimal, as COTS components are selected . For *SUS-FW-1.12* scores a 10: the assembly has been made easy due to the use of COTS components As for the Society criteria, *SUS-FW-1.13* scores a 10 for a mandatory compliance to all laws, and *SUS-FW-1.14* is given a 4, as Saft and AzurSpace are not small businesses. The *SUS-FW-1.15* criterion is given a 9: the effect of an potential improvement to an existing project enhances market presence. The Gross Domestic Product (GDP) could potentially be improved, and thus *SUS-FW-1.16* is given an 8. The market share can be improved if the SPS-2 FF is successful, but this is not guaranteed and hence *SUS-FW-1.17* is given a 7. The maintainability is only possible before launch: for this, it is also low due to the high number of miniaturised components that are present in the power converters, and thus *SUS-FW-2.1* is a low 3. For *SUS-FW-2.2*, the topology optimisation decision yields the highest efficiency possible when combined with market-leading solar cells: this gives the PGD&S subsystem a score of 9 due to the limitation to COTS components. The power subsystem does not affect the decommissioning of the SPS, and is not considered. Overall, the equal-weights average grade is calculated to be an 8.2.

10.10. Explanation of Used Software

In this section, the software used will be elaborated upon. Then, a basic block diagram will be added to outline its functionality.

10.10.1. Software Used and Its Functions

The software used for the Detailed PGD&S subsystem design was a singular Python script, designed with easy modification in mind. Loops were not necessary, as average power values were assumed. Adaptability between steps was an early feature, such that the user could select the step and approximate values for the solar array area and battery capacity. However, it was retooled with more accurate subsystem power values for Step 1, and the power modes were outlined. In Step 2, the values are simply modified from within the script. This program was exceedingly simple, and was introduced as a faster replacement for calculation by hand with a calculator, as values for certain subsystems would often change. The complexity of the program is perhaps the lowest of all software used in this DSE project: however, it helped greatly with reduction of time wasted on power system sizing reiterations.

10.10.2. Software Block Diagram

To get an early overview of the required inputs to get to the desired outputs, a software diagram was made. It is depicted in Figure 10.7 and was used to set up the software in an efficient manner.

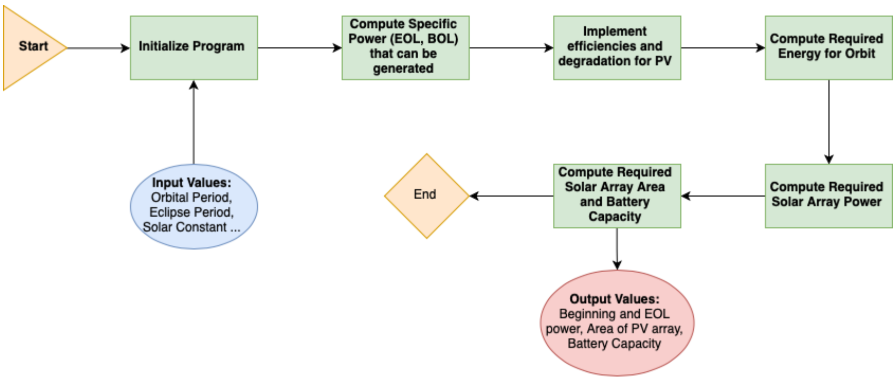

Figure 10.7: PowerMain.py Software Block Diagram

As can be seen, the software requires no loops and no input data processing. This means that verification was able to be performed through calculation by hand.

10.11. Sensitivity Analysis

For the Step 1 design to be complete, a Sensitivity Analysis needs to be performed. The impacts of sizing process input alteration will be considered.

Alteration of QuadPack Number

If the number of QuadPacks attached to the SPS-2 FF varies, the power system would need to change. The main change driver will be the loss or gain of solar panel surface area available: if a decrease in the number of QuadPacks is done, the design would no longer be viable. The solar panel area for a 50 W payload cluster is now at the limit, meaning that at least 6 QuadPacks are required. If the number of Quadpacks is increased, the solar panels can be distributed closer to the center of gravity, as the roofs of the QuadPacks would not need to be completely covered.

Alteration of Orbit

Given that this is unlikely, this situation is not analysed in detail. However, the orbit can already be altered by the AVUM+ to some extent, which can yield different eclipse times. Since the worst-case eclipse time is already considered, the Step 1 orbital inclination change does not cause changes to the design.

Alteration of Payload Power

If the Step 1 payload power is decreased, the power system could naturally be scaled down. However, assuming that the maximum area that can be covered is 5.7 QuadPacks in total (0.606 m^2), the limiting case is a power increase. In fact, a mere 6 W increase to the operational power will increase the required solar array area to 0.6054 m^2, which means a payload of 56 W is the limit unless hinged solar arrays in addition to those already present are allowable: for the sake of simplicity and adherence to cost limits, this is not an option.

Alteration in Solar Cell technology

As the system is operating at its limit already in terms of solar cell area, decreasing the solar cell efficiency would be fatal. A decrease of 22% efficiency yields a solar panel area of 0.82 m^2, which is unacceptable. Thus, cells that are not multi-junction would require a lower payload power. For compliance with the solar panel area limitations, Silicon cells with 23% efficiency will require the payload power to be reduced to a maximum of 26.5 W. This is, of course, a serious option if cost is to be cut on the solar panels.

Alteration In Power Transfer Efficiency

An alteration in power transfer efficiency will have a large effect on the sizing of the subsystem. Considering a decrease in battery efficiency, a drop from the assumed 0.98 to 0.79 yields an upper-limit area of 0.604 m^2. Thus, some safety with regards to transfer efficiency is allowed, as the decease used here for analysis alone is strongly exaggerated. However, the power distribution and transfer efficiency may not be decreased far beyond 0.833: if it decreases by a mere 3%, the PV panel area required is already an excessive 0.61 m^2. Thus, only lower-efficiency batteries are allowable.

Conclusion of Sensitivity Analysis

As seen from these examples, the increase that can be done to the overall power is very limited with the available space. Given a cost-viable Step 1, 6 W is the maximum total operational day power increase allowed. It is possible to use Silicon cells instead of Triple-Junction cells, but that cuts payload power to 26.5%. A battery power delivery efficiency decrease will not significantly impact the possible payload power. The PV panels will thus not require a redesign unless a battery efficiency drop in excess of 15% is achieved. However, the power distribution efficiency must not decrease by a value beyond 2.5%: this is absolutely critical to performance. However, this value is already heavily under-estimated for this feasibility analysis, and is not deemed an issue.

11
THERMAL CONTROL STEP 1

The thermal design of a satellite comprises of identification of the components which require a specific temperature range, the analysis of the temperature environment and if necessary the design of passive or active means in order to control the temperature of different satellite components. For the SPS-2 FF two architecture types will be considered. The first, proposed by an Airbus feasibility study[4], is to thermally isolate the mounting ring and the service module. The advantage of this is that the ring will be able to sustain more extreme temperatures than the electronics in the service module and thus by separating them thermally only the service module needs to be thermally controlled. The alternative option is to not isolate the service module and ring thermally thus giving rise to the need of having the temperature range of the entire satellite in a range acceptable to the most sensitive component. In section 11.1 the choice of architecture is presented and the reasoning outlined. It can be seen that section 11.2 subsequently describes the steady state thermal analysis conducted for the ring and the system implemented in order to obtain a suitable temperature range. Next to the ring the steady state worst case temperature of the service module is calculated in section 11.3. After these preliminary means of analysis a transient thermal model is established and used to analyse the temperature of the main components of the SPS2-FF in section 11.4. In section 11.5 the risk of the design is discussed. Lastly a conclusion for the thermal control design is presented and recommendations for future work presented in section 11.6.

11.1. OVERALL ARCHITECTURE

The choice of overall system architecture has to be made previous to the analysis as it determines if thermally the spacecraft can be treated as two separate entities or as one. In order to make a distinction it is first essential to identify the temperature range in which different subsystems can operate. The temperature ranges for different components are shown in Table 11.1.

Table 11.1: Operating Temperature of components sensitive to this

Component	Min temperature(°C)	Max Temperature(°C)
Saft batteries (76065 xtd)	-30	80
power Conversion, regulation, transmission network	-20	45
Solar Panels (AzurSpace cells)	-20	50
ANT2000 (antenna)	-40	85
TR-600 (transceiver)	-40	85
NanoDock SDR (motherboard)	-20	85
NanoMind z7000 (cpu)	-40	85
RW1 (reaction wheel)	-40	70
TQ-15 (redundant wind) (magnetorquer)	-55	70
NanoSSOC-A60 (Sun sensor)	-30	85
QRS116 (gyroscope)	-55	85
NMRM-001-485 (magnetometer)	-25	70
GNSS receiver	-40	85
Al-7075-T6 Ring Structure	-273	635

From Table 11.1, one can conclude that the electronics stored in the service module will require the most stringent temperature control in a range from 0-40°. According to [1], the temperature of a spacecraft in LEO can be controlled to be in a range from 50°-150° by passive thermal control.

Thus in order to have an architecture were the service module is not thermally isolated from the ring, the ring itself would have to employ more complex thermal control in order to meet the stringent temperature range of the service module. This subsequently means that the thermal control system of the ring will be over designed in order to compensate for the fact that it will conduct to the service module. This will significantly increase the complexity of the system, its power usage and mass. Due to this, the architecture of isolating the service modules from the ring will be used for step 1 of the design.

11.2. RING THERMAL ANALYSIS & CONTROL

In order to establish a preliminary temperature range which the ring will be subjected to in the case of isolated service module a worst case approach is chosen. For this the max and min temperature experienced are computed based

[1] URL:http://webserver.dmt.upm.es/ isidoro/tc3/Spacecraft%20Thermal%20Modelling%20and%20Testing.pdf, Cited: 5th June 2019

on the assumption that the ring is in thermal equilibrium. Due to this assumption is is possible to equate the power input to the power output, ignoring the energy change of the satellite itself. The power input can be contributed to four main factors. These are the power due to direct sunlight, the power due to indirect sunlight (albedo), the power input due to Earths infra-red radiation, and the power dissipated internally. As the ring itself does not host any energy dissipating elements this term can be neglected. The power output on the other hand consist exclusively of the power radiated away by the exposed outside surface of the ring. This does not include the area of the ring which is covered by the QuadPacks and service module of which there are assumed to be 6.

The equation for each component, obtained from SMAD, are given by Equation 11.1-Equation 11.4. As the view factor is specific to each component it is not included in these general expressions but discussed separately.

$$P_{Sun} = q_s \cdot A_{Sun} \cdot \alpha^{th} \quad (11.1) \qquad P_{IREarth} = q_{Earth} \cdot \frac{R_E}{R_E + h}^2 \cdot A_{IREarth} \cdot \epsilon \quad (11.2)$$

$$P_{Albedo} = q_s \cdot A_{albedo} \cdot \alpha^{th} \cdot albedo \quad (11.3) \qquad P_{radiated} = \eta^{th} \cdot \sigma \cdot A_{radiated} \cdot T^4_{equilibrium} \quad (11.4)$$

The above equation are subsequently applied for each of the two possible orbits in order to determine the worst case temperature profile.

11.2.1. ORBIT OPTION 1: POLAR, SUN-SYNCHRONOUS, ORBITAL PLANE PERPENDICULAR

This orbit option refers to the situation in which the polar, Sun-synchronous is such that its orbital plane is perpendicular to the incident sunlight, thus causing the satellite to be in constant sunlight. For step 1 the orientation of the SPS2-FF in the P-frame is such that z-axis aligns with the incoming sunlight. It is however vital to take into account the fact that there exists a Sun pointing offset of the SPS-2FF which will cause both the outside and inside of ring structure to be illuminated by sunlight. This can be accounted for by multiplying Equation 11.1-Equation 11.4 for the outside and inside area with the cosine of the angle of incidence which is given by ϵ_{error}. The Infra-Red and reflected solar radiation (albedo) will on the other hand be incident on the side surface of the ring. In this case the pointing offset is neglected as the combination of low energy Earth radiation and shallow incidence angle on a comparably small surface yields in just a small contribution to the total heat flux input. This is exemplified by using the situation where the Earth IR radiation would be perfectly perpendicular on the side surface of the ring in case of an ideal ADCS system, see Figure 11.1, and computing the height of inside ring which is illuminated in case of $\epsilon_{error} = 0.5°$. This height can be calculated based on the geometry shown in Figure 11.1, which yields in Equation 11.5.Based on this height and the Earth IR radiation in combination with the angle of incidence the total power input due to this can be computed by Equation 11.6.The small magnitude of this results is used as reasoning for the decision to neglect its contribution.

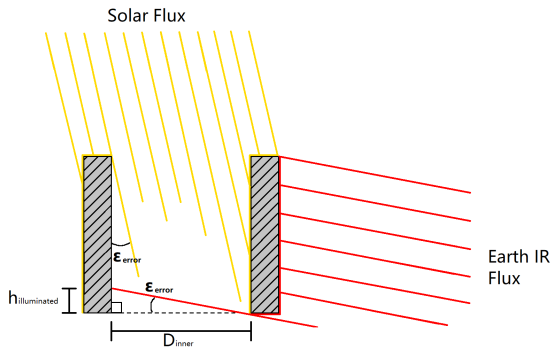

Figure 11.1: Side View of the cross-section of the SPS2-FF showing the effect of non-ideal Sun pointing on the heat flux input

$$h_{illu} = tan(\epsilon_{error}) \cdot D_{inner} = tan(0.5) \cdot 0.936 = 0.008168 m^2 \quad (11.5)$$

$$Q_{Earth} = A_{inside} \cdot q_{IR} \cdot cos(\epsilon_{error}) = q_{IR} \cdot \pi \cdot R_{inner} \cdot height_{illu} \cdot cos(\epsilon_{error}) = 0.027W \quad (11.6)$$

The outside area illuminated by the solar radiation is taken as the product of the diameter and the height of the cylinder in order to account for the fact that the radiation will not be perpendicular to the entirety of the curved surface. In order to also account for the fact that part of the surface is covered by QuadPacks which are treated as thermally isolated a packing factor is included which is calculated as the ratio of the total uncovered surface area of the ring divided by the total area, Equation 11.7.

$$F_{pg} = \frac{2 \cdot \pi \cdot R_{outer} \cdot h_{ring} - 6 \cdot (Base_{quad} \cdot Width_{quad})}{2 \cdot \pi \cdot R_{outer} \cdot h_{ring}} \quad (11.7)$$

Using Equation 11.1-Equation 11.7 and the values for physical constants, the properties of the ring and its attitude as shown in Table 11.2, the equilibrium temperature of the ring can be found to be **94.96°C**. As this orbit option does not present the satellite with an eclipse, no worst case eclipse steady state temperature needs to be calculated.

Table 11.2: Variables used to calculate the equilibrium temperature of the Ring structure of SPS2-FF

Properties of the Ring	Sign	Value	Unit	Orbit and Attitude Related Variables	Sign	Value	Unit
Outer Radius		0.4785	*[m]*	Orbital Altitude		350	*[km]*
Inner Radius		0.4685	*[m]*	Area Perpendicular to Solar Radiation		0.02975	*[m^2]*
Height		0.45	*[m]*	Area Perpendicular to Earth Albedo Radiation		0.28935	*[m^2]*
Outside Surface Area Ring		1.3529	*[m^2]*	Area Perpendicular to Earth IR Radiation		0.28935	*[m^2]*
Interface Area Quad-Ring		0.443904	*[-]*	**Constant Properties**	**Sign**	**Value**	**Unit**
Packing Factor		0.6718	*[m^2]*	Solar Radiation in LEO		1365	*[W/m^2]*
Area Radiating Away		0.289	*[-]*	Earth Radiation		258	*[W/m^2]*
Absorptivity Aluminium		0.15	*[-]*	Earth Albedo		0.35	*[-]*
Emissivity Aluminium		0.05	*[-]*				

11.2.2. OPTION 2: POLAR, SUN-SYNCHRONOUS, ORBITAL PLANE PARALLEL

The second orbit option is such that the orbital plane of the polar Sun-synchronous orbit is parallel to the incoming solar radiation giving rise to an orbit that experiences eclipse. Due to this the worst case temperature is split into two aspects. The worst cold case is such that the area on which the Earth radiation impinges is minimal, which is the case when the z-axis of the ring is pointing exactly towards Earth. This gives an exposed area as calculated in Equation 11.8.

$$A_{IREarth} = \pi \cdot R_o^2 - \pi \cdot R_i^2 = 0.02975 m^2 \tag{11.8}$$

Other than this area and the orbital height, which for the worst case cold temperature is set to 850km, the values from Table 11.2 can be used to compute the worst case minimum temperature of **-68.3570°C**.

For the hot case all variables needed for the calculation are equivalent to the ones stated in Table 11.2 giving rise to a worst case maximum equilibrium temperature of **94.96°C**.The results of the thermal analysis for the ring are presented in Table 11.3.

Table 11.3: Summary of the thermal ranges experienced by the ring structure for the different orbit options

	Worst Case Upper Equilibrium Temperature	Worst Case Lower Equilibrium Temperature
Orbit Option 1	*94.96°C*	*[-]*
Orbit Option 2	*94.96°C*	*-68.3570°C*
Temperature Range which the Ring has to sustain= -68.36°C to 94.96°C		

11.3. SERVICE MODULE THERMAL ANALYSIS & CONTROL: ORBIT OPTION 1

For the preliminary sizing and layout the assumption that the service module and ring structure are completely isolated is taken forward. For power generation, the side panel which faces in the direction of positive Z-Axis(Side 3) is to be covered by a solar panel and constantly orientated towards the Sun. As an initial estimate it was considered to place a radiator(high emissivity surface) on the top surface of the service module(Side 2), however upon iteration and consultancy with the electronics subsystem it became apparent that cooler temperatures during the sunlight phase were preferred as too cold temperatures during eclipse could be mitigated by running more of the electronics and thus an additional high emissivity surface is placed on the side opposite to the solar panel(Side 4). The remaining side panels are covered by Multi Layer Insulation (MLI) (Side 5,6). To simplify initial calculations the orientation error of the body mounted solar panel w.r.t the Sun will be neglected. Additionally the assumption is made that the service module is perfectly isolated from the ring structure (Side 1). The effective thermal absortivity of the solar panels is given by Equation 11.9 and is based on the solar panel efficiency (η^{th}), the absorptivity of the solar panels α^{th} and the packing factor of the individual solar cells F_{pg}.

$$\alpha_{eff}^{th} = \alpha^{th} - \eta^{th} \cdot F_{pg} \tag{11.9}$$

As this orientation stays fixed during the sunlight part of the orbit causing the solar flux input to stay constant, the maximum heat flux input is present when the area of the service module facing Earth radiation at a perpendicular angle. This occurs when the SPS is in between the Earth and Sun such that the side panel on the opposite side of the solar panel covered side is perpendicular to the Earth infrared radiation and the reflected albedo. Additional to these heat flux inputs the electronics within the service module dissipate an estimated 81 W as heat, see chapter 10. Using Equation 11.15-Equation 11.7 and the variable values given in Table 11.4 gives a max heat input off 201.38W.

During eclipse Sun pointing can no longer be relied upon and the orientation of the SPS2-FF is treated as unknown. Furthermore the eclipse internal power dissipation is quantified as 43W in chapter 10. For the worst case cold estimate the surface of the service module which yields in the minimum combination of area exposed and emissivity is used as this yields in minimum power input. For MLI made from Teflon film together with a radiator emissivity of 0.888 and an assumed geometry of the service module equal to that of the service module pack (272mm x 272mm x 391mm), this worst case orientation is given when one of the MLI coated sides is pointed at Earth and results in a power input of 50.4W.

Table 11.4: Geometric and Thermal Surface Properties of the Service Module Sides

	Side 1	Side 2	Side 3	Side 4	Side 5	Side 6
Dimension 1	272mm	272mm	272mm	227mm	272mm	272mm
Dimension 2	272mm	272mm	391mm	391mm	391mm	391mm
Absorptivity	0	0.248	0.805	0.49	0.49	0.49
Emissivity	0	0.888	0.825	0.3	0.3	0.3
Packing Factor	[-]	[-]	0.8	[-]	[-]	[-]

Using Equation 11.1 - Equation 11.4 and the values of absorptivity and emissivity in Table 11.4 in combination with the worst case power input values provided above the worst case max and min temperatures can be calculated to be,

- Maximum Temperature=53.2230$°C$
- Minimum Temperature=-41.4625$°C$

At this preliminary stage it was decided that it was worth refining the method of thermal design used, instead of trying to achieve the needed thermal range for the electronical components by placing high power heaters and more high emissivity surfaces and solely relying on steady state thermal analysis.

11.4. ITERATION 1: TRANSIENT NODAL THERMAL ANALYSIS

Different from a steady state thermal analysis in a transient thermal analysis the thermal inertia of the components, as well as the variation in heat flux input, is taken into account. Furthermore by increasing the number of nodes used to represent the satellite to four it is possible to represent all of the major components (Service Module,Mounting Ring, and QuadPacks) with their own respective node. In order to model the interactions between them an analogy to electrical circuits is used were the thermal conductance is represented by resistors, the power flow is represented by current and the temperature difference between nodes causing said power flow by a voltage difference. This yields in the nodal model of the SPS2-FF which can be observed in Figure 11.2.

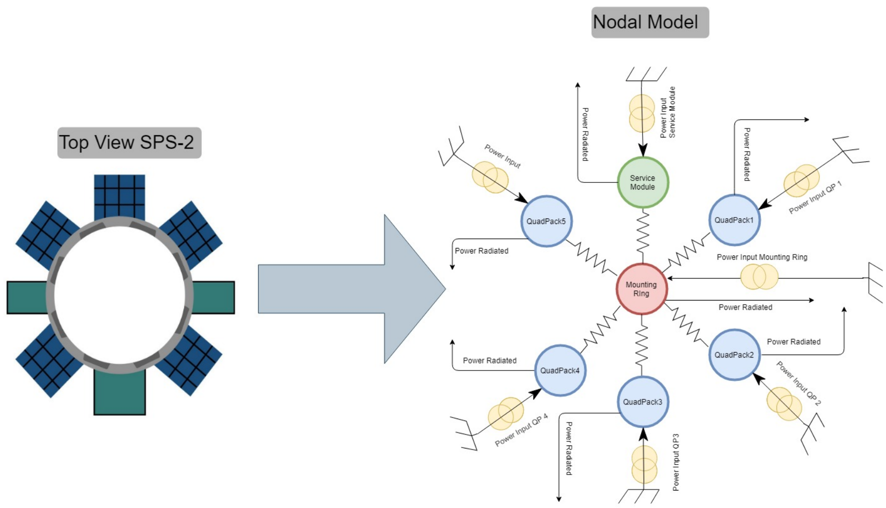

Figure 11.2: Nodal Representation of the SPS2-FF used in the transient thermal analysis

From the above figure the energy balance for each node can be constructed. In general an energy balance consists of three distinct components. These are the power input, the power output, and the power stored. In this specific case, the power input for the service module can be further split into two components. The first is the internal power dissipated as heat by the electronical subsystems in the service module. This has been quantified as 81W in sunlight and 43W in eclipse chapter 10. The second component is the flux input from the environment, which consists of Earth Infrared, Sun direct and Sun Albedo. For both the QuadPacks and the mounting ring there exists no internal power dissipation such that the power input reduces to the environmental factors. The power output by each node is based on its radiation towards the environment and conduction to the other nodes.

It is important to note that the assumption is made that the part of the power absorbed from the nodes by the radiation of the other nodes is small. In order to support this assumption the amount of power transfer between two QuadPacks separated by a small distance with their major area (272mm x 391mm) pointed towards each other is calculated. The worst case hot temperature, of 326.7 K, from the steady state analysis of the service module (section 11.3) is used for this generalised situation. Furthermore the emissivity of the sides is assumed to be that of blue anodised aluminium (ϵ = 0.7), such that the power radiated by the first QuadPack is given by Equation 11.10. The power subsequently absorbed by the second is given by Equation 11.11.

$$P_{radiated} = \sigma \cdot \epsilon \cdot A_{q1} \cdot T_q^4 = 5.67 \cdot 10^{-8} \cdot 0.7 \cdot (0.271 \cdot 0.391) \cdot 326.7^4 = 47.9W \tag{11.10}$$

$$P_{absorbed} = P_{radiated} \cdot A_{q2} \cdot \epsilon = 47.9 \cdot (0.271 \cdot 0.391) \cdot 0.7 = 3.6W \tag{11.11}$$

Comparing this to the power input by the environment to the QuadPacks as calculated in subsection 11.4.1 serves as justification for neglecting this small quantity.

Lastly the power stored term describes the thermal inertia the components have with respect to the time and energy it takes to increase their respective temperatures. This is summarised in Equation 11.12. The following subsections are used to establish the values and variations of each of these terms for each of the components.

$$m \cdot c_p \cdot \frac{dT}{dt} = P_{in} - P_{out} \tag{11.12}$$

11.4.1. POWER INPUT

The power input from the environment and internally dissipated varies for each of the nodes due to their different orientations towards the Sun and Earth. As the attitude of the SPS2-FF w.r.t to rotation about the Z-axis is currently unknown the two orientation of the service module which yield in the worst case situation are used. In Figure 11.3 the QuadPack highlighted in red represents the worst case hot orientation of the service module, as in this orientation the input albedo and infrared radiation will be maximum. On the contrary the QuadPack highlighted in blue represents the service module in its worst case cold attitude. Upon entering eclipse the ADCS can no longer provide Sun pointing capabilities and thus it is assumed that the SPS2-FF will rotate to a position where the cold case attitude experiences the absolute minimum flux input. For position 1 both attitudes are effected by the same environment heat flux input and thus are both highlighted red.

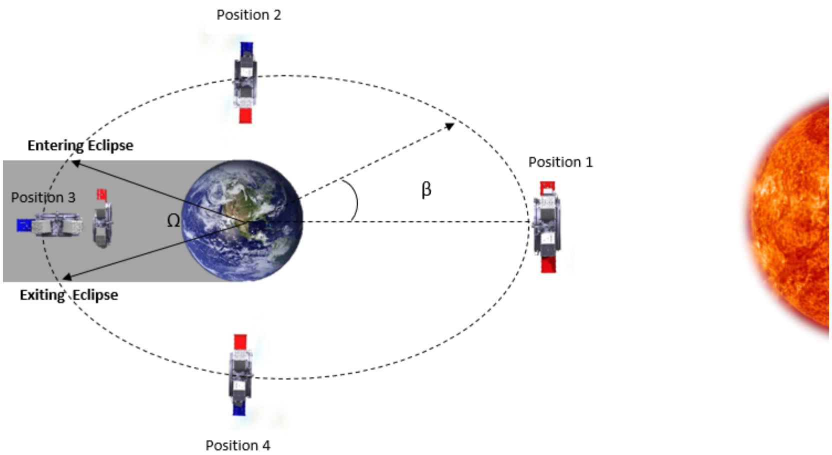

Figure 11.3: Attitude with respect to Sun and Earth at different points during the orbit. The orbital position is given by β

The heat flux input for the service module in its red configuration from position 1 to position 2 from the Sun is given by Equation 11.13 in which the assumption from the steady state thermal analysis is taken forward, such that the ADCS Sun pointing error is not taken into account. As the ADCS maintains this attitude from position 1 to position 2 this represents a constant power input. The same applies for the cold case.

$$P_{Sun} = q_s \cdot A_{SolarPanel} \cdot (\alpha_3^{th} - (\eta^{th} \cdot F_{pg})) \tag{11.13}$$

The power input from the Earth on the other hand varies as the attitude of the SPS2-FF changes with respect to it. For the red attitude both radiator sides (side 2,4) experience an input from Earth. While side 4 varies from a maximum input at position 1, due to the perpendicular radiation input from the Earth, to a minimum as it is out of sight to Earths radiation in position 2. The opposite is true for side 2. It starts from being out of sight of Earth radiation in position 1 to being exposed to at a perpendicular angle at position 2. This yield in Equation 11.14 which describe the power input into the service module which is highlighted in red as it traverses from position 1 ($\beta^{th} = 0°$) to position 2 ($\beta^{th} = 90°$).

$$\begin{aligned} P^{In}_{HotCaseEarth} =& q_{IR} \cdot \epsilon_{side2} \cdot A_{side2} \cdot cos\left(\frac{\pi}{2} - \beta^{th}\right) + q_{Sun} \cdot albedo_{Earth} \cdot \alpha^{th}_{side2} \cdot cos\left(\frac{\pi}{2} - \beta^{th}\right) \\ &+ q_{IR} \cdot \epsilon_{side4} \cdot A_{side4} \cdot cos\left(\beta^{th}\right) + q_{Sun} \cdot albedo_{Earth} \cdot \alpha^{th}_{side4} \cdot cos\left(\beta^{th}\right) \end{aligned} \tag{11.14}$$

Subsequently the total power input to the service module in its hot case orientation from position 1 to position 2 is given by Equation 11.15.

$$P^{In}_{HotTotal1} = P_{Sun} + P^{In}_{HotCaseEarth} + P_{internal} \tag{11.15}$$

For the worst case cold case, highlighted blue in Figure 11.3, the heat flux input follows the same progression for side 4. Different to the worst case hot scenario however in the cold case no other side is pointed towards Earth as the SPS2-FF orbits from position 1 to position 2. This yield in Equation 11.16.

$$P^{In}_{ColdCaseEarth} = q_{IR} \cdot \epsilon_{side4} \cdot A_{side4} \cdot cos\left(\beta^{th}\right) + q_{Sun} \cdot albedo_{Earth} \cdot \alpha^{th}_{side4} \cdot cos\left(\beta^{th}\right) \tag{11.16}$$

Subsequently the total power input to the service module in its cold case orientation from position 1 to position 2 is given by Equation 11.17.

$$P^{In}_{ColdTotal1} = P_{Sun} + P^{In}_{ColdCaseEarth} + P_{internal} \tag{11.17}$$

The second segment of the orbit is the movement from position 2 until the satellite enters eclipse, the angle at which this occurs can be calculated by assuming that when it enters eclipse the orbital height = 350km. This yields in an angle of $\Omega = 133.4705°$, thus the second segment analysed covers the power input for $\beta^{th} = 90°$ to $\beta^{th} = 113.26°$. For both hot(red) and cold(blue) service module orientations the direct solar radiation input is the same and constant as the satellite keeps its attitude constant. Due to this Equation 11.13 continues to be valid for the solar flux input. For the hot case during segment 2 of its orbit the heat flux input from Earth is incident on both side 2, were the incident angle becomes more shallow, and the solar panel side(3), were it increases from a 0° angle of incident to $\frac{\Omega}{2}$. This results in the power input by Earth as described in Equation 11.18 for the power input from Earth IR and albedo.

$$\begin{aligned} P^{In}_{HotCaseEarth} =& q_{IR} \cdot \epsilon_{side2} \cdot A_{side2} \cdot cos\left(\frac{\pi}{2} - \beta^{th}\right) + q_{Sun} \cdot albedo_{Earth} \cdot \alpha^{th}_{side2} \cdot cos\left(\frac{\pi}{2} - \beta^{th}\right) \\ &+ q_{IR} \cdot \epsilon_{side3} \cdot A_{side3} \cdot \left[-cos\left(\beta^{th}\right)\right] + q_{Sun} \cdot albedo_{Earth} \cdot \alpha^{th}_{side3} \cdot \left[-cos\left(\beta^{th}\right)\right] \end{aligned} \tag{11.18}$$

Subsequently the total power input to the service module in its hot case orientation from position 2 to the point where it enters eclipse is again given by the summation of Equation 11.13, Equation 11.18 and the internal heat dissipation during sunlight.

For the cold case orientation on the other hand the flux input from the Earth is limited to the to side 3 and varies in the same manner as for the hot case orientation of the service module, such that the power input in cold case orientation is given by Equation 11.19.

$$P^{In}_{ColdCaseEarth} = q_{IR} \cdot \epsilon_{side3} \cdot A_{side3} \cdot -cos\left(\beta^{th}\right) + q_{Sun} \cdot albedo_{Earth} \cdot \alpha^{th}_{side3} \cdot -cos\left(\beta^{th}\right) \tag{11.19}$$

Subsequently the total power input to the service module in its blue case orientation from position 2 to the point where it enters eclipse is similarly given by the summation of Equation 11.13, Equation 11.19 and the internal heat dissipation during sunlight.

Different to previous segments, in eclipse the attitude is treated as unknown in order to ensure that the thermal control subsystem does not limit the orientation preferred by the ADCS or payload. In this case the two worst case hot and cold orientation of the service modules also correspond to different orientations of the SPS2-FF. This is visualised in Figure 11.3 by displaying two distinct attitudes of the SPS2-FF at position 3 and highlighting the service module in its worst case cold position blue and red in its worst case hot orientation. The worst case cold position causes the service module to have no environmental power input and thus only the internal power dissipation is present. The worst case hot orientation, on the other hand, is given when the IR radiation from Earth is incident at a 90° onto the side of the service module with the highest product of emissivity and area. This is given when the larger of the two radiator areas is pointing towards Earth(side 4). In the hot case the total power input is thus given by Equation 11.20 and for the cold case by Equation 11.21.

$$P^{In}_{HotTotal3} = (q_{IR} \cdot A_{side4} \cdot \epsilon_{side4}) + P_{internalEclipse} \tag{11.20}$$

$$P^{In}_{ColdTotal3} = P_{internalEclipse} \tag{11.21}$$

Upon coming out of eclipse the conservative assumption is made that the SPS2-FF is orientated such that the service module orientation is still the same worst case position as before going into the eclipse. This means from position 3-1 the power input is the mirrored version of the power input from position 1-3. Using Equation 11.13-Equation 11.21 and the values for absorptivity,emissivity and area in Table 11.4 the variation of the power input into the service module can be constructed. Due to the possibility of any combination of worst case hot and cold orientation of the service model in sunlight and eclipse four distinct power input plots can be constructed, see Figure 11.4. As all of them represent a viable scenario, all are used in the nodal analysis to check that the system works for any possibility.

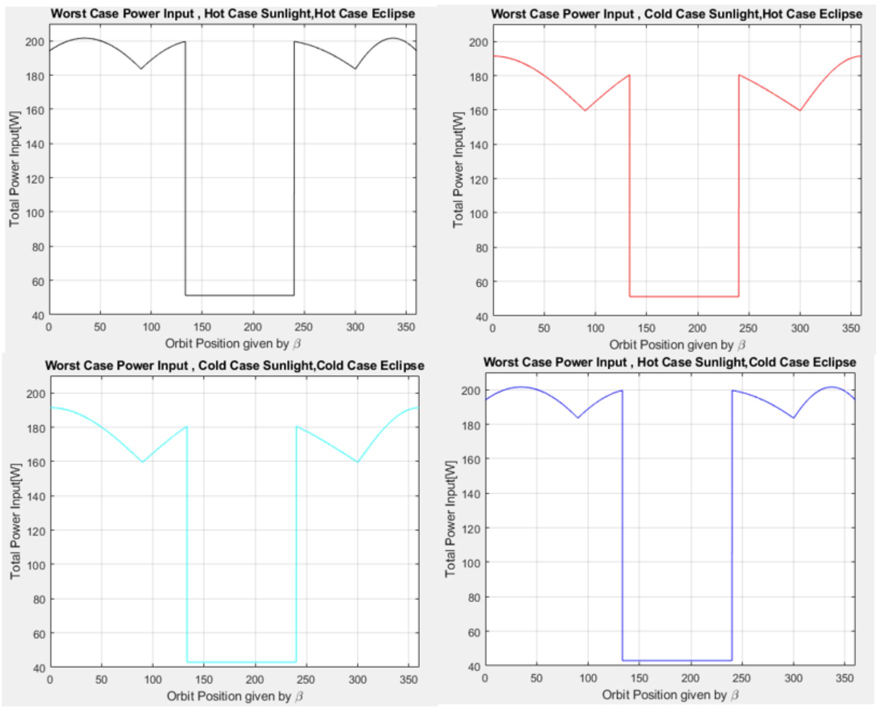

Figure 11.4: power Input variations for the Service Module over one orbit for the different combinations of worst case scenarios

Next to the service module itself, the environmental power input to the mounting ring to which the service module is to be attached has to be considered. The attitude of the ring follows from the orientation of the service module in Figure 11.3. As expressed in section 11.2 for the ring the effect of the Sun pointing error caused by the ADCS cannot be neglected. While in sunlight (position1 to entering eclipse) the maximum power input to the mounting ring is given at the maximum ADCS Sun pointing error of 0.5°. Due to this pointing error the power input from the Sun is split over three surfaces as shown Figure 11.1. The worst case hot situation corresponds to this offset error being constant during sunlight and the power input by the Sun is thus described by Equation 11.22.

$$\begin{aligned} Q_{RingSun} =& q_s \cdot A^{Ring}_{lip} \cdot \alpha^{th}_r \cdot cos(E_{ADCS}) + qs \cdot A^{Ring}_{In} \cdot \alpha^{th}_r \cdot cos\left(90° - E_{ADCS}\right) \\ &+ qs \cdot A^{Ring}_{Out} \cdot \alpha^{th}_r \cdot cos(90° - E_{ADCS}) \end{aligned} \tag{11.22}$$

The worst case cold case on the other hand occurs when the Sun pointing ADCS error is zero and thus the power input from the Sun is solely input through the lip of the mounting ring(Equation 11.23).

$$Q_{RingSun} = q_s \cdot A^{Ring}_{lip} \cdot \alpha^{th}_r \cdot cos(E_{ADCS}) \tag{11.23}$$

As explained in subsection 11.2.1 for the Earth IR and albedo radiation the ADCS error will not be considered. As the SPS2-FF orbits from position 1 to position 2 the angle of incidence on the lip of the ring varies from being perpendicular to not being exposed. In contrast the inside and outside surface of the mounting ring are not exposed at position 1 but have a 90° angle of incidence from the radiation at position 2. This is described in Equation 11.24.

$$\begin{aligned} Q_{Earth} =& q_{IR} \cdot \epsilon_{ring} \cdot A_{lip}^{Ring} \cdot cos(\beta^{th}) + q_{IR} \cdot \epsilon_{ring} \cdot A_{In}^{Ring} \cdot cos(90° - \beta^{th}) \\ &+ q_{Sun} \cdot albedo \cdot \alpha_{ring}^{th} \cdot A_{Out}^{Ring} \cdot cos(\beta^{th}) + q_{Sun} \cdot albedo \cdot \alpha_{ring}^{th} \cdot A_{In}^{Ring} \cdot cos(90° - \beta^{th}) \end{aligned} \tag{11.24}$$

As the ring does not have internal heat dissipation the total power input from position 1 to position 2 can be described for the hot case by Equation 11.22+Equation 11.24 and for the cold case by the summation of Equation 11.23 and Equation 11.24. From position 2 to until entering the eclipse a similar procedure is applied as from positions 1 to position 2 for the service module computations and yields in Equation 11.25 for the hot worst case,for which the ADCS error = 0.5°, and Equation 11.26 for the cold worst case for which the ADCS error = 0°.

$$\begin{aligned} P_{InHot}^{Ring} =& q_{Sun} \cdot A_{lip}^{Ring} \cdot \alpha_{ring}^{th} \cdot cos(E_{ADCS}) + q_{Sun} \cdot A_{In}^{Ring} \cdot \alpha_{ring}^{th} \cdot cos(90 - E_{ADCS}) \\ &+ q_{Sun} \cdot A_{out}^{Ring} \cdot \alpha_{ring}^{th} \cdot cos(90 - E_{ADCS}) + q_{IR} \cdot \epsilon_{ring} \cdot A_{lip}^{Ring} \cdot \left[-cos(\beta^{th})\right] \\ &+ q_{IR} \cdot \epsilon_{ring} \cdot A_{In}^{Ring} \cdot cos(\beta^{th} - 90°) + q_{Sun} \cdot albedo \cdot \alpha_{ring}^{th} \cdot A_{lip}^{Ring} \cdot \left[-cos(\beta^{th})\right] \\ &+ q_{Sun} \cdot albedo \cdot \alpha_{ring}^{th} \cdot A_{In}^{Ring} \cdot cos(\beta^{th} - 90°); \end{aligned} \tag{11.25}$$

$$\begin{aligned} P_{InCold}^{Ring} =& q_{Sun} \cdot C \cdot \alpha_{ring}^{th} \cdot cos(E_{ADCS}) + q_{IR} \cdot \epsilon_{ring} \cdot A_{lip}^{Ring} \cdot \left[-cos(\beta^{th})\right] \\ &+ q_{IR} \cdot \epsilon_{ring} \cdot A_{In}^{Ring} \cdot cos(\beta^{th} - 90°) + q_{Sun} \cdot albedo \cdot \alpha_{ring}^{th} \cdot A_{lip}^{Ring} \cdot \left[-cos(\beta^{th})\right] \\ &+ q_{Sun} \cdot albedo \cdot \alpha_{ring}^{th} \cdot A_{In}^{Ring} \cdot cos(\beta^{th} - 90°); \end{aligned} \tag{11.26}$$

Lastly for eclipse conditions the worst case cold scenario(Equation 11.28) is given for an ADCS error=0° and for the blue highlighted service module orientation in Figure 11.3, while the worst case hot scenario(Equation 11.27) is given for the red highlighted service module orientation in Figure 11.3. Similar to the service module eclipse conditions, the worst case orientation is assumed to be constant while the satellite moves through eclipse.

$$P_{InHot}^{Ring} = q_{IR} \cdot \epsilon_{ring} \cdot A_{Out}^{Ring} \cdot F_{pg}; \tag{11.27}$$

$$P_{InCold}^{Ring} = qIR \cdot \epsilon_{ring} \cdot P_{InHot}^{Ring}; \tag{11.28}$$

For each segment of the orbit there are thus 2 options for the power input to the mounting ring. For the parts in the sunlight the power input to the mounting ring can be treated as independent from the service module orientation and all possible combinations of the worst case power inputs will be checked in the nodal analysis. In eclipse the same applies, however here the orientation of the mounting ring and service module are not independent of each other and thus only two possible orientations exists. This resulting power input possibilities for the mounting ring are shown in Figure 11.5.

The last type of node for which the power input from the environment has to be discussed are the 5 QuadPacks. It is essential to note that for this analysis it has been assumed that the QuadPacks have already released the CubeSats they carry and are thus empty. This assumption is conservative as it reduces and thermal inertia of the QuadPacks and subsequently increases the temperature variation. The placement of the QuadPack opposite to the service module depends on the position of the service module. Thus similar to the service module there are two options for the power input, the worst case hot and worst case cold orientation. For these the power input can be calculated using the same procedure as for the service module. Different to the service module, the QuadPacks will not have any MLI or high radiative surface. The only alteration made, is to attach a solar panel to side 3 of each. The surface properties of the other sides have been estimated from the ISIS brochure [2] and are shown in the Table 11.5.

The remaining four QuadPacks are symmetrically distributed around the mounting ring. Due to this the power input to each is, preliminary estimated to be the average of the power input to the worst case hot service module and worst case cold service module for the surface properties of the QuadPacks. The resulting two possible power input variations for the QuadPack opposite to the service module and the average power input variation used for the other four nodes are shown in Figure 11.6.

[2] URL:'https://www.isispace.nl/product/QuadPack-CubeSat-deployer/', Retrieved:21-6-2019

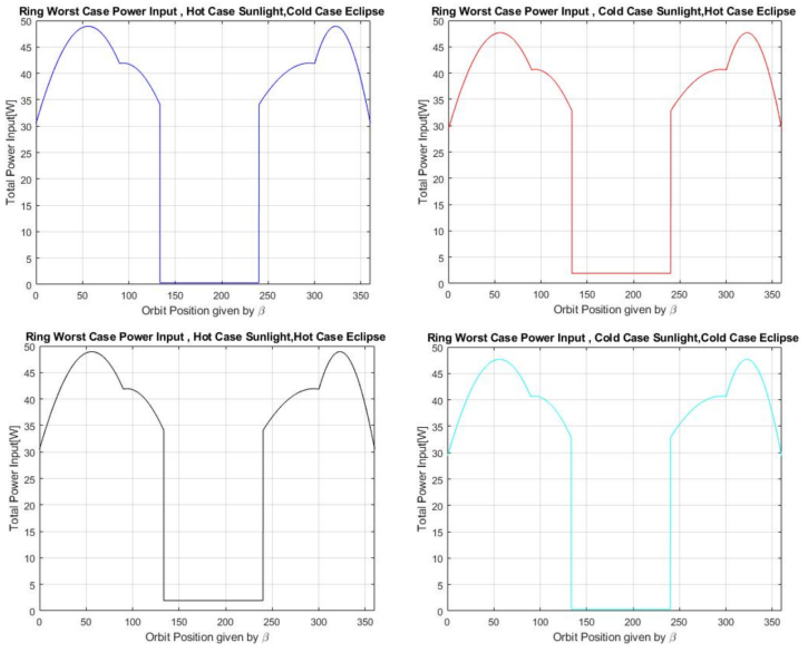

Figure 11.5: Power Input variations for the Ring over one orbit for the different combinations of worst case scenarios

Table 11.5: Surface Thermal Properties of the QuadPacks, where AA stands for Anodised Aluminium.

	Side1	Side2: Black AA	Side3: Solar Panel	Side 4: Blue AA	Side 5:Blue AA	Side 6:Blue AA
Dimension 1 $[mm]$	272	272	272	272	272	272
Dimension 2 $[mm]$	272	272	391	391	391	391
Absorptivity	0	0.65	0.805	0.53	0.53	0.53
Emissivity	0	0.82	0.825	0.82	0.82	0.82
Packing Factor	[-]	[-]	0.8	[-]	[-]	[-]

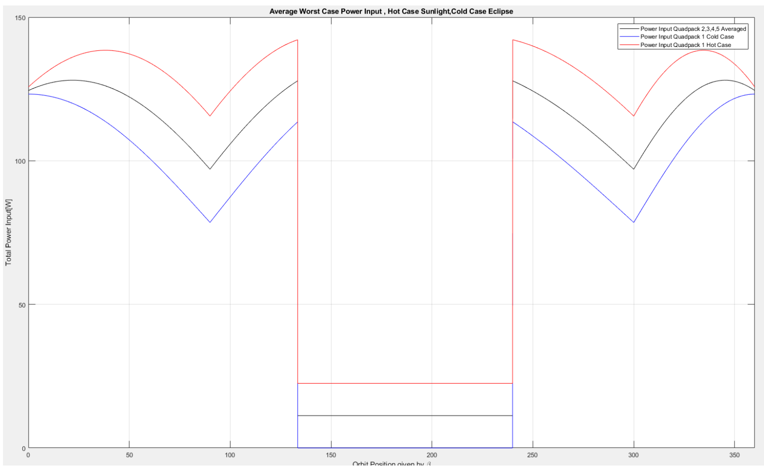

Figure 11.6: Power Input for the QuadPack nodes. Both possibilities for QuadPack 1 are shown.

11.4.2. POWER INTO ENVIRONMENT

The power radiated by each of the three node types towards space is dependent on the components temperature, surface properties,and the temperature of the environment. For space this temperature is ~ 3 K and for this analysis is treated as absolute zero. Both QuadPacks and the service module radiate with all sides except side 1(interface with mounting ring) towards the environment. The area of each of these sides and the emissivity values are given in Table 11.2 and Table 11.4. For the ring only the outside surface not covered by QuadPacks radiates in combination with the top and bottom lip. For the mounting ring polished aluminium surface properties are used,such that the absorptivity=0.35 and the emissivity=0.05. The general equation that is applied for each node is given in Equation 11.29.

$$P^i_{radiated} = \sigma\Sigma(\epsilon^i_j \cdot A^i_j \cdot T^{i\,4}_j) \tag{11.29}$$

11.4.3. CONDUCTIVITY INTERACTION BETWEEN NODES

Each of the QuadPacks and the service module conducts to the mounting ring via their respective interfaces. For the QuadPacks the bottom side is bolted to the ring via 16 bolts and thus has a aluminium to aluminium interface. For this first iteration of the nodal model only the conductance over the aluminium interface is considered and not through the bolts. This assumption is regarded as conservative as less conduction between the components allows for less dissipation and averaging of the power input and thus yields in higher temperature ranges of the components. The conductance over the interface is highly dependent on the surface finish and the contact pressure. It is furthermore different in space due to the lack of heat transfer via convection. Gap conductance for a rough aluminium interface in vacuum are specified to be from $150\frac{W}{m^2K}$ to $500\frac{W}{m^2K}$[3]. The gap conductance for a smooth aluminium interface in atmospheric condition,on the other hand, is given to be from $2000\frac{W}{m^2K}$ to $12000\frac{W}{m^2K}$. Due to the preliminary design stage this value can not be obtained accurately for a smooth aluminium interface in a vacuum and thus is estimated to be in between the two ranges at a value of $1000\frac{W}{m^2K}$. Furthermore a sensibility analysis is conducted in subsection 11.4.6 to check the effect on the temperature range in case this value is changed between $150\frac{W}{m^2K}$ and $2000\frac{W}{m^2K}$. For the service module-mounting ring interface, due to the architecture design decision made in section 11.1 to thermally isolate the service module from the ring, a 10mm isolation layer made from Makrolon GV 30, a glass fiber reinforced polymer made for space application, with a conductivity of $k_{GV30} = 0.16\frac{W}{mK}$.

11.4.4. NODAL SETUP & NODE ENERGY BALANCE

The nodal approximation, as presented in Figure 11.2, can be further simplified into 4 nodes. One node to represent the service module, one node to represent the mounting ring, one node to represent the QuadPack opposite to the service module and one node to represent the remaining 4 QuadPacks for which the power input is the same. In order to use the energy balance Equation 11.12 to iterate the orbit, the first order derivative of the temperature with respect to time is approximated by a first order Taylor approximation as shown in Equation 11.31. This computational modelling scheme is stable as long as the time-step is below 1 second. For this reason the time-step is set to 0.1 seconds.

$$\frac{\delta T}{\delta t} = \frac{T_{i+1} - T_i}{\Delta t} \tag{11.30}$$

Thus the energy balance equation Equation 11.12 can be simplified to Equation 11.31. Note that the power in and out terms include the power conducted between nodes.

$$m_i * cp_i \cdot \frac{T_{i+1} - T_i}{\Delta t} = P_{In} + P_{out} \tag{11.31}$$

Based on the inputs from the ring, the energy balance for it can be constructed,see Equation 11.32. By definition the conduction is taken as from the ring to the service module and QuadPacks.

$$m_r \cdot cp_r \cdot \frac{T_{i+1} - T_i}{\Delta t} = \sigma \cdot \Sigma(\epsilon^r_{out,lip} \cdot A^r_{out,lip}) \cdot T^4_{r,i} + P^{IR,Alb,Sun}_r - \frac{k_{MakGV30} \cdot A_{int}}{L_{int}} \cdot (T_{r,i} - T_{SVM,i}) - \frac{k_{r-QP1} \cdot A_{int}}{L_{int}} \cdot (T_{r,i} - T_{SVM,i}) \tag{11.32}$$

Similar equation can be written for the other 3 nodes and represented in a matrix equation of the form $\mathbf{A} \cdot \tilde{x} = \mathbf{B}\dot{u}$, where the vector $\tilde{x}$ contains all $T^{i+1}_{node1,2,3,4}$ terms and $\tilde{u}$ all input variables such as the power input to each node and the temperature of the node at the previous time-step.

$$A = \begin{pmatrix} \frac{m_r c_{pR}}{\Delta \cdot t} & 0 & 0 & 0 \\ 0 & \frac{m_{SVM} c_{pSVM}}{\Delta \cdot t} & 0 & 0 \\ 0 & 0 & \frac{m_{QP1} c_{pQP1}}{\Delta \cdot t} & 0; \\ 0 & 0 & 0 & \frac{m_{QPo} c_{pQPo}}{\Delta \cdot t} \end{pmatrix}$$

[3]URL:'http://mhtl.uwaterloo.ca/courses_old/ece309/notes/conduction/cont.pdf',Retrieved:'21-6-2019'

$$B =$$

$$\begin{pmatrix} \frac{m_r c_{pR}}{\Delta \cdot t} - (\frac{k \cdot A}{L})_{R-SVM} - (\frac{k \cdot A}{L})_{R-QP1} - 4 \cdot (\frac{k \cdot A}{L})_{R-QPo} & -\sigma \cdot \epsilon_r \cdot A_r & (\frac{k \cdot A}{L})_{R-SVM} & 0 & (\frac{k \cdot A}{L})_{R-QP1} & 0 & 4 \cdot (\frac{k \cdot A}{L})_{R-QPo} & 0 & 1 & 0 & 0 & 0 \\ (\frac{k \cdot A}{L})_{R-SVM} & 0 & \frac{m_{SVM} c_{pSVM}}{\Delta \cdot t} - (\frac{k \cdot A}{L})_{R-SVM} & -\sigma \cdot \epsilon_{SVM} \cdot A_{SVM} & 0 & 0 & 0 & 0 & 0 & 1 & 0 & 0 \\ (\frac{k \cdot A}{L})_{R-QP1} & 0 & 0 & 0 & \frac{m_{QP1} c_{pQP1}}{\Delta \cdot t} - (\frac{k \cdot A}{L})_{R-QP1} & -\sigma \cdot \epsilon_{QP1} \cdot A_{QP1} & 0 & 0 & 0 & 0 & 1 & 0 \\ (\frac{k \cdot A}{L})_{R-QPo} & 0 & 0 & 0 & 0 & 0 & \frac{m_{QP0} c_{pQP0}}{\Delta \cdot t} - (\frac{k \cdot A}{L})_{R-QP0} & \sigma \cdot \epsilon_{QPo} \cdot A_{QPo} & 0 & 0 & 0 & 1 \end{pmatrix}$$

$$\tilde{x} = \begin{pmatrix} T_r^{i+1} \\ T_{SVM}^{i+1} \\ T_{QP1}^{i+1} \\ T_{QPo}^{i+1} \end{pmatrix} \tag{11.33}$$

$$\tilde{u} = \begin{pmatrix} T_r^i \\ T_r^{i\,4} \\ T_{SVM}^i \\ T_{SVM}^{i\;\;4} \\ T_{QP1}^i \\ T_{QP1}^{i\;\;4} \\ T_{QPo}^i \\ T_{QPo}^{i\;\;4} \\ P_{in}{}^r \\ P_{in}{}^{SVM} \\ P_{in}{}^{QP1} \\ P_{in}{}^{QPo} \end{pmatrix} \tag{11.34}$$

Table 11.6: Key Parameters used for the thermal transient analysis/

	Mounting Ring	**Service Module**	**QuadPacks**	**Units**
Specific heat(cp)	910	300	910	J/kgK
Mass	15	40	7.5	kg
AreaRing_lip	0.02975	[-]	[-]	m^2
AreaRing_OutsideIlluminated	0.4685	[-]	[-]	m^2
AreaRing_InsideIlluminated	0.4735	[-]	[-]	m^2
Packing Factor	0.6718	[-]	[-]	[-]
AreaRing_Radiating	0.4735	[-]	[-]	m^2
Gap Conductance Quad-Ring		1000		W/m^2K
Area Interface Quad-Ring	0.051076	[-]	0.051076	m^2
Interface Conductance SVM-Ring		0.16		W/mK
Area Interface SVM-Ring	0.051076	0.051076	[-]	m^2
T_intial	273.5	273.5	273.5	K

For the worst case hot orientation of the QuadPack and subsequent placement of the QuadPack opposite to the service module in the worst case cold position in combination with the worst case hot power input to the ring yields in the temperature distribution over the course of 10 orbits shown in Figure 11.7. Note that the initial condition has been set to $0°C$. This initial condition has to be chosen in order to solve the energy balance. It has limited influence on the results as all nodes will converge to a temperature around which they oscillate based on their thermal properties and the power input. The closer the initial condition is chosen to this value, the less orbits are needed before the node converges to its oscillation temperature. Additional properties of the nodes are furthermore summarised in Table 11.6. Due to the early stage of the design phase accurate values on the specific heat capacity of the service module are not available. The values shown in Table 11.6 are thus merely estimates and should be refined at a later stage. In order to account for the possibility of errors in the estimation of the specific heat capacity a sensitivity analysis has been conducted for changing values of the specific heat capacity of both the service module and QuadPack which is presented in subsection 11.4.6. Lastly due to the in orientation and power input an additional safety factor of 1.25 has been applied.

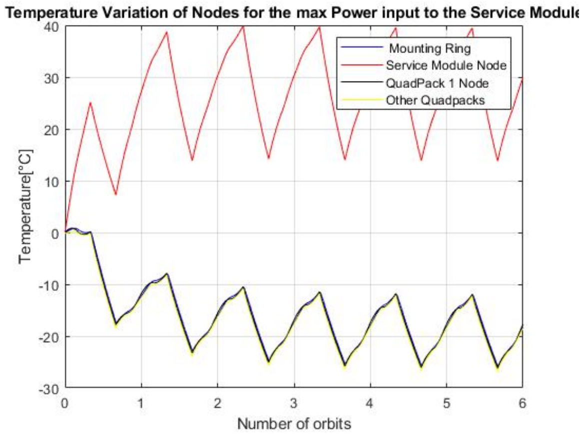

Figure 11.7: Temperature variations of the nodes as a function of Orbit.

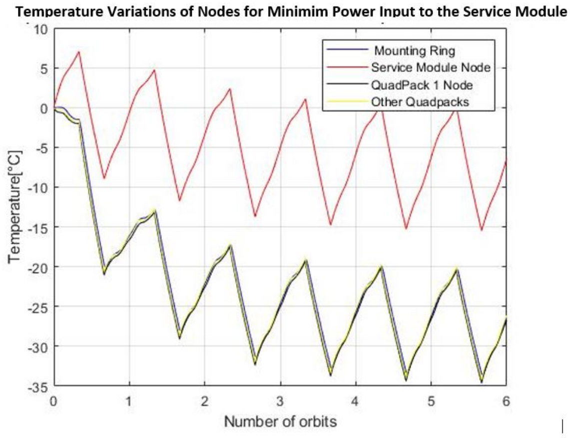

Figure 11.8: Temperature variations of the nodes as a function of Orbit for the minimum power input to the QuadPack.

Figure 11.7 visualises the affect of isolating the service module from the mounting ring. While the QuadPacks, which are not thermally isolated from the mounting ring, tend to a similar equilibrium temperature as the mounting ring, the service module oscillates at a much higher temperature. The other worst case combination of all power inputs which has been identified occurs when the service module is in its worst case cold orientation such that the QuadPack opposite to it is in its worst case hot position in combination with the mounting ring in its worst case cold orientation. The results of this combination are shown in Figure 11.8. Again a similar behaviour of service module and mounting ring can be observed however with this combination in a slightly lower temperature range. From these two scenarios for the placement of the service module a maximum temperature range can be computed.

- Service Module= Range from a minimum of -15°C to a maximum of 40°C
- Mounting Ring= Range from a minimum of -35°C to a maximum of -26°C
- QuadPack 1= Range from a minimum of -35°C to a maximum of -12°C
- other QuadPacks= Range from a minimum of -35°C to a maximum of -12°C

Upon comparison of the temperature range for the service module with the allowed operational temperature ranges of the components in the service module, as shown in Table 11.1, shows that the thermal control system works for either the worst case hot or worst case cold placement of the service module Figure 11.3.

11.4.5. ITERATION 2: UPDATE DUE TO PAYLOAD PLACEMENT

Upon iteration of the SPS2-FF with respect to payload placement two causes for iteration were identified. The first is the actual placement/orientation of the service module during the orbit will be such that it is in its blue orientation for half of the orbit and in its red orientation for the other half,see Figure 11.3. Additionally due to the volume taken up by subsystems in the service module, the maximum amount of volume available for payload in the service module is 90mm x 90mm x 180mm. This allows for the placement of one GNSS receiver in the service module which dissipates 5W as heat. The total power dissipated in the service module is thus not the previously used value of 81 W but 36 W as not all of the power allocated to the payload will be dissipated in the service module, see Table 10.3.2. This in combination with the iterated upon orientation of the service module yields in temperature variation as shown in Figure 11.9. As the temperature variations are satisfy the operating temperature of all components

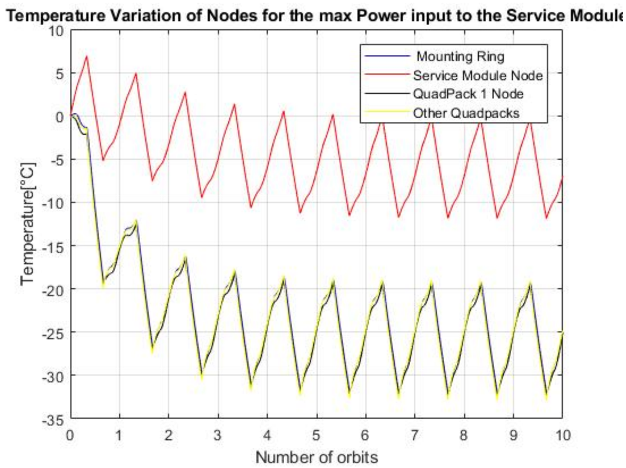

Figure 11.9: Temperature variation based on the updated power dissipation and service module orientation

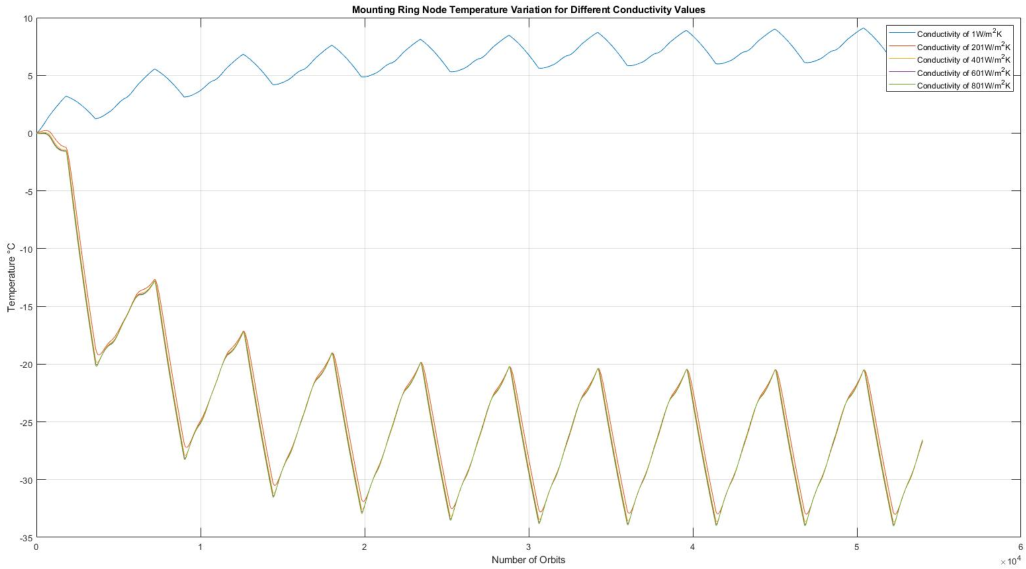

Figure 11.10: Mounting ring node temperature variations for different QuadPack-Ring conductivity values

the passive architecture is regarded as satisfactory.

11.4.6. SENSITIVITY ANALYSIS

The sensitivity analysis is split into two different aspects. The first concern the effect of changing the conductivity between the interfaces and the effect this has on the temperature fluctuations of the nodes. The main reason to investigate this for the SVM and QuadPack interface is that due to the limited time frame of this project, it has not been possible to study the increase in conductance due to the bolted connection through the insulation layer. Additionally the effect of changing the specific heat capacity of the service module has been investigated. The reason for this is that this parameter remains largely unknown and has only been estimated based on the electrical components inside, the structural mass and material choice of each. For the conductance over the QuadPack-mounting ring interface the model has been propagated over 6 orbits for varying numbers of gap conductance. The largest variation in behaviour are observed for the mounting ring, see Figure 11.10. For small values of conductivity the QuadPacks and mounting ring are quasi-isolated causing the ring to oscillated at a higher temperature than observed for higher conductivity values, see figure Figure 11.10. These fluctuations however do not exceed the operating temperature range of the aluminium mounting ring. The observed effect of the conductivity on the temperature of the service module is negligible due to the insulation between the service module and the ring. This aspect of the sensitivity analysis should however be revisited upon further detailed design of this interface. The sensitivity and importance of this interface(service module-mounting ring) is further exemplified by repeating the process for it. The results of increasing the conductivity across the interface are shown in Figure 11.11. These clearly highlights the need for an effective insulation system as else the temperature fluctuations occur too close to the minimum operating temperature of the batteries. As previously stated the current conductivity value arises solely from the conductance through the isolation layer and the additional conductance through the bolts has not been accounted for. If during further design it is revealed that this interface is too conductive, a decrease in the radiator area of the service module shall be investigated. This area covers both sides 2 and 4, could however be reduced by application of a thermal paint. This allows for straight forward adaption of the thermal control system upon further detailed design.

Last the specific heat capacity effect of the specific heat capacity is investigated. This value was estimated by investigating general reference values for PCBs [4], aluminium, silicates and polymers [5] as these make up the majority of the service module. None of the mention components showed a specific heat value below 300 J/kgK and thus this value was chosen as a conservative estimate. The effect of changing this value is shown in Figure 11.12.

[4]URL:'http://www.electronics-cooling.com/2002/08/simplified-transient-model-for-ic-packages/',Accessed:'23.06.19'
[5]URL:'https://www.engineeringtoolbox.com/specific-heat-capacity-d_391.html',Accessed:'23.06.19'

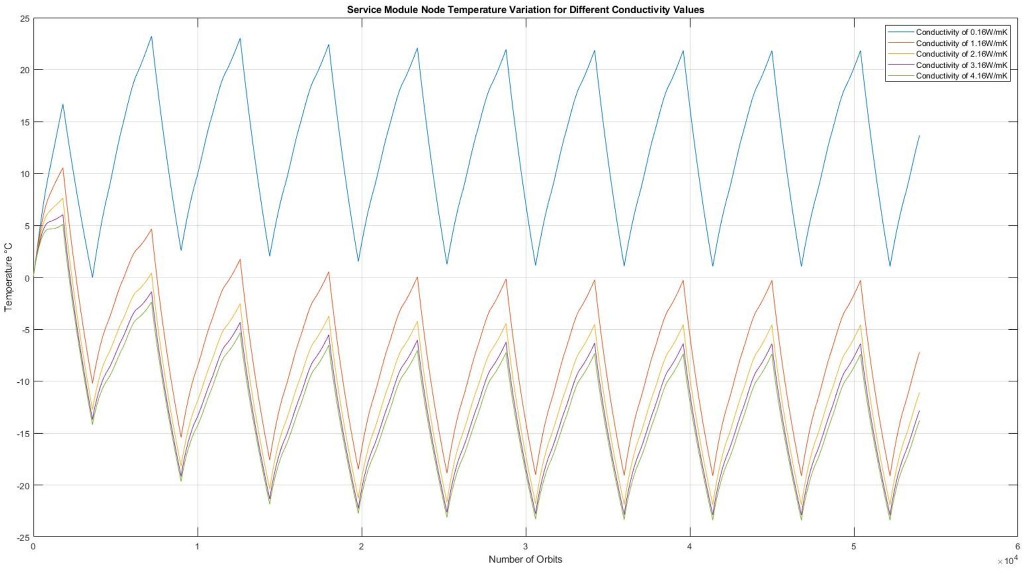

Figure 11.11: Temperature variations of the nodes as a function of Orbit and conductivity between the service module and mounting ring

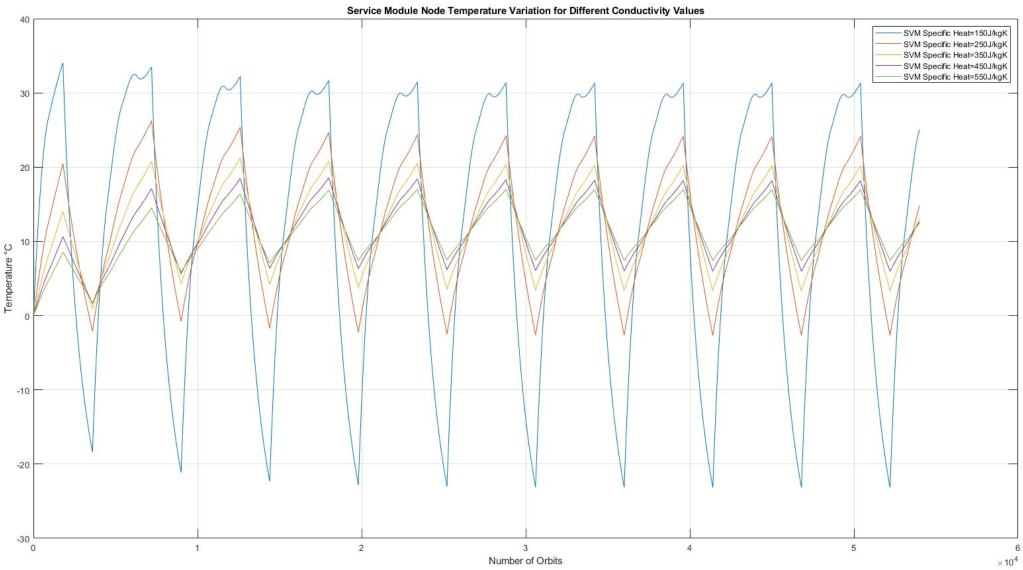

Figure 11.12: Temperature variations of the Service Module Node as a function of Orbit and specific heat capacity between the

11.5. THERMAL RISKS

This section will discuss the risks associated with the thermal subsystem.

11.5.1. RISK ASSESSMENT

- RAD-1: Radiator fails to export heat to space: this causes certain parts to heat up. In case the rise in temperature is significant, the reliability of the hardware will be lowered, making them more prone to failure. However as it doesn't affect the performance directly, the impact is considered *significant*. The probability is *unlikely*, due to the fact that this is not a complex mechanism. Furthermore, it will take time before the heat causes failures, while the mission lifetime is rather short.
- DEG-1: Degradation of surface components, leading to changing properties: this can cause a loss of perfor-

mance of the outer material, which affects its ability to capture/transfer/export heat. This degradation can happen in an irregular way, leading to concentrated areas with trapped heat. The impact of this event occurring is *significant*. Materials in space are affected by the local environment, the probability that it causes changes in the thermal analysis is *likely*.

11.5.2. Risk Mitigation

- RAD-1: The thermal subsystem is designed with margins on the thermal requirements of the components. This decreases the probability to *rare*.
- DEG-1: The thermal subsystem uses well known materials and techniques that are known in the aerospace industry and have been flight proven. Furthermore, these methods have been studied and tested thoroughly making it possible to estimate the effects of the space environment on the system. This lowers the impact to *minor*.

11.6. Conclusions & Recommendations

Based on the analysis discussed in this section, the thermal control of the service module can be accomplished by the use of passive means. This greatly reduces the development step needed to go from the SPS1 to the SPS2-FF system. Furthermore the mass associated with these passive means is small and there is no risk of active component failure. The final layout of the thermal design is as follows.

- High emissivity surface finish on the side opposite to the solar panel and on top. This ensures these surfaces do not face the Sun at any time thus maximising their efficiency.
- Body mounted solar panel on side 3 to generate power for the service module
- All other sides exposed to space are wrapped in Kapton Multi Layer insulation
- Thermal isolation between the mounting ring and the service module in the form of Makrelov GV30 reinforced thermoplastic insulation

The key aspect of this design is however its modularity. As previously stated if during a later design stage it is necessary to shift the temperature range of the service module either to a higher or lower temperature this can be done by passive means. More specifically if the temperature range needs to be shifted upwards the radiator on the side opposite to the thermal insulation can be decrease in favour of a surface finish which offers less emissivity. On the contrary if th temperature range is to be shifted downwards, the thermal insulation between the mounting ring and the service module can be decreased thus using the mounting ring as a heat sink.
For future design iterations it is recommended that the transient thermal model should be further verified. Additionally commercially available software should be used in order to evaluate the power input from the environment into the components in more detail. This refers especially to components shadowing each other. Furthermore it is recommended that the insulation between service module and mounting ring is investigated in more detail and a nodal model is set up which accounts for the heat transfer through the bolts. Lastly it has to be noted that for the thermal nodal analysis only the orbit option with eclipse condition has been considered. For the other orbit option, because the SPS-2 FF is in continuous sunlight, it is anticipated that the temperatures reached will be in excess of the maximum operating temperatures of the components in the service module and that controlling this temperature will represent a significantly larger delta than for the other orbit option. Thus it is recommended that without further investigation this orbit option shall be avoided.

12
Structural Design & Analysis Step 1

The main requirement for the structural design of the SPS-2 FF is that the development cost from the SPS-1 should be as little as possible. As a result, the 'delta' of the structural design from the SPS-1 to the SPS-2 should be minimised.

The first step in achieving a small 'delta' is determining all load cases that act on the spacecraft during launch, as given by section 12.1. A detailed explanation of the material selection will be given in section 12.2. The geometry and dimensions of the structure shall then be determined in section 12.3. The structure of the Service Module (SVM) will be elaborated in section 12.4. The SPS-2 FF should be able to separate from the AVUM+ after orbit insertion. At last, a structural mass estimation and recommendations for steps 2 and 3 will be given in section 12.5 and section 12.6, respectively.

12.1. Load Cases During Launch

From *Vega-C User Manual* [8] the Quasi-Static Loads (QSL) that act on the spacecraft can be obtained, as shown in Table 12.1. Using Equation 12.1, the forces based on the QSL's can be calculated. Here, m is the PPL mass which is taken as 1500 kg. The results are shown in Table 12.2.

$$F = QSL \cdot m \cdot g \tag{12.1}$$

Table 12.1: Table stating the Quasi Static Load factors (in g) from the Vega C users manual

Load Event		QSL (g) (+ = tension; - = compression		
		Longitudinal		Lateral
		Compression	Tension	
1	Lift off Phase	-4.5	+3.0	± 1.35
2	Flight with maximum dynamic pressure (Q_{max})	-4.0	+1.5	± 0.9
3	First stage flight with maximal acceleration and tail off	-5.0	+1.0	± 0.7
4	Second stage ignition and flight, Third stage ignition	-5.0	+3.0	± 1.3
5	Third stage maximal acceleration	-5.5	NA	± 0.2
6	AVUM flight	-1.0	+0.5	± 0.7

Table 12.2: Table stating the loads in [N] during each of the launch phases in compression, tension and lateral direction

Load Event		Compression (-) [N]	Tension (+) [N]	Lateral (+/-) [N]
1	Lift-off phase	66218	**44145**	**19865**
2	Flight with maximum dynamic pressure (Qmax)	58860	22073	13244
3	First stage flight with maximum acceleration	73575	14715	10301
4	Second stage ignition and flight, Third stage ignition	73575	**44145**	19130
5	Third stage maximal acceleration	**80933**	N/A	2943
6	AVUM flight	14715	7358	10301

Before any structural calculations can take place, a coordinate system has to be defined for the uppers stage. Figure 12.1 demonstrates the coordinate system in relation to the SPS-2 FF, the launcher structure and the PPL.

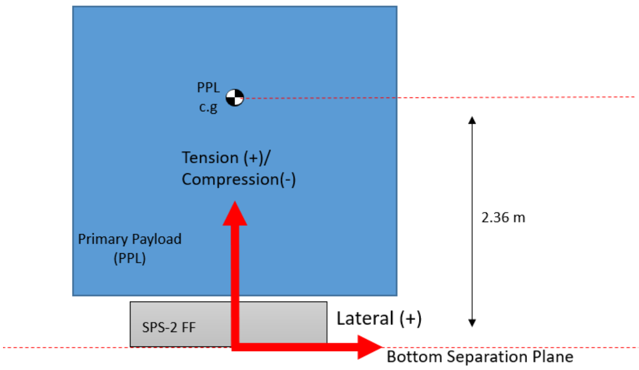

Figure 12.1: Axis system that is defined for the structural calculations.

Included in Figure 12.1 is also the distance from the bottom separation plane and the centre of gravity of the PPL . This is used for the calculation of the Margins of Safety (MS), in the following chapters.

12.2. Material Selection

Although the design of the SPS-2 FF should be based mostly on the design of the SPS-1, it is still worthwhile to investigate whether savings can be obtained when using different materials. The mission that the SPS-2 FF has to perform is much more exhaustive on the structure than what the SPS-1 has had to endure, as it has to stay in orbit for longer periods, has to perform complex pointing and perhaps in the step 3 design it might have to perform propulsive manoeuvres as described in section 13.3. Therefore, it is worthwhile to investigate what other material choices are available and define whether the material choice for the SPS-1 is still the correct choice.

In this chapter the materials used for the structural analysis will be defined, and their relevant properties are given. First the reasoning behind the material choice will be given, with an explanation as to why these materials are particularly suited for the SPS-2 FF structure. After this the mechanical properties of the materials are discussed, such as the yield stresses, the ultimate stresses and the fatigue properties. After this several other aspects of the materials are discussed such as the manufacturability, the price of the material and how sustainable the material is. Finally, a trade off between the suitable materials will take place in subsection 12.3.4.

12.2.1. Selected Materials

Three materials will be investigated:

- Aluminium 7075-T6
- Titanium Ti-6Al-4V
- Carbon Fibre/epoxy UniDirectional (UD) Preimpregnated (Prepreg)

Aluminium 7075-T6 has been chosen as this is the material that the SPS-1 has been made of. The material has been widely used in the aerospace, automotive and sporting goods industry due to its high strength and its relatively low density compared to other metals such as steel or titanium. This is quite important for the SPS-2 FF as it is a highly stressed component, which will need to be light as well. Every kilogram that is saved on the 'dry' mass can be spent on more payload or instruments [12].

Titanium Ti-6Al-4V is used as this material features a very high strength to weight ratio, excellent corrosion resistance and high temperature resistance. The SPS-2 FF requires a material to be strong and lightweight, and will have to endure a harsh space environment with changing temperatures. This material is also widely used in the aerospace industry mainly due to the aforementioned properties of the material. Additive manufacturing is also frequently using this material to print complex parts for the medical and aerospace industry. The advantage of this is that short cycle times can be obtained, offering flexibility for prototyping and the design process. This can be useful for the SPS-2 FF as the design requires adaptability and flexibility to support multiple different payloads for each flight.

Carbon Fibre/Epoxy UD Prepreg was chosen as it offers a new lightweight alternative, and can be specifically tailored to every specific strength, stiffness, temperature, chemical resistance and fatigue requirement. The choice of fibres and matrix can be specifically chosen and adjusted to the needs, as well as the layup that can be used. This combination of composite materials are widely used in aerospace, automotive and other industries where a high strength and low weight is required. For all the following sections a quasi-isotropic laminate is used made from the UD Prepreg, as this provides the easiest comparison to the other materials.

12.2.2. Mechanical Properties

In this section the yield stress, ultimate stress and fatigue properties are discussed. It starts with the Aluminium 7075-T6 alloy, followed by the Ti-6Al-4V alloy and ends with the Carbon Fibre/epoxy UD prepreg material. The data in this subsection is taken from the *CES EduPack* Database [12], where datasheets for each of the materials were obtained.

Table 12.3: Mechanical properties of the three chosen materials [12]. Values with * taken from[1].

Mechanical Property	Material			Unit
	Al 7075-T6	Ti-6Al-4V	CF/Epoxy UD Prepreg	
Density	2.77e3 - 2.83e3	4.41e3 - 4.45e3	1.55e3 - 1.58e3	[kg/m^3]
Young's modulus	69 - 76	110 - 119	49.7 - 60.1	[GPa]
Yield Strength (Elastic Limit)	359 - 530	786 - 910	603 - 738	[MPa]
Tensile Strength	434 - 580	862 - 886	603 - 738	[MPa]
Compressive Strength	393 - 530	848 - 1080	542 - 657	[MPa]
Shear Modulus	26 - 28	40 - 45	33 - 47	[GPa]
Shear Strength	330 - 360	620 - 675	210-260	[MPa]
Fatigue Strength @ 10^7 cycles	152 - 168	529 - 566	137 - 231	[MPa]
Service Temperature Range	-273 - 635	-273 - 420	-123 - 220	[° C]

The yield stress, ultimate stress and fatigue properties are far superior for the titanium alloy, at the expense of increased density. The composite material is following on several aspects, but lacking in the young's modulus and the fatigue strength. The aluminium is set between the titanium alloy and the composite material on some of the mechanical properties, and with others it is last. Additional graphs can be made to provide more insight how the materials relate with each other regarding the density and the young's modulus and the yield strength. Figure 12.2 shows the yield strength of the different materials, plot against the density of each.

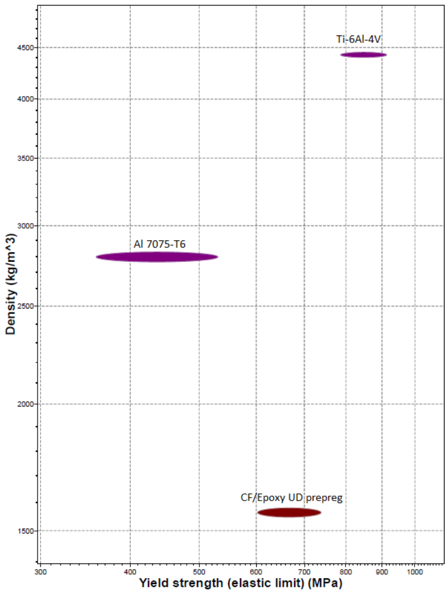

Figure 12.2: Graph illustrating the density versus the yield strength of the selected materials.

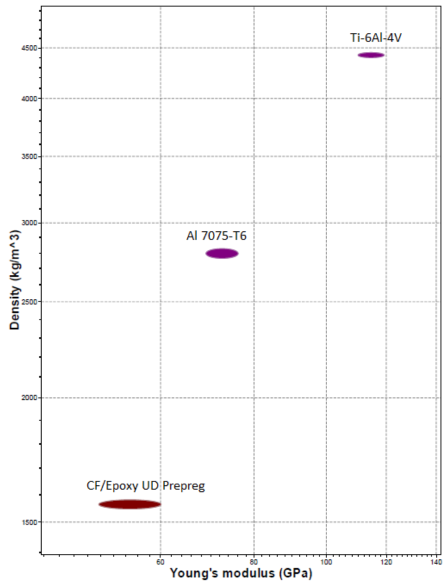

Figure 12.3: Graph illustrating the density versus the Young's modulus of the selected materials.

From Figure 12.2 it can be seen that the titanium alloy has the highest yield strength, yet also has a density that is significantly higher than the other materials. The CF/Epoxy UD prepreg has the lowest density, and its performance is in between the aluminium alloy and the titanium alloy. The aluminium alloy scores the lowest yield strength, and has a density that is in between the two other materials, as such it does not score that well for this mechanical property. Another important mechanical property is the Young's modulus, which can also be plotted against the density and is shown in Figure 12.3. From Figure 12.3 it is clear that once again the titanium alloy has the superior mechanical property, but now the CF/Epoxy UD prepreg performs the worst. The aluminium alloy scores considerably well for this important characteristic as well. Both these characteristics are quite important for the shell, as it has to be stiff to make sure that the primary payload does not deflect much, as that it can withstand the vibrations of the launch. Furthermore, the tensile strength is important as this governs the strength of the SPS-2 FF during flight, and makes sure that it keeps the structural integrity. The compressive strength is also important for launcher structures, however for all these materials it is close to the yield strength as such the yield strength will be used. The structural analysis performed in section 12.3, uses these three materials and will investigate the mass of the structure using these different materials.

[1]URL: http://www.performance-composites.com/carbonfibre/mechanicalproperties_2.asp, Cited: 13th June 2019

12.2.3. TEMPERATURE EFFECTS ON MATERIAL PROPERTIES

For the metals only, *CES EduPack* also indicates the effect that temperature has on selected properties. In this section the mechanical properties will be placed in the thermal environment which is described in section 11.1. In that section the thermal environment for the structures is described as ranging from -45 to +65 °C. As the young's modulus and the yield strength were analysed in subsection 12.2.2, these will also be analysed and placed in the temperature range of the structure.

First, the aluminium alloy will be analysed. The yield strength compared to the temperature takes a steep decline past 100 °C, as can be seen in Figure 12.4. For temperatures of above 100°C the yield strength takes a significant fall, and thus the thermal subsystem should be designed to avoid these temperatures or the structure should be designed to allow for the reduced strength.

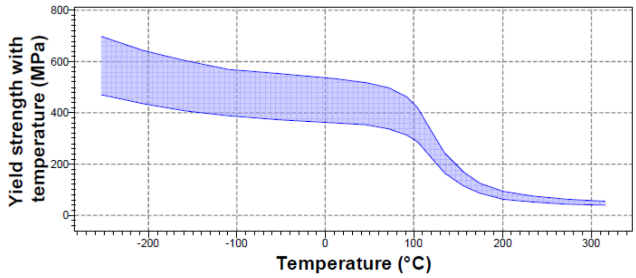

Figure 12.4: Temperature effect on the yield strength of the aluminium 7075-T6 alloy

For the Young's modulus, the same graph is made. The Young's modulus does not take as significant as fall a with the yield strength, but declines in a more steady manner. It can be seen that the Young's modulus is around half at around 300°C, which is a temperature that will not be encountered during nominal operation of the SPS-2 FF. The decrease in Young's modulus is minor across the temperature range that is specified for the structure of the SPS-2 FF, but will be verified with structural calculations.

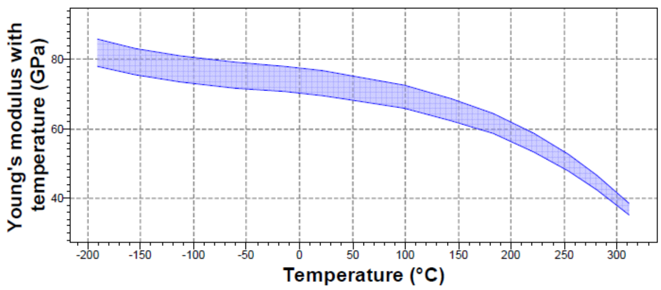

Figure 12.5: Temperature effect on the Young's modulus of the aluminium 7075-T6 alloy

Second, the Titanium Ti-6Al-4V alloy. For the yield strength of the alloy, the drop in strength is significant and the rate decreases as the temperature increases. This can be seen in Figure 12.6. In the temperature range provided the yield strength does vary significant, and thus the reduced strength has to be verified with structural calculations.

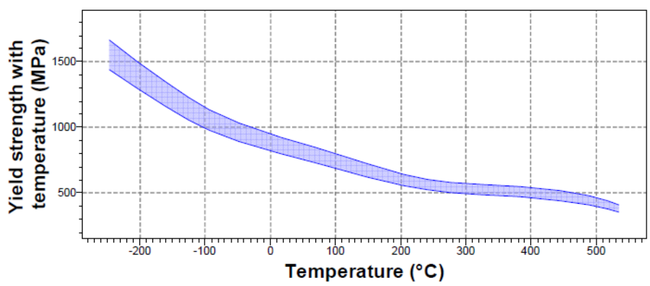

Figure 12.6: Temperature effect on the yield strength of the Titanium Ti-6Al-4V alloy

The effect of temperature on the Young's modulus for the Titanium Ti-6Al-4V alloy can be seen in Figure 12.7. The graph has the same shape as for the aluminium alloy, and the drop in the modulus is minor across the temperature range. For the temperature below 0°C there is no data, and the value at 0°C will be taken. although the drop is minor, it should be verified whether this has any significant effect on particularly the vibrational loading on the structure.

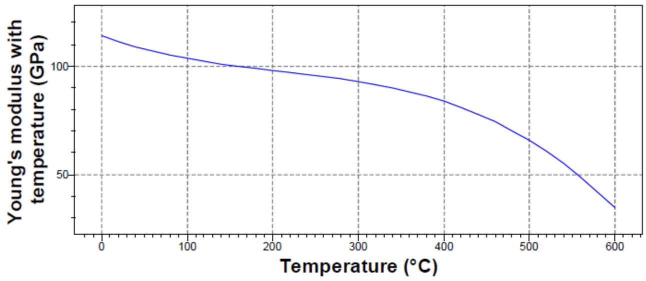

Figure 12.7: Temperature effect on the Young's modulus of the Titanium Ti-6Al-4V alloy

As there is no concrete information on temperature affecting the properties of CF/Epoxy UD Prepreg, only the metals have been analysed. Both the metals show degradation of the mechanical properties when the temperature increases, and structural verification will have to be performed on the structure as to verify whether the structure can retain its structural integrity during all phases of the flight.

12.2.4. MANUFACTURABILITY, PRICE & SUSTAINABILITY

It is important to also look at other aspects of the materials, and not only at the mechanical properties. Therefore information has also been collected on the manufacturing, price of the raw material, and sustainability aspect of the materials. This data is based on the CES Edupack database [12] and is summarised in Table 12.4.

Table 12.4: Table giving information on the manufacturing, price and sustainability aspects of the selected materials [12].

Material Property	Material			Unit
	Al 7075-T6	**Ti-6Al-4V**	**CF/Epoxy UD Prepreg**	
Manufacturability	Easy	Medium	Hard	[-]
Price (raw material)	3.37 - 3.7	17.7 - 18.2	31.7 - 35.2	[EUR/kg]
Primary Production Energy CO2 Footprint	12.5 - 13.8	38.4 - 42.3	45.8 - 50.5	[kg/kg]
Primary Production Embodied Energy	184-203	665-722	655-723	[MJ/kg]
Recycling	Yes	Yes	No	[-]
Recycle fraction in current supply	40.5 - 44.7	20.9 - 23.1	0.1	[%]

The table presents the data on manufacturing in the terms easy, medium and hard, this is based on the machining speed of the metal materials, and the complexity of manufacturing. The aluminium alloy has been given the value easy, as the SPS-1 is also made from this material and there is thus some experience with producing such a structure from this material. The titanium alloy has been designated as the same production process can be followed as the aluminium alloy, only with different processing parameters, such as feedrate and RPM. The CF/Epoxy UD Prepreg material is much more complex to produce as a new production method will have to be used, rather than something that has been done before, therefore it is denoted as hard.

The price of each of the raw materials has also been given. This is based on an estimate but still provides an insight into how the materials relate to each other. Taking the aluminium alloy as a base, the composite costs around 10 times more, and the titanium costs around 5 times more. This is only an estimate for the raw material costs, but it does indicate that the aluminium is the obvious cheaper choice. Another aspect highlighted is the sustainability of the material by quantifying the production energy CO2 footprint, the recycling possibility and how much of the current supply is recycled. Taking these aspects into account, the aluminium is the best choice as it has the lowest CO2 production foot print, has plenty recycling options and around 40% of the current supply is recycled aluminium. The composite material is the obvious worst as it has the largest footprint, no recycling options and almost none of the current supply is recycled. The titanium alloy scores in between these two, but much better than the composite material.

12.3. SPS-2 FF Geometry Sizing

The geometry and dimensions of the SPS-2 FF shall be selected in this section. The following subsections contain structural computations for different kinds of geometries and materials. Together with the sustainability and thermal performance (chapter 11) a trade-off of the geometry and materials can be made for the SPS-2 FF structure.

12.3.1. Solid Cylinder Structure

This subsection will describe the steps taken to determine the dimension of the SPS-2 FF structure. Here, a cylindrical structure with the same diameter and height as the SPS-1 is chosen, based on the separation system used. These dimensions have values 937 and 455 mm respectively and are retrieved from Airbus' technical drawings. Furthermore, from communication with the client it can be retrieved that the limit of the Center of Gravity (CG) for a PPL mass of 1500 kg is equal to 2.36 m with respect to the bottom separation plane. All known parameters that are relevant to the structure of the SPS-2 FF are given by Table 12.5. These parameters will be extensively used in the vibrational and structural performance, as described in the following subsections.

Table 12.5: General known parameters that are relevant to the structure of the SPS-2 FF.

Parameter	Symbol/Abbreviation	Value	Unit
Distance CG PPL & Bottom Separation Plane	d_{CG}	2.36	m
Height SPS-1 Cylinder	L	0.455	m
Diameter SPS-1 Cylinder	D	0.937	m
Primary Payload Mass	m_{PPL}	1500	kg
Total SPS-2 Mass	m_B	250	kg
Natural Frequency (Lateral)	$f_{n_{lateral}}$	20	Hz
Natural Frequency (Longitudinal)	$f_{n_{axial}}$	75	Hz
Factor of Safety (Yield)	FS_{yield}	1.1	-
Factor of Safety (Ultimate)	FS_{ult}	1.25	-
Margin of Safety	MS	0.25	-

Vibrational Analysis Solid Cylinder

From *Space Mission Analysis And Design (SMAD)* [22] a preliminary estimation of the vibrational performance of the structure can be conducted. As shown in Figure 12.1, it can be assumed that the SPS-2 FF is clamped to the AVUM+. In reality, the structure of the AVUM+ will vibrate itself which should be taken into account when conducting a more detailed vibrational analysis. Furthermore, it is assumed that the Primary Payload (PPL) is a tip mass that rests on the SPS-2 FF structure. At last, the cylinder is assumed to be solid which means that attachment points, holes and flanges are neglected in this approximation. From SMAD it can therefore be assumed that the structure is *complex*, as illustrated in Figure 12.8(a). Corresponding natural frequencies in lateral $f_{n_{lateral}}$ and axial $f_{n_{axial}}$ direction are given in Equation 12.2 and Equation 12.3 respectively.

$$f_{n_{lateral}} = 0.276\sqrt{\frac{EI}{m_{PPL}d_{CG}^3 + 0.236 m_B d_{CG}^3}} = 0.276\sqrt{\frac{E\pi R^3 t}{m_{PPL}d_{CG}^3 + 0.236 m_B d_{CG}^3}} \tag{12.2}$$

$$f_{n_{axial}} = 0.160\sqrt{\frac{AE}{m_{PPL}d_{CG} + 0.333 m_B d_{CG}}} = 0.160\sqrt{\frac{2\pi R t E}{m_{PPL}d_{CG} + 0.333 m_B d_{CG}}} \tag{12.3}$$

Here the variable E is the Young's Modulus, I is the Area Moment of Inertia (AMOI), d_{CG} the distance between the Center of Gravity (CG) of the PPL and bottom separation plane, R is the radius, t is the thickness of the cylinder, m_{PPL} is the mass of the PPL and m_B is the mass of the SPS-2 cylinder. The frequency requirements described in the *Baseline Report* [11] show that natural frequency has to be equal or larger to 75 and 20 Hz in axial and lateral direction respectively. Combining these requirements with the known geometries (Table 12.5) of the SPS-2 and Equation 12.2-Equation 12.3 results in a minimum cylinder thickness for the three materials, as given by Table 12.6.

Table 12.6: Thickness of the ring for the three materials, based on a preliminary vibrational analysis.

	Material		
Parameter	**Al7075-T6**	**Ti-6Al-4V**	**CF/Epoxy UD Prepreg**
Thickness [mm]	4.62	2.89	6.03
Mass [kg]	17.37	17.15	12.64

STRUCTURAL ANALYSIS SOLID CYLINDER

From Table 12.3.1 a minimum cylinder thickness for the vibrational analysis can be obtained. After this, a structural analysis is to be conducted where the structure is sized for strength and stability. For stability of the structure, the critical buckling stress σ_{cr} has to be determined first. The equation for cylinder buckling stress is given by Equation 12.4-Equation 12.6.

$$\phi = \frac{1}{16}\sqrt{\frac{R}{t}} \tag{12.4}$$

$$\gamma = 1.0 - 0.901(1.0 - e^{-\phi}) \tag{12.5}$$

$$\sigma_{cr} = 0.6\gamma\frac{Et}{R} \tag{12.6}$$

$$P_{cr} = A \cdot \sigma_{cr} \tag{12.7}$$

The second step requires an estimation of the equivalent combined axial, lateral and bending loads on a cylinder as given by Equation 12.8[22].

The ultimate load P_{ult}, which takes a safety factor into account, can be determined as follows: $P_{ult} = P_{eq} \cdot FS$, where FS is the Factor of Safety (FS). This is also illustrated in Figure 12.8(b).

$$P_{eq} = P_{axial} \pm \frac{2M}{R} \tag{12.8}$$

Equation 12.7 and Equation 12.8 can be used as input for the Margin of Safety (MS), as given by Equation 12.9. The MS describes if the structure can withstand a specific type of stress. If this is not the case, the process has to be reiterated, by increasing the thickness of the skin which increases the stiffness of the structure. From *Spacecraft Structures* [38] it can be obtained that a MS of values greater or equal to 0.25 results in an optimal design.

Table 12.7: Table containing Margin of Safety's for different load cases and materials.

	Margin of Safety [-]		
Loading Condition	**Al7075-T6**	**Ti-6Al-4V**	**CF/Epoxy UD Prepreg**
Buckling	8.64	4.26	12.47
Tensile Yield	139.75	147.59	244.03
Tensile Ultimate	139.85	157.98	214.63
Compression	69.44	91.14	118.50
Bending	13.01	17.41	11.45
Shear	205.83	214.16	56.85
Bending + Tensile	13.25	14.04	23.80
Bending + Compression	12.14	12.87	21.87

$$MS = \frac{AllowableLoad/Stress}{AppliedLoad/Stress} - 1.0 \geq 0.25 \tag{12.9}$$

The QSL's described in section 12.1 and the mechanical properties described in Table 12.3 can be used to determine the tensile yield σ_{ty} (Figure 12.8(c)), tensile ultimate σ_{tu}, compression σ_c (Figure 12.8(d)), shear stresses σ_s (Figure 12.8(e)) and bending σ_b (Figure 12.8(f)) (Equation 12.10-Equation 12.14) that act on the structure. Combinations of combined bending with compression stress $\sigma_{comb_{b+c}}$ and bending with tensile stress $\sigma_{comb_{b+t}}$ (Equation 12.15-Equation 12.16) will also be taken into account. Again, the MS is calculated for each type of stress and is iterated if the value of MS ≤ 0.25. From the results, given by Table 12.7, it can be obtained that the vibrational analysis is the limiting factor in designing the thickness of the ring, since the MS of all loading conditions are ≥ 0.25.

$$\sigma_{ty} = \frac{P_{tension} \cdot FS_{yield}}{A} \tag{12.10}$$

$$\sigma_{tu} = \frac{P_{tension} \cdot FS_{ult}}{A} \tag{12.11}$$

$$\sigma_c = \frac{P_{compression} \cdot FS_{yield}}{A} \tag{12.12}$$

$$\sigma_b = \frac{(P_{lateral} \cdot (d_{CG} - \frac{L}{2}) + P_{lateral_{SPS}} \cdot \frac{L}{2})FS_{yield} \cdot R}{I} \tag{12.13}$$

$$\sigma_s = \frac{P_{lateral} \cdot FS_{yield}}{A} \tag{12.14}$$

$$\sigma_{comb_{b+c}} = \sigma_b + \sigma_c \tag{12.15}$$

$$\sigma_{comb_{b+t}} = \sigma_b + \sigma_t \tag{12.16}$$

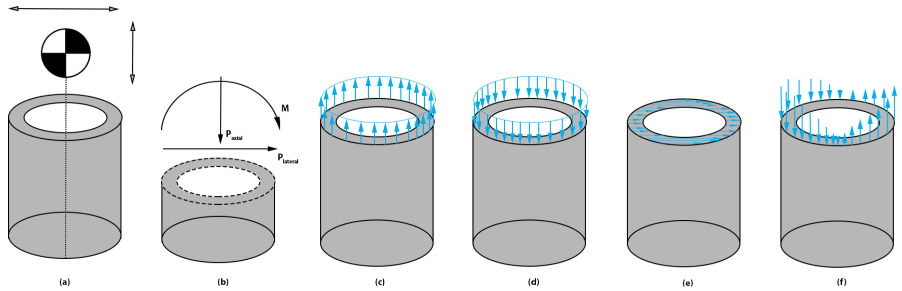

Figure 12.8: Complex beam for the frequency analysis illustrated in (a)[2]. The equivalent load is shown in (b). Tension, compression, shear and bending stresses are illustrated in (c), (d), (e) and (f) respectively.

12.3.2. SKIN-STRINGER CIRCULAR STRUCTURE

This section describes if adding stringers to the skin is beneficial for the overall performance of the structure. The stiffness of the overall structure increases if stringers are added to the skin. Consequently, the thickness and mass of the skin can be decreased. However, the increase in the amount of stringers will mean that the stringer mass also increases. An optimum is to be found for the thickness of the skin and the amount of stringers implemented in the structure. In this approach it is assumed that the skin will not buckle, which means that the skin helps to stringers in carrying the applied loads. Furthermore, two stringers will be used in the first calculation and an iteration with more stringers will follow afterwards. From Table 12.3.1 it can be obtained that the thickness of the solid circular skin is constraint by the frequency analysis. This means that the Area Moment Of Inertia (AMOI) I_{lat} in Equation 12.2 should remain constant. The formula for the AMOI of the stringers is given by Equation 12.17 and can be computed if a smaller skin thickness compared to the solid cylinder skin is chosen.

$$I_{stringers} = I_{lat} - (I_{skin})_{new} = I_{lat} - \pi R^3 t \qquad (12.17)$$

$$I_{stringers} = \sum A_{stringer} d^2 \qquad (12.18)$$

The parallel axis theorem can be used to calculate the area of each stringer $A_{stringer}$ as shown in Equation 12.18. The AMOI around the stringer's own Center of Mass (CoM) is negligible compared to its corresponding steiner term ($I_{cm} << \sum A_{stringers} d^2$) and can therefore be neglected. Equation 12.18 shows that d is the distance from each cylinder to the neutral axis and $A_{stringer}$ the cross-sectional area of the stringer. Subsequently, this can be used as input for the combined mass of the stringers and ring as given by Equation 12.19. Here, n is the number of stringers and ρ the density of the material of the stringer. This material type is assumed to be the same as the materials used in subsection 12.3.1.

$$m = m_{stringers} + m_{ring} = (nA_{stringers} + 2\pi R t)L\rho \qquad (12.19)$$

$$\sigma_{cr} = \frac{k\pi^2 E}{12(1-\nu^2)}\left(\frac{t}{b}\right)^2 \qquad (12.20)$$

The stability of this chosen panel has to be checked to see if the structure can withstand the applied loads that act on the spacecraft. The formula for the compressive buckling stress of a panel is given by Equation 12.20. Here, k depends on factor Z (Equation 12.21) and its relation is illustrated in *Space Mission Analysis And Design, Fig. 11-34* [22]. Furthermore, ν is the Poisson Ratio and b is the distance between each stringer. Again, as described in Table 12.3.1, the MS can be applied to ensure it is capable of withstanding the applied loads. If $MS \geq 0.25$ the thickness should be decreased and the process should be iterated till a convergent solution is found. After this, an extra stringer should be added and the process shall repeat itself. This process is done for the three materials selected in section 12.2 and the corresponding results are given by Table 12.8. The combined masses are larger compared to the respective masses of the solid ring structure, as given by Table 12.6. For this design it is therefore not preferable to include stringers in the structure.

$$Z = \frac{b^2}{rt}(1-\nu^2)^{1/2} \qquad (12.21)$$

[2] URL: https://autodesk.i.lithium.com/t5/image/serverpage/image-id/199600i36F29371130CFE28?v=1.0 [cited on 23th of June 2019]

Table 12.8: Results of the implementation of stringers in the circular structure.

Al7075-T6	**Number of Stringers**			**Ti-6Al-4V**	**Number of Stringers**			**CF/Epoxy UD**	**Number of Stringers**		
Parameter	**4**	**8**	**12**	**Parameter**	**4**	**8**	**12**	**Parameter**	**4**	**8**	**12**
Thickness Ring [mm]	1.32	1.51	1.52	Thickness Ring [mm]	2.43	2.43	2.43	Thickness Ring [mm]	5.07	5.07	5.07
Mass Skin [kg]	4.97	5.69	5.73	Mass Skin [kg]	14.42	14.42	14.42	Mass Skin [kg]	10.63	10.63	10.63
Mass Stringers [kg]	16.48	13.31	12.66	Mass Stringers [kg]	3.64	3.12	2.98	Mass Stringers [kg]	2.68	2.30	2.19
Combined Mass [kg]	21.46	19.00	18.39	Combined Mass [kg]	18.06	17.54	17.40	Combined Mass [kg]	13.31	12.92	12.82

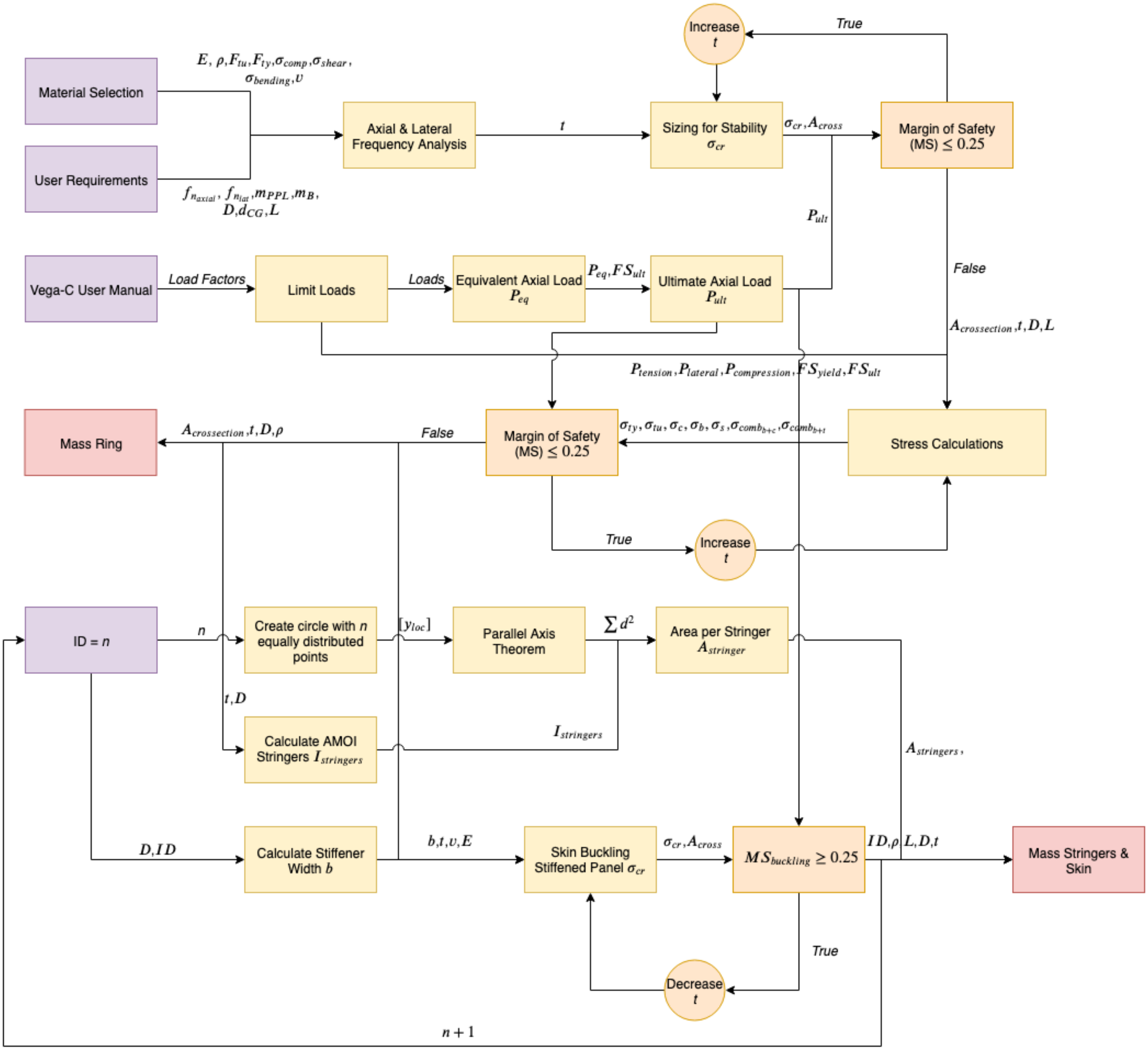

Figure 12.9: Software block diagram of the skin and stringer calculations.

12.3.4. TRADE-OFF GEOMETRY & MATERIAL

Based on the material and geometry analysis described in section 12.2 and section 12.3 respectively, a trade-off of the overall structure can be made. The first parameter in the trade-off will be the geometry of the structure. Table 12.8 shows that increasing the number of stiffeners results in a lower combined skin and stringer mass. From subsection 12.3.3 it can be obtained that increasing the number of stiffeners beyond 12 results in a minimum decrease of mass (around 0.02 kg per added stringer). Comparing the masses of the circular and circular stiffened structure, as described in Table 12.6 and Table 12.8, results in a small differential between the two in favour of the circular ring. Therefore, a circular solid ring is considered.

The second parameter to be considered is the material of the skin. The criteria used in this trade-off are listed below and are given weights between 1 and 5.

1. **Mass:** The mass of the ring is important in this trade-off (**SPS-2-LEI-MASS-1**), since it determines how much dry mass can be put on the spacecraft. Therefore, it has been granted a weight of 4.
2. **Cost:** Because of the budget given by the client (**SPS-2-CS-BUD-1**), it is important to consider the cost of the product. This includes the raw material, production and labour costs. Thus, this criteria has been given a weight of 5.
3. **Manufacturability:** Based on the past experience with a certain material it might be easier to work with that specific material. However, for other materials, a different production process might be necessary, which has to be taken into account. Therefore, this criteria is given the weight 3.
4. **Sustainability:** Four launches per year are to be expected to launch from 2022 onwards. The CO_2 emissions released and energy used during production should therefore be limited (**SUS-FW-1.4** & **SUS-FW-1.6** [11]). Furthermore, the percentage of raw materials that are wasted should also be limited and should be recycled as much as possible (**SUS-FW-1.10**). Therefore, this criteria has been given a weight of 2.

Starting with the mass criteria, it can be obtained from Table 12.6 that the CF/Epoxy UD structure is the most lightweight structure, followed by the aluminium and titanium alloy. To quantify this as a number from 1-10 in the Trade-Off, it is chosen that one kg deficit is equal to one point off. Therefore, the aluminium and titanium alloys have been given a 5 and the CF/Epoxy UD structure is given a 10. For the cost, a quick glance at Table 12.4 shows that the aluminium alloy is by far the cheapest material followed by titanium alloy. Furthermore, production of the CF/Epoxy UD Prepreg material costs ten times more than aluminium, not including the labour cost that are substantial when using CF/Epoxy UD Prepreg. It is chosen such that a deficit of 10 EUR/kg results in one point off the grade. Adding the large labour cost for CF/Epoxy UD Prepreg results in a grade of 2. The aluminium and titanium alloys have been given a 9 and 7, respectively. From Table 12.4 it can be obtained that the manufacturability is easy, medium and hard for aluminium alloy, titanium alloy and CF/Epoxy UD Prepreg respectively. Furthermore, as mentioned in subsection 12.2.4, since an aluminium alloy is already known to be used in the SPS-1, it is easier for the production crew to reproduce a similar ring of Al7075-T6. subsection 12.2.4 also mentions that the titanium alloy has the same production process as the aluminium alloy. For CF/Epoxy UD Prepreg, a new production method has to be used, which increases the complexity for the production crew. This could increase the risk of making mistakes and increases the development cost. Therfore, it has been chosen that aluminium, titanium and CF/Epoxy UD Prepreg have been given a 8, 7 and 4 respectively. Table 12.4 can be used again for the sustainability criteria, where it is obtained that the aluminium and titanium alloy are recyclable and CF/Epoxy UD Prepreg is not. Furthermore, twice as much material of the aluminium alloy can be recycled compared to titanium alloy. The CO_2 emissions and energy used for production of the material is small for the aluminium alloy and large for both the titanium alloy and CF/Epoxy UD Prepreg. Therefore, the aluminium alloy has been given a 9, titanium alloy a 5 and CF/Epoxy UD Prepreg a 1.

The grades for each parameter is given by Table 12.9. Here, grades 1-3 are illustrated in Red (R), 4-5 in Orange (O), 6-7 in Blue (B) and 8-10 in Green (G). From the total grade it can therefore be determined that Al7075-T6 will be used as material for the SPS-2 structure.

Table 12.9: Material Ring Trade-Off Table.

Material	Mass	Cost	Manufacturability	Sustainability	Score
Al7075-T6	5 O	9 G	8 G	9 G	7.6
Ti-6Al-4V	5 O	7 B	7 B	5 O	6.1
CF/Epoxy UD	10 G	2 R	4 O	1 R	4.6

12.3.5. Sensitivity Analysis Trade-Off Material

A sensitivity analysis is conducted on the material trade-off given in subsection 12.3.4. This is to check if the outcome of the trade-off still stays the same if certain weights or parameters are changed. The weight of the mass can for example be increased if more emphasis is to be put in this parameter in the design. Increasing the weight from 4 to 5 will result in a increase of +0.3 points for the CF/Epoxy UD Prepreg, but no net increase for the aluminium and titanium alloy. It can therefore be concluded that changing the weight of the mass does not change the outcome of the trade-off. Less emphasis can be put on the manufacturability criteria if for example the client has experience in working with titanium and composite structures. If this is the takes, it can be assumed that the manufacturability criteria is less important in the trade-off and its weight can be decreased from 3 to 1 for example. Calculating the new scores for the materials results in ±0.1 difference compared to its old score. Therefore, it can be concluded that changing the weight of the manufacturability criteria does not change the outcome of the trade-off. At last, an increase in the weight of the sustainability criteria can be applied. This can be increased if for example the client wants to put a lot of emphasis on reducing the CO_2 emissions and maximising the amount of material that can be recycled. A weight change from 2 to 5 is to be applied, which results in an even more deficit between the grade of the aluminium alloy and the titanium alloy. This means that this change in weight will not result in a change of the outcome of the trade-off. With these three changes in mind, it can be therefore concluded that the aluminium alloy will still be chosen even for different weight configurations.

12.4. Design of the Service Module

This section will focus on the Service Module, which will house all the subsystems of the SPS-2 FF. First the purpose and the relevant requirements for the service module will be discussed, after which a section will focus on the integration of the service module. Next several structural concepts for the service module will be outlined, with a trade off selecting the best option for the SPS-2 FF. Following this is the configuration of all the subsystem components into the service module, and the final layout of the service module. Finally, a structural and vibrational analysis will be done on the service module, verifying that the design will meet the structural requirements, and a concluding overview is given of the service module.

12.4.1. Purpose Service Module & Relevant Requirements

The purpose of the Service Module (SVM) is to protect the subsystems from the environment. This includes the loads induced during launch and the harsh environment in space. Furthermore the same QSL's as defined in Table 12.2 will be used, but now with regards to the centre of gravity and mass of the service module. In order to make a baseline design of the service module, requirements have to be set on the size and the mass of the service module. For now this results in the following design requirements:

- **SPS-2-SVM-1:** The mass of the complete service module (structure and components) shall be no more than 35kg.
- **SPS-2-SVM-2:** The size of the service module shall be no more than 30x30x40cm (approximate size of a QuadPack)

12.4.2. Interface with SPS-2 FF Ring

The interface of the service module with the SPS-2 FF ring can be done in several ways. The easiest method is to use an existing interface that is present on the SPS-1 ring. Two options are present here, it is possible to use the IMDC sequencer integration points, or use one of the QuadPack integration ports. For the first option, there is the possibility to mount the Service Module in between two QuadPack integration points. The connection to the SPS can be done via means of a bracket and utilising the holes present in the ring. There are however several reasons why these integration points cannot be used:

- Currently in the configuration there is only one IMDC sequencer on the SPS, however Airbus Defence and Space requested that the option to have two sequencers on the SPS remain open.
- The IMDC sequencer is currently 160x170x250mm, which will most likely not be large enough for all the subsystem components. There is also not enough room to allow for a larger structure at these locations.
- In the case of the solar panels, only extension in the axial axis is possible, as the QuadPacks are close to the integration point which will not allow for radial deployment. If the structure was to be longer, the solar panels could be deployed in the radial direction, however they could cross the deployment trajectory of the payloads in the neighbouring QuadPacks.

Due to these reasons, utilising the integration ports of the IMDC sequencer is not a viable option for the SPS-2 FF. However, another integration port is also possible. For instance, the Service Module could use the integration port used for a Quadpack. There are 6 possible locations that the Service Module could be placed at, where each one of them is identical to one another. A front view of the integration of the QuadPack can be found in Figure 14.2. Using the QuadPack integration points has several advantages:

- All integration points are identical, thus the service module placement is flexible
- There is room to fit a larger and heavier Service Module
- The structure already has the structural strength and stiffness to accommodate a maximum QuadPack payload

The Service Module will thus utilise the same integration ports that have been used for the QuadPacks, as this has several advantages over the integration port of the IMDC Sequencer. For the analysis in the detailed design phase, the Service Module has been placed in the 'centre' of the ring, as shown in Figure 12.10.

12.4.3. STRUCTURAL CONCEPT OF THE SERVICE MODULE

In this subsection several structural concepts for the service module will be presented, and a final concept is chosen. When the concept has been chosen, a preliminary design can be made, which will be further investigated in the sections that follow. Three options have been outlined for the Service Module:

- Commercial Off The Shelf Concept: A concept which will use a QuadPack outer structure and COTS inner structure.
- Hybrid Concept: A concept which will feature a QuadPack as the outer structure, and a custom designed inner structure which will have integrated integration points in the structure
- Custom Designed Concept: a concept which features a custom designed outer structure and a custom designed inner structure with integrated integration points.

These three options will be investigated and on four criteria: Performance, Sustainability, Risk and Cost. These criteria are chosen as they are most relevant for the Service Module and will allow for a proper concept choice.

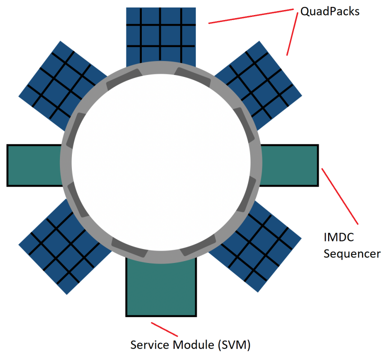

Figure 12.10: Placement of the service module relative to the other QuadPacks and the IMDC sequencers.

PERFORMANCE

For the performance, the concepts are rated in the following categories: subsystem component integration, space environment resistance and mass. The performance requirements which are important for the design are also shown in chapter 3. The Commercial Off the Shelf concept scores well for the space environment resistance and worse for both the subsystem component integration and the mass. The COTS concept has been acceptance tested and has flight heritage and is thus properly designed to resist the space environment. In terms of thermal management it also scores well as it can use the same exact systems that are used on the other QuadPacks. The subsystem component integration and mass score low as the COTS concept has not been specifically designed for this and is thus not optimised. Therefore the integration of the subsystems will require more supporting and mounting structures, which negatively influences the mass of the system. The Hybrid concept scores well for the space environment resistance and the subsystem component integration categories. The space environment resistance is delivered by the COTS outer structure, which also allows for the same thermal management systems as the other QuadPacks. The subsystem component integration is made easier as the inner structure design can be adapted such that it integrated well with the outer structure, and that it also has easy integration with each of the subsystem components. For the mass it does score lower, as the outer structure is still not optimised for the function it has to provide. However, the inner structure will be mass optimised as such it still scores higher than the COTS concept. The Custom Designed concept scores good for the subsystem component integration and the mass, but scores less for the space Environment Resistance. The system can be completely optimised for the functions of the Service Module and thus can provide optimal mass and subsystem component integration. The space system environment resistance can also be designed for, however this will not be as robust as what the QuadPacks already have, and another system will be necessary to operate the thermal management.

SUSTAINABILITY

Each of the concepts will be rated on the sustainability of the design, as it is a requirement from the client chapter 3, to ensure that the ecological footprint of the structure is as low as possible, and to have an overview of the resources spent producing it. For the Commercial Off The Shelf, all components are produced by external companies. This means that the ecological footprint of the production is normally lower than if everything is custom made, as the production volume for COTS component is much higher. Furthermore, no significant resources have to be spent on designing, testing and production of the components as this has already been done by the supplier. Therefore, the COTS scores well on the sustainability criteria. For the Hybrid concept, the outer structure scores well on the sustainability as it is a COTS component but scores less for the inner structure. The inner structure will have to be custom made, which includes the design, testing and production. As this is a custom made component the ecological footprint will be larger than for the COTS component, as a production cycle has to be set up for this component only and the production volume is low compared to COTS components. Therefore, the hybrid concepts scores average on the sustainability of the concept. The Custom Made concept scores the worst of all on the sustainability as it only features custom made components, which will require significant resources to design, test and produce. Each of the components is custom made, which means that the production volume will be low, and thus will have a larger ecological footprint compared to the other concepts.

RISK

Each of the concepts will be rated on the number of risks, the potential magnitude, potential mitigation and the effect of this mitigation. An important requirement is also the technical feasibility of the design, which is closely related to the risk factors of the concept. For the Commercial Off The Shelf Concept, there are not a not a large number of risks related to the design, testing and production, as all of this has already been performed. A large risk for the concept is that every component is currently from a sole supplier, which creates a significant problem if the supplier changes the design, cannot deliver the products on time, or is in financial problems and ceases to exist. This can be solved with contracts with the sole supplier obligating them to deliver the products for the foreseeable future, or adapt the design to also allow for integration of components from other suppliers. The effect of this will be in the form of financial compensation in order to obligate the supplier, and adapting the design to allow for other components might result in delays in the design and production process. This concept scores the best out of the three for the risks. For the Hybrid concept, the same risks apply for the outer structure as with the Commercial Off The Shelf concept. For the inner structure new risks can be defined. The inner structure will require a redesign, will require testing and a production process. Risks can be defined regarding the planning and resources. Risks can be mitigated by proper planning and having the design and production done by external companies. This will not completely remove the risk related to the design, production and verification of the components but it will make sure that much less resources are necessary from the company in terms of time. The effects of this will result in an increase in necessary financial resources, but will allow for better planning and risk mitigation, as resources can be spent elsewhere. This concept scores average for the risk management, as the external structure scores well but the inner structure scores less good. For the Custom Made concept the number of risks are the greatest, and with the largest magnitude. Doing the design, production and verification brings many risks with it, especially for the planning. Therefore attention has to be paid to the resource allocation, and perhaps certain design phases can be outsourced to other companies. The effect of this is that it will require significant financial resources, as with this concept more things will have to be outsourced, and more control on the design may be lost. This concept scores the worst for the risk characteristics.

COST

Each of the concepts will be analysed for their costs, including the development cost, production cost and in the case of the Commercial Off The Shelf concept the actual price of the components. Taking the cost of a concept into account is necessary as there is a limited budget for the SPS-2 FF design, as described in section 24.2. The Commercial Off The Shelf, will have the lowest development and production cost, but the actual listing price is fairly high. The inner structure is quoted as at least € 11,950 for the 12U version, and the deployer has no cost attributed on the website. However, some cost will have to be added to this as work has to be done on the integration of the subsystem components into the inner structure. Therefore the concept does score average, as there has to be significant cost attributed to the integration of the subsystem components. Due to this, the concept scores average on cost. For the Hybrid concept the same cost for the external structure can be used as for the Commercial Off The Shelf concept, as the same external structure is used. The inner structure will be more expensive as the COTS inner structure from the COTS concept. As this has to be designed, it will increase the development cost for the concept. However, this concept will have much less costs related to the subsystem integration to the structure. Changing the design from step 1 to step 2 will also be less of a delta, as the production process for the structure exists and should not need changing. This concept therefore scores average on cost. For the Custom Designed concept, the costs are mainly for the development, production and testing. Doing an entire design cycle for each of the components will significantly increase the cost, therefore the Custom Designed concept scores the lowest in terms of cost.

TRADE-OFF STRUCTURAL CONCEPT SERVICE MODULE

Now that all the relevant aspects have been discussed for each of the concepts, a trade off can be held. A table with the trade off criteria and the ratings is shown in Table 12.10. The Performance of the service Module has been given a weight of 5, as integration and the mass of the structure are of high importance. The sustainability has been given a weight of 2, due to the number of launches that are planned for the SPS, which can result in a large ecological footprint if the design is not sustainable. The Risk of the concept has been given a weight of 1, as it still has to be taken into account due to the launch schedule. The cost of the concept has been given the weight of 2, as the recurring cost has to be kept below the required 2 million.

Table 12.10: Trade-Off Structural Concept Service Module.

Criteria	Concept				
	Performance (5)	**Sustainability (2)**	**Risk (1)**	**Cost (2)**	**Score**
Commercial Off The Shelf	3 R	8 G	8 G	9 G	**5.7** O
Hybrid	8 G	6 B	6 B	7 B	**7.2** B
Custom Design	10 G	3 R	4 O	4 O	**6.8** B

From this it is clear that the Hybrid concept scores the highest. However, it is important to check whether the results of the trade off matrix change when the weights of the criteria are altered. When the weight of the Performance is decreased to 3, the Commercial Off The Shelf concept scores a 6.4, the Hybrid concept scores a 7, and the Custom Design scores a 6 . Thus when the weight is decreased, the outcome of the trade off does not change. When the Sustainability criteria is increased to 3, the Commercial Off The Shelf concept scores a 5.9, the Hybrid scores a 7.1, and the Custom Design scores a 6.45. Thus the outcome does not change. When the Risk is increased to 3, the score of the Commercial Off The Shelf concept will become 6.1, the Hybrid concept scores a 7 and the Custom Concept scores a 6.3. Thus once again, the outcome of the trade off matrix does not change. The last criteria to change is the Cost of the concepts, and when this is increased to have a weight of 4, the Commercial Off The Shelf concept scores a 6.25, the Hybrid concept scores a 7.2, and the Custom Design scores a 6.3. Thus the outcome of the trade off matrix does not change when a criteria becomes higher or lower. Therefore the structure of the Service module will feature an outer structure which is the QuadPack, and will feature a custom designed inner structure for integration with the subsystem components.

12.4.4. Configuration Subsystems in Service Module for Step 1

Once the structure of the Service Module has been determined, the components of the other subsystems can be implemented. These components with the product ID, number and mass are given by Table 12.11.

Table 12.11: Components of the subsystem that are integrated in the Service Module. The values containing a (*) suggest that these components are partly integrated in the Service Module. Therefore, an estimation of these parts that *are* in the Service module is estimated.

Step 1					
ID	**Product Name**	**Subsystem**	**#**	**Total Mass [kg]**	**Description**
RW-08	RW1	ADCS	4	3000	Reaction Wheel (angled at 32° from x or y axis)[3]
SS-02	NanoSSOC-A60	ADCS	2	8	Sun Sensor (both placed on top of the SVM in positive Z)[4]
MM-04	NMRM-001-485	ADCS	3	201	Magnetometer (placed in x, y and z direction)[5]
MT-13	TQ-15	ADCS	3	2181	Magnetorquer (placed in x, y and z direction)[6]
GS-1	QRS116	ADCS	3	180	Gyroscope (placed in x, y and z direction)[7]
GPS-1	GPSRM 1 Kit Pumpkin space	ODCS	1	109	GNSS Receiver Module[8]
POW-BATT	Saft MP 176065 xtd	Power	10	2025	10 batteries for eclipse ops[9]
POW-SOL	AzurSpace Solar Cells 3C44C Assembly	Power	1	190*	PV panels placed on top of QuadPacks[10]
POW-DR	Harness & converters	Power	1	600*	All of the connective electronics
C&DH-1	NanoDock SDR 27	Operation	1	76.4	Motherboard[11]
C&DH-2	NanoMind Z7000	Operation	1	76.8	CPU[12]
C&DH-3	NanoCom TR-600	Operation	1	65.3	Transceiver[13]
Antenna	NanoCom ant2000-11	Operation	3	330	Antenna
			Total Mass	9.04	

All these subsystem components have to be integrated into the inner structure of the service module, and also fit within the external structure. First all the components are placed roughly within the inner structure, and afterwards

[13]URL: https://storage.googleapis.com/blue-canyon-tech-news/1/2019/05/BCT_DataSheet_Components_ReactionWheels.pdf [cited on 24th June 2019]
[13]URL: https://www.cubesatshop.com/product/Nano-ssoc-a60-analog-sun-sensor/ [cited on 24th June 2019]
[13]URL: https://www.cubesatshop.com/product/nss-magnetometer/ [cited on 24th June 2019]
[13]URL: https://www.zarm-technik.de/products/magnetic-torquer/ [cited on 24th June 2019]
[13]URL: https://www.systron.com/gyroscopes/qrs116-single-axis-tactical-grade-analog-gyroscope-non-itar [cited on 24th June 2019]
[13]URL: http://www.pumpkininc.com/space/datasheet/710-00908-D_DS_GPSRM_1.pdf [cited on 24th June 2019]
[13]URL: https://www.saftbatteries.com/products-solutions/products/mp-vl-batteries-launchers [cited on 24th June 2019]
[13]URL: http://www.azurspace.com/index.php/en/products/products-cpv/cpv-solar-cells [cited on 24th June 2019]
[13]URL: https://gomspace.com/shop/subsystems/docks/NanoDock-sdr.aspx [cited on 24th June 2019]
[13]URL: https://gomspace.com/shop/subsystems/command-and-data-handling/NanoMind-z7000.aspx [cited on 24th June 2019]
[13]URL: https://gomspace.com/shop/subsystems/communication/NanoCom-tr-600.aspx [cited on 24th June 2019]

the components are integrated into the structure itself. The placement of the subsystem components will be done in terms of the relevant subsystems, in order to provide a good overview. The axis system used for the Service module follows the same definition of the P-frame used in the ADCS analysis. This can be found in Figure 9.7.

ADCS Components

The ADCS subsystem contains four RW-1 reaction wheels, three MM-04 magnetometers, three MT-13 Magnetorquer, two SS-02 Sun Sensors and three GS-1 Gyroscopes. The Reaction Wheels have to be placed at an angle of 32 ° with respect to the axis that they operate on. The next components to be placed are the magnetometers. These have to be placed in the x- y- and z-axis respectively. The magnetorquers are nearing the limit of what can fit inside the QuadPack as it is defined now. These have to be placed in the x- y- and z-axis respectively as well. The SS-02 Sun Sensors have to be placed on the external structure, as they need to have a direct line of sight to the sun. Two are placed on each ends of the external structure. The GS-1 gyroscopes again have to be placed in the x- y- and z-axis, and are mounted on the inner structure. A figure demonstrating the placement of all the subsystems that are placed on the inner structure is shown in Figure 12.11. The sun sensors are mounted on the external structure, which can be seen in Figure 12.12.

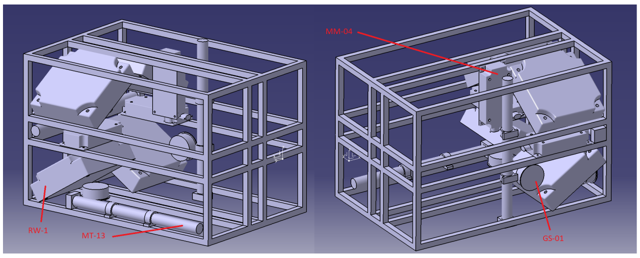

Figure 12.11: Placement of the ADCS subsystem components on the inner structure.©ISIS

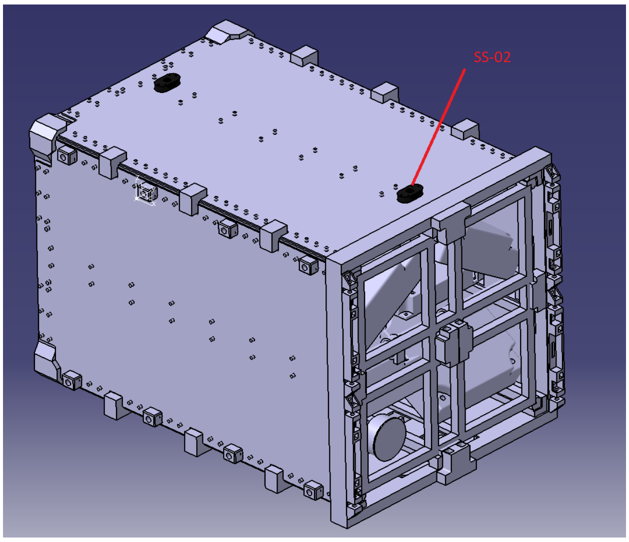

Figure 12.12: Placement of the ADCS subsystem components on the external structure.©ISIS

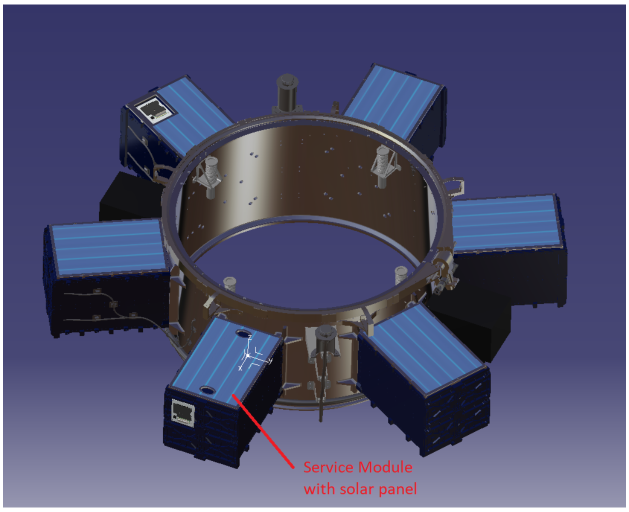

Figure 12.13: Placement of the solar panels on each of the QuadPacks.©Airbus Defence and Space Netherlands ©ISIS

ODCS

The ODCS has one component that has to be placed in the Service Module: A GNSS receiver from Pumpkin aerospace, designated the GPS-1. This receiver can be placed on the inside and will be placed in the xy plane. The placement of the receiver can be seen in Figure 12.11.

Power Subsystem

The power subsystem contains the architecture for power generation and distribution. On the outside of each of the QuadPacks, a solar panel will be mounted on the top, 10 batteries will be placed inside the inner structure and the harness and converters have to be added as well. For the harness and the converters, there were no models and sizes available so these have been omitted at this phase in the design. A figure demonstrating the solar panels on top of each of the QuadPacks is shown in Figure 12.13.

Operations

For the operations of the SPS-2 FF several components are required: a NanoDock to dock a NanoMind Z7000 and a NanoCom TR600 to, and three antenna's in different locations and orientations. The NanoDock, NanoMind Z7000 and NanoCom TR600 can be placed on the inner structure, and the antenna's have to be placed on the outer structure. In Figure 8.12 the configuration of the antenna's can be seen, and in Figure 12.14 the placement of the antenna's on the structure is shown. In Figure 12.15 the placement of the NanoDock, NanoMind and NanoCom is shown.

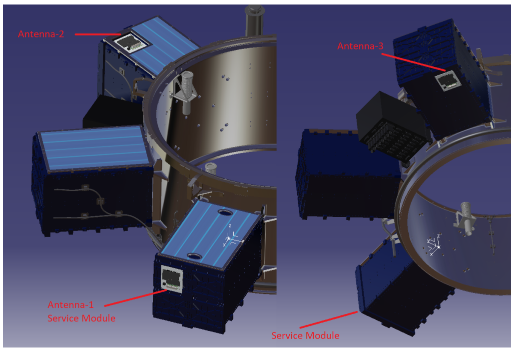

Figure 12.14: Placement of the three antenna's on the different locations on the SPS-2 FF ©ISIS ©Airbus Defence and Space Netherlands

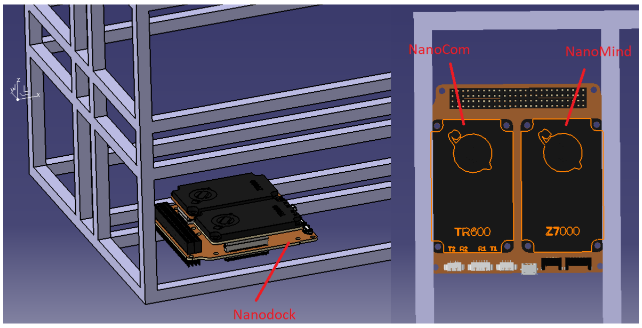

Figure 12.15: Placement of the NanoDock, NanoMind and the NanoCom in the inner structure ©ISIS

These are all the components that have to be placed into the service module for Step 1. The additional components that have to be added to the Service Module for step 2 will be discussed in Table 20.1.

12.4.5. Material & Manufacturing

The inner structure of the Service Module is custom made, and thus a manufacturing method and material has to be defined for it. The structure is complex in nature as it will incorporate the integration of the subsystem components into the shell like inner structure. In order to make these complex structures whilst still being strong and cost effective, additive manufacturing is a nice solution. Additive manufacturing is making its way to the aerospace industry by allowing for complex nozzle and combustion chamber designs [14]. Additive manufacturing would be a better choice compared to traditional manufacturing methods such as cnc machining, as this allows for more complex geometries to be designed, which in turn allow for lower structural masses. Another aspect of additive machining is that it is only required to use the material from which the part will consist of, instead of with traditional subtractive manufacturing methods, where material is removed to obtain the component. Therefore, the method will allow for a more sustainable production process. The risks associated with Additive manufacturing methods are related to the defect free producing of the components and the reliability of the process. These risks will decrease once a fixed working production process is defined for the inner structure.

Aluminium and titanium alloys are selected for the inner structure as both these materials offer a high strength to density ratio. These materials are also able to be printed by current machines, and machines are available which can handle the size of the inner structure [15]. These materials offer similar properties as described in Table 12.3, whilst using an entirely different production method. These properties are obtained from printed components and tested

[14]https://www.cnbc.com/2019/02/20/brooklyn-rocket-start-up-launcher-gets-largest-single-piece-3d-printed-engine.html accessed at 24-06-2019

[15]https://www.3dsystems.com/3d-printers/dmp-flex-350 accessed 24-06-2019

using the ASTM testing standards [16] [17]. However, as the production technique is vastly different from the traditional methods, extra care has to be taken to verify and validate the structural models that are used for the initial structural prototypes. It is proposed that these materials are used to produce structural prototypes of the inner structure, which can be used for vibration, structural and integration testing. This will provide critical information on the properties of these materials and will allow for trade off between the two materials.Furthermore, the same material and manufacturing method shall be used for both step 1 and step 2, as this will offer the greatest flexibility for the integration of new components.

12.4.6. Vibrational Analysis Service Module

A vibrational analysis of the Service Module will be conducted in this section. It is first assumed that the ring will carry all the loads induced during launch. This means that the ring can be assumed to be a fixed end. A distributed load of the component masses that are in the SVM is to be assumed. Thus, a cantilever beam with a distributed load can be assumed, which is given by Equation 12.22[18], where q is the uniform distributed load. The output of Equation 12.22 yields a natural frequency of 609 Hz which is much larger than the requirements given by **SPS-2-PERF-STRUC-5** and **SPS-2-PERF-STRUC-6**.

$$f_{nat} = 0.56 \cdot \left(\frac{EI}{qL^4}\right)^{0.5} \tag{12.22}$$

A structural analysis is not conducted for the Service Module, because in reality the components are not distributed equally in the Service Module. This causes stress concentrations that can not be accounted for in analytical analysis. Therefore, it is recommended to make a model using FEM-software and make a more accurate estimation of the structural capabilities of this Service Module.

12.4.7. Step 1 Service Module Design Overview

The Service Module design for step 1 is shown in Figure 12.16. It includes all the components listed in Table 12.11, and consists of the QuadPack as an outer structure and a custom designed inner skeleton model with integrated connections for the subsystem components. The outer structure is a commercial off the shelf solution, and the inner structure shall be manufactured using additive manufacturing.

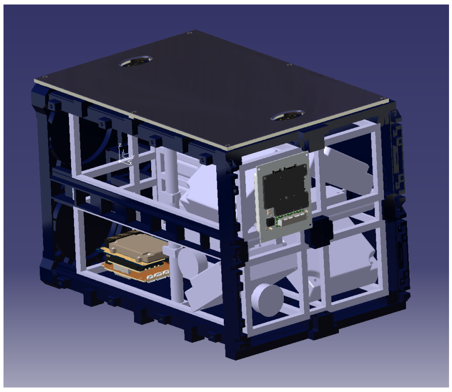

Figure 12.16: Overview of the Service module from the side, with the front doors and side panel removed. ©ISIS

12.5. Structural Mass Estimation

An overview of the structural component masses is given by Table 12.12.

Table 12.12: Mass estimation of the structural components of the SPS-2 FF.

Component	Mass [kg]
Marman Clamp (2x) [39]	12.4
Cylindrical Structure	17.37
Service Module Structure	1.60
Total Mass	31.37

12.6. Recommendations & Step 3

A lot of analysis has been done on the structure of the SPS-2 FF, however certain aspects are left out due to the project's time constraint. Therefore, a recommendation for the structure and a conceptual design of step 3 for the structure is given in this section. The list of recommendations is listed below.

- The material of the ring, service module and bolts have a certain fatigue life that has to be taken into account. Therefore, fatigue loading calculations have to be done to account for this.
- A more detailed analysis on the stiffener calculation can be made. By specifying the the shape of the stiffener, a more accurate calculation of the AMOI can be made. Furthermore, the stiffener also locally strengthens the

[16] https://www.3dsystems.com/sites/default/files/2017-12/3d-systems-laserform-stainless-ti-gr5%28a%29-datasheets-us-a4-2017-12-07-web.pdf accessed 24-06-2019

[17] https://www.3dsystems.com/sites/default/files/2018-11/3D-Systems_Laserform_AlSi7Mg0.6%28A%29_DATASHEET_A4-us_2018.11.06_WEB.PDF accessed 24-06-2019

[18] URL: https://www.engineeringtoolbox.com/structures-vibration-frequency-d_1989.html [cited on 24th of June 2019]

skin (i.e. effective sheet width) which increases the allowable buckling stress of the panel. This can be taken into account to make a more accurate prediction of the possibility of implementing stringers in the structure.
- With a circular structure you can not fully utilise every part of the skin. Different geometries like hexagonal or octagonal structures can therefore be considered for further research.
- For the CF/Epoxy UD Prepreg, a sandwich panel between the skin can be considered, which increases the AMOI of the structure significantly. However, inserts have to then be integrated in the sandwich panel to be able to mount the QuadPacks to the structure.
- The cables that connect to the subsystems in the Service Module have to be specified to check if there is still sufficient space available in the Service Module.

For step 3 there is minimum to no change in the structure of the ring. The components in the Service Module will change which means that the dimensions of the SVM might change. This means that the vibrational and structural analysis of the SVM should be done again.

12.7. SPACE ENVIRONMENT

The radiation endured on the spacecraft in space has to be accounted for in the structural design of the SPS-2 ring. An overview of sources of radiation and its influence on the SPS-2 FF will be described in subsection 12.7.1 and subsection 12.7.2 respectively.

12.7.1. SOURCES OF RADIATION

As the two orbits used are both in Low Earth Orbit (LEO) and are both relatively close to each other, there will not be much difference in radiation between the orbits. The main radiation sources are the so called space weather, which is the impact that the sun has on the earth due to for instance solar wind particles and its photons. The other influence is due to the Earth's magnetosphere and its upper atmosphere, which consist of the thermosphere and ionosphere. In the thermosphere molecular nitrogen and Oxygen, atomic Oxygen hydrogen and helium exist. Atomic Oxygen has the lowest atomic mass, which makes it most prevalent in the operational altitude of the SPS-2 FF. Atomic Oxygen could cause problems for the spacecraft due to adsorption of atomic Oxygen. The biggest sources of radiation acting on a spacecraft in orbit are given in the list below. The effects of these sources are depicted in Figure 12.17.

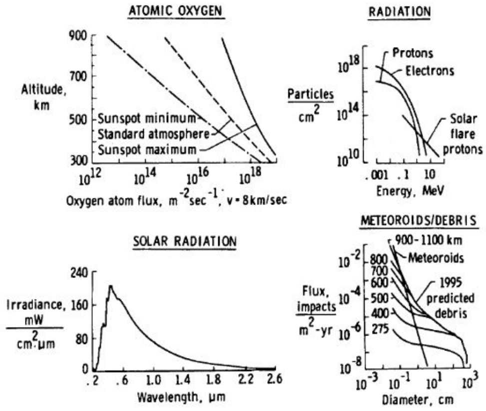

Figure 12.17: Main influences of radiation on satellites in LEO [17].

- Effects due to space weather (Ultraviolet, surface charging, communication interference)
- Trapped electrons and protons
- Debris
- Atomic Oxygen

12.7.2. RADIATION EFFECT ON THE SPS-2 FF

As the material was chosen to be aluminium, the resistance to radiation effects of aluminium will be discussed hereafter. From communication with the client the Total Ionizing Dose (TID) of aluminium for different values of thickness of the protection layer is known, this is depicted in Table 12.13.

Table 12.13: Total radiation exposure doses for different mission durations and aluminium protection layers .

Mission duration	TID at 1mm Alu protection[rad]	TID at 3mm Alu protection[rad]	TID at 5mm Alu protection[rad]
1 month	$7.75\ 1 \cdot 10^3$	$1.43 \cdot 10^2$	$5.50 \cdot 10$
6 months	$4.65 \cdot 10^3$	$8.58 \cdot 10^2$	$3.30 \cdot 10^2$
1 year	$9.30 \cdot 10^3$	$1.72 \cdot 10^3$	$6.60 \cdot 10^2$
3 years	$2.79 \cdot 10^4$	$5.15 \cdot 10^3$	$1.98 \cdot 10^3$

Also from communication with the client it was made evident that that radiation dose exerted on the aluminium ring during operational time will not endanger the operation of the SPS-2 FF. Therefore no protection is needed over this aluminium. For the IOD payloads, the radiation protection will be provided by the IOD payload provider itself, if necessary. This is obviously not necessary for IOD payloads testing the time the payload can be exposed to radiation. As the main structure of the service module itself is made of aluminium, the main structure will provide a protective layer of 1-2 mm of aluminium in all directions. This will also protect the components of the spacecraft. Further analysis will have to be done on the individual resistance to radiation exposure of all components to check if they will survive the space environment for at least 6 months. This will mean they have to be able to resist a TID of $4.65 \cdot 10^3 [rad]$.

13 PROPULSION

Propulsion on spacecraft consists mainly of low thrust, high specific impulse thrusters. These can be used on very small satellites, like Nanosats and CubeSats to change orbit. For heavier spacecraft, like the SPS-2, the low thrust of several milliNewtons will not suffice to make substantial orbital changes. Therefore ion, and other low thrust thrusters are mainly used for attitude control, orbit maintenance or used to desaturate reaction wheels, for spacecraft like the SPS-2. In this chapter an analysis will be performed on the necessity of thrusters for nominal operation of the SPS-2 Free Flyer through its design steps.

13.1. STEP 1

During step one the SPS-2 FF will be flying a 850x350 km orbit, with an estimated de-orbiting time of 1.6 years. As the set lifetime by the client is 3-6 months up to max 1 year, no station keeping is needed. Together with the fact that propulsion is not needed for the ADCS, no thrusters will be added to the SPS in Step 1.

13.2. STEP 2

In step 2 the orbit and the proposed lifetime have not changed. Therefore the SPS in this step will also not include thrusters. The delta will be non-existent.

13.3. STEP 3

In step 3 the methane mission will be employed on the SPS-2, leading to a more strict pointing accuracy and a different orbit. The new orbit will be a 450 km circular orbit. De-orbiting from this orbit can be done passively as the orbit will degrade enough within the prescribed 25 years. To get to the desired orbit from the orbit of the primary payload, the required ΔV can be provided by the AVUM+ stage or the SPS-2.

Both methods have advantages over the other. The required ΔV is independent of the spacecraft size and mass, with the given I_{sp} and mass fractions of the AVUM+ stage and possible cold-gas thrusters for the SPS-2. It was calculated that the AVUM+ would need to expend more propellant mass to perform the same manoeuvre. Furthermore, being hosted on the AVUM+ stage will also require additional funds. Mounting a propulsion subsystem on the SPS-2 will lead to more mass, added delta between steps and complexity to the structure, therefore leaving less mass for potential payload.

Communication with the client lead to insights that propulsion will not be necessary for station keeping. During the mission lifetime the degradation of orbital height will not be detrimental to the performance of the methane mission instruments.

Further, more detailed analysis will have to be conducted to get a definite answer whether or not to use a propulsion subsystem in step 3. The cost of manufacturing, integration and testing of the propulsion subsystem together with the potential loss of payload capacity will have to be traded off against the additional costs of being hosted on the AVUM+ stage. Important information currently lacking is for instance a cost estimation of reserving fuel mass on the AVUM+ stage.

14
Configuration

The configuration of the SPS-2 will be greatly influenced by the amount of payloads to be carried. Multiple payload configurations and deployer options are possible for the SPS, but in this chapter only one of these will be outlined. The configuration used in this chapter is the maximum payload capacity whilst using the QuadPack deployer systems on each of the attachment points.

14.1. Integration In The Launch Vehicle

The SPS will be launched in the fairing of the VEGA-C launcher normally, but to maintain a bigger business case, it may also be flown on different launchers. To accommodate for this fact, a standard diameter is used, 937 mm. This way commercial of the shelf products can be used, like Marman clamps already properly and used in the SPS-1. On the SPS-2, these clamps will be on top, to attach the SPS-2 to the primary payload, and on the bottom, to make detachment of the SPS-2 from the AVUM+ stage possible.

14.2. Structural Configuration

The Marman clamps will be attached to the primary structure of the SPS-2, being a round aluminium structure of, again, 937 mm diameter. This will be conveniently placed in between the two clamps. An overview of the already developed structure showing one of the two clamps can be seen in Figure 14.1.

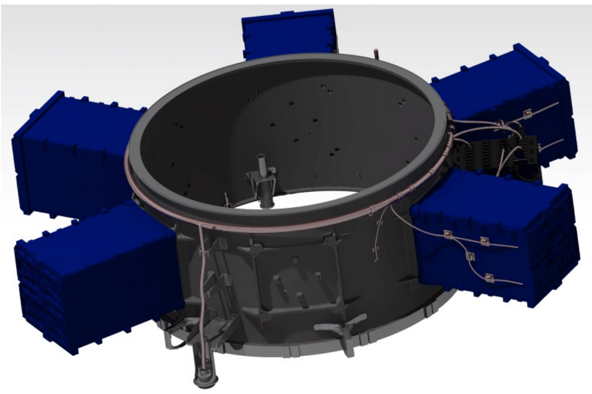

Figure 14.1: Front view of the SPS-1 with one QuadPack hidden to see the attachment point. ©Airbus Defence and Space Netherlands, ©ISIS

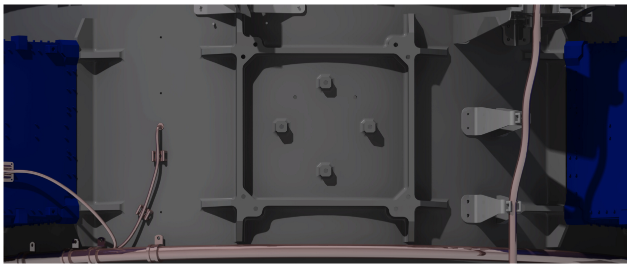

Figure 14.2: Close up of the holes used to attach a single QuadPack. ©Airbus Defence and Space Netherlands

14.2.1. Existing structural complexities

The structure itself will contain certain holes and extrusions to make attachment of the secondary payloads, cables and the umbilical chord possible. The total amount of holes for the attachment of secondary payloads, which will be packed in QuadPacks from ISIS[1], has been defined and tested by analysis on the SPS-1. The amount of holes for bolts will be 12 per secondary payload. In the case for the SPS-2 with capacity for 5 secondary payload devices, this will result in 60 holes possibly endangering structural integrity. The layout of these holes is depicted in Figure 14.2

Furthermore, there will be one sequencer[40] between the secondary payloads, which controls its deployment. This will also lead to extra holes and already leads to an unsymmetrical structure. Other holes will also be introduced on the surface, for instance for attachment of the detachment springs, attachment of the umbilical cord and other holes for different purposes. In total there will be more than 100 holes. These holes have all been included in vibrational and strength testing of the SPS-1 and are therefore excluded from further analysis. Although there are more holes in the structure, the most important ones are depicted in Figure 14.3. In this picture, a nice overview of the umbilical chord can also be seen.

[1] URL:"https://www.isispace.nl/product/quadpack-cubesat-deployer/, cited on [13/06/2019]

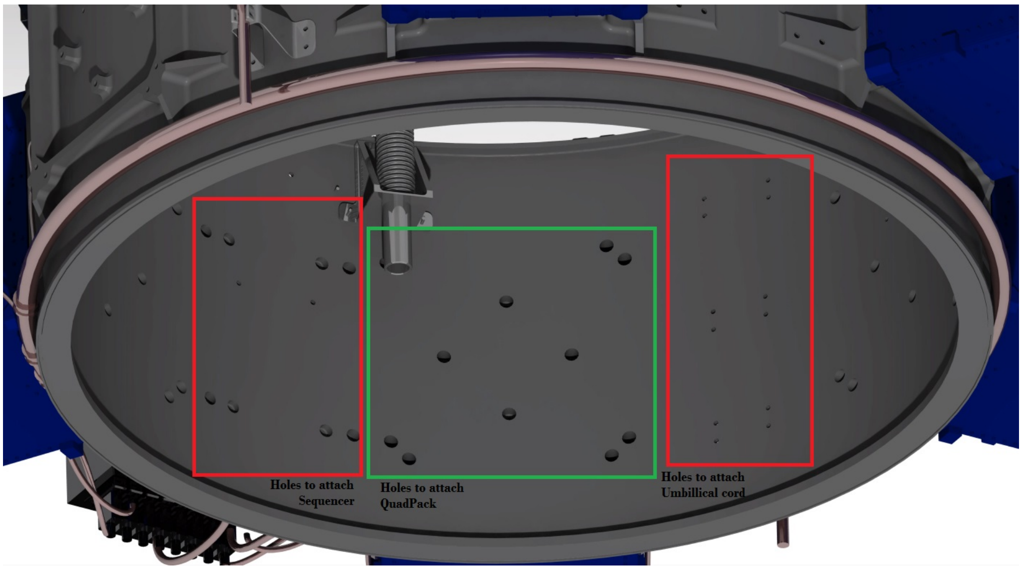

Figure 14.3: Overview of the most important holes used for the attachment of components to the SPS. ©Airbus Defence and Space Netherlands

14.2.2. CHANGED OR ADDED COMPLEXITY TO THE STRUCTURE

As the adaptations to make the SPS a free flying device will change a spot for a secondary payload on the SPS-1 in a spot for the service module, the attachment to the structure might also have to be changed. It is convenient for symmetry to make the service module of the same size and weight as a secondary payload, as this might not be possible the implications of this change will have to be looked at.

14.3. ATTACHMENT OF SECONDARY PAYLOADS & SERVICE MODULE

As mentioned before, the main structure of the SPS-2 contains holes and extrusions to fit the primary payloads on. The size of these extrusions and placement of the holes has been designed to perfectly fit a QuadPack in. Naturally it will be optimal to design the service module to fit perfectly in these already specified extrusions and holes. A QuadPack has a volume of 10x10x30 cm^3. The longest side will point radially outwards from the structure. This is also where the “doors” are to make deployment possible. The volume of the sequencer will depend on the amount of ports needed, as four are needed for every QuadPack, a minimum of 20 ports is needed. Using the holes, the QuadPacks will be bolted on, to make deployment of CubeSats inside the QuadPack possible, the QuadPack is connected to the IMDC sequencer via cables. These cables are distributed from the sequencer using a centralised line around the perimeter of the structure. Every QuadPack will be connected by four lines. These lines will also be connected to the umbilical chord.

15 Manufacturing, Integration & Testing

As part of the design of a spacecraft, Manufacturing, Integration and Testing has to be considered. In this case, the focus will be on how this changes between steps, as the desired result is a small delta between steps.

To get the optimal efficiency out of the Manufacturing, Integration and Testing (MIT) a production plan will be made. This production plan will provide guidelines on the sequence of MIT. Parts of MIT have already been performed. Namely, all of it that has to be performed on the ring itself and the attachment points to QuadPacks. Adding a service module will have minimal effects to the structural properties of the entire SPS-2 assembly. Minor additional testing will still be needed to confirm that for instance the attachment point is compliant with loads occurring during launch, as well as testing to confirm that the vibrations of the SVM will not have a disadvantageous effect on the structure of the SPS-2.

Since the MIT for the SPS-2 has already been performed partly on the SPS-1 design, focus will be on the SVM in this section. All components of the SVM are COTS products, therefore it can be assumed that they will work nominally. Nevertheless, some analysis and testing will be done to confirm all functionality is working nominally. Although this testing will not be done to the extent as would be done for developed products, the testing is still crucial in obtaining a perfectly working object.

All the COTS products will have to be ordered by their respective manufacturers, as not all products might be needed at the same time, the ordering sequence will be an integral part of the integration. If parts will be ordered late they might heavily delay the integration process of the SVM.

When the required parts have been obtained, they will have to be integrated together to form the SVM. Integration of the SVM will have to be done in an enclosed environment with highly regulated particle control. As the SPS-2 is developed for Airbus D&S, which have available space in clean rooms, the desired environment for integration will not be a problem. Another thing to consider about the integration of the COTS parts are the people integrating them. They have to be qualified and capable of using the parts. As the SVM will be integrated at Airbus D&S, numerous qualified people will be available, therefore this will not pose a problem for the integration.

After integration is done the SVM will have to be tested, as depicted in Figure 15.1. There are numerous tests to be considered, which, when all completed will lead to a fully working and space worthy system.

The MIT plan as described by [17] is depicted in Table 15.1. The time the entire process takes is also estimated in Table 15.1, the estimation is quite broad, but will likely be on the low side for the SPS-2. This is due to that only the SVM has to be fully tested as opposed to the entire spacecraft. Still the MIT process will take a lot of time, as most spacecraft projects do.

For the case of the SPS-2 the parts procurement and test has been assumed to take as little as 1 month for mechanical parts and 4 months for electronic parts, as all parts will be obtained off the shelf and their manufacturers have already been decided on. As the components have not been used together before, no easy guide for this consists. Therefore the component assembly will take around 3 months, to account for potential interface issues. This complication will also be present in the component acceptance test, therefore taking a high 3 months. For the qualification the components of the SPS-2 will again have an advantage due to being off the shelf, the components have been designed for in orbit use so there should already be a sufficient overview of the fragility of all components. Therefore this step will take as low as 2 months. In the integration and test step much timewise gain might not be possible, as the service module will have to go through extensive testing. Testing is needed for the service module itself and the SVM attached to the ring. Vibrational analysis of the ring with only QuadPacks will not be valid anymore unfortunately. But test equipment and some test procedures might only need minor adaptations. This leads to a estimated time for integration and testing of 12-13 months. In total the MIT phase of the SPS-2 would than take around two years.

As spacecraft products are very prone to delays. This will result in a very unlikely first launch in 2022, thereby not complying to the set requirement of first launch in 2022.

Fast MIT for spacecraft has been performed before, as described by [41]. So this might be a possibility for the SPS-2 as well. But to have this as a baseline would be too prone to delays. But it might be used as a perfect launch opportunity arises and a different MIT strategy is the only option to reach the deadline.

Table 15.1: steps used for manufacturing, integration and testing of the spacecraft

Step	Description	Comments
Prepare engineering data	Complete drawings and all supporting information such as material and part and processing methods	Engineering data will consist of hundred drawings for each component, specifications for each piece-part type process , assembly drawings, and equipment data
manufacture component	stages: 1. Manufacture planning 2. parts procurement and test 3. component assembly 4. component acceptance test	typical timing: 1. In parallel with engineering-data preparation 2. Mechanical parts and materials 1-6 months. electronic parts 3-18 3. 1-3 months 4. 1-3 months; acceptance test includes functional test and environmental exposure
Qualify component	Functional test and exposure	Takes 1-6 months depending on complexity and fragility of component, severity of environment and number of failures
Integrate and test spacecraft	Mechanical assembly, functional test, and environmental exposure	Takes 6-18 months

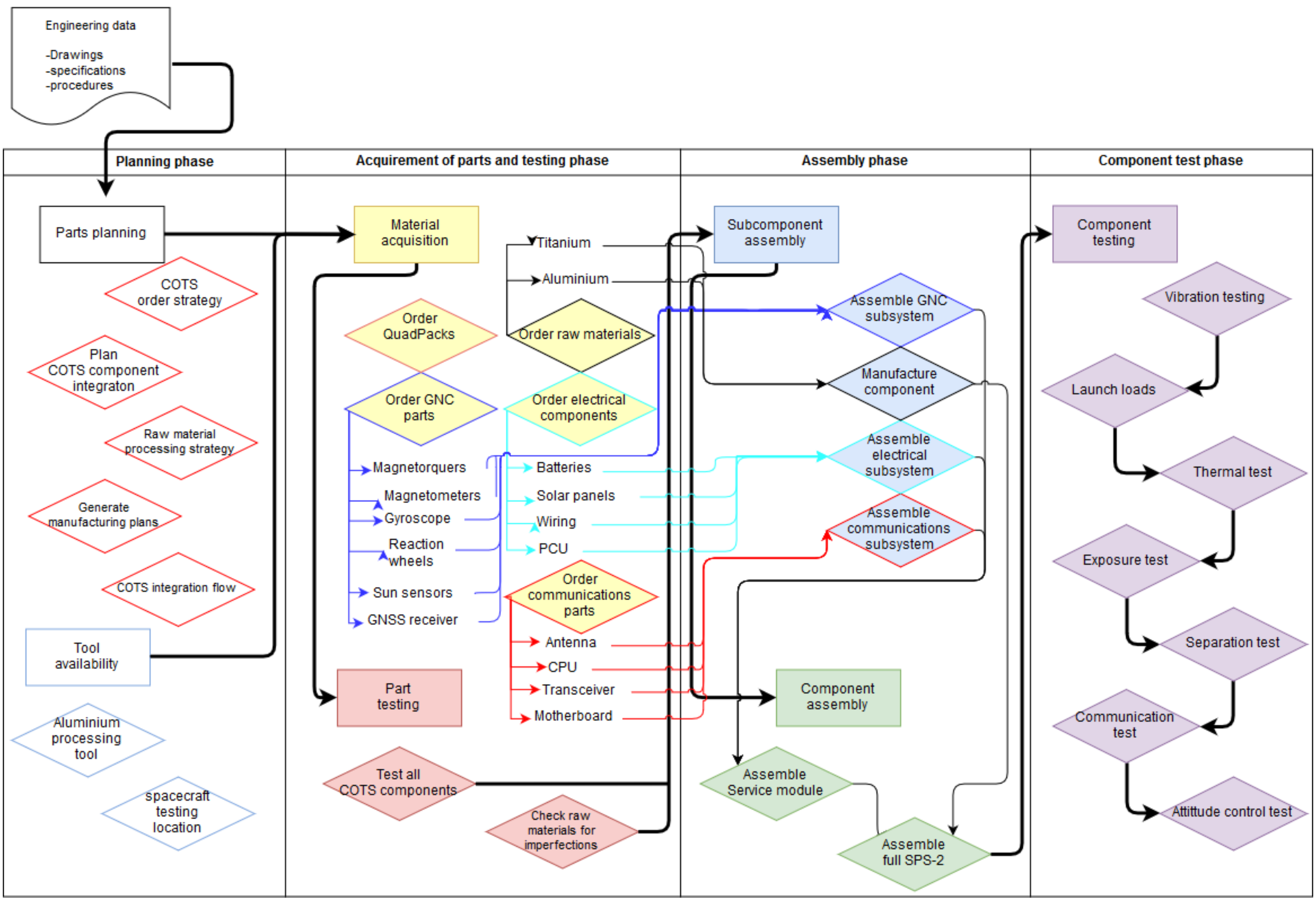

Figure 15.1: Production flow diagram.

16
Mission Operations Step 2

This chapter presents the necessary updates to be implemented for the operation of the SPS-2 FF Step 2. It also includes the design improvements and adjustments needed to ensure that the data handling and communications subsystems meet the requirements of the new product phase. The initial operational model, product selection and general subsystem design presented in chapter 8 are developed to minimise the necessary changes for the new product phase. Most of the topics covered in the design of Step 1 are omitted in this chapter, as they will be shared by Step 1 and Step 2. This chapter only outlines the necessary corrections for the successful operation of more complex combinations of payloads. The basis behind the design of a ground segment network and operations model are reused from Step 1. Only further considerations for the improvement of data handling and mission communications are covered in this chapter.

16.1. Data Generation

The data generated by the payloads for step 2 can be seen in Table 16.1. Step 2 has payloads that generate $100 kbps$ of data. In the worst case this leads to 5 payloads that produce this data rate. This is multiplied with 1.5 again, to include overhead data, and $1 kbps$ is added for the service module. This results in a data generation of $4.349792 Gbits$ per orbit. Given that the chosen product has a data storage of $32GB = 256Gbits$, it will take $t = \frac{256}{4.349792} = 58.9 orbits$ to fill up the storage, when ignoring the software storage needed for operations. Since, the average communication time is $561.17s$ this leads to a communication data rate of $15503485 bps$ for step 2. This is inputted for R in the link budget, which is found in subsection 16.2.1.

Table 16.1: IOD requirement table, indicating the IODs for each step and their telemetry needs [4].

	OBCs/ OBPs	RF Comms system	GNSS Receiver	ADCS sensor	Optical P/L	RF Payload	Space Weather P/L	Radiation Hardness	CubeSats
Step 2	x	x	x	x		x	x	x	x
Telemetry needs	n.a.	n.a.	<1 kbps	<1 kbps	few GB per day	<100 kbps	<100 kbps	<1 kbps	n.a.

The analysis of the data generation requirements and the orbit propagation data leads to an initial set of communication characteristics summarised in Table 16.2. These values are used during the link budget design presented in subsection 8.7.2. Based on the orbital period and the aforementioned data generation rate, two cases for the required downlink rates have been calculated: using the average number of station passes and using only one station pass for communications.

Average Passes Per Orbit	3.69
Data Generation Rate (kbps)	751
Orbit Storage (Gb/orbit)	4.35
Downlink Rate (mbps) ***(Average Passes / orbit)***	4.2
Downlink Rate (mbps) ***(1 Pass / orbit)***	15.5

Table 16.2: Overview of communication characteristics.

16.2. Communication System

The main aspects of the communication subsystem of Step 2 are presented in this section. It includes an updated overview of the communication flow between the subsystems of the spacecraft and the revision of link budget calculations for the new payload requirements. The design of antenna coverage, which is based on the antenna performance analysis, is directly taken from the design of Step 1, as well as the considered ground stations and their average availability for contact during the previously covered 224 orbit cycle. However, additional considerations regarding the amount of stations needed to meet the new payload requirements are explained in the following subsections.

16.2.1. Link budget

Once more, the link budget can be calculated following the same procedure as described in subsection 8.7.2. The equation can be seen in Equation 16.1. [20] The parameters in orange represent the parameters that are determined by the chosen product.[6] The parameters in blue are affected by the chosen product. The SNR, signal to noise ratio, needs to be at least 3 dB in order to close the link as specified by the client and the TU Delft. [21]

$$SNR[\text{dB}] = P + L_l + G_t + L_s + L_a + L_{pr} + G_r + L_r - 10\log_{10} R + 228.6 - 10\log_{10} T_s \tag{16.1}$$

The formula includes the following parameters:

- P = power by transmitter, equal to $8.9W = 9.5dBW$.
- L_l = loss from transmitter, equal to 0 dB, as the loss is included in the gain.
- G_t = gain from transmitter, equal to 8 dBi.
- L_s = space loss, equal to -155.7 dB.
- L_a = transmission path losses, mainly atmosphere and rain attenuation, equal to -14.3 dB
- L_{pr} = antenna pointing loss, equal to -0.13 dB
- G_r = gain receiver, equal to $18dB$, for a diameter of 2.4 m and 25.3 dB, for a diameter of 5.5 m.
- L_r = loss receiver, equal to -0.46 dB using an efficiency of 0.9
- R = data rate [bit/s], equal to 15.5 $Mbits/s$ = 71.9 dB
- k = Boltzmann's constant = $1.38{\cdot}10^{-23}$ $\frac{J}{K}$ = -228.6 dB
- T_s = system noise temperature, equal to 135 K = 21.3 dB for downlink.

Finally, this leads to a signal to noise ratio of 0.3 dB for the 2.4 m diameter disk of Redu-3. Therefore, this ground station antenna can't be used, but the others at Redu can. The second smallest antenna from the ground stations is the 5.5 m diameter of Santa Maria. This station has an SNR of 7.5 dB. Therefore, the link closes as the SNR is bigger than 3 dB. However, when the antenna is radiating under an angle of 90°, the link budget does not close (0.24 dB). Therefore, the communication time needs to be increased in order to lower the data rate. If the SPS communicates with two ground stations during an orbit, only the biggest (15 m diameter) antennas work 3.2 dB. This limits the number of available stations to three. The communication time can also be increased further, by connecting to three ground station per orbit. This allows for the use of 12 m diameter dishes (3.1 dB). This decreases the amount of available ground stations to seven stations with 10 antennas. The data rate for this scenario is $5.2Mbits/s$.

16.3. COMMUNICATION ARCHITECTURE

Due to the fact that the SPS-2 FF will be Earth pointing from Step 2 onwards, the communication architecture can be optimised. Only one antenna would be sufficient. However, two are selected for redundancy. They will be placed on the bottom of the spacecraft, Earth pointing, side of the SPS-2 FF. They will both be placed on the service module to reduce wiring.

17
Guidance, Navigation & Control Step 2

The Guidance, Navigation and Control (GNC) system has also been designed for step 2. Step 1 was designed in such a way that the change from step 1 to step 2 was as small as possible. Firstly, the ODCS for step 2 is explained in section 17.1. After that, the changes for the ADCS is designed for in section 17.2.

17.1. ODCS

The requirements on orbit determination do not change between step 1,2 and 3, nor do they need to change based on other changes between these steps. Therefore it was deemed that the GNSS receiver was sufficient for all steps and will be thus kept the same in order to prevent any unnecessary delta's.

17.2. ADCS Design For Step 2

As the ADCS in step 1 has be designed for changes to step 2 and 3, not much changes in the components has to be done. What exactly changes for the architecture is explained in subsection 17.2.1. After that, the mission operations for step 2 are shown in subsection 17.2.2. Next, the science mode is analysed in subsection 17.2.3. Then, another risk analysis is executed in subsection 17.2.4. Lastly, recommendations regarding step 2 are written out in subsection 17.2.5.

17.2.1. Additional Sensors

As the reaction wheels have a very high control accuracy [17], no new actuators have to be designed for to accomplish control in step 2 and 3. However, in step 2 an attitude knowledge of at least 0.5° while Earth-pointed [7] is required. Sun sensors are not sufficient anymore as the attitude control cannot be guaranteed solely relying on the gyroscope during eclipse, and they do not provide 3-axis knowledge and the required accuracy for Earth-pointing.

All sensors from step 1 are also implemented in step 2. The magnetometers are still needed for detumbling and momentum dumping, the gyroscope is needed for small corrections and detumbling and the Sun sensors are needed for the safe mode, which is explained later this section. This is the case, because the ADCS in step 1 has been designed to make the delta from step 1 to step 2 is as small as possible.

There are two design options considered to provide the increase required in pointing accuracy. A star tracker could be added or an Earth sensor. For more information see section 9.4. Star trackers have a very high accuracy. The disadvantage is that star trackers are therefore also more expensive and require a large database and much computing data [17]. An Earth sensor on the other hand does not have an accuracy as high as a star tracker. However, it is cheaper and very useful for the Earth pointing requirements. Thus, an Earth sensor will be used.

An effort has been made to find possible Earth sensors. Many Earth sensors for sale did not meet the accuracy requirements, but three did, as can be seen in Figure B.6. The MAI-SES IR[1], with ID ES-01 is a clear winner just from looking at the mass and power consumption. Two of these sensors will be implemented for redundancy. They will be placed on the far side of the SVM, so as much as possible in the positive x_P-direction. This way the sensors' view will not be obstructed and they will be able to see the Earth's curvature at all times during nominal operations.

17.2.2. Mission operations

As the requirements are different in step 2, the modes implemented in the spacecraft differ as well, as can be seen in Figure 17.1. The detumbling still occurs in the same fashion as in step 1, using the magnetorquers, magnetometers and gyroscope.

The Earth Acquisition mode (EA) differs from the SA in step 1 that the Earth is now looked for by the Earth sensor (block 2-3).

Then Science Mode (SM) is initiated (block 5), but now the spacecraft has a constant slew to stay pointed in nadir direction. This will be controlled by the reaction wheels, magnetorquers, magnetometers, gyroscope and Earth sensor. If the Earth measurement is lost for a time longer than <TBD>, the EA will start again.

If a failure occurs within the spacecraft and time is needed to analyse it, or a certainty for power is needed, the safe mode can be implemented (block 6-11). In this mode the spacecraft will orient itself towards the Sun, just like

[1] URL: https://www.cubesatshop.com/product/mai-ses-ir-earth-sensor/ [cited on 23rd of June]

in step 1. If the spacecraft is able to return back to SM, it will first have to go through EA again. The nice part about the safe mode is that it is the same as the operations in step 1, so no extra development has to be done for sensors, actuators, coding and implementation to make the delta step as small as possible from step 1 to 2.

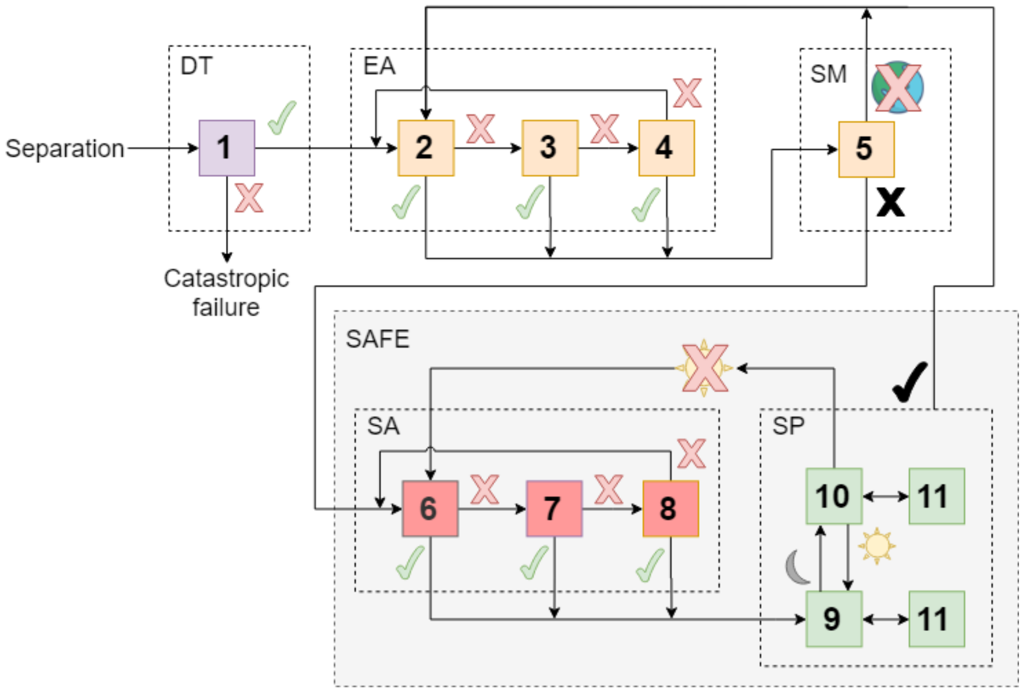

Figure 17.1: Mode switching diagram of step 2. DT = Detumbling mode, EA = Earth Acquisition mode, SM = Science Mode, SA = Sun Acquisition mode, SP = Sun-Pointing mode

17.2.3. Science Mode Analysis

After Earth-pointing has been achieved, the spacecraft needs a minimum slew rate to stay Earth-pointing. This torque required to achieve the minimum slew rate has been calculated in [7] to be $7.115 \cdot 10^{-5} Nm$. This torque will be exerted on the spacecraft by the magnetorquers. Due to the nature of the slew rate being opposite and equal for every half orbit, the reaction wheels will not saturate significantly faster than from resisting the disturbance torques only. The saturation time will fluctuate by about half the orbit, as the reaction wheel will only de-saturate itself after half this orbit.

Furthermore the detumble time requirement and orbit will not change between steps. Therefore the chosen magnetorquers will be the same as used in step 1. Due to the magnetorquers as well as the reaction wheels remaining the same, the desaturation requirement of < 2 orbits will also be met.

As the spacecraft is not Sun-pointing anymore, the effect of solar flux will create a moment on the spacecraft. This effect will be less than the other disturbance torques [28]. Due to the lesser influence and time constraints this disturbance has not been addressed in this reports.

In [7], the difference between used IOD payloads in step 1 and step 2 is listed. It can be seen that for the pointing accuracy a requirement is now set, but to reduce Δ and as a consequence of other requirements, this was already taken into account and realised for step 1. Also an actual requirement for the stability has been set for an ADCS sensor payload($<1\ deg/s$). This accuracy was already obtained in step 1 and therefore no changes are needed.

17.2.4. Risk analysis

The risk stay the same as step 1, but one risk is added since a new component is added. Furthermore, there is a safe mode which decreases the overall risk of mission failure.

- **E-1:** *Earth Sensor Failure.* The probability is *unlikely* as these devices are known aerospace instruments that are well known. In case of failure, the sps-2 FF can not guarantee accurate Earth pointing, making the impact *fatal.*

This risk is mitigated by redundancy, two Earth sensors will be used. Furthermore, the sensors do not contain any moving part and are flight proven. This reduces the impact to *critical.*

17.2.5. Recommendations

Just as for step 1, there are also recommendations for step 2, which are stated here. This gives an overview of what can be improved if there is time for further research of the system.

To get a more complete overview of the disturbance torques acting on the spacecraft, including an analysis on the solar pressure would be beneficial. Due to time limitations this analysis was excluded. However, it would be useful as in step 2 the spacecraft's orientation differs with respect to the Sun. Even though the disturbance torque of the solar radiation is small compared to the other disturbance torques [28], it is still important to implement.

Also, the attitude should be altered. As of now, step 2 has been designed for the disturbance torques of step 1. However, in step 2 the spacecraft is Earth-pointed, so the disturbance torques will change. The magnitude might not change that much [28] [26], but the directions of the disturbance vectors will change, which will affect the time before the wheels' momentum capacity is reached.

Furthermore, the detumbling analysis can be investigated further. It should be investigated how the Earth sensors are used optimally, to improve the detumbling time. Furthermore, it can be used to improve the nadir pointing stability by analysing the Earth sensors' operations in further detail.

18
Power Generation, Distribution & Storage Step 2

The Step 2 of the PGD&S (Power Generation, Distribution and Storage) subsystem retains many of the elements of the first Step's architecture. This is deliberate: a low design delta between steps was a critical requirement from the client, and thus was implemented in the design process. Firstly, the expected solar array size and battery capacity will be stated, followed by the assumptions that differ from Step 1 chapter 10. Then, it shall summarise the critical components and their principal characteristics, possible changes for this step and will demonstrate the feasibility of the PGD&S subsystem in the context of the increased power required.

18.1. Summary of Preliminary Sizing Values and Assumptions

The following summary can be made for the Step 2 power system sizing, using the same methods as outlined in chapter 10:

Table 18.1: Summary of Step 2 Preliminary Sizing.

	Value	Units
Max. Power Required (Day)	152.2	W
Required Solar Array Area	2.2	m^2
Required Battery Capacity	151	Wh

The assumptions that must be made are presented below. The last two assumptions are analogous to those utilised in Step 1, which is a consequence of a low-delta design philosophy.

- The average incidence angle is 70°, which is the reason for the drastic increase in solar panel area. This value is large due to the fact that there is no longer any Sun-pointing present, and thus the solar panels have a significant incidence angle with respect to the Sun.
- The night/eclipse power remains equal to 40% of the maximum day power, as in Step 1
- The thermal coefficient for the solar panel efficiency remains -0.00168 /deg [34, 35]

18.2. Unchanged Components from Step 1

As mentioned in the introduction, many of the components used in the PGD&S subsystem are retained from Step 1. These will be outlined here. The regulation and distribution network, as well as the harness, must remain the same as those used in the first Step. The change in the power that must be delivered to all subsystems does not undergo significant change between Steps 1 and 2, and thus the distribution and regulation will function efficiently for both Steps. For the battery, the system was grossly over-designed for Step 1, it can remain the same for Step 2. The Python script used yields a value of 197.1 Wh, which is below the 204 Wh designed for the first Step.

18.3. Detailed Array Architecture Concepts and Trade-off

The solar array area required was computed for an incidence angle of 70° on average. However, this area is of 2.2 m^2 is simply too large as more than triple the area of that available on the top of the QuadPacks would be required. Since this would already require hinging, the only remaining option would be to have solar panels that are actuated and actively pointed towards the Sun. This can be done in several ways, which will be listed below.

18.3.1. Trade-Off Criteria for Concept Selection

The concepts will be ranked on the following criteria:

- Flexibility
- Ease of Implementation
- Potential Cost
- Risk

Flexibility denotes the degree to which the design can adapt during the mission to different orbits (for instance, fully sun-exposed with no eclipse) or be adapted to them before launch. *Ease of Implementation* takes into account the number of different parts used, testing required, expected TRL of various parts used the design and other design-specific factors. *Potential Cost* is strongly linked to the *Ease of Implementation*: it is not a fully orthogonal metric as often the

18.3.2. Concept 1: Service Module Only

An option for the solar panel integration for the Step 2 design is a set of fully actuated panels placed on the service module. These will fold out outwards from their resting position, and adjust to point towards the Sun. Assuming all solar panels have a pointing accuracy of 10°, the incidence angle with no shadowing will be 10°. This yields a required solar panel area of 0.785 m^2. In order for this to be achievable, all of this area needs to be fully rotatable. The key features of this configuration are that:

- The area can be effectively contained in 8 QuadPack sized surfaces
- The surfaces are placed a the front of the service module, as shown in the illustration
- The surfaces can be folded around a single QuadPack for launch

18.3.3. Concept 2: Partial Service Module, Partial Body

Here, the service module only has 6 QuadPack Sized PV arrays placed on the service module. This requires some to be placed on the body of the QuadPacks. Again assuming a pointing accuracy of 10° for the actuated panels, and an average orbital incidence angle of 70° for the body-mounted solar panels, the computations go as follows. Firstly, the area that is allowed on the Service Module panels is a total of 0.638 m^2. From the Python script used and [17], the required power from the solar arrays is given as a total of $P_{req} = 194.92W$, and the EOL power delivered by the frontal area is

$$P_{front} = A_{sa} * v_{sol} * SolFlux * Id * cos(\theta) * (1-D)^L \tag{18.1}$$

which gives

$$P_{front} = 0.638 * 0.258 * 1360 * 0.72 * cos(10) * (1-0.005)^{0.5} = 158.36W$$

Where v_{sol} is the total solar panel efficiency (including the temperature-induced efficiency loss), SolFlux is the solar flux [W/m^2], Id is the inherent degradation of the solar cells, θ is the incidence angle [deg], D is the yearly degradation constant and L is the mission life [years]. As can be seen, the power that remains to be generated by the unmovable panels is 194.92 - 158.36 = 36.56 W , which requires an area of 0.4242 m^2 for the body-mounted panels as computed by the Python code. This means that 4 QuadPack tops must be covered in fixed solar panels. The specifications are as follows:

- The area can be effectively contained in 4 articulating QuadPack sized surfaces on the Service Module and another non-movable 4 on the body
- The surfaces are placed in the most symmetric fashion possible
- The front surfaces can fold around a single QuadPack for launch, while others have no effect on the placement

This yields a more flexible concept, as the greater symmetry can be achieved with more panel weight being offset to the other side of the SPS.

18.3.4. Concept 3: The Rogue Concept

This concept is identical to Concept 2: 6 articulating panels on the service module and another 4 fixed panels on the body. However, the additional feature here is the fact that the body panels can articulate too, but to a smaller extent: an angle of 45° both ways can be attained due to compact actuators. This means that the only difference will be a decrease in required body panel area, to approximately 0.205 m^2, assuming an average incidence angle of 45° instead of 70°. This means that 2 QuadPack need to be covered with solar cells instead of 4.

18.3.5. Trade-off Weight Allocation and Concept Grading

In this section, the trade-off criterion weights will be specified and justified. Then, each concept will be graded from 1-5 in terms of ascending performance with regards to each trade-off criterion

Weights and Justification

The weighting given to the criteria goes as follows:

- *Flexibility:* this gets a weight of 3. Flexibility allows for the orbits to be altered without significant change or reconfiguration, and it is important for fast program deployment, avoiding additional costs and testing, and simply producing a more versatile design. It therefore gets a higher weight.

- *Ease of Implementation:* The Ease of implementation differs between these concepts to a large extent and is an important factor in the success of the development of the SPS-2 FF. For this reason, it is allocated a weight of 3.
- *Potential Cost:* The potential cost is an important factor as the limit costs that must be adhered to for the customer are a paramount requirement. Due to this, a weight of 3 is deemed appropriate.
- *Risk:* this criterion gets a weight of 1. While risk is important, it is not too different between these concepts and despite its importance may not prove to be decisive, Therefore, the lower weight of 1 is given.

CONCEPT GRADING: FLEXIBILITY

The concepts can be graded and ranked in terms of Flexibility as follows:

1. Concept 1, Grade: 5
2. Concept 3, Grade: 4
3. Concept 2, Grade: 3

Here, Concept 1 comes out ahead as the fully actuated solar panels allow for the greatest amount of flexibility. Concept 3 is second-best, as limited actuation is available for the top-mounted panels.

CONCEPT GRADING: EASE OF IMPLEMENTATION

The concepts can be graded and ranked in terms of Ease of Implementation as follows:

1. Concept 2, Grade: 4
2. Concept 1, Grade: 3
3. Concept 3, Grade: 2

Concept 2 is easiest to implement: the lower number of actuated panels leads to an easier design overall. For Concept 1, it is the baseline and outperforms Concept 3 as the latter requires additional actuation for the top-mounted panels.

CONCEPT GRADING: POTENTIAL COST

The concepts can be graded and ranked in terms of Potential Cost as follows:

1. Concept 3, Grade: 4
2. Concepts 1 and 2, Grade: 3

For the overall cost, the development of the hinges for the top-mounted panels is deemed to be minimal. Thus, the overall decrease in actuated front panels and lower area than Concept 2 is expected to yield the lowest cost. Concept 2 trails concept 3 purely due to the increased amount of solar panel area needed.

CONCEPT GRADING: RISK

The concepts can be graded and ranked in terms of Risk as follows:

1. Concept 2, Grade: 3
2. Concept 1, Grade: 2
3. Concept 3, Grade: 1

Here, Concept 2 is dominant as it has the simplest overall actuation requirement and thus the least risk of failure. The other two concepts are difficult to distinguish in terms of potential failure, and thus tie with a lower score.

18.3.6. TRADE-OFF SCORE TOTAL AND SELECTED DESIGN

The scores are computed with the given weights and the following ranking and point sums are achieved:

1. Concept 1, Score: 35
2. Concept 2, Score: 33
3. Concept 3, Score: 31

The winning concept is thus Concept 1, the fully-actuated fold-able Service-Module mounted array that is actuated to track the Sun . It is advisable that a similar panel deployment method is used in later design stages.

RENDER OF CONCEPT 1

The winning Concept 1 looks as follows:

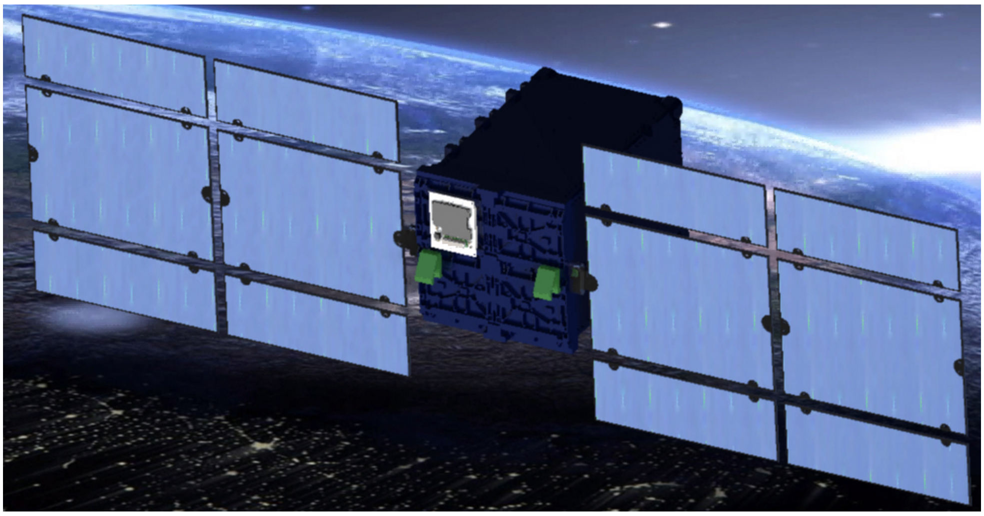

Figure 18.1: Render of Winning Service Module Concept CAD Model. ©ISIS

18.4. Coarse Cost Estimation

Here, an attempt will be made to estimate the expected mass of the PGD&S subsystem.

18.4.1. Coarse Cost Estimation

Just as for Step 1, the component costs can be totalled. In fact, the only alterations that must be made to the PGD&S subsystem come in the form of solar arrays: the increase in cost can be modelled from that alone. From chapter 10, the cost was estimated to be as follows:

Table 18.2: Power Subsystem: Preliminary Cost Estimation for Step 2.

Component and (Quantity)	Unit Cost [$]	Quantity [-]	Total Cost[$]
Batteries: Saft MP 176065 xtd	7,000	10	70,000
Solar Array Assembly	176,800	1	176,800
Harness, Power Conversion and PPT mechanism	100,000	1	100,000
Total Subsystem Cost			346,800

The Solar Array assembly now requires 16 6U panels: this yields, as per section 10.9, a cost of $16 \cdot 8500 = 136{,}000$ $. As the assembly and integration, as well as the hinge addition and actuation mechanism costs are unknown, these are factored in with a larger safety factor of 1.3, giving a total cost of approximately 176,800 $ for the solar panels. As for the total cost, the value is given to be 346,800 $, which is within the limit stated in section 10.9: this means that the Step may indeed be feasible.

18.5. Changes in Risk Approach

The risks for Step 2 only differ with regards to Step 1 when it comes to the redesigned PV panels. This results in several additional risks as seen below:

Additional Step 2 Risks

- **P-3:** *The actuation mechanism experiences a failure.* This has an *unlikely* probability, as the hinges and actuators are mechanical mechanisms and despite testing, certain regimes can cause premature failure. The impact of actuation failure is *fatal*, as insufficient solar power is generated.
- **P-4:** *The deployment mechanism experiences a failure.* This also has an *unlikely* probability, as the hinges and actuators are mechanical mechanisms and despite testing, certain regimes can cause premature failure. The impact of actuation failure is *fatal*, as insufficient solar power is generated and the payload can no longer operate at its required power.

18.6. Changes in Sustainability Approach

The sustainability of the concept is slightly decreased due to additional structures and materials required for Step 2 compliance. However, there will also be an increase in the sustainability due to additional created jobs and GDP. Therefore, the sustainability rating is deemed to not vary significantly between the Steps.

19
Thermal Control Step 2

The delta needed in order to go from the first development stage to the second development stage of the SPS-2 FF for the thermal control system is mainly caused by the change in attitude of the satellite and the larger power dissipation. The precise deltas of the subsystem relevant to the thermal control are given below.

- Payload: In step two the sun pointing for the body mounted solar panels and payloads is sacrificed for earth pointing payload capabilities in conjunction with deployable sun pointing solar panels. This will significantly alter the power input to the system. The deployed solar panels in particular will have to sustain a larger temperature variation than the body mounted ones.
- ADCS: Due to the use of a different ADCS architecture the sensors and actuators will have a different pointing offset with respect to the earth for the payload and with respect to the sun for the solar panels.
- Power dissipation: Due to the more power consuming electronic subsystems needed for step two the power dissipation has been altered for both the sunlight phase of the orbit and eclipse.
- Component temperature range changes: Lastly considerations have to be made in order to account for the fact that many electrical components will be altered during step 1 and step 2 such that there is the potential shift in allowable temperature range.

Due to these changes the thermal behaviour of each of the vital components will have to be re-analysed. Due to time constraints it was however chosen to focus only on the most crucial part, thus the service module, as this houses the most essential and vulnerable components.

19.1. Transient Thermal Analysis

Different to the nodal analysis presented in section 11.4. In this case the only one isolated node for the service module will be considered. Thus the energy balance for the service module simplifies to $m \cdot c_p \cdot \frac{dT}{dt} = P_{in} - P_{out}$.

Each of the terms in the energy balance will now be analysed separately and subsequently the differential equation will be solved. Separately the energy balance for the deployed solar panels will be set up in order to assess their temperature variations.

19.1.1. Power Input to Service Module

The orientation of the SPS2-FF for the second step is such that the Z-axis constantly points towards earth. From the service module an array of solar panels is deployed which can be rotated to track the sunlight. The preliminary architecture of the outside of the service module is kept the same except that the solar panel on side 3 is replaced by white space-rated paint. This is done in order to reduce the necessary delta from step 1 to step 2.

The power input is computed using the same procedure as for step 1. The internal power dissipation in the service module is 54.6 W in sunlight and 30 W in eclipse (chapter 18). The resulting power input from position 1 to position 2 is shown in Equation 19.1, the power input from step 2 to step 3 is shown in Equation 19.2 and lastly the power input from position 3 to the position at which $\beta = 180°$ is shown in Equation 19.3.

$$\begin{aligned} P^{in}_{1-2} =& q_{sun} \cdot A_{side3} \cdot \alpha^{th}_{side3} cos(\beta) + q_{sun} \cdot \alpha^{th}_{side1} \cdot A_{side1} \cdot cos(90-\beta) + \\ & q_{IR} \cdot \epsilon_{side4} \cdot A_{side4} + q_{sun} \cdot albedo \cdot \alpha^{th}_{side4} \cdot A_{side4} + Q^{sun}_{internal} \end{aligned} \tag{19.1}$$

$$\begin{aligned} P^{in}_{2-3} =& q_{sun} \cdot A_{side1} \cdot \alpha^{th}_{side1} cos(\beta - 90) + q_{sun} \cdot \alpha^{th}_{side4} \cdot A_{side4} \cdot -cos(\beta) + \\ & q_{IR} \cdot \epsilon_{side4} \cdot A_{side4} + q_{sun} \cdot albedo \cdot \alpha^{th}_{side4} \cdot A_{side4} + Q^{sun}_{internal} \end{aligned} \tag{19.2}$$

$$P^{in}_{3-ecli} = q_{IR} \cdot \epsilon_{side4} \cdot A_{side4} + q_{sun} \cdot albedo \cdot \alpha^{th}_{side4} \cdot A_{side4} + Q^{eclipse}_{internal} \tag{19.3}$$

The power input to the service module as a function of orbital angle β is visualised in Figure 19.1.

19.1.2. Power Radiated to the Environment

For the power radiated away from the service module the same basic principles holds as for step 1 subsection 11.4.2 and is summarised by Equation 19.4.

$$P^{i}_{radiated} = \sigma \Sigma(\epsilon^i_j \cdot A^i_j \cdot T^{i^4}_j) \tag{19.4}$$

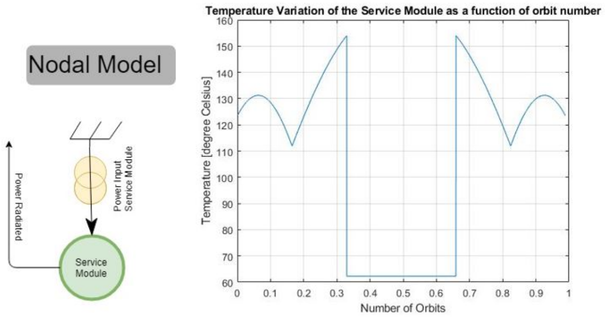

(A) (B)

Figure 19.1: (A) Service Module represented by one isolated node. (B) Variation of power input to the service module as a function of orbital angle.

19.1.3. ENERGY BALANCE & PROPAGATION

The energy balance for this single node can be set up in the same form as previously done with the key difference that there is no conduction from the mounting ring to the service module.

$$m_{SVM} * cp_{SVM} \cdot \frac{T_{i+1}^{SVM} - T_i^{SVM}}{\Delta t} = Power_{In}^{SVM} - \sigma \cdot \Sigma(\epsilon_{SVM} \cdot A_{SVM}) \cdot T^{i4}_{SVM} \tag{19.5}$$

Re-arranging for T_{i+1}^{SVM} yields in Equation 19.6.

$$T_{i+1}^{SVM} = \frac{m_{SVM} \cdot cp_{SVM}}{\Delta t} \cdot T_i^{SVM} + Power_{In}^{SVM} - \sigma \cdot \Sigma(\epsilon_{SVM} \cdot A_{SVM}) \cdot T^{i4}_{SVM} \tag{19.6}$$

Propagating this equation for 6 orbits yields in the temperature variation of the Service Module node shown in Figure 19.2. Note that the only change to the thermal design has been changing the body mounted solar panel for white paint surface finish on side 3. For all other parameters Table 11.6 applies.

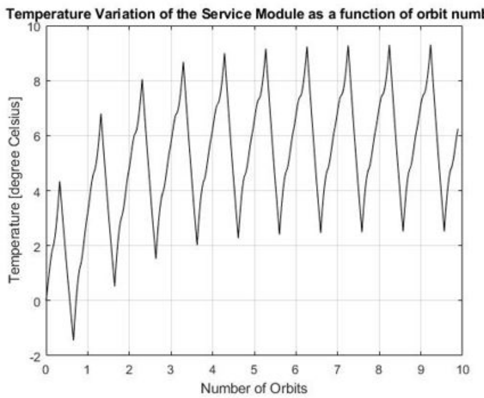

Component	Min temperature(°C)	Max Temperature(°C)
Saft batteries (76065 xtd)	-30	80
Power Conversion, regulation, transmission network	-20	45
Solar Panels (AzurSpace cells)	-20	50
ANT2000 (antenna)	-40	85
TR-600 (transceiver)	-40	85
NanoDock SDR (motherboard)	-20	85
NanoMind z7000 (cpu)	-40	85
RW1 (reaction wheel)	-40	70
TQ-15 (redundant wind) (magnetorquer)	-55	70
NanoSSOC-A60 (Sun sensor)	-30	85
QRS116 (gyroscope)	-55	85
NMRM-001-485 (magnetometer)	-25	70
GNSS receiver	-40	85
Al-7075-T6 Ring Structure	-273	635

(A) (B)

Figure 19.2: (A) Temperature variation of the service module as a function of the orbit. (B) Service Module components operating temperatures.

The temperature variations are well within the operational limits of all components in the service module and thus passive thermal control is deemed satisfactory for this step. Upon comparison with step 1 it is clear that the addition of a white paint surface, which reduces the heat flux input to the service module, is more than balanced by the additional power dissipation by the electronical components in the service module.

19.2. CONCLUSION & RECOMMENDATIONS

The incremental development is small for step two as there is no active control necessary, just as step one. For the thermal control the main changes with respect to step 1 are that instead of the body mounted solar panel on side

3 it has to be coated in space grade white paint. Additionally, as only passive means are employed, the thermal design can still be adjusted with ease in case of changing internal heat dissipation or upon incorporation of the more detailed nodal model, especially the heat transfer from the solar panels. Upon further design iterations the temperature variations of the solar panels and their heat transfer to the service module shall be considered. Additionally the nodal model for step 1 should be used for step 2. Consequent to this the same recommendations applies as outlined in section 11.6.

20
Structural Design & Analysis Step 2

All changes corresponding to step 2 for the structure are to be described in this chapter.

20.1. Step 2 Service Module Configuration

For step 2, additional components have to be added to the Service Module. An overview of these can be found in Table 20.1.

Table 20.1

ID	Product Name	Subsystem	#	Total mass	Description
Step2					
Mai-SES S2	Mai-SES IR	ADCS	2	66 [g]	Step 2 earth sensor
POW-SOL S2	Azurspace Solar Cells 3C44c assembly	Power	1	4490 [g]	PV panels on top of Service Module
		total mass including step 1		13.41	

20.1.1. Step 2 Service Module Configuration

For step 2 two earth sensors have to be added, which need to be placed on the outer structure. This is shown in Figure 20.1.

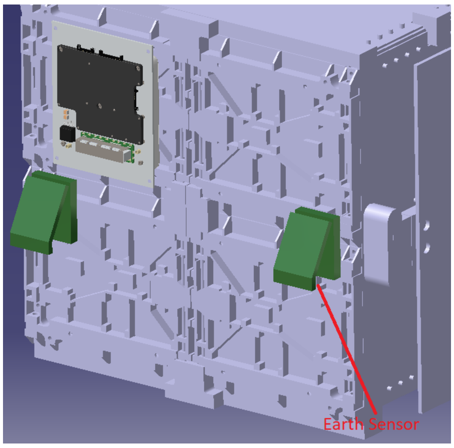

Figure 20.1: Placement of the two earth sensors for the ADCS subsystem in the step 2 design. ©ISIS

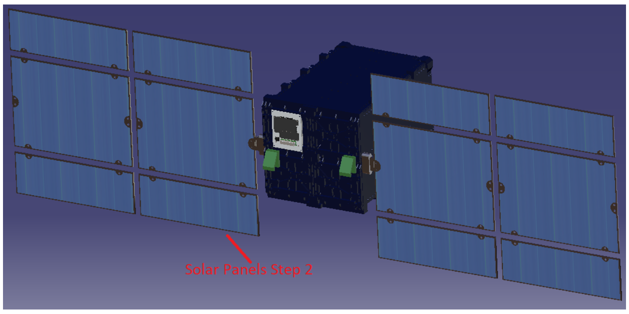

Figure 20.2: Placement of the solar panel configuration for step 2. ©ISIS

20.1.2. Power

For the power, the solar panels on each of the QuadPacks are removed, and a new configuration of solar panels is used. There is a need for solar panels that can keep pointing at the sun whilst in orbit, as such a rotating solar panel arm is used. The new configuration is shown in Figure 20.2.

This concludes the design of the service module for the second step, the rest is kept the same and no more changes are made to the design of the structure itself. An overview of the service module with the extra components can be seen in Figure 18.1.

21 DEVELOPMENT CONSIDERATIONS STEP 3

21.1. ASTRODYNAMICS

Due to the required mission altitude for step 3, the SPS-2-FF will be put at a circular 450 km altitude orbit after Primary Payload (PPL) separation, and will be kept there for the duration of the mission. After the mission lifetime, and before the maximum lifetime of 25 years, the SPS-2-FF will deorbit after 3.6 years through passive orbit decay. However to bring the SPS-2-FF into this orbit and to circularise it, a great amount of ΔV is required from the AVUM+ module. This greatly increases the delta from step 2 to 3, not in technical design but mission complexity and cost. This is traded off against giving the SPS-2-FF its own propulsion system, and is found to be more cost and weight effective, as it allows the SPS-2-FF to carry more payload, while making the most use of the leftover propellant in the AVUM+ module after PPL separation. The required inclination for this orbit to be sun-synchronous is 97.2°. As with the elliptical orbit, this is outside the range of the 98° to 108° polar range. Once again however, the difference is deemed negligible and therefore the inclination used for step 3 orbit will be 97.2°.

21.1.1. ORBIT PARAMETERS

The final parameters of the orbit design for all steps are shown in Table 21.1.

Table 21.1: Orbital parameters for all three steps.

Parameter	Step 1	Step 2	Step 3
altitude (km)	350x850	350x850	450
semi-major axis (km.)	6971	6971	6821
eccentricity (-)	0.04	0.04	0
orbital period (min.)	97	97	93
eclipse period (min.)	35	35	36
inclination (deg.)	97.8°	97.8°	97.2°
lifetime all QuadPacks attached (yrs)	4.8-7.0	4.8	3.6

21.2. OPERATIONS

The payloads that generate the most data for step three are the optical payloads. They generate “a few GB per day” of data [4]. Only one of these payload will be placed on the SPS-2 FF for the third step. This changes the amount of data generated to a total of 9.56 $Gbitsperorbit$. When using one pass in an orbit and a gain of 8 dB, the link budget closes for all ground station antenna’s except the 2.4 m diameter for Redu.

The link budget does not close for any antenna when the antenna radiates under an angle of 90° (-3.2dB). Even when increasing the contact time by three, the link budget does not close (1.6 dB). In order to close the link budget for the bigger stations ($\geq$ 12 m diameter), the angle can be maximum of 65 °. This corresponds to a gain of -4 dB, with a data rate of 11.4 $Mbits/s$. As a result the SPS-2 FF has to point more accurately towards the ground station. If this is not possible, new antenna’s need to be chosen which increases the design effort.

21.3. ADCS

Step 3 has the most stringent requirements of all steps, with a pointing accuracy of <0.03° [7]. The reaction wheels are still capable of performing this job [17]. The one thing that needs to be added for step 3 are star trackers. The implemented Earth sensors and Sun sensors are still needed for the needed Earth and Sun acquisition. However, the accuracy is not good enough [1]. Star trackers can have an accuracy that is <0.03°[1].

This means that all ADCS components in step 1 and 2 can be used for step 3 as well, with two star sensors added, taking redundancy into account. As one can see, the delta from step 1 to 2 and from step 2 to 3 are as small as possible. The only thing that must be added is a sensor for each consecutive step.

[1] URL: https://www.cubesatshop.com/product/mai-ss-space-sextant/ [cited on 23rd of June 2019]

21.4. POWER

For the Step 3 Feasibility of the power generation and distribution subsystem, the required arrays and batteries must be sized, Their subsequent requirements in terms of mass and volume will be attempted to be verified. This will allow for a preliminary evaluation of what can be done and whether the transition to Step 3 is at all possible for the PGD&S subsystem. Firstly, the solar area and battery capacities will be computed. Then, cost will be estimated, followed by a discussion of feasibility.

21.4.1. POWER GENERATION COMPONENT RE-SIZING

As the pointing conditions do not change significantly from Step 2, only supplementary area is needed on the actuated front panels. The required area is computed to be 1.12 m^2, which requires 10.6 QuadPack top-equivalent surfaces. These will increase the weight of the PGD&S subsystem significantly to 9.713 kg and cost to $413,000, with the same coarse estimation methods as used for Step 2 and 1.

21.4.2. FEASIBILITY DISCUSSION

The feasibility of the PGD&S subsystem is questionable for Step 3. For instance, the cost of the assembled subsystem alone without development costs is $413,000 (€362,450 for FY2019) is higher than the allocated 17,5 % (€350,000). However, the excess is only €12,450, and thus this is still deemed feasible with modifications and cost-reducing measures taken post-DSE. For the mass allocated, the total comes out to be 9.713 kg as per chapter 24, which is 3.9 % of the total allowable mass of 250 kg. This is deemed to be reasonable and feasible for the full design. Due to a shortage of time, the computational aspect of the implementation of Step 3 could not be further elaborated upon. However, the following aspects must be further investigated for a full assessment of the feasibility:

- The power generated and energy stored need to be integrated over the mission lifetime and the overall power delivery capability needs to be verified for consistency over the full operational life of the subsystem
- The topology of the power distribution system must be designed and verified for functionality for all Steps.
- The degradation of the PV panels needs to be accurately modelled

Given the scope and time-frame of this project, this further analysis could not be performed. However, purely in terms of the technical budgets as seen in chapter 24, the Step is deemed *feasible*.

22 Risk Map

All the aforementioned risks are listed below and can be combined in a risk map. Two maps are made, one before mitigation (Table 22.1 and one after mitigation (Table 22.2). The detailed explanation of the risks can be found in the corresponding chapter.

- OP-1: Computer program GMAT mistakes, causing communication issues.
- HW-1: Hardware failure.
- GC-1: No data downlink possible for a long period of time.
- S-1: Sun sensor failure.
- R-1: Reaction wheel failure.
- MM-1: Magnetometer failure.
- MT-1: Magnetorquer failure.
- G-1: Gyroscope failure.
- B-1: Batteries cease working prematurely.
- B-2: Batteries experience a wiring issue.
- B-3 Supplier refuse to source batteries at given price.
- P-1: The solar panels fail prematurely.
- P-2: Supplier refuse to source cells/assemble panels at given price.
- RAD-1: Radiator fails to export heat to space.
- DEG-1: Degradation of surface components, leading to changing properties.

Additional risks for step 2:
- E-1: Earth sensor failure.
- P-3: The actuation mechanism experiences a failure.
- P-4: The deployment mechanism experiences a failure.

The external risks were discussed before in the Baseline report. [11] These remained invariable over time except risk E5: requirements change. This probability of this risk decreases as the project developed and the requirements got more defined.

Table 22.1: Risk map before mitigation, with the red coloured areas indicate high risk, the orange part shows medium risk and green is low risk. The operational risk are coloured in orange, the power risks in blue, the ADCS risks in green and the thermal risks in red.

Very likely	LOW	MEDIUM	HIGH		
Likely			DEG-1		
Moderate			G-1, B-3, P-2	B-2	
Unlikely			OP-1, GC-1, RAD-1		R-1, E-1, B-1, P-1, P-3, P-4
Rare				MM-1, MT-1	HW-1, S-1
Probability/Impact	Negligible	Minor	Significant	Critical	Fatal

Table 22.2: Risk map after mitigation, with the red coloured areas indicate high risk, the orange part shows medium risk and green is low risk. The operational risk are coloured in orange, the power risks in blue, the ADCS risks in green and the thermal risks in red.

Very likely	LOW	MEDIUM	HIGH		
Likely		DEG-1			
Moderate					
Unlikely		GC-1	G-1, B-3, P-2	R-1, E-1, B-2	P-3, P-4
Rare		OP-1, MM-1	RAD-1, MT-1	HW-1, S-1	B-1, P-1
Probability/Impact	Negligible	Minor	Significant	Critical	Fatal

23
VERIFICATION & VALIDATION

It is critical that during the detailed design of the SPS-2 FF verification and validation is conducted, in order to ensure that the requirements are met by the design and that the system performs in the way intended and to the customer's satisfaction. If this is done, and the validation of the whole system is successful, the functionality of the design can be proven. A flowchart illustrating the procedural flow of all verification and validation tasks is shown in Figure 23.1. A thorough explanation of each step can be found in the previous midterm report. This chapter will focus on the implementation of V&V on the detailed design of the SPS-2 FF. In the first section, the verification and validation of the used models is explained. Following this, the product verification methods suited for the SPS-2 FF are discussed. Finally the last section is dedicated to the SPS-2 FF product validation.

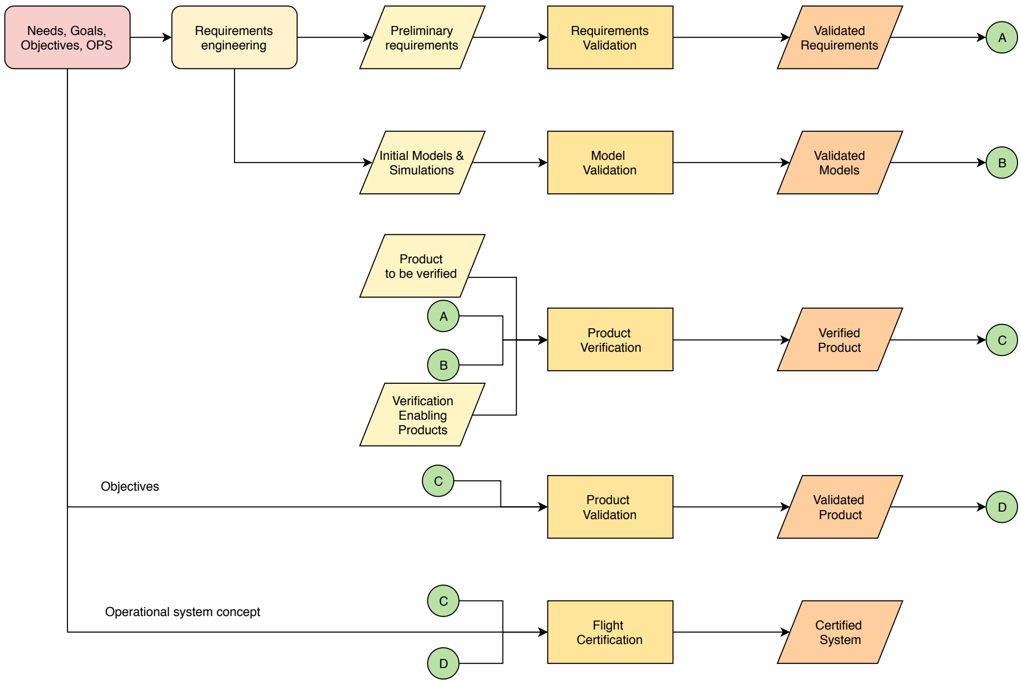

Figure 23.1: The chronological flow of the verification and validation procedures [42].

23.1. MODEL VERIFICATION

Simulation model verification contains code verification and calculation verification, in order to prove that the model accurately represents the chosen physical model. Code verification is done through inspecting whether code has been implemented correctly, and without syntax errors. Calculation verification is done through bottom-up testing through the following tests:

- Unit(feature) Test
- Integration Test
- System Test
- Acceptance Test

These models were used by the s15 group members individually, to each verify their own programs. Any other pre-existing models which were used by group S15 were deemed to be sufficiently validated by the organisations who developed or used these models, as they had a long and well known heritage. For instance, SPENVIS is a widely used and highly verified tool. These models were only subjected to acceptance tests: SPENVIS' orbit propagation tool, for instance, was verified to produce an adequate number of usable data-points.

Furthermore, physical models can be used to inspect aspects such as geometry and interfaces before the real subsystems are made. However, as the SPS-2 FF will use COTS components and will remain as close as possible in terms of design to the SPS-1 to decrease the inter-step delta, it is deemed more convenient and time-efficient to not construct a separate physical model, as most components already physically exist and are easy to procure. This reduces the risk of having to produce a system which turns out to be fully unusable, as most parts are already produced or will be produced for either the SPS-1, or are commercially available, resulting in no extra investment for the production capability, only a one-time purchase or cost for the production for one extra ring for example.

23.2. MODEL VALIDATION

The methods can be validated based on the following methods:

- **Experience**
- **Analysis**
- **Comparison/test**

Most of the models developed by group S15 were developed not because no independent proven models existed for the physical models to be simulated, but because no access to those was available. Therefore they could also not be validated through comparison. For these a combination of experience and analysis was used. For the experience use was made of the available tutors and experts from Airbus to validate results, and otherwise careful and thorough analysis was done by group S15. For this analysis, tests such as those for verification were used for the whole model. This includes using reference models from literature of which the inputs and outputs are known for testing. The orbital propagation performed by the group was cross-checked with SPENVIS.

23.3. PRODUCT VERIFICATION

The 4 methods existing for verification of a product, according to [43], are:

- Test, including demonstration
- Analysis, including similarity
- Review Of Design
- Inspection

It will depend on each subsystem and component what verification method is possible and preferred due to limitations in size, budget and nature of the purpose of the component. For each subsystem the preferred method will shortly be discussed. In general, it would be advised to do an entire vibration test on the service module of the SPS-2 FF, and more vibration tests on subsystems with moving parts.

23.3.1. ADCS

The ADCS subsystem can be exposed to multiple verification methods in order to test adherence to the requirements. The preferred method would be testing the ADCS subsystem in a simulated environment. Tests such as performance tests before, after or during vibration, radiation exposure and thermal tests are advised. The topmost level of this would require the SPS-2 FF system to be placed in a 3-axis gimbal harness, preferably in a vacuum, and the attitude determination and control tested through simulated inputs to the determination subsystem, or using simulated attitude sensor data.

On the analysis that has been performed to achieve the current design verification has already been performed to guarantee that the obtained results were compliant with the desired result.

Verification of the Coordinate Transform Models

The data from the SPENVIS models implemented is already verified by the creators of the models. The software that converts this data has been verified in numerous ways. Firstly, it has been checked by inspection and comparison. The coordinate transformations have been checked using unit tests and analytical calculations for several samples of the dataset. Furthermore, the implementation of the coordinate transformation has been checked to see if the distance of the spacecraft with respect to the centre of the Earth remained the same for every datapoint in every reference frame. Also other values, such as velocity have been checked to see if the magnitude remained the same. Furthermore, the reference vectors to calculate certain transformation angles have analytically been checked to see if they were implemented correctly. From this it was discovered that the reference vector in the z_C did not correctly tranform to other frames, as a unit vector was used. It was then changed to an unlimitedly long vector to tackle the problem. This vector has been used to also verify the orientation of the spacecraft which has been implemented. The altitude, longitude, latitude and normalised Sun vector have been used to analytically check the attitude of the spacecraft with respect to the Sun and the Earth. Also, inspections have been executed to check if units and unit transformation have been implemented correctly in the simulation.

Lastly, the results from the simulation have been checked with the results from [26, 28]. However, their magnitude differs from the results obtained in the simulation by around a factor 10. Another full break-down of the model occurred and every line of code was checked and verified once more. The analytic calculations executed in the program are quite simple expressions, see section 9.3 and have the correct magnitude. Therefore, the model is deemed to be correct. The discrepancy is thought to be a result from [28] and [26] using a different and more advanced model from Airbus D&S. Next to that, the mass and size of the SPS-2 was different when their research occurred and thus they use a different MMOI. In their analysis the spacecraft is also Earth-pointing instead of Sun-pointing. This means that the attitude is different, which alters the results. Furthermore, as the attitude is different, their models include the solar radiation pressure as a disturbance factor as well.

Verification of the Detumble Time Simulation

The software written to simulate detumbling after release from the AVUM+ stage was verified using inspection, and comparison. Also contact with the client was used to employ experience in the verification procedure. Results from the angle calculations for instance were manually inspected to never exceed 90° as that would mean the magnetorquer was not working as it would in real life. Also the control method was analysed such that the magnetic field induced by the magnetorquer would always create the desired force direction exerted on the spacecraft. Furthermore, a comparable analysis was found in literature, which did not take all factors into account as in our program. The program was run using the same factors as the analysis in literature to confirm that that part of the simulation was compliant [28].

Verification of the Desaturation Simulation

The verification of the desaturation simulation was done similar to the verification of the detumble time simulation. Here also the intermediate values were inspected to make sense and reviewed with respect to values found in literature if applicable. Furthermore, logic was used to verify that additions to the simulation, like the magnetorquer/magnetometer ratio would indeed increase the desaturation time and not decrease it as would be impossible.

Verification of the Reaction Wheel Analysis

The code used for the reaction wheel performance analysis has been verified by checking all calculations analytically. Furthermore, the implementation of the angles has been checked by analysing the torque difference over the axes if different inclination angels are implemented.

23.3.2. ODCS

The simple ODCS system can be tested by a test setup where a transceiver sends out a simulated GNSS signal to the GNSS receiver, which then updates the on-board Vinti orbit propagator with the simulated orbital location and parameters. The output of Vinti, both the instantaneous location and velocity as well as the location and velocity propagated over a certain time period can then be compared with the original simulated data and it's respective propagated location. Furthermore, a radiation test could be conducted in order to test the system in cases of heavy radiation doses. A thermal range is already given for the receiver, -40 to $+85°C$ but it would be suggested to test the receiver together with the entire service module for thermal behaviour.

23.3.3. PGD&S

The methods that are applicable to the verification of the PGD&S subsystem product verification include Testing, Analysis and Inspection. The specifics of applicability of these two methods will be outlined here. After this, the software and calculation verification of the design process will be discussed.

TESTING OF PGD&S SUBSYSTEM

Testing for the PGD&S subsystem can be performed for multiple components and for the entire assembly. The photovoltaic panels can be tested for their power capability generation at beginning of life, as well as for integration on the structure. The MPP tracking and power distribution can easily be tested for a range of currents and voltages, and is the most important component to test as it must be topology-optimised and designed from the ground up. The batteries can be tested over some charge-discharge cycles, and all of the components can be tested for compliance with specified power standards when functioning together. Another set of components that can be tested is the Step 2 and 3 torsional spring assembly for solar panel deployment: the solar panels must deploy without damage and be still during operation. In addition, every component can be tested for its temperature range adherence. For end-of-life power, only analysis can be performed. Some additional tests that can be performed for the Power Generation assembly (PV panels and hinges) are[44]:

- UV Exposure for Encapsulant Materials: A multitude of other reports cite discoloration in the encapsulate materials. This effect is also reflected in the degradation of the short-circuit current I_{sc}. This testing is deemed to have already been performed by AzurSpace.
- UV Exposure for Backsheets
- UV Exposure for Cables and Connectors
- Bypass Diode Thermal Test
- Thermal Cycling Test
- Hinge Stress Test

Testing the actuation and deployment mechanism for the PV assembly is perhaps the most critical aspect to be tested. Therefore, it is recommended that this testing is performed rigorously as the mechanism is a significant source of failure if the failure modes are not properly investigated and designed for.

Analysis Of PGD&S Subsystem

The analysis of the PGD&S subsystem is very useful for verification: this allows the system to be verified for the end-of-life power delivery compliance. In the short development span available, full-scale testing for end-of-life is not feasible. An important aspect to note here would be the use of more detailed computational models than the ones used in this design stage: the degradation would have to be modelled accurately over the propagated lifetime. Since models of the present particulates and solar radiation can be implemented, the detailed modelling of the panels themselves will allow for analysis of the end-of-life conditions. The recommendation for further design and subsequent subsystem verification is to replace the simple sizing performed here by an orbital propagation including parameters such detailed varying solar flux, attitude and particle density-related degradation.

Inspection of PGD&S Subsystem

Some components in the PGD&S, such as the batteries, will be COTS. Thus, inspection and acceptance testing of those components and very basic testing can be sufficient. For the batteries, the capacity, charge and discharge voltage and temperature parameters should be simple to verify by simple inspection.

Verification of Detailed Design Computation for PGD&S

For the tools used in this DSE project, code and calculation verification were performed. For the code, the syntax was thoroughly checked and all errors were corrected. As for calculation verification, the code used for the PGD&S subsystem computations was very simple and could be verified by hand. This hand-verification was unit testing at first, as sub-components of the code were verified to output the same values given identical inputs. Then, the entire program was verified in the same fashion.

23.3.4. Thermal Control

The verification and validation for the thermal control subsystem is split into two distinct aspects. The first is presented in subsection 23.3.4 and explains the procedures undertaken in order to verify the transient thermal nodal model to the largest extent possible. Next to this the possible validation techniques are outlined in Table 23.3.4.

Model Verification

In order to fully verify the module there are three distinct aspects which have to be verified. These are the power input and output to the nodes, the conduction between nodes, the energy storage of the nodes. Due to the stringent time frame it was not possible to establish a detail verification procedure for each of these. Instead the verification for the nodes will be done based on comparison with the steady state worst case estimated made in section 11.2 and section 11.3. For the steady state the assumptions are that the nodes/components are isolated from each other, such that no heat transfer between them occurs and that they no not poses thermal inertia, such that they react to power input changes instantly. In order to replicate these conditions with the nodal model, the conductivity between nodes is decreased to 0.001 W/mK and the mass and specific heat capacity set to 1. The resulting maximum and minimum temperature for the service module and mounting ring node are

Table 23.1: Comparison of the values obtained by using the steady state equations or the Nodal model

	Mounting Ring	*Service Module*
Temperature Steady State Max	139.3563°C	53.2230°C
Temperature Nodal Model Max	139.2587°C	54.8076°C
Δ	0.0976°C	-1.5846°C
Temperature Steady State Min	-61.9908°C	-41.4625°C
Temperature Nodal Model Min	-61.8215°C	-41.4743°C
Δ	-0.1693°C	0.0118°C

compared to the steady state values in Table 23.1. Note that different to section 11.2, the power input equation used for the thermal equilibrium calculations for this section have been revised in order to reflect the effect of the ADCS sun pointing error. This yields in a higher power input during the sunlight phase for which reason the calculated thermal equilibrium temperature presented in this section is higher than the one presented in section 11.2. The comparison in Table 23.1 shows that both methods predict nearly identical results. For this preliminary stage this is deemed sufficient as the time necessary in order to setup a comparable transient thermal model exceeds the time frame of this detailed design phase.

VALIDATION OF THERMAL CONTROL

The possible validation techniques of the thermal control subsystem of the SPS2-FF are summaries below.

- *(Unit Test)* Conduction Across Service Module-Mounting Ring Interface
- *(Unit Testing/System Testing)* Thermal Cycling Testing: Variable exposure of components or the overall system to the worst case hot and worst case cold temperature. Used to reveal production deficiencies.
- *(System Testing)* Thermal Vacuum Test: Temperature Cycling of the system in a vacuum. Frequently used as it is one of the most realistic replication of the actual operation environment of the satellite.[1]

The internal heat generation can be tested, and the dissipation through the ring structure could be tested through a heat input at the service module interface. Solar flux and IR flux from the earth however will have to be analysed.

23.3.5. STRUCTURE

The calculation of the structure of the cylinder is to be verified in this section. A method to verify both calculations of the solid and skin-stiffened cylindrical structure is given in the following subsections, respectively.

VERIFICATION SOLID CYLINDER STRUCTURE

The first step in verification of the calculation of the structure are the unit steps in the system. Figure 12.9 shows the corresponding unit blocks, illustrated in yellow. To check if one unit block is correctly implemented in Python, values from an example exercise in *Space Mission Analysis and Design (SMAD)* [22] can be used as input. The output of the unit block can then be compared to the results given by *SMAD*, by means of a value comparison or unit check. No differentials between the Python Code and the results of *SMAD* where therefore found. The input values of *SMAD* are now replaced by the values corresponding to the SPS-2 FF structure. To check if the system as a whole outputs a good approximation, comparison with *Concept study of Stackable Platform Structure: Structural Analysis of SPS-1 and SPS-2* about the SPS-2 FF can be made [45]. Results of the frequency analysis, mass and thickness of the ring were used to compare to the results of the python code. From the comparison it is found that the results of the Python Code were almost the same as the results from the aforementioned report.

VERIFICATION SKIN-STRINGER STRUCTURE

The same procedure in the aforementioned subsection can be used to verify the calculations for the skin-stringer structure. A difference in output was however observed between results from *SMAD* and the unit block *Skin Buckling Stiffened Panel* σ_{cr}. This differential can be explained due to the calculation of buckling coefficient k, illustrated in *SMAD, Fig. 11-35, p. 479* [22]. Here, k can only be read off the graph based on the skin-stringer dimensions. To iterate, a formula of this buckling coefficient must be used in the Python Code. Since $\frac{r}{t} << 500$, the theoretical curve is chosen and a polynomial was approximated with the given values. To make the approximation more accurate, an exact formula for k should be used that is based on the skin-stringer dimensions. For the system verification a comparison with the aforementioned report in the previous section can be made again. The values of the Python Code were almost the same as what was given in the report. It can therefore be concluded that the results are verified correctly.

23.3.6. MECHANISM

The release mechanism for the Marman Clamps should be verified, as well as the CubeSat QuadPack deployment and the unfolding of solar panels for step 2 and 3. The Marman Clamp release has already been tested for the connection to the PPL for the SPS-1, thus it only needs to be verified through testing for the connection to the Vega-C connector. The same goes for all the CubeSat QuadPack deployers, and therefore this design does not need to be verified anymore. Finally the solar panel deployment will need to be tested. Due to the small size of the solar panels and the expertise of ADS NL this is expected to not pose any problems, thus the verification of this aspect of the SPS-2 FF is deemed relatively uncomplicated.

[1] URL:'https://pdfs.semanticscholar.org/35fb/b8424e70bdf568e233db7d77875405ed31ed.pdf',Accessed:'24.06.19'

23.3.7. Operations
There are four elements involved in the design of the ground operations model, communications system and data handling system. The verifiability of these mission and spacecraft components depends on five main elements: mission requirements, simulation software, specifications of the selected off-the-shelf products, the literature consulted for reference and the analytic methods used. The vast majority of requirements have been used as design input throughout the different design phases of the product. These requirements, such as payload data generation rate or data handling interfaces, have been verified by review of design after their detailed update when initiating a new design phases. The accuracy of requirements increased over time, being updated on a weekly basis by constant contact between the project team and the client.

GMAT has been used for the simulation of orbit propagation, while MATLAB has been used for the modelling of antenna signal propagation. Both design environments have been acquired from official and reliable sources, and are therefore assumed to provide trustworthy analysis of the physical models they are intended to represent. The compatibility of system requirements and commercial off-the-shelf products is based on the predicted performance of these products. Despite being provided by the manufacturers, the technical specifications of the products considered to be included as subsystem components have been critically studied and extensively compared among the available product catalogues. Furthermore, only products with certified acceptance testing and flight heritage have been considered. Therefore, the verification of the subsystem components has been already performed in the form of testing by the suppliers.

Literature has been consulted to estimate design variables at the beginning of each iteration and to confirm the feasibility of our iteration outputs. Verification through similarity has been used by comparing analogous mission and/or products throughout the design, specially during the verification of signal reception by ground stations. The mathematical expressions behind analytically obtained values are explicitly derived, appropriately referenced or thoughtfully explained throughout the report. Moreover, the limited set of calculations performed manually have been compared and cross-verified, after being repeated independently by different members of the design team.

23.3.8. Payload Interface
Besides verifying the deployment of CubeSats by the ISIS' QuadPack deployer, only significant interfaces will be necessary for IOD payloads, as any deployed CubeSats will be independent of the SPS-2 FF. The verification of these interfaces depends on the IOD, but this is expected to include testing the power supply, possible data rates and structural connections. For structural connections it is advised to conduct vibration tests and load tests, while for the rest simulated input tests will suffice.

23.4. Product Validation
For the final product validation is necessary to confirm that the design performs as intended, accomplishes it's intended purpose and is suitable for the mission. The validation of the SPS-2 FF will be done through the 3-step approach. The initial flight of step 1 will validate the primary functions of the system, structural integrity, stabilisation and sun pointing. Step 2 will demonstrate the capability of the SPS-2 FF system to provide a platform to host the wide range of expected IOD missions, including the power and interfaces required for this as well as the capability to achieve more accurate attitude control. For the dedicated methane mission of step 3 no initial mission which will be followed by more of its exact kind will exist, and it is not preferred to validate the satellite at the moment when it is supposed to accomplish its mission successfully. Therefore step 3 will have to be validated by a combination of analysis, demonstrating subsystems and the whole system in an accurately simulated environment and situation. This will mostly be reduced to the mission payload and the interaction of this payload with the SPS-2 FF as most of the SPS-2 FF has already been validated in step 3.

In which terms the phases will prove that the system can perform the mission are stated below.

Phase 1
- Structure
- Basic ADCS
- Basic power

Phase 2
- Fine ADCS
- High power range
- Long possible lifetime

Phase 3
- Mission specific payload integration

24
Budget Control

In this chapter the general budgets and budget estimations used in the design process of the SPS-2 FF will be discussed. These can be divided into 4 parts: Mass, Power, Propellant and Cost. Mass will be discussed in section 24.1, Power is discussed in the Power subsystem section, subsection 10.3.2. As the SPS-2 FF does not require any propulsion subsystem, no Propellant budget is required. Finally the Cost budget and estimations are discussed in section 24.2.

24.1. Mass Budget

Mass wise the SPS-2 FF should adhere to the requirements **SPS-2-LEI-MASS-1** and **-2**: the maximum dry mass of the SPS-2 FF shall be less than 200 kg in launch state and less than 250 kg for wet mass. In order to ensure this, multiple weight estimation models were considered. However these were based on general satellite design's such as the weight estimations used in *SMAD* [17]. As the SPS-2 FF is far from ordinary, the assumptions and equations for these estimations could not provide a satisfactory and realistic approximation. A big difference for example is that the SPS-2 FF has a very large portion of its weight invested in the structure, as it is supposed to also be a load carrying structure for the PPL, thus it should be structurally strong. Furthermore, the nature of the payload is different as well. While the IOD payloads are still close to normal payloads on a satellite, deployable CubeSats which become a tertiary payload have their own service module already on them, increasing their weight as compared to just being instruments, due to them requiring their own bus.

24.1.1. Step 1

For step 1, an in-depth analysis has been made for all budgets. This is as the detailed design is focused around step 1, with step 2 and step 3 illustrated through their respective delta's.

Initial Mass Estimation

Initially an estimation was made by combining the estimation for the service module in the report from C. Hobijn [46] with the report on the structure made by DutchSpace [45], adding to this component weights of which it was certain that they would be used such as the Marman Clamps and CubeSat deployers, and finally adding to this estimations taken from SMAD [17] if necessary. The resulting budget can be seen in Figure 24.1. For more detail please refer to Figure C.2 in Appendix C. The amount of CubeSat deployers was calculated by subtracting structural, mechanical and service module mass from the maximum dry mass, and then dividing this resultant payload mass by the mass of a single, filled, CubeSat QuadPack. The payload mass was based on using filled QuadPacks, IOD missions can be swapped for one or multiple QuadPacks, depending on the required mass.

Final Mass Estimation

The aforementioned method and model were maintained and updated throughout the design as more accurate estimates and values became available for the components and subsystems to be used. The main improvement and update to this initial mass estimation was the choice to not include any propellant nor propulsion system. This was made possible due to the realisation that all orbits would decay within the 25 year maximum, while staying in orbit longer than the minimum required orbital lifetime. This freed up an extra 50 kg for the dry mass, a fifth of the total mass. This resulted in an increase of the amount of QuadPacks that could be carried on the ring, which now came to match a convenient 5. In combination with one service module this meant that the aluminium ring did not require any changing, as it allowed for six attachment points. This helps to keep the delta low, while maximising the amount of QuadPacks due to the removal of propellant mass. This resulted in the final mass balance shown in Figure 24.1.

Initial	Mass fraction (%)	Mass (kg)	Quadpacks possible	Step 1	Mass fraction (%)	Mass (kg)	Quadpacks possible
Payload	66.3	132.7	4	Payload	77.6	194.1	6
Structure	13.6	27.3		Structure	10.9	27.3	
Mechanism	8.2	16.4		Mechanism	6.6	16.4	
Power	3.5	7.0		Power	2.4	6.0	
Operations	3.1	6.1		Operations	0.2	0.5	
ADCS	5.2	10.4		ADCS	2.2	5.6	
ODCS	0.1	0.1		ODCS	0.0	0.1	
Non-Payload Dry mass	33.7	67.3		**Non-Payload Dry mass**	22.4	55.9	
Total Dry mass	100.0	200.0		**Total Dry mass**	100.0	250.0	
Propellant	20.0	50.0		Propellant	0.0	0.0	
Total Wet mass	100.0	250.0		**Total Wet mass**	100.0	250.0	
Step 2	**Mass fraction (%)**	**Mass (kg)**	**Quadpacks possible**	**Step 3**	**Mass fraction (%)**	**Mass (kg)**	**Quadpacks possible**
Payload	76.9	192.1	6	Payload	76.2	190.4	6
Structure	10.9	27.3		Structure	10.9	27.3	
Mechanism	6.6	16.4		Mechanism	6.6	16.4	
Power	3.2	8.0		Power	3.9	9.7	
Operations	0.2	0.4		Operations	0.2	0.4	
ADCS	2.3	5.6		ADCS	2.3	5.6	
ODCS	0.0	0.1		ODCS	0.0	0.1	
Non-Payload Dry mass	23.1	57.9		**Non-Payload Dry mass**	23.8	59.6	
Total Dry mass	100.0	250.0		**Total Dry mass**	100.0	250.0	
Propellant	0.0	0.0		Propellant	0.0	0.0	
Total Wet mass	100.0	250.0		**Total Wet mass**	100.0	250.0	

Figure 24.1: Final mass balance of SPS-2-FF.

24.1.2. STEP 2

For step 2, the two main delta's are the change in ADCS and in the Power generation and storage system. These will get heavier, due to an increased performance necessary of both. The increase in the ADCS is due to the requirement of earth pointing, which imposes a set of Earth sensors onto the ADCS system. The results from this are also represented in Figure 24.1.

24.1.3. STEP 3

For step 3, the SPS-2 FF does not only need to be Earth pointing, it also needs to be capable of much more accurate attitude determination. This is accomplished by a set of two star sensors. This once again increases the mass of the system. The mass budget updated for step 3 is also present in Figure 24.1.

24.2. COST BUDGET

In order to adhere to the cost requirements **SPS-2-CS-CE** and **SPS-2-CS-BUD** set by Airbus as well as to aid in the design process and trade-offs, an initial cost estimate of the SPS-2 FF needs to be made, which should be evaluated throughout the project in order to update it and see if the budget is in danger of being exceeded. This has been done for all steps, which are shown in the following subsections.

24.2.1. STEP 1

For the initial cost estimation use was made of the TUDelft's SMAD-based estimation sheets[1]. These can be seen in Figure C.1 and Figure 8.19. Multiple things should be noted however. Firstly "The SMAD model is known to dramatically overestimate the cost of modern (post 1985) small (<500kg) satellites"[1]. Furthermore there is the fact that the SPS-2 FF is far from an ordinary satellite and therefore most often not agreeable with SMAD on system level, especially considering the relation of the payload to the development of the actual system. Therefore not only should some components of the cost be neglected, the remaining values need to be taken as very rough order of magnitude (ROM) values which are very likely to be overestimated. Components to be removed are launch and ground development costs, as ridesharing is used, and the ground support used already exists. This model results in the ROM cost estimation Table 24.1 for a series of 10 satellites.

Table 24.1: Step 1 ROM cost estimate.

Segment	Cost (2019 M €)
Total for 10 SPS-2-FF's	52.3
Recurring cost SPS-2-FF	2.76
Space segment	49.7
Investment	17.2
Total Production	18.7
Launch operations	7.5
Program level	6.3
Ground segment	2.6
Development	-
Operations and support	2.6

In order to provide a more detailed look at these costs, a balance has been made of the production costs of the SPS-2 FF, which can be compared to the model's estimations. This balance

[1] URL: http://lr.home.tudelft.nl/fileadmin/Faculteit/LR/Organisatie/Afdelingen_en_Leerstoelen/Afdeling_SpE/Space_Systems_Eng./Space_Links/doc/Space_mis [cited on 24th of June 2019]

can be seen in Figure 24.3. It can be seen that neither requirement **SPS-2-CS-CE-4**: Recurring platform cost of the SPS-2 FF shall be less than €2 million (FY2019), nor **SPS-2-CS-BUD-1.2**: The total mission development of the SPS-2 FF shall have a budget of €10 million (FY2019). Now the development costs are €17.2 million, and the recurring costs are €2.76 million per satellite. The launch operations costs are €0.75 million per satellite. This only includes the operations, not the launch itself. Although it is known that this model dramatically overestimates the costs for this type of satellite, this does not give a guarantee that the real costs will be low enough to still fit within the original budget of Airbus. What can be said however, is that it is deemed very unrealistic that the real costs will exceed these values and that it seems likely that the recurring costs could in reality be within or very close to the original budget of €2 million. A more lengthy and thorough cost analysis would be required in order to give a more definitive estimation.

DEVELOPMENT COSTS

For the development costs the service module will make up the major part of the costs, while a small part will be taken up by the development of the structural and mechanical changes with respect to the SPS-1, such as the release mechanism from the Vega-C launcher. These however should still be quite small, as a lot of development can be based upon the similar, already developed mechanisms and structures of the SPS-1.

The service module is, instead of the structure and release mechanisms of the SPS-1, fully a new system, and therefore needs to be developed. It cannot taken from a pre-existing design, which results in high development costs. It does however function as any ordinary service module does, and won't have to provide any exotic services. Therefore the design itself can be based upon common design methods and knowledge, lowering the costs.

24.2.2. STEP 2

For the initial step 2 cost estimation, the two inputs that change in the final model are the mass of both the ADCS and the Power system. The effect of this on the R&D and Testing costs, in combination with an even faster learning curve of 70% instead of 80%, due to the gained experience with the SPS-2 FF step 1 can be seen in Figure 24.2. Please note that this is not fully representative as the model assumes that the satellite is a new type for every step, and simply looks at the mass. Therefore the masses are grossly overestimated, but the relative difference between them can provide a ROM cost increase estimate. Also a production cost balance can be seen in Figure 24.3.

step 1

Subsystem RDT&E cost (FY 2000)	k€	Subsystem TFU cost (FY 2000)	k€
Structure	4247	Structure	715
Thermal	223	Thermal	27
Electrical Power	332	Electrical Power	388
TT&C	304	TT&C	398
ADCS	180	ADCS	124
Propulsion	0	Propulsion	0
Total	5287	Total	1652
3. Integration Assembly & Test (IAT)	2198	3.\IAT	2237

step 2

Subsystem RDT&E cost (FY 2000)	k€	Subsystem TFU cost (FY 2000)	k€
Structure	4247	Structure	715
Thermal	223	Thermal	27
Electrical Power	442	Electrical Power	482
TT&C	304	TT&C	398
ADCS	206	ADCS	140
Propulsion	0	Propulsion	0
Total	5423	Total	1762
3. Integration Assembly & Test (IAT)	2237	3.\IAT	2256

step 3

Subsystem RDT&E cost (FY 2000)	k€	Subsystem TFU cost (FY 2000)	k€
Structure	4247	Structure	715
Thermal	223	Thermal	27
Electrical Power	536	Electrical Power	559
TT&C	304	TT&C	398
ADCS	415	ADCS	262
Propulsion	0	Propulsion	0
Total	5725	Total	1960
3. Integration Assembly & Test (IAT)	2280	3.\IAT	2277

Figure 24.2: The R&D, testing and integration cost delta's between step 1, 2 and 3 per subsystem. TFU stand for Theoretical First Unit.

Production	cost
Total Step 1	**€890,174**
Total Step 2	€955,382
Total Step 3	€1,047,502
Structure	**€25,000**
Ring	€25,000
Mechanism	**€250,000**
Clampband (2x)	€250,000
Power Step 1	**€259,600.00**
Storage	€61,600.00
Control&distribution	€88,000.00
Generation Step 1	€110,000.00
Generation Step 2	€155,584.00
Generation Step 3	€213,928.00
Communications	**€44,440.00**
Motherboard	$24,640.00
CPU	included with motherboard
Transceiver	included with motherboard
Antenna (3x)	$19,800.00
Antenna (2x)	$13,200.00
Antenna (2x)	$13,200.00
ADCS Step 1	**€304,133.60**
Reaction Wheel (4x)	€211,200.00
Sun Sensor (2x)	€4,400.00
Magnetometer(3x)	€45,000.00
Magnetorquer(3x)	€31,680.00
Gyroscope(3x)	€11,853.60
+ Earth sensor (2x)	€26,224.00
+ Star tracker (2x)	$60,000.00
ODCS	**€7,000.00**
GNSS receiver module	€7,000.00

Figure 24.3: The production or acquisition costs of the components of the SPS-2-FF

24.2.3. STEP 3

For step 3, the delta will be even bigger in terms of ADCS due to the addition of star trackers for the more accurate determination, while to power will increases as well. Furthermore other changes can still occur during the detailed design of step 3, or will already be expected while the design of step 2 is in process. These cannot be predicted in this early stadium yet, and thus a very ROM estimation is obtain by updating the model for the step 3 subsystem masses. The result of this can be seen in Figure 24.2 and the updated production cost balance can be seen in Figure 24.3.

25
Business Case

In this section the business case for each step will be discussed in detail. This takes into account the cost breakdown presented in chapter 24 as well as the mass budget and power budget in order to determine the number of payloads which can be supported and other parameters of interest. Using the table below, data about the IOD payloads which are considered for each step can be summarised.

Table 25.1: Types of IOD payloads and technical characteristics.

	OBCs	**RF Comms system**	**GNSS Receiver**	**ADCS Sensor**	**Optical P/L**	**RF P/L**	**Space Weather**	**Radiation Hardness Assurances**	**CubeSats**
Mass(kg)	2	4	1	3	30	2	5	1	30
Power(W)	20	70	5	5	15	5	5	2	2
Volume(L)	2	4	1	3	30	2	5	1	16
Market Share									
Altitude Constraints	none	none	none	none	none	none	none	none	none
Inclination Constraints	>45	>50	>45	>45	45-98	45-98	>45	none	>50
Duration	several months	several months	several months	several months	several months	several months	several months	several months	[-]
Pointing Accuracy	none	0.5-2	30	none	<<1	2.0-5.0	<2	none	none
Stability	none	none	none	<1	none	none	none	none	<5
Step 1	x		x					x	
Step 2	x	x	x	x		x	x	x	x
Step 3	x	x	x	x	x	x	x	x	x

Additionally, due to the fact that a substantial part of the information about potential customers and market aspects like the market volume and development could not be verified, to a larger extent than the general interest of companies in the system, a sensitivity analysis must be conducted. It aims at assessing the consequences and the possible adaptations needed if the future need of companies shifts away from IOD payloads and towards CubeSats or back to larger satellites.

25.1. General Outline Of Business Strategy

Here, the general business strategy will be outlined. The general steps look as follows:

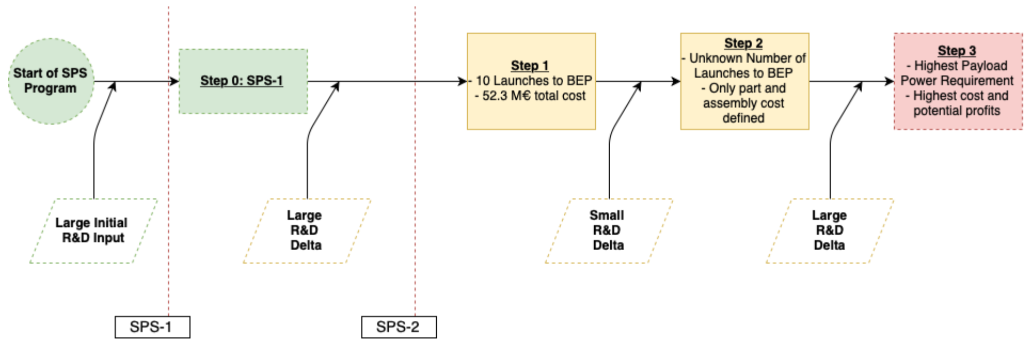

Figure 25.1: Business Plan Layout.

The initial step in the business analysis is to compare the possible revenue generation capability of the SPS-2 FF system to that of the SPS-1. Although the development cost of the SPS-1 is the unknown the comparison is used to establish whether or not the SPS-2 FF is capable of generating revenue in excess of that generated by the SPS-1. Failure to generate more revenue than the SPS-1 would make a re-evaluation of the overall business idea behind the SPS-2 FF necessary followed by a more thorough analysis of the market needs and potential. The second aspect is the analyses of the development cost and revenue generation in order to determine different possible break even points depending on assumptions made with respect to the market. This process is subsequently also done for the step 2 iteration of the SPS-2 FF.

25.1.1. REVENUE GENERATION COMPARISON

The SPS-1 is solely used as a secondary payload adapter in order to meet the increasing demand for CubeSat launches. It has the capability to bring twenty four 3U CubeSats into LEO. Based on a market analysis conducted for the SMILE launcher [1] the cost per kg of CubeSat into LEO should be approximately 50 k€/kg in order to be competitive on the commercial market. Using this figure as a baseline in combination with the fact that by definition $1U = 1.33kg$[2] yields in a a total amount of revenue generated per launch= $4.788M€$.

In order to obtain a comparable value for the SPS-2 FF two distinct scenarios will be considered. According to the executive summary of the GMV [47] for the market analysis conducted the cost per kg which could be charged is in the order of magnitude of $200,000\$/kg$. This unit of measurements is however misleading as it does not take into account the different power levels supplied to the payloads. Additionally the demand of each IOD payload remains unknown. Due to this the first scenario which will be considered is that of infinite demand. This assumption subsequently leads to a hosted payload choice solely driven by revenue maximisation. Determining the cost using this premise gives an optimal payload configuration of only radiation hardness assurance payloads. This is due to the fact that this type of payload has the most efficient mass/power and mass/volume ratio for step 1. Carrying the maximum amount of 25 (due to power limitations) leaves an additional mass of $175 - 25 = 150kg$ for carrying CubeSats. Additionally, as every Radiation hardness assurance IOD uses a maximum of 1 litre of volume, all can theoretically be fitted into one QuadPack. This leaves, next to the service module, 4 QuadPacks which can be fitted with CubeSats such that 16 x 3U CubeSats can be carried. Given the price per kg of the IOD payloads and that of the CubeSats yields in a total revenue per launch=$25kg \cdot 200000\frac{euro}{kg} + (16 \cdot 3 \cdot 1.33)kg \cdot 50000\frac{euro}{kg} = 8.192Meuro$. This represents an revenue increase by a factor of 1.7. It is however realised that the assumption of infinity demand is not conservative. For this reason the calculation of revenue generation is repeated for the case where the distribution of IOD types for step 1 is kept more balanced. Due to the excess space in the service module of (90mm x 90mm x180mm) one GNSS receiver will be placed there. Additionally, constraint by the power, 3 more GNSS receivers can be placed in a QuadPack redesigned for IOD hosting, together with one OBC IOD and 3 radiation hardness assurances IOD. The remaining mass and volume can be filled by 4 QuadPacks with CubeSats. As the IOD payloads do not take up the entire remaining QuadPack deployer it could be possible to split it into separate compartments in order to carry two addition 3U CubeSats. This more reasonable payload configuration yields in a total revenue generated per flight = 5.391M€ representing an increase by a factor of 1.12.

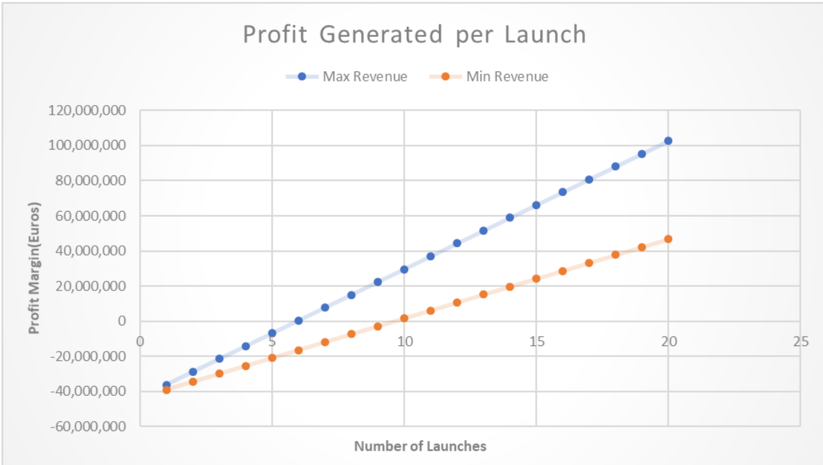

Figure 25.2: Profit generated as a function of number of launches

25.1.2. DEVELOPMENT COST SPS-2 FF

From Table 24.1 the total cost of 10 SPS-2 FF launches is given to be 52.3 Million Euro (59,600,819 $). This includes both the development cost and production cost for 10 SPS-2 FF. Thus to obtain just the development cost the production cost has to be subtracted out. The production cost per SPS-2 FF is estimated to be 878,320€ such that the total non-recurring cost is = $52.300,000 - 10 \cdot 878,320€$ = 43,516,800€. The break even point for the two different cases of revenue generated per launch can be calculated based on Equation 25.1.

$$P = n * Revenue - n * production - development \tag{25.1}$$

Where P=Profit Margin, n=number of Launches, and production and development represent the cost associated with each. This relation is plotted in Figure 25.2. It visualises at what launched number the break even point is reached and the Return on Investment as a function of number of launches. For the infinity demand this point is

[1] URl='https://link-springer-com.tudelft.idm.oclc.org/content/pdf/10.1007%2F978-3-319-32817-1.pdf',[Cited: 2nd of May 2019], see pg.64

[2] URL:'http://www.CubeSat.org/',Accessed:'25.06.19'

reached after 6 launches and for the more conservative approach after 10. Due to the quantification of 4 launches per year by the client this represents a breaking even point after 18 months and after 30 months.

The main conclusions which can be drawn from the above figure are as follows. For both payload configurations the SPS-2 FF will become profitable. The time frame in which this occurs is however strongly dependent on the demand and price/kg which can be obtained from the customer. Thus more concrete research should be done into the variation of this value with system level performance, such as power supplied and down-link data rate available.

25.2. STEP 2

For the second development stage of the SPS-2 FF the same procedure as previously is applied. In this case the maximum power available for the payload is limited to 70 W while the payload mass stays approximately the same, as well as the available volume constraint. Again if a maximisation based on infinite demand is conducted the payload configuration will solely consists of the IoD payload with the highest mass/power ratio, which for step 2 is the Space Weather IoD payload. A maximum of 14 of these could be placed within 2.5 quadpacks. The remaining 2.5 QuadPacks can subsequently be filled with CubeSats. This configuration results in a total revenue generation per launch equal to 15.995$Meuro$. A more conservative approach on the other hand could yield in a payload configuration of 1 OBC,3 GNSS Receivers, 3 ADCS Sensors,1 RF payload,2 Space Weather IODs, and 2 radiation hardness assurance payloads. As this only takes up 1 quadpacks volume, an additional 16x3U CubeSats could be attached. This yields in a total revenue generated per flight of 8.792$Meuro$. In this case the RoI is based on the delta development cost from step 1, which is estimated to be 136000$euro$. The small magnitude of this value is explained by the fact that the most expensive aspects, the design, development and testing of the structural components has already been done with Step 1. Due to this the break even point occurs within 1 launch for both payload configurations.

25.3. SENSITIVITY ANALYSIS

This section reviews the consequences of an unexpected decrease in the demand for IoD hosted payloads. The main competitor of this system are cheap, flight proven,off the shelf components, mainly based on the CubeSat standard, which allow companies cheap development of their own platforms for testing. This in combination with dedicated smallsat launchers has the potential to rival hosted payload services. An analysis of this market and potential adaptations of the SPS have previously been researched in detail and analysed in [11]. The main conclusion was that a possible adaption would be offering ΔV capabilities to the CubeSats in order to allow quicker deployment of constellations.

25.4. CONCLUSION

Overall the business analysis conducted supports the feasibility of the SPS-2 FF step 1 and step 2 as the revenue generated by these systems is higher than the revenue generated by the current SPS-1. More importantly the stepwise development makes it possible to have a very profitable step 2 of the SPS-2 as the main cost factors can be split over the launches of the SPS-2 FF step 1. Furthermore it shows that within a moderate time span it is possible to achieve a positive RoI. It does however also highlight the fact that in order to gain a better understanding of the market more research will have to be conducted, especially with regards to the demand metrics of the customers. While this can prove difficult to do, perhaps a statistical analysis technique can be implemented.

26
POST-DSE PROJECT DEVELOPMENT

This chapter covers an overview of the project planning procedures to be used for further development steps of the SPS-2 FF. The project life cycle to be implemented for the different step of the SPS-2 FF programme is outlined, and the main flow of activities to be performed between steps is shown.

26.1. PROJECT LIFE CYCLE

Based on the Space Flight Program and Project Management Handbook [9], the highest level phases of a general project life cycle for space development projects is presented in Figure 26.1.

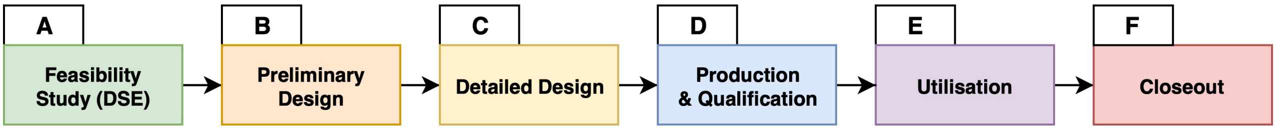

Figure 26.1: Main phases of the proposed project life cycle.

The Feasibility Study of the project (Phase A), corresponds to the work scope included in the current Design Synthesis Exercise (DSE). The activities that will be performed after the DSE (Phase B to Phase F) are broken down in detail in this section. Note that the detailed description of the Utilisation Phase (Phase E) can be found in the complete system Functional Analysis presented in chapter 5. Figure 26.2 shows the detailed flow between the project life cycle activities, their dependencies and the milestone product delivery points. The latter are dependent on the project maturity, and are constantly updated to ensure a smooth transition between project phases. They are essential to allow the project management office coordinate the progress of the project. The following lists of milestone products are adapted versions from the product framework used in the Space Flight Program and Project Management Handbook [9].

Preliminary Design Review Products:
- Technical, Schedule, & Cost Control Plan
- Safety & Mission Assurance Plan
- Technology Development Plan
- Systems Engineering Management Plan
- Product & Life-Cycle Management Plan
- Information Technology Plan
- Environmental Management Plan
- Integrated Logistics Support Plan
- Science Data Management Plan
- Configuration Management Plan
- Technology Transfer Control Plan
- Communications Plan
- Knowledge Management Plan
- Technology Readiness Documentation
- Design Documentation
- Engineering Development Assessment
- Payload Safety Process Deliverables

System Readiness Review Products:
- Mission Operations Plan
- Science Data Management Plan
- Project Protection Plan
- Security Plan

Critical Design Review Products:
- Safety & Mission Assurance Plan
- Verification & Validation Plan
- Environmental Management Plan
- Integrated Logistics Support Plan
- Technology Transfer Control Plan
- Communications Plan
- Design Documentation

Systems Integration Review Products:
- Risk mitigation plans & resources
- Documented Cost & Schedule Baselines
- Documentation of Basis of Estimates
- Verification & Validation Plan
- Threat Summary
- Design Documentation
- Technology Readiness Documentation
- Payload Safety Process Deliverables
- Operations Handbook

- Human Rating Certification Package
- End of Mission Plans
- Decommissioning/Disposal Plan
- Design Documentation

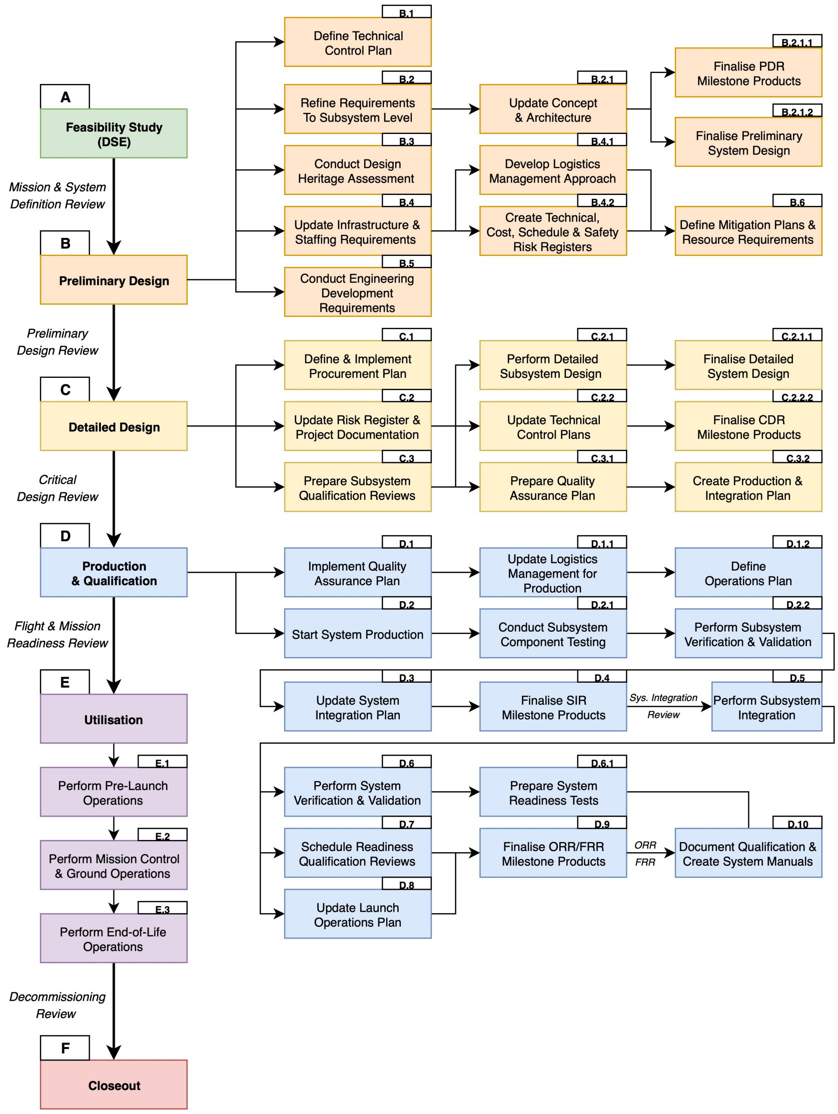

Figure 26.2: Detailed project life cycle activity flow.

26.2. PRODUCT DEVELOPMENT PLANNING

The activities of the previously discussed project life cycle of Step 1 are included in a gantt chart in Figure 26.3. The ongoing DSE activities are considered part of the feasibility study, i.e., Phase A. It is also assumed that Phase B will take place right after the completion of the DSE.

WBS	TASK DESCRIPTION	PROGRESS	PLAN START	PLAN END	PLAN DAYS	ACTUAL START	ACTUAL END	ACTUAL DAYS
A	**Feasibility Study**	100%	5/1/19	7/4/19	65	5/1/19	7/4/19	65
	Concept & Mission Definition	100%	5/1/19	6/1/19	30	5/1/19	6/1/19	30
	Other DSE Activities	100%	6/1/19	6/20/19	15	6/1/19	6/20/19	15
	Concept Trade-Off	100%	6/1/19	6/20/19	15	6/1/19	6/20/19	15
	Project Approval	100%	6/20/19	7/4/19	7	6/20/19	7/4/19	7
B	**Preliminary Design**		7/4/19	7/4/20	367	7/4/19	7/4/20	367
	Define Technical Control Plan		7/4/19	10/4/19	90	7/4/19	10/4/19	90
	Refine Requirements		7/4/19	9/4/19	60	7/4/19	9/4/19	60
	Update Concept & Architecture		9/4/19	11/4/19	60	9/4/19	11/4/19	60
	Finalise PDR Products		11/4/19	2/4/20	90	11/4/19	2/4/20	90
	Finalise Preliminary System Design		11/4/19	2/4/20	90	11/4/19	2/4/20	90
	Conduct Design Heritage Assessment		9/4/19	11/4/19	60	9/4/19	11/4/19	60
	Update Infrastructure & Staffing Requirements		11/4/19	2/4/20	90	11/4/19	2/4/20	90
	Develop Logistics Management Approach		2/4/20	5/4/20	90	2/4/20	5/4/20	90
	Create Project Risk Registers		2/4/20	5/4/20	90	2/4/20	5/4/20	90
	Define Mitigation Plans & Resource Requirements		5/4/20	7/4/20	60	5/4/20	7/4/20	60
	Conduct Engineering Development Plan		7/4/19	3/4/20	240	7/4/19	3/4/20	240
C	**Detailed Design**		7/4/20	7/4/21	366	7/4/20	7/4/21	366
	Define & Implement Procurement Plan		7/4/20	10/4/20	90	7/4/20	10/4/20	90
	Update Risk Registers & Project Documentation		7/4/20	10/4/20	90	7/4/20	10/4/20	90
	Perform Detailed Subsystem Design		10/4/20	4/4/21	180	10/4/20	4/4/21	180
	Update Technical Control Plans		10/4/20	12/4/20	60	10/4/20	12/4/20	60
	Prepare Quality Assurance Plan		10/4/20	12/4/20	60	10/4/20	12/4/20	60
	Prepare Subsystem Quaslification Reviews		10/4/20	12/4/20	60	10/4/20	12/4/20	60
	Finalise Detailed System Design		4/4/21	7/4/21	90	4/4/21	7/4/21	90
	Finalise CDR Products		12/4/20	7/4/21	240	12/4/20	7/4/21	240
	Create Production & Integration Plan		4/4/21	7/4/21	90	4/4/21	7/4/21	90
D	**Production & Qualification**	100%	7/4/21	5/1/22	302	7/4/21	5/1/22	302
	Implement QA Plan		7/4/21	8/4/21	30	7/4/21	8/4/21	30
	Update Logistics Management for Production		8/4/21	9/4/21	30	8/4/21	9/4/21	30
	Define Operations Plan		8/4/21	10/4/21	60	8/4/21	10/4/21	60
	Start system Production		7/4/21	12/4/21	150	7/4/21	12/4/21	150
	Conduct Subsystem Component Testing		11/4/21	12/4/21	30	11/4/21	12/4/21	30
	Perform Subsystem V&V		11/20/21	1/1/22	30	11/20/21	1/1/22	30
	Update System Integration Plan		1/1/22	2/1/22	30	1/1/22	2/1/22	30
	Finalise SIR Milestone Products		2/1/22	3/1/22	30	2/1/22	3/1/22	30
	Perform Subsystem Integration		3/1/22	4/1/22	30	3/1/22	4/1/22	30
	Perform System V&V		4/1/22	5/1/22	30	4/1/22	5/1/22	30
	Prepare System Readiness Tests		4/1/22	5/1/22	30	4/1/22	5/1/22	30
	Schedule Readiness Qualification Reviews		4/1/22	4/4/22	3	4/1/22	4/4/22	3
	Update Launch Operations Plan		4/1/22	4/16/22	15	4/1/22	4/16/22	15
	Finalise ORR/FRR Milestone Products		4/1/22	5/1/22	30	4/1/22	5/1/22	30
	Document Qualification & Create System Manuals		4/1/22	5/1/22	30	4/1/22	5/1/22	30
E	**Utilisation**	100%	5/1/22	2/1/23	277	5/1/22	2/1/23	277
	Perform Pre-Launch Operations 1 meses		5/1/22	6/1/22	30	5/1/22	6/1/22	30
	Perform Mission Control & Ground Operations		6/1/22	1/1/23	180	6/1/22	1/1/23	180
	Perform End-of-Life Operations		1/1/23	2/1/23	30	1/1/23	2/1/23	30
F	**Closeout**		2/1/23	TBC	TBC	2/1/23	TBC	TBC

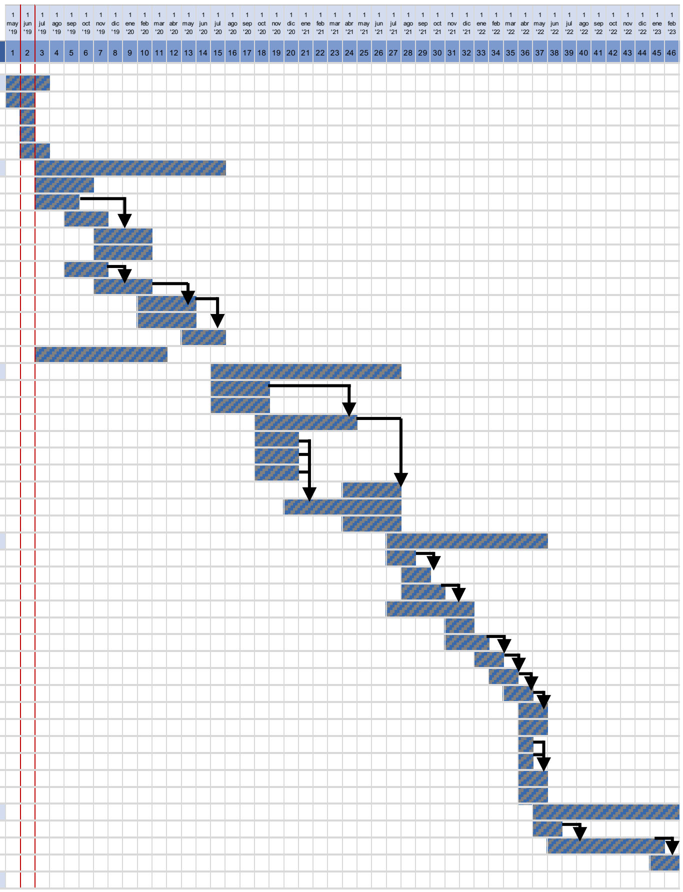

Figure 26.3: SPS-2 FF Step 1 Project Development Gantt Chart.

Once Step 1 is successfully completed, knowledge transfer can be performed. Design heritage will accelerate the design and production of Step 2. There are other factor that will also make the development of the second version of the SPS-2 FF faster than its predecessor. For example, the procurement plan for launch services has been previously covered, as well as an already existing supplier and contractor network. Due to time constraints, the feasibility study for Step 2 has not been completed. The next step is to perform a detailed concept exploration, like the detailed subsystem design presented in this report for Step 1. The project approval of Step 2 will be based on that detailed concept feasibility study. Regarding the development of Step 3, this report only includes qualitative analysis of the design sensitivity, given the drastic update of requirements necessary to upgrade the system from Step 1 to Step 3. Exhaustive study for the correct design adaptation and subsystem upgrade to comply with the requirements of the final SPS-2 FF product version has still to be performed to achieve accurate technology development needs, as well as reliable cost estimations.

27 CONCLUSION

The SPS-2 FF has been studied in detail within this report. This has been done from both a technical perspective and an organisational perspective. The subsystems have been analysed in such a way that COTS products could be selected and integrated into a full working design. The clients wishes and the requirements are aimed to be fulfilled, while taking into account the adaptability of the design to later design phases. This is achieved by dividing the design in steps of which two are worked out in detail. The third step has been considered conceptually.

The design for step 1 is a sun pointing aluminium (7075 T6) ring, which host basic IOD missions. A total of five QuadPacks are allocated to these payloads. One extra QuadPack is allocated to the service module. The upper parts of these QuadPacks are filled with solar panels and one antenna. An other antenna is located on the bottom of one QuadPack and one on the hatch of the service module. The service module includes various ADCS components and the OBDH subsystem. The recurring cost for this step is 2.76M euro, with an estimated development cost of 17.2M euro.

For step 2, the design changes to an Earth pointing satellite. The biggest change from step 1 to 2 are the solar panels. The area needs to be increased and the panels need to be deployable. Besides this, extra ADCS components are added and more complex IOD payloads are possible. This increases the amount of data generated, however this does not alter the design of the communication subsystem. Te additional recurring cost is estimated to be 100k euro, combined with an additional development cost of 150k euro.

Step 3, will have the possibility to include an optical payload. Since this is only worked out conceptually, no specific values can be given. Therefore, it is advised to perform a more detailed analysis for this part of the design. For power it can be estimated that the solar panel area will increase. However, no redesign of the mechanism should be performed. For the ADCS, star trackers will be added for improved pointing accuracy. The communications components can be retained if the communication plan is revised. The estimated additional development cost for this final step consists of 300k euro and an additional recurring cost of 200k euro on top of the costs from step 2.

Bibliography

[1] *ESATRACKING STATIONS (ESTRACK)FACILITIES MANUAL (EFM)*, EUROPEAN SPACE AGENCY (2008).

[2] GOMspace, *NanoDock SDR Datasheet* ().

[3] GOMspace, *NanoMind Z7000 Datasheet* ().

[4] N. Ruitenbeek, *Designing the evolutionary process of the SPS free-flyer platform*, Master's thesis, Faculty of Aerospace Engineering, Delft University of Technology (2018).

[5] GOMspace, *NanoCom TR-600 Datasheet* ().

[6] GOMspace, *NanoCom ANT2000 Datasheet* ().

[7] Group 15, *Midterm report: Sps free flyer for low earth orbits,* (2019).

[8] Arianespace, *Vega C User's Manual*, issue 0, revision 0, 1st ed. (Arianegroup, 2018).

[9] *NASA Space Flight Program and Project Management Handbook*, National Aeronautics and Space Administration (2014).

[10] M. Oomen, *Sps-2 specification sheets,* ().

[11] A. Cabrera *et al.*, *SPS FF for Low Earth Orbits - Baseline Report V1.2* (Delft University of Technology, 2019) p. 18.

[12] C. Edupack, [2018].

[13] Consultative Committee for Space Data Systems, *Mission Operations Services Concept (Informational Report)* (NASA, Space Operations Mission Directorate).

[14] GSC-18094-1, *General mission analysis tool version (gmat),* Goddard Space Flight Center, NASA (R2018a).

[15] Ames Research Center, *State of the Art Small Spacecraft Technology* (NASA, December 2018).

[16] EXPLORATION AND SPACE COMMUNICATIONS PROJECTS DIVISION, *453-nenug: Near earth network (nen) users' guide,* (2016).

[17] J. Wertz *et al.*, *Space Mission Engineering: The New SMAD*, Vol. 23 (Space Technology Library Springer Microcosm Press, 2011).

[18] G. Palem, *Condition-based maintenance using sensor arrays and telematics,* International Journal of Mobile Network Communications & Telematics (2013).

[19] GOMspace, *NanoCom SDR Datasheet* ().

[20] A. Cervone, *Aerospace design and system engineering elements ii: Lecture 07 spacecraft telecommunications,* (2018), lecture slides.

[21] A. Cervone, *Aerospace design and system engineering elements ii: Lecture 11 spacecraft: Recap, practical examples and excerises,* (2018), lecture slides.

[22] J. Wertz and W. Larson, *Space Mission Analysis and Design*, 3rd ed. (Space Technology Library Microcosm Press, Kluwer Academic Publishers, 1999).

[23] A. Cervone, *Aerospace design and system engineering elements ii: Lecture 08 spacecraft telecommunications,* (2018), lecture slides.

[24] J. N. Chinchilla, *Analysis Model to Optimize Ground Stations in Built-up Areas*, Master's thesis, UNIVERSIDAD POLITÉCNICA DE MADRID (2017).

[25] K. Voormansik, *Satellite Signal Strength Measurements with the International Space University Ground Station and the University of Tartu Ground Station*, Master's thesis, UNIVERSITY OF TARTU (2009).

[26] P. Munatsi, *Design of the Attitude Control System for the SPS-2 satellite for the science mode*, Master's thesis, TU Delft (2016).

[27] J. Mulder *et al.*, *Lecture Notes AE3202, Flight Dynamics* (Control and Simulation division, Delft University of Technology, 2013).

[28] M. Oomen, *The design of an Attitude Control System for the SPS- 2 satellite For the Rate Damping, Sun Acquisition and Sun Pointing Modes*, Master's thesis, TU Delft (2016).

[29] B. Wie, *Space Vehicle Dynamics and Control*, edited by J. Przemieniecki (American Institute of Aeronautics and Astronautics, Inc., 1801 Alexander Bell Drive, Reston, VA 20191, 1998).

[30] M. Oomen, *Sps-2 specification sheets,* (2016).

[31] M. M. Oomen, *SPS-2 specification sheets - An overview of the specification sheets of the sensors and actuators which have been considered for the SPS-200mission* ().

[32] B. Zandbergen, *Aerospace design & systems engineering elements i part: Spacecraft (bus) design and sizing,* (2015), lecture slides.

[33] V. B. Malcolm Macdonald, *The International Handbook of Space Technology* (springer, 2014).
[34] K. Misiakos and D. Tsamakis, *Accurate measurements of the silicon intrinsic carrier density from 78 to 340 k,* Journal of Applied Physics **74**, 3293 (1993).
[35] G. Siefer and A. W. Bett, *Analysis of temperature coefficients for iii–v multi-junction concentrator cells,* Progress in Photovoltaics: Research and Applications **22**, 515 (2014).
[36] ISIS, *Quadpack cubesat deployer,* .
[37] T. Soeira, *EE3125TU Advanced Electronics for Robotics- PE Lecture 3* (TU Delft, Delft, The Netherlands, 2018).
[38] J. Wijker, *Spacecraft Structures* (Springer, Leiden, The Netherlands, 2008).
[39] O. S. Cooperation, *Minotaur IV*, release 2.2 ed. (Distribution Unlimited, 3380 S. Price Road, Chandler, AZ 85248, 2015).
[40] J. Rotteveel, *Launch results from the qb50 pre-cursor launch campaign flight qualification of the qb50 launch system,* Cubesat workshop , 14 (2014).
[41] J. H. N. T. C. Z. Christian D. Grimm, Jan-Thimo Grundmann, *Going beyond the possible, going beyond the "standard" of spacecraft integration and testing!* (2014).
[42] P. D. E. Gill, *As4-s12-10 - verifying and validating,* (2018), lecture slides.
[43] ECSS, *Space engineering verification,* (2018).
[44] M. K. Sarah Kurtz, John Wohlgemuth *et al.*, *Photovoltaic module qualification plus testing,* .
[45] J. van der Ploeg, *Concept study of stackable platform structure,* (2014).
[46] C. Hobijn, *The preliminary design of the SPS-2*, Master's thesis, Hogeschool van Amsterdam (2015).
[47] I. team, *Executive summary iodisplay,* (2016).

Figure C: Communication & Hardware Flow Diagram for step 1 and 2, with SLOC estimations[17].

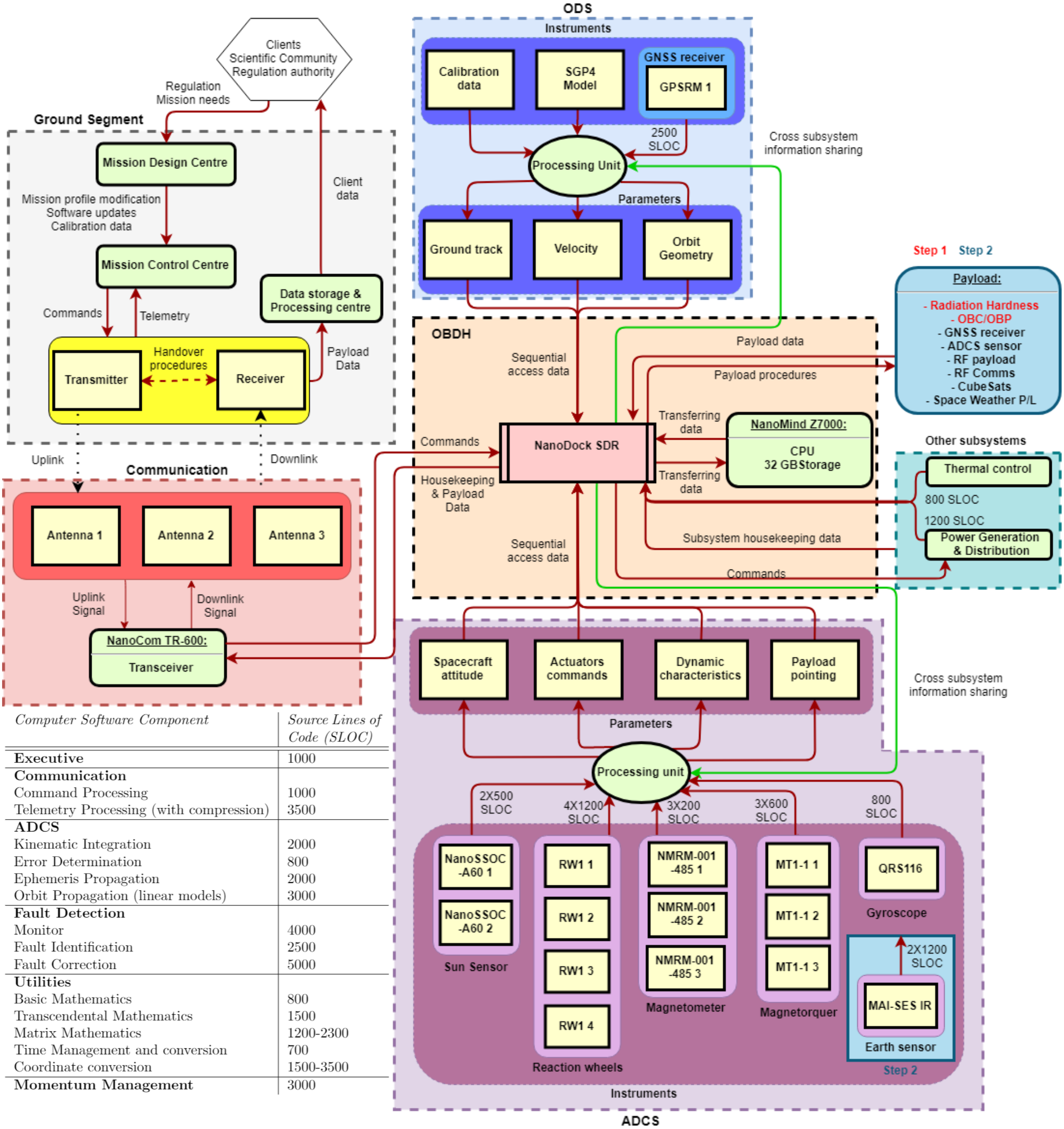

Computer Software Component	*Source Lines of Code (SLOC)*
Executive	1000
Communication	
Command Processing	1000
Telemetry Processing (with compression)	3500
ADCS	
Kinematic Integration	2000
Error Determination	800
Ephemeris Propagation	2000
Orbit Propagation (linear models)	3000
Fault Detection	
Monitor	4000
Fault Identification	2500
Fault Correction	5000
Utilities	
Basic Mathematics	800
Transcendental Mathematics	1500
Matrix Mathematics	1200-2300
Time Management and conversion	700
Coordinate conversion	1500-3500
Momentum Management	3000

A
Simulation Software

A.1. SPENVIS Configuration

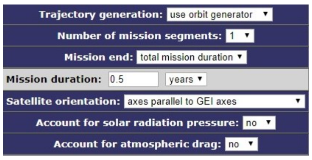

Figure A.1: First settings page used in the SPENVIS orbit generator.

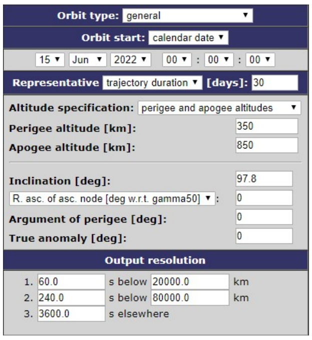

Figure A.2: Second settings page used in the SPENVIS orbit generator.

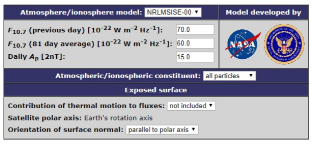

Figure A.3: Settings page used in the SPENVIS atmoshpere/ionosphere model.

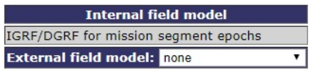

Figure A.4: Settings page used in the SPENVIS magnetic field model.

A.2. GMAT Configuration

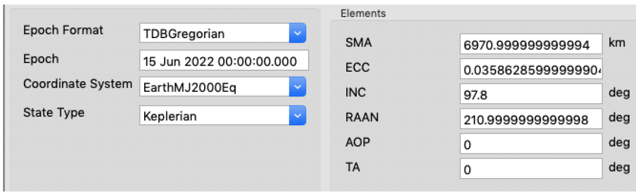

Figure A.5: GMAT settings for SPS-2-FF.

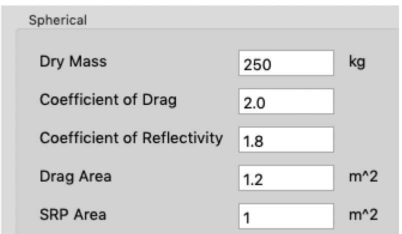

Figure A.6: GMAT spacecraft ballistic coefficients.

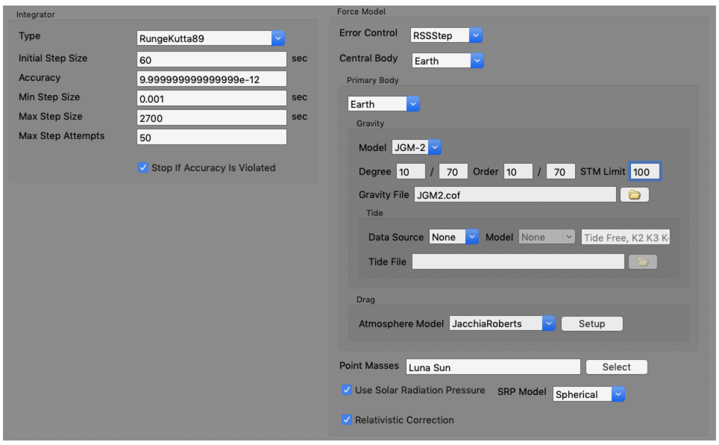

Figure A.7: GMAT orbit propagator settings.

B
Component Architecture

ID	Product Name	Size (LxWxH) [mm]	Mass [kg]	Linear Dipole Moment [Am^2]	Linear Power [W]	Linear Voltage [V]	Price
MT-01	MT-10-2-H	330.0x17x17	0.35	10	1	10	-
MT-02	MT-10-2-AIR	1120x584x95	2.7	10	1.1	11	-
MT-03	MT15-1	329.5x17x17	0.43	15	1.11	14	-
MT-04	MT30-2	404.5x29x29	1.4	30	1.5	12.5	-
MT-05	MT0.1-1	55x3.5x3.5	3.00E-03	0.1	2.95E-01	5	-
MT-06	MT0.2-1	70x5x5	7.00E-03	0.2	3.00E-01	5	-
MT-07	MT0.2-1	85x6x6	9.00E-03	0.2	1.40E-01	5	-
MT-08	MT0.3-1	90x5x5	9.00E-03	0.3	3.15E-01	5	-
MT-09	MT0.5-1	100x9x9	3.00E-02	0.5	2.75E-01	5	-
MT-10	MT0.5-1	95x12x12	3.50E-02	0.5	3.00E-01	5	-
MT-11	MT1-1	132x13.5x13.5	6.00E-02	1	2.30E-01	5	-
MT-12	TQ-15 (single wind)	228	4.00E-01	15	2.8	28	$11,000
MT-13	TQ-15 (redundant wind)	237	7.27E-01	15	2.8	28	$12,000
MT-14	TQ-40	338	8.25E-01	42	2.8	28	$14,000

Figure B.1: Possible magnetorquers considered.

ID	Product Name	Size (LxWxH) [mm]	Mass [kg]	Speed range (RPM)	Momentum Cap [Nms]	Torque Cap [mNm]	Power (Idle) [W]	Power (SS) [W]	Power (Peak) [W]	T Range [°C]	Design Life [yrs]	Price
RW-01	MSCI MicroWheel 1000	130x130x90	1.50	±10,000	1.1	30.0	2	9 (<10,000 RPM)	45 (tau = 30 mNm)	-30/+60	>7	-
RW-02	CubeWheel Large	57x57x31.5	0.2	±6,000	0.03	2.3	-	1.8E-02	-	-30/+60	-	€6,500
RW-03	MAI-400 Reaction Wheel	33x33x38.4	0.09	-	0.011076	0.6	0.45	0.85 (500RPM)	2.2	-40/85	-	€7,100
RW-04	Reaction Wheel VRW-02	70x70x48	1	±6,500	0.2	20.0	1	3.0 (4000 RPM)	25	-20/70	-	-
RW-05	Reaction Wheel VRW-05	115x115x77	1.3	±6,500	0.5	25.0	1	3	25	-20/70	-	-
RW-06	Reaction Wheel VRW-1	115x115x77	1.8	±6,500	1.0	25.0	1	3	25	-20/70	-	-
RW-06	RWA-1000	150x140x40	0.98	±6,000	1.0	100	2	graph on site	15	-40/70	-	$60000 (+$9900 per 4)
RW-07	4RW0	43.5x43.5x24	0.137	±6,500	0.02	3.2	4.50E-02	0.15 (1000 RPM)	3.00E+00	-40/85	-	Can be requested
RW-08	RW1	110x110x38	0.75		1.0	100			9		>10	$60,000

Figure B.2: Possible reaction wheels considered.

ID	Product Name	Size (LxWxH) [mm]	Mass [kg]	Accuracy [°]	Measurement range [mu T]	Voltage [V]	Power [W]	T Range [°C]	Price
MM-01	MAG-3	82.8x35.1x32.3	1.00E-01	±0.75	±100	15-34	0.375-0.85	-55/+85	-
MM-02	Spacemag (3 axis)	106x88x30	2.75E-01	±0.5	±100	15	0.57	-55/+125	-
MM-03	TAM-2 (3-axis)	143x76.2x44.5	0.5	±1.0	±100	21-38.6	0.525-0.965	-39/+76	-
MM-04	NMRM-001-485	96x45x20	6.70E-02	±1.0	±60	5	0.55	-25/70	$15,000

Figure B.3: Possible magnetometers considered.

ID	Product Name	Size (LxWxH) [mm]	Mass [kg]	Bias stability [°/hr]	Voltage [V]	Power [W]	T Range [°C]
GY-01	QRS116	41.275x41.275x16.38	6.00E-02	3	5	0.1	-55/+85
GY-02	ButterflyGyro STIM210	38.6x44.8x21.5	5.20E-02	0.3	5	1.5	-40/+85

Figure B.4: Possible gyroscopes considered.

ID	Product Name	Size (LxWxH) [mm]	Mass [kg]	Accuracy [°]	FOV [°]	Voltage [V]	Power [W]	T Range [°C]	Price
SS-01	Cubsat Sun sensor (SSBV)	33x11x6	5.00E-03	0.5	114	5	0.05	-25/+50	-
SS-02	NanoSSOC-A60	27.4x14x5.9	4.00E-03	0.5	60	3.3/5	0.0066/0.01	-30/+85	€2,200
SS-03	NanoSSOC-D60	43x14x5.9	6.50E-03	0.5	60	3.3/5	0.00759/0.0115	-30/85	€3,600
SS-04	SSoC-A60	40x30x12	2.50E-02	0.3	60	5 - 12	3.60E-02	-40/+85	€7,200
SS-05	SSoC-D60	60x30x12	3.50E-02	0.3	60	5	0.6	-40/+85	€12,200
SS-06	Fine Sun Sensor	108x108x52.5	3.75E-01	0.3	128	15	0.25	-50/+85	-

Figure B.5: Possible Sun sensors considered.

ID	Product Name	Size (LxWxH) [mm]	Mass [kg]	Accuracy [°]	Power [W]	FOV wide [°]	FOV narrow [°]	Price
ES-01	MAI-SES IR	4.33x3.18x3.18	0.033	0.25	0.132	60	7	$14,900
ES-02	IRES N2	-	2.3	0.08	3.5	5.5	11	-
ES-03	IRES-C	-	1.3	0.8	3.3	86	-	-

Figure B.6: Possible Earth sensors considered.

C
System Budgets

Space Segment Cost Estimation

Space segment cost summary		
Inflation factor		1.49
Cost item	FY2000$M	FY2019$M
Investment cost	13.1	19.5
Total production costs	14.2	21.2
Production costs first unit	5.5	8.2
Launch operations costs	5.7	8.5
Program level costs	4.9	7.2
Total costs		56.5

For cost details, see below.

Inputs					
Payload		S/C mass data (kg)		Other data	
Infra-Red (yes/no)	no	Attitude determination	0.389	Number of production satellites	10
Visible (yes/no)	no	Propulsion	0		
Communications (yes/no)	no	Power	6	Apogee kick motor (AKM); yes/no	no
IR aperture diameter (m)	0.54	Structure	62	AKM dry mass (kg)	0
Visible aperture diameter (m)	0	Thermal	0.5	Learning curve slope; S	0.8
Antenna mass (kg)	0.11	acking, Telemetry & Command	0.55		
Electronics (kg)	2	Payload mass	175		

S/C bus dry mass (kg)	69.464
S/C bus + payload dry mass (kg)	244.464

B. Zandbergen:
In case AKM is "yes", than this mass also includes AKM dry mass.

RDT&E cost (FY2000)		TFU cost (FY2000)		Production cost (FY2000)	
1. Payload	0	1. Payload	0	B	0.678072
1.1. Infra-Red	0	1.1. Infra-Red	0	Learning curve factor; L	4.765099
1.2. Visible	0	1.2. Visible	0	Production cost for total lot	14233
1.3. Communications	0	1.3. Communications	0	1st unit	5529
2. S/C bus	7016	2. S/C bus	2987	2nd unit	3318
3. Integration Assembly & Test (IAT)	2497	3. IAT	2542	3rd unit	2800
4. Program Level	3369	4. Program Level	1019	4th unit	2509
				5th unit	2312
5. Ground Equipment	2728	5. Launch operations	1198	Total launch operations	5708
				Total program level costs	4853
Total	12882	Total	7746		

B. Zandbergen:
Based on S/C bus dry

Subsystem RDT&E cost (FY 2000)		Subsystem TFU cost (FY 2000)	
Structure	4826	Structure	812
Thermal	254	Thermal	31
Electrical Power	378	Electrical Power	441
TT&C	346	TT&C	452
ADCS	205	ADCS	141
Propulsion	0	Propulsion	0
Total	6008	Total	1877

Figure C.1: Space segment cost estimation sheet.

Mass Estimates

Mechanism	8.2	16.4							Mechanism	6.6	16.4		
Power	3.5	7.0							Power	2.4	6.0		
Operations	3.1	6.1							Operations	0.2	0.5		
ADCS	5.2	10.4							ADCS	2.2	5.6		
ODCS	0.1	0.1							ODCS	0.0	0.1		
Non-Payload Dry mass	33.7	67.3							**Non-Payload Dry mass**	22.4	55.9		
Total Dry mass	100.0	200.0							**Total Dry mass**	100.0	250.0		
Propellant	20.0	50.0							Propellant	0.0	0.0		
Total Wet mass	100.0	250.0							**Total Wet mass**	100.0	250.0		
Each subsection:									**Each subsection:**				
PAYLOAD			**POWER**			**ODCS**			**PAYLOAD**			**POWER**	
ISIS Quadpack launcher	7500	gr	Generation	2970	gr	GNSS Receiver Module	109	gr	ISIS Quadpack launcher	7500	gr	Generation	2500
Max weight of a 3U Cubesat	6000	gr	Storage	3762.5	gr	Complete ODCS	109	gr	Average weight of a 3U Cubesat	6000	gr	Storage	2025
Mass of 1 filled quadpack unit	31500	gr	Control&distribution	1500	gr	**OPERATIONS**			Mass of 1 filled quadpack unit	31500	gr	Control&distribution	1500
STRUCTURE			Complete power	8232.5	gr	CDHU	748	gr	**STRUCTURE**			Complete power	6025
Aluminium Ring	17370	gr	**ADCS**			PCDU	1432	gr	Aluminium Ring	17370	gr	**ADCS**	
Service module (external+internal)	9100	gr	magneto meters	157	gr	Comms	322	gr	Service module housing	9100	gr	magneto meters	201
Estimated Bolts	800	gr	Sun sensors	73.5	gr	Instrumentation	297		Estimated Bolts	800	gr	Sun sensors	8
Complete structure	27270	gr	Reaction wheels	7560	gr	Complete computer system	2799	gr	Complete structure	27270	gr	Reaction wheels	3000
MECHANISM			Magneto Torquers	2290	gr	Antenna's	3350	gr	**MECHANISM**			Magneto Torquers	2181
2x Marman Clamp type 937S	6200	gr	Gyrometer	0	gr	Complete operations	6149	gr	2x Marman Clamp type 937S	6200	gr	Gyrometer	180
ISIS IMDC sequencer	2000	gr	Earth sensor		gr				ISIS IMDC sequencer	2000	gr		
Complete mechanism	16400	gr	Star sensor	315	gr				Complete mechanism	16400	gr		
			Complete ADCS	10395.5	gr							Complete ADCS	5570
Step 2	**Mass fraction (%)**	**Mass (kg)**	Quadpacks possible						**Step 3**	**Mass fraction (%)**	**Mass (kg)**	Quadpacks possible	
Payload	76.9	192.1	6						Payload	76.1	190.2	6	
Structure	10.9	27.3							Structure	10.9	27.3		
Mechanism	6.6	16.4							Mechanism	6.6	16.4		
Power	3.2	8.0							Power	3.9	9.7		
Operations	0.2	0.4							Operations	0.2	0.4		
ADCS	2.3	5.6							ADCS	2.4	5.9		
ODCS	0.0	0.1							ODCS	0.0	0.1		
Non-Payload Dry mass	23.1	57.9							**Non-Payload Dry mass**	23.9	59.8		
Total Dry mass	100.0	250.0							**Total Dry mass**	100.0	250.0		
Propellant	0.0	0.0							Propellant	0.0	0.0		
Total Wet mass	100.0	250.0							**Total Wet mass**	100.0	250.0		
Each subsection:									**Each subsection:**				
PAYLOAD			**POWER**			**ODCS**			**PAYLOAD**			**POWER**	
ISIS Quadpack launcher	7500	gr	Generation	4490	gr	GNSS Receiver Module	109	gr	ISIS Quadpack launcher	7500	gr	Generation	6188
Average weight of a 3U Cubesat	6000	gr	Storage	2025	gr	Complete ODCS	109	gr	Average weight of a 3U Cubesat	6000	gr	Storage	2025
Mass of 1 filled quadpack unit	31500	gr	Control&distribution	1500	gr	**OPERATIONS**			Mass of 1 filled quadpack unit	31500	gr	Control&distribution	1500
STRUCTURE			Complete power	8015	gr	NanoDock SDR 27	78.4	gr	**STRUCTURE**			Complete power	9713
Aluminium Ring	17370	gr	**ADCS**			NanoMind Z7000	76.8	gr	Aluminium Ring	17370	gr	**ADCS**	
Service module housing	9100	gr	magneto meters	201	gr	NanoCom TR-600	65.3	gr	Service module housing	9100	gr	magneto meters	201
Estimated Bolts	800	gr	Sun sensors	8	gr	Complete computer system	218.5	gr	Estimated Bolts	800	gr	Sun sensors	8
Complete structure	27270	gr	Reaction wheels	3000	gr	Antenna's	220	gr	Complete structure	27270	gr	Reaction wheels	3000
MECHANISM			Magneto Torquers	2181	gr	Complete operations	438.5	gr	**MECHANISM**			Magneto Torquers	2181
2x Marman Clamp type 937S	6200	gr	Gyrometer	180	gr				2x Marman Clamp type 937S	6200	gr	Gyrometer	180
ISIS IMDC sequencer	2000	gr	Earth sensor	66	gr				ISIS IMDC sequencer	2000	gr	Earth sensor	/
Complete mechanism	16400	gr							Complete mechanism	16400	gr	Star sensor	330